306318916.

NEURAL VULNERABILITY IN MODELS OF PARKINSON'S DISEASE

Thesis submitted for the Degree of Doctor of Philosophy
Hilary Term 2007

Mimi Shin Ning Mo

Christ Church & Department of Pharmacology
Oxford University

Supervisor: Dr Susan Totterdell

RADCLIFFE SCIENCE LIBRARY OXFORD
DEPOSITED
22 MAY 2008
THESIS

NEURAL VULNERABILITY IN MODELS OF PARKINSON'S DISEASE

Thesis submitted for the Degree of Doctor of Philosophy

Hilary Term 2007

Mimi Shin Ning Mo

Christ Church

Oxford University

ABSTRACT

Parkinson's disease (PD) is a neurodegenerative disorder with no known cure. This thesis explores the degenerative process in two neurotoxin-based models, the 6-hydroxydopamine and the chronic 1-methyl-4-phenyl-1,2,3,6-tetrahydropyridine (MPTP)/probenecid mouse models, to yield important information about the pathogenesis of PD.

Neuronal survival patterns in Parkinsonian patients and animals are heterogeneous. More dopaminergic neurons are lost from the ventral tier of the substantia nigra (SN) than from the dorsal tier or the adjacent ventral tegmental area, possibly due to differential expression of the calcium-binding protein, calbindin D28K. Brain sections were processed for tyrosine hydroxylase (TH) and calbindin (CB) immunocytochemistry to distinguish the dopaminergic subpopulations. I show that more TH+/CB- and TH-/CB+ than TH+/CB+ neurons are lost in both models, suggesting that CB confers some degree of protection for dopaminergic neurons. With respect to connectivity, I show that both TH+ and CB+ neurons receive striatal and dorsal raphe inputs.

I investigated the possibility of a progressive loss in midbrain neurons by prolonging the post-lesion survival period. In both models, there is an irreversible neuronal cell loss of TH+, CB+ and TH+/CB+ neurons but the effects of survival time and lesion treatments differ for the three neuronal types. The lesions also appear to be toxic to GABAergic neurons.

I explore whether, once neurodegeneration has started, neurons can be rescued by pharmacological intervention. Salicylic acid appears both to reduce microglial activation and significantly improve TH+, but not CB+ or TH+/CB+ neuronal survival.

PD appears multifactorial in origin and may involve complex interactions between genetic and environmental influences. I show that a xenobiotic-metabolising enzyme, arylamine *N*-acetyltransferase may fulfil a neuroprotective role in the SN by limiting the environmental risks. Taken together, this study provides a body of information on two different mouse PD models and highlights possible genetic predispositions to PD neuropathology.

Acknowledgements

First and foremost, I must thank Sue, my supervisor. I would not know where or how to express my gratitude for her support and help throughout my DPhil. I dare not call myself a scientist but with Sue's teaching, I feel that I could be one. She is my mentor and I would not have done this without her.

I also thank Wendy, for her scientific advice but more importantly, the love and care she gives to everyone. She teaches me the virtue of patience and being passionate in life. Electron microscopy sounds less laborious compared to her fly-fishing or making tapestry, and definitely less risky than going up on a hot-air balloon.

I am grateful for all the lab members, Sarah, whose guidance was central to my "early DPhil development" and the girls, Claire, Xiao Xiao and Henrike, to my "late-phase DPhil maintenance". Thank you for making me feel at home in your lab.

There are so many people that made my work possible here in the Department. It is like a symphony orchestra – without oboe player No.2, even the best first violin cannot make the music work. So I thank the Sim lab (the String section, for winding me up and cutting me some slacks under different circumstances) especially Larissa, Hilary, Akane, Isaac, Matt and Liz; to Dr Trevor Sharp's group ("Percussion"), Katie, Josie and Qin in particular, and for the use of their microscope; Viv and Debbie at the Biomedical Unit and even the securities who let me in during the weekends and gave me chocolate on Christmas Eve, Christmas Day and New Years Eve.

Last but not least, I thank Professor Sim, for giving me the opportunity to work in her lab as a summer research student even when I was still an undergraduate. She secured the MRC funding for my doctoral work and showed me how to be professional. I am truly blessed to have started my learning and career here.

Abbreviations

ABC	Avidin-biotin-peroxidase complex
ANOVA	Analysis of variance
BG	Basal ganglia
CB	Calbindin-D28K
DA	Dopaminergic
DAB	3,3'-diaminobenzidine tetrahydrochloride
EM	Electron microscopy
GABA	Gamme-amino-butyric acid
GAD	Glutamate decarboxylase
LM	Light microscopy
NAT	Arylamine *N*-acetyltransferase
pABA	*para*-aminobenzoyl glutamate
PAP	Peroxidase anti-peroxidase
PB	Phosphate buffer
PBS	Phosphate buffer saline
PD	Parkinson's disease
PFA	Paraformaldehyde
SA	Salicylic acid
SEM	Standard error of the mean
SG	Slate grey
SN	Substantia nigra
SNC	Substantia nigra pars compacta
SNR	Substantia nigra pars reticulata
SNL	Substantia nigra pars lateralis
TH	Tyrosine hydroxylase
VTA	Ventral tegmental area
TH+	Tyrosine hydroxylase-immunoreactive only
CB+	Calbindin-immunoreactive only
TH+/CB+	Immunoreactive for both tyrosine hydroxylase and calbindin

Table of Contents

1 Introduction 5
1.1 The Basal Ganglia and Disorders of Movement 6
1.1.1 The normal basal ganglia 6
1.1.2 Parkinson's disease 9
1.2 Genetic Basis of Parkinson's Disease 11
1.2.1 α-Synuclein 11
1.2.2 LRRK2 (also known as dardarin) 12
1.2.3 Parkin 12
1.2.4 DJ-1 13
1.2.5 PINK1 13
1.2.6 UCHL-1 13
1.3 Murine Models of Parkinson's Disease 15
1.3.1 6-hydroxydopamine (6-OHDA) 16
1.3.2 MPTP/probenecid (MPTP/p) 17
1.4 Differential Neuronal Vulnerability in Parkinson's Disease 20
1.5 Neuroprotective Strategies for Parkinson's Disease 21
1.6 Environmental Risks in Parkinson's Disease 24

2 General Materials and Methods 29
2.1 Animal models 30
2.1.1 6-hydroxydopamine-lesioned mouse model 30
2.1.2 MPTP/probenecid-lesioned mouse model 31
2.1.3 GAD65-GFP mouse model 31
2.1.4 Arylamine N-acetyltransferase (Nat) transgenic mice 32
2.2 Stereotaxic surgery 33
2.2.1 Lesion injections 34
2.2.2 Anterograde tracer injections 35
2.2.3 Tissue fixation 36
2.3 Tissue preparation prior to immunohistochemistry 37
2.3.1 Sectioning of the brain 37
2.3.2 Penetration enhancement 38
2.4 Immunohistochemistry 39
2.4.1 Immunofluorescence 40
2.4.2 Immunohistochemistry for light microscopy 41
2.4.3 Immunohistochemistry for electron microscopy 42
2.4.3.1 Use of the Avidin-Biotin-Peroxidase Complex (ABC) bridge method 43
2.4.3.2 Use of the Peroxidase Anti-Peroxidase (PAP) method 44
2.4.4 Electron microscopy 45
2.4.4.1 Post-fixation, dehydration and resin embedding 45
2.4.4.2 Correlated light and electron microscopy 46
2.4.4.3 Ultrathin sectioning 46
2.5 Image capture 47
2.6 Statistical analysis 48

3 Viability of Midbrain Neurons in the 6-hydroxydopamine and MPTP/probenecid Mouse Models of Parkinson's Disease 55
3.1 Introduction 56
3.2 Aims 59
3.3 Methods 59

3.3.1 Animals and lesions ... *59*
3.3.2 Immunohistochemistry and immunofluorescence ... *60*
3.4 Results ... **65**
3.4.1 Normal expression of TH and CB in mouse ... *65*
3.4.2 Effects of 6-OHDA in the striatum one month post-treatment ... *66*
3.4.3 Effects of 6-OHDA in midbrain neural degeneration one month post-treatment 67
3.4.3.1 Dopaminergic neurons ... *67*
3.4.3.2 GABAergic neurons ... *69*
3.4.3.3 Total neuronal number and total volume of the midbrain ... *69*
3.4.4 Effects of MPTP/probenecid in the striatum one month post-treatment ... *70*
3.4.5 Effects of MPTP/probenecid in midbrain neural degeneration one month post-70
3.4.5.1 Inclusion formation ... *70*
3.4.5.2 DA neurons ... *71*
3.5 Discussion ... **73**

4 Progressive Neurotoxicity to Midbrain Neurons in Mouse Models of Parkinson's disease ... **81**
4.1 Introduction ... **82**
4.2 Aims ... **84**
4.3 Methods ... **84**
4.3.1 Animals and lesions ... *84*
4.3.2 Immunohistochemistry and immunofluorescence ... *85*
4.3.3 Image analysis ... *85*
4.3.4 Quantitative and statistical analysis ... *85*
4.4 Results ... **86**
4.4.1 Effects of 6-OHDA in midbrain neural degeneration 3 months post-treatment 86
4.4.1.1 Nigro-striatal projections in the striatum ... *86*
4.4.1.2 DA neurons in the midbrain ... *87*
4.4.1.3 GABAergic neurons in the midbrain ... *89*
4.4.2 Effects of MPTP/probenecid in midbrain neural degeneration 3 months post-treatment 89
4.4.2.1 Nigro-striatal projections in the striatum ... *89*
4.4.2.2 DA neurons in the midbrain ... *90*
4.5 Discussion ... **91**

5 Anatomical and morphological evidence that striatal and dorsal raphe afferents innervate TH+ and CB+ neurons in the mouse midbrain ... **97**
5.1 Introduction ... **98**
5.2 Aims ... **100**
5.3 Methods ... **101**
5.3.1 Triple Immunofluorescence ... *101*
5.3.2 Electron microscopy ... *102*
5.4 Results ... **103**
5.4.1 Anterograde tracing into the striatum – injection site and projections to the VTA observed under fluorescence ... *103*
5.4.2 Striatal terminals forming synaptic junctions with TH+ and CB+ neurons in the VTA 104

5.4.3 Anterograde tracing from the dorsal raphe – injection site and projections to the VTA observed under fluorescence *106*
5.4.4 Dorsal raphe terminals forming synaptic junctions with TH+ and CB+ neurons in the VTA *108*
5.5 Discussion **109**
5.5.1 Striato-nigral pathway in the mouse *109*
5.5.2 Striatal afferents terminating onto TH+ and CB+ neurons in the VTA *111*
5.5.3 Raphe-nigral pathway in the mouse *112*
5.5.4 Dorsal raphe afferents terminating onto TH+ and CB+ neurons in the VTA *113*
5.5.5 Functional significance of the striato-nigral and raphe-nigral projections to the TH+ and CB+ neurons *114*

6 Effects of Salicylic Acid on Nigral Neurons in the MPTP/probenecid Mouse Model **116**
6.1 Introduction **117**
6.2 Aims **119**
6.3 Methods **119**
6.3.1 Animals and experimental protocols *119*
6.3.2 TH and CB immunostaining *120*
6.3.3 Macrophage antigen complex-1 (MAC-1) immunostaining *120*
6.3.4 Cell counting and statistics *121*
6.4 Results **121**
6.4.1 Administration of SA in the MPTP/p mouse model *121*
6.4.2 Effects of salicylic acid on TH+, CB+, and TH+/CB+ nigral neurons *122*
6.4.3 Nigral microglia activation *125*
6.5 Discussion **126**

7 Arylamine N-acetyltransferase as a Vulnerability Factor in Sporadic Parkinson's Disease **132**
7.1 Introduction **133**
7.2 Aims **135**
7.3 Materials and Methods **136**
7.3.1 Chemicals *136*
7.3.2 Generation of Nat2-/- mice *136*
7.3.3 Antibody generation *137*
7.3.4 Tissue homogenisation *137*
7.3.5 Dot blotting and Western blotting *138*
7.3.6 X-gal staining *138*
7.3.7 Immunohistochemistry *139*
7.3.8 Acetyl Coenzyme A (AcCoA) hydrolysis assay *140*
7.3.8.1 Substrate Screening *140*
7.3.8.2 Inhibitor Screening *140*
7.3.9 Behavioural tests using SHIRPA *140*
7.4 Results **141**
7.4.1 Genotyping of Nat wildtype and knockout mice *141*
7.4.2 Characterisation of hNAT1/mNAT2-specific antiserum 183 ..... *142*
7.4.3 Expression of mouse Nat2 in the adult brain *143*
7.4.4 Screening compounds as substrates/inhibitors of mouse NAT2 ..... *144*
7.4.5 SHIRPA behavioural study on NAT2 wildtype and knockout mice *145*
7.5 Discussion **146**

8 Discussion 151
8.1 6-OHDA and MPTP/p Mouse Models of Parkinson's Disease 153
8.1.1 Differences between the 6-OHDA and MPTP/p models 154
8.1.2 Limitations of the animal models 155
8.2 Midbrain CB+ and CB- Dopaminergic Neurons 156
8.3 Changes in Dopaminergic and GABAergic Neurons in Parkinson's Disease Models 159
8.4 The Relationship Between Early Neurotoxin Exposure and Progressive Neurotoxicity in Parkinson's Disease 161
8.5 Salicylic Acid As an Anti-oxidative and Anti-inflammatory Therapy for Parkinson's Disease 163
8.6 Gene-environment Interactions in Sporadic Parkinson's Disease 164

1 Introduction

1.1 The Basal Ganglia and Disorders of Movement

1.1.1 The normal basal ganglia

The basal ganglia (BG) are the largest subcortical structures in the human forebrain. Their anatomy puts them in the prime position to influence the forebrain's executive functions, such as planning for movement and even cognitive behaviours. In addition to this tight linkage with the frontal cortex, the BG send outputs to brainstem nuclei involved in motor control, including the superior colliculus (Graybiel, 2000). Lesions of the BG lead to devastating motor disorders such as Parkinson's disease (PD) and Huntington's disease, although unlike the motor cortex, which has direct connections with motor neurons, the BG influence movements by acting on the descending pathways (Martin, 2003).

These BG pathways are formed by a complex network of neuronal circuits organised in parallel to integrate activity from different cortical regions (Obeso et al., 2002). On the basis of their connections, the BG can be divided into three categories: input nuclei, output nuclei, and intrinsic nuclei. The input nuclei receive afferent connections from brain regions other than the BG and project to the intrinsic and output nuclei. The output nuclei project to regions of the diencephalon and brainstem that are not part of the BG. The connections of the intrinsic nuclei are largely restricted to the BG (Martin, 2003).

The striatum, the input nucleus of the BG, receives afferent projections from the cerebral cortex. Three subnuclei comprise the striatum: the caudate nucleus, which participates in eye movement control and cognition; the putamen, which participates in control of limb and trunk movements; and the nucleus accumbens, which participates in emotions.

There are three output nuclei: the internal segment of the globus pallidus (GPi), the substantia nigra pars reticulata (SNR), and the ventral pallidum. The axons of output nuclei

project to thalamic nuclei, including the ventrolateral, ventral anterior, and medial dorsal nuclei, which innervate different frontal lobe areas. The output nuclei also project to the peduncolopontine nucleus (PPTg) at the junction of the midbrain and pons, implicated in limb and trunk control during locomotion, and to the superior colliculus, which controls axial orientation and saccadic eye movement. The path from the striatum to the output nuclei (GPi/SNR) and then to the thalamus and brainstem promotes the production of movement. This circuit is termed the "direct pathway". Neurons in the direct pathway establish a monosynaptic, inhibitory connection and they contain mainly D_1 dopamine receptors and co-express the substance P and dynorphin (Gerfen, 1992; Obeso et al., 2002).

The BG have four intrinsic nuclei: the external segment of the globus pallidus (GPe), the subthalamic nucleus (STN), the substantia nigra pars compacta (SNC), and the ventral tegmental area (VTA). The pathway from the striatum to the GPe and STN comprises the "indirect pathway". Striatal neurons in the indirect pathway express mainly D_2 dopamine receptors and the peptide enkephalin. They send their GABAergic axons to the GPe, which connects with the STN, which in turn projects to the GPi/SNR. The STN uses glutamate as a neurotransmitter and therefore exerts an excitatory effect on the GPi/SNR and other brainstem nuclei that it innervates (PPTg and SNC). Output neuronal activity in the GPi/SNR is thought to be under a dual control mechanism. Therefore increased activity in the direct pathway gives rise to inhibition, or pauses, of neuronal firing in the GPi/SNR, leading to disinhibition of their projection nuclei (thalamus, PPTg, superior colliculus etc.) whereas, activity in the indirect pathway increases excitation of the STN and augments inhibition from the GPi/SNR onto their projection nuclei (Albin et al., 1989; DeLong, 1990; Obeso et al., 2002).

The anatomy of BG connections suggests that, at least in part, these structures operate as part of recurrent circuits (loops) within the cerebral cortex (Alexander and Crutcher, 1990; Graybiel, 2000). Five anatomical loops have been identified: 1) motor, 2) oculomotor, 3) associative, 4) limbic, and 5) orbitofrontal. The motor loop, which comprises of the direct and indirect pathway, is most relevant to the pathophysiology of movement and has several internal (or "closed) loop circuits to regulate the excitability of the BG (Gimenez-Amaya et al., 2000; Obeso et al., 2000). A summary of the main connections of the motor loop is shown in Figure 1A.

The dopaminergic (DA) system innervates all BG nuclei. The mesencephalic DA system stems from three main cellular populations known as areas A8 (retrorubral area - RRA), A9 (substantia nigra, SN), and A10 (VTA). Mesencephalic DA neurons can be divided according to their topographical distribution and chemical characteristics (Gerfen, 1992). Neurons in the dorsal tier of the SN mesencephalic region (including some SN neurons, VTA, and RRA) are loosely spaced and are positive for calbindin D_{28K} but contain relatively low levels of dopamine transporter and tyrosine hydroxylase. These neurons project mainly to the limbic and associative areas of the striatum. On the other hand, neurons from the ventral region of the SN mesencephalic region, which are calbindin D_{28K}-negative but rich in dopamine transporter, give rise to the major DA projection to the motor regions of the BG (Gerfen, 1992). Two different types of axonal projections have been distinguished (Prensa et al., 2000): a) neurons with a long axon travelling directly to the striatum that do not give rise to collaterals, and which mainly innervate specific zones of the striatum known as "patches" or striosomes; and b) neurons with profusely arborized axons that mainly innervate extrastriatal nuclei such as the GPe, GPi, STN, and even the thalamus. The latter type of neurons in the ventrolateral tier of the SN, which appear arranged in columns penetrating into the SNR, seems to be the first to degenerate in PD.

1.1.2 Parkinson's disease

The pathophsyiological hallmark of PD is increased neuronal activity in the output nuclei of the BG (GPi/SNR) leading to excessive inhibition of the thalamocortical and brainstem motor systems (Fig. 1B). Dopamine is deficient in PD, which leads to reduced inhibition of GABAergic striatal neurons in the indirect pathway and decreased facilitation of GABAergic neurons in the direct pathway neurons (Gerfen, 1992; Guridi et al., 1996; Gimenez-Amaya et al., 2000). Reduced inhibition of neurons in the indirect pathway leads sequentially to over-inhibition of GPe, dis-inhibition of STN, and increased excitation of GPi/SNR. Decreased activation of neurons in the direct pathway reduces its inhibitory effect on GPi/SNR and contributes to their excessive output activity. Together these effects drastically reduce the thalamic signals to the cortex. For the premotor and motor cortical areas, this reduces cortical outflow along the corticospinal and corticobulbar tracts and reduces production of motor behaviours such as hypokinesia (Martin, 2003).

Both familial and sporadic PD have a common endpoint – neurodegeneration of nigrostriatal DA neurons, which is the major pathological characteristic of PD. Neuronal loss in the SNC produces a marked deficit of dopamine content in the striatum, thus impinging directly onto the motor circuit as described above. This progressive loss of midbrain DA neurons is also accompanied by loss of non-DA populations in more advanced stages (Jellinger, 2001). An understanding of BG circuitry helps to explain the clinical features of PD, for example, impairment in initiating movement (akinesia), poverty of movement (hypokinesia), slowness of movement (bradykinesia), rigidity and tremor at rest. ***In Chapters 3 and 4, changes in DA and GABAergic neurons are examined in two 'parkinsonian' models, which illustrate the importance of BG circuits in this movement disorder.***

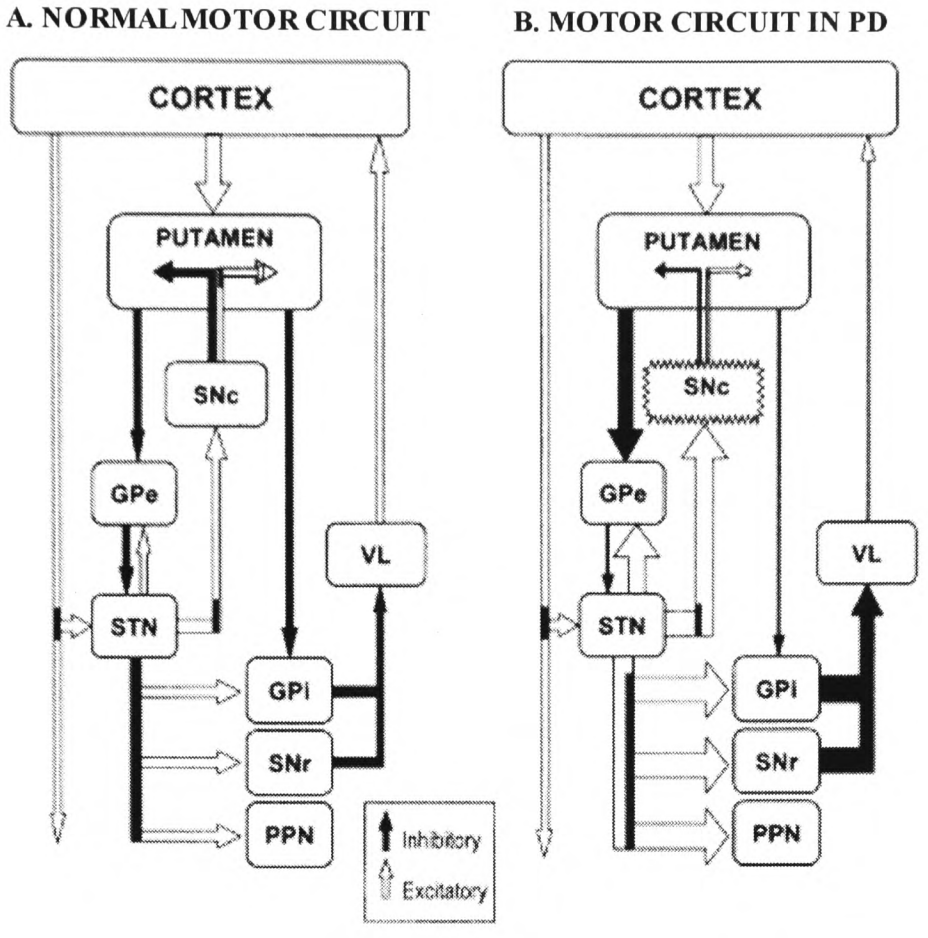


Figure 1. Summary of the main connections of the "motor circuit" of the basal ganglia.

In the normal state, the putamen receives afferents from the motor and somatosensory cortical areas and communicates with the GPi/SNR through a direct inhibitory pathway and through a multisynaptic indirect pathway (GPe, STN). Dopamine is believed to modulate striatal activity, mainly by inhibiting the indirect and facilitating the direct pathways. In Parkinson's disease (PD), dopamine deficiency leads to increased inhibitory activity from the putamen onto the GPe and disinhibition of the STN. Consequently, STN hyperactivity by virtue of its glutamatergic action produces excessive excitation of the GPi/SNR neurons, which overinhibits the thalamocortical and brainstem motor centres. SNc, substantia nigra pars compacta; SNr, substantia nigra pars reticulata; GPe, external segment of the globus pallidus; GPi, internal segment of the globus pallidus; STN, subthalamic nucleus; VL, ventrolateral thalamus; PPN, pedunculopontine nucleus. Figure modified from (Obeso et al., 2002).

1.2 Genetic Basis of Parkinson's Disease

PD generally arises as a sporadic condition but about 5-10% of the cases are inherited in a Mendelian fashion. Although sporadic and familial PD are very similar, the inherited form usually begin at earlier ages and are associated with atypical clinical features (Vila and Przedborski, 2004). In total, two autosomal-dominant genes (*α-synuclein* and *LRRK2*) and three autosomal-recessive genes (*parkin, DJ-1* and *PINK1*) have been definitively associated with inherited PD (Polymeropoulos et al., 1997; Kitada et al., 1998; Bonifati et al., 2003; Paisan-Ruiz et al., 2004; Valente et al., 2004; Zimprich et al., 2004; Jain et al., 2005). A summary of the PD genes involved is listed in Table 1 and the associations among the genetic factors are illustrated in Figure 1.2

Locus	MOI	Gene (protein)	Protein function	Clinical presentation	Neuropathology	Age at onset
PARK1 (PARK4)	AD	*SNCA* (α-synuclein)	Unknown synaptic function	Duplications: Idiopathic PD; some postural tremor; slow progression	LBs	Mid 30–mid 60
				Triplications: PD; PD with dementia; diffuse LBs disease; aggressive course	LBs and LNs; ± glial inclusions; hippocampal CA2 and CA3 loss	Mid 20–30
				Mutations A53T, A30P, E46K: Idiopathic PD; parkinsonism and diffuse LBs	LBs and LNs; ± tau inclusions; amyloid plaques	30–60
PARK2	AR	Parkin	E3 ubiquitin ligase	Parkinsonism; slow progression	Variable presence of LBs	Juvenile to 40
PARK5	AD	*UCHL1*	Ubiquitin hydrolase and ligase	PD	Unknown	30–50
PARK6	AR	*PINK1*	Mitochondrial Ser–Thr kinase	Parkinsonism	Unknown	30–50
PARK7	AR	*DJ-1*	Oxidative stress response?	Parkinsonism	Unknown	20–40
PARK8	AD	*LRRK2* (dardarin)	Unknown protein kinase	PD	Diffuse LBs; LNs; ± tau inclusions; ± amyloid plaques	40–60

Abbreviations: AD, autosomal dominant; AR, autosomal recessive; LBs, Lewy bodies; LNs, Lewy neurites; MOI, mode of inheritance; OE, overexpressed; PD, Parkinson's disease.

Table 1. Mendelian PD genes. (Figure modified from (Wood-Kaczmar et al., 2006)

1.2.1 α-Synuclein

Three missense mutations (A53T, A30P and E46K) in the gene encoding α-synuclein, *SNCA*, are linked to a dominantly inherited PD (Polymeropoulos et al., 1997; Kruger et al., 1998; Zarranz et al., 2004). Genomic duplications and triplications at the *SNCA* locus can also

cause autosomal dominant, early onset PD (Singleton et al., 2003; Farrer et al., 2004; Nishioka et al., 2006) It is a major component of the Lewy body in both idiopathic and inherited PD (Spillantini et al., 1997) but whether α-synuclein inclusions are directly toxic or if the α-synuclein protofibrils are the pathogenic species remain to be elucidated. It is thought that the soluble, oligomeric forms of α-synuclein are the toxic species rather than the insoluble fibrils within the inclusion body (Conway et al., 2000). (See Section 1.5 for further details on the role of α-synuclein in familial PD)

1.2.2 LRRK2 (also known as dardarin)

At least 9 pathogenic mutation in the leucine-rich repeat kinase 2 (*LRRK2*) gene have been identified so far, including two that map to the kinase domain (Paisan-Ruiz et al., 2004; Albrecht, 2005; Khan et al., 2005). One of the mutations, the G2019S substitution, causes parkinsonism closely resemblig idiopathic PD, and accounts for ~5% of familial PD and 1.5% of sporadic cases (Gilks et al., 2005). The function of LRRK2 and the consequent effects of pathogenic mutations remain unclear – mutations that lie outside the kinase and GTPase domain might be pathogenic via dominant negative mechanism (Wood-Kaczmar et al., 2006).

1.2.3 Parkin

Mutations in the parkin gene are the predominant cause of juvenile and early onset recessive parkinsonism (Kitada et al., 1998). Inactivation of parkin leads to reduction in ubiquitin-proteasome system (UPS)-mediated degradation of its substrates (Shimura et al., 2000; Sriram et al., 2005). This accumulation results in selective toxicity to DA neurons, which has been demonstrated for certain substrates only (von Coelln et al., 2004). Interestingly, parkin

seems to display a protective function in mitochondria (Palacino et al., 2004), although the mechanism is yet unknown.

1.2.4 DJ-1

Rare mutations in *DJ-1* also cause autosomal recessive early onset PD (Bonifati et al., 2003). DJ-1 is oxidatively damaged in the brains of idiopathic PD patients, suggesting a mechanism of protein aggregation in these diseases that is mediated by high levels of oxidative stress (Choi et al., 2006).

1.2.5 PINK1

Homozygous or compound heterozygous mutations in the *PINK1* gene cause PD with a wide phenotypic spectrum, for early onset with atypical features to late-onset PD that is identical to sporadic cases. At least 20 pathogenic mutations have been reported. *PINK1* mutations are the second most common cause of autosomal recessive PD after parkin (Hatano et al., 2004; Klein and Schlossmacher, 2006; Wood-Kaczmar et al., 2006).

1.2.6 UCHL-1

The clinical features as a result of mutations in the *UCHL-1* gene were typical of idiopathic PD. The gene could potentially interact in the same pathway as *parkin*, but also has hydrolase activity that could result in proteosomal degradation of proteins (Liu et al., 2002; Nishikawa et al., 2003; Osaka et al., 2003).

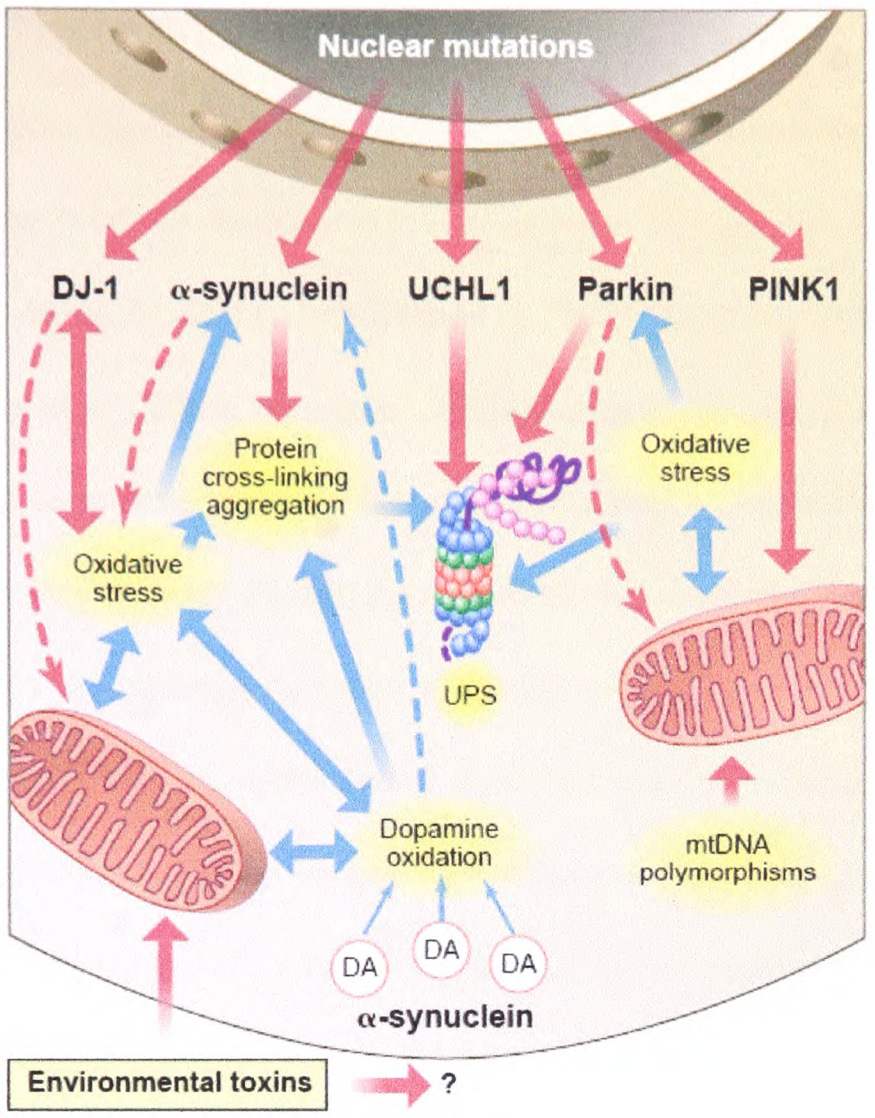


Figure 1.2 Genetic factors associated with Parkinson's disease

Five nuclear genes are known to carry mutations that cause PD. These genes encode DJ-1, α-synuclein, UCHL1, parkin, and PINK1. Mutations or altered expression of these proteins contributes to PD pathogenesis through common mechanisms that result in mitochondrial impairment, oxidative stress, and protein mishandling.

Red arrows indicated putative primary causes of PD; dashed arrows indicate effects that are probably secondary. Blue arrows indicate mechanisms of PD that are probably secondary to primary genetic or environmental causes.

Figure modified from (Greenamyre and Hastings, 2004)

1.3 Murine Models of Parkinson's Disease

The specific aetiology of PD is unknown, making it difficult to study the disease and its treatment. Approaches to modelling PD in animals depend either on disease-related genes (e.g. synuclein-based models (Abeliovich et al., 2000; Masliah et al., 2000); *parkin* knockout mice (Goldberg et al., 2003; Itier et al., 2003)) or toxin-based models. These two classes of animal models complement each other. Models based on mutations known to cause PD in humans offer a way to study the full extent of PD pathology and permit identification of early pathogenic steps in neurodegeneration, although only 1-2% of PD is familial (Dawson et al., 2002). On the other hand, toxin-based models have been invaluable in developing new symptomatic therapies, but a major limitation is that they mainly reproduce loss of nigrostriatal DA neurons with little effect in other brain regions or peripheral organs, which could precede nigrostriatal cell loss in the actual PD pathology (Levine et al., 2004).

A consensus has been reached that an ideal PD model should have the following characteristics (Beal, 2001; Petroske et al., 2001): first, a normal complement of dopamine neurons at birth with selective and gradual loss of DA neurons commencing in adulthood. The losses should exceed 50% and be readily detectable using biochemistry and neuropathology. Second, the model should have easily detectable motor deficits, including the clinical symptoms of PD. Third, the model should show the development of characteristic Lewy bodies. Fourth, if the model is genetic, it should be based on a single mutation to allow robust propagation of the mutation, as well as crossing with enhancer or suppressor strains. Finally, it should have a relatively short disease course of a few months, allowing rapid and less costly screening of therapeutic agents.

Most neurotoxin-based animal models have studied rats or non-human primates. With an increasing availability of genetically modified mice that model PD, characterising toxin-

induced lesions in mice is highly warranted. ***In the present study, neurotoxin-based murine models by 6-hydroxydopamine and MPTP/probenecid lesions were used to decipher the neuronal dysfunction in PD.***

1.3.1 6-hydroxydopamine (6-OHDA)

This was the first agent used to model PD (Ungerstedt, 1968). Inside neurons, 6-OHDA accumulates in the cytosol, generating reactive oxygen species and inactivating biological macromolecules by generating quinones that attack nucleophilic groups (Cohen, 1994). Its toxicity is relatively selective for monoaminergic neurons, resulting from preferential uptake by DA and noradrenergic transporters (Luthman et al., 1989) and inducing cell death without apoptosis *in vivo* (Jeon et al., 1995). On the other hand, *in vitro* studies showed that 6-OHDA toxicity is initiated via extracellular auto-oxidation and that hydrogen peroxide plays a central role in evoking neuronal cell death, as well as hydroxyl radicals in the presence of iron (Sachs and Jonsson, 1975). In addition, 6-OHDA caused mitochondrial dysfunction, activation of pro-apoptotic protein kinase Cδ, caspases 3/7, which lead to nuclear fragmentation and apoptosis (Hanrott et al., 2006). Similar to PD, there is a differential sensitivity to 6-OHDA between the ventral midbrain DA neuronal groups: greatest loss is observed in the SNC, while tuberoinfundibular neurons are almost completely resistant (Jonsson, 1980).

Unlike 1-methyl-4-phenyl-1,2,3,6-tetrahydropyridine (MPTP), 6-OHDA does not cross the blood-brain barrier and must be administered directly by local stereotaxic injection. In this study, 6-OHDA is injected into the medial forebrain bundle, which carries ascending dopaminergic and serotonergic projections to the forebrain. After injection, DA neurons start "dying back" within 24 hours and die without apoptotic morphology (Jeon et al., 1995).

6-OHDA is an effective toxin in rats, mice, cats and primates that is predominantly used to produce unilateral lesions (Beal, 2001), with the contralateral side servicing as control (Ungerstedt, 1971). Consequently, the injection produces an asymmetric circling behaviour in the animals, the magnitude of which depends on the degree of the nigrostriatal lesion (Ungerstedt and Arbuthnott, 1970; Hefti et al., 1980; Przedborski et al., 1995). Following 6-OHDA administration in a rat, can be binding of a specific ligand ^{11}C-CFT (2β-carbomethoxy-3β-(4-fluorophenyl) tropane) to presynaptic dopamine transporters, monitored by positron emission tomography (PET) imaging, was markedly reduced in the striatum, indicating DA degeneration (Cicchetti et al., 2002).

The disadvantages of 6-OHDA are that the mechanism by which it kills DA neurons may differ from the key molecular features in PD; the lesion does not result in Lewy bodies in the SN and it can produce non-specific damage to other neurons. Nevertheless, it is still extensively used for investigating time-dependent alterations of nigrostriatal DA neurons (Iwata et al., 2004). Its also has a major advantage in quantifying motor deficit (rotation), assessed by amphetamine and apomorphine administrations (Beal, 2001; Dauer and Przedborski, 2003), and spontaneous motor tests (Iancu et al., 2005).

1.3.2 MPTP/probenecid (MPTP/p)

Perhaps the best-characterised model of PD uses the toxin, MPTP (Bloem et al., 1990). Rats are generally resistant to MPTP neurotoxicity (Heikkila et al., 1984; Lau and Fung, 1986; Zuddas et al., 1994) but mice such as C57BL strain are susceptible (Heikkila et al., 1984; Lau and Fung, 1986; Hamre et al., 1999). The toxin is highly lipophilic and it readily crosses the blood-brain barrier. It is converted into its active metabolite, 1-methyl-4-phenylpyridinium (MPP^+) by monoamine oxidase B (an enzyme involved in catecholamine degradation) in glia and serotonergic neurons, the only cells that contain this enzyme (Dauer and Przedborski,

2003). MPP^+ is taken up by the plasma membrane dopamine transporter, for which it has a high affinity, or by vesicular monoamine transporters (VMAT). Intracellular MPP^+ is concentrated in mitochondria, where it inhibits complex I of the electron transport chain (Tipton and Singer, 1993). This reduces ATP generation and increases free radical production, particularly in the striatum and ventral midbrain (Chan et al., 1991; Fabre et al., 1999). The subsequent apoptotic events and/or inflammation contribute to the nigrostriatal cell death. A comparison between the action of 6-OHDA and MPTP is illustration in Figure 1.2.

MPTP damages the dopaminergic pathways in a pattern similar to that seen in PD, including relatively greater cell loss in the SNC than the VTA and a preferential loss of neurons in the ventral and lateral segments of the SNC (Sirinathsinghji et al., 1992; Varastet et al., 1994). Although MPTP toxicity replicates all the clinical signs of PD (Burns et al., 1983; Bloem et al., 1990) and its administration leads to the accumulation and nitration of α-synuclein in the cytosol of SNC DA neurons (Vila et al., 2000; Przedborski et al., 2001), it is an acute insult (Dawson et al., 2002). Moreover, in mice, frequent injections of large, hepatotoxic doses of MPTP are required (Petroske et al., 2001) and the dopamine system recovers over time.

In this chronic MPTP/p model, striatal DA levels do show some recovery: there was a 95-98% depletion 1 and 3 weeks after chronic treatment, and 76% loss after 6 months. Additionally, 1, 3 weeks or 6 months after the MPTP/p treatment, striatal DA uptake in the striatal terminals remained persistently depressed (72% loss was found in the 6-month post-treatment group) (Petroske et al., 2001). These results were in contrast to chronic treatment of MPTP alone, where striatal DA levels and striatal DA uptake recovered 80-100% after 6 months (Petroske et al., 2001).

In this model, tyrosine hydroxylase-immunopositive (TH+) processes in the striatum were progressively lost in both the caudate-putamen and nucleus accumbens. Fibers were first reduced in medial and central, dorsal striatum and the core of nucleus accumbens at 1 week post-treatment, then in dorsolateral caudate-putamen and lateral shell of nucleus accumbens in the 3 weeks post-MPTP/p treatment group. In the midbrain, TH+ processes were greatly reduced throughout the SN and to a lesser extent in the VTA, at 1 and 3 weeks post-MPTP/p treatment. By one week post-treatment, DA neurons had been lost from the pars lateralis (SNL), and from the middle of the SNC at 3 weeks post-treatment. The loss of TH+ neurons throughout the SNC and VTA was still observed after 6 months, though both the pattern and extent of TH+ fibers partially recovered. The volume of the SN and the behavioural consequences of the MPTP/p treatment have been described in detail (Petroske et al., 2001; Novikova et al., 2006). Taken together, the data provide the basis for comparison with the present study, and demonstrate that neurochemical, immunohistochemical and behavioural experiments can be performed to assess the extent of neuronal loss in PD.

1.3.3 Action of Probenecid

MPTP neurotoxicity might be enhanced by agents that inhibit the central clearance of MPP^+ and/or the renal excretion of MPTP. Probenecid (a uricosuric agent) as an adjuvant, potentiates neurotoxicity by reducing the clearance of MPTP and its metabolites from kidney and brain. The effect of probenecid in the MPTP-treated mice was examined by Lau *et al.* because mice injected with radiolabelled [^{3}H]methyl-MPTP excreted ~42% of the total injected [^{3}H] in the urine within 3 hours after drug administration. The urinary volume and excretion of MPTP metabolites were inhibited by pretreating the animals with probenecid (Lau et al., 1988). The effects on striatal DA depletion are chronic and do not reverse even 6 months after treatment (Lau et al., 1990).

The mechanism by which probenecid delays the excretion of MPTP metabolites in urine is not fully understood. It seems that probenecid retarded the formation of urine and reduced the total amount of metabolites excreted in the urine. It has been known to affect excretion of, e.g. penicillin, by decreasing their excretion through inhibition of tubular secretion, but does not directly affect the enzymatic property of flavin-containing monooxygenase or monoamine oxidase to convert MPTP to MPTP N-oxide or MPP+ (Lau et al., 1988). Probenecid appears to block transport of organic acids from the brain and cerebrospinal fluid into the blood (Gordon et al., 1976).

In mice, inhibition of transport of acidic metabolites from the brain by administration of probenecid does not increase levels of a dopamine metabolite, 3,4-dihydroxyphenylacetic acid (DOPAC), and even after inhibition of O-methylation the increase in DOPAC levels does not reflect the decrease in another dopamine metabolite, homovanillic acid (HVA) (Murphy et al., 1969; Roffler-Tarlov et al., 1971). Taken together, probenecid prolongs MPTP neurotoxicity in mice by acting mostly in the brain and kidney.

1.4 Differential Neuronal Vulnerability in Parkinson's Disease

Three tiers of DA cells are identified in the rodent and primate SN: a dorsal tier of the SNC, and the two ventral tiers; one within the SNC proper with the other occupying the SNR. The SN dorsal tier may be distinguished from the ventral tiers by cytological criteria, and expression of the calcium binding proteins calbindin-D-28k (CB) and/or calretinin (CR) in rodents, non-human primates and humans (Cote et al., 1991; McRitchie and Halliday, 1995; Liang et al., 1996a). In PD, the pattern of progressive midbrain DA neuronal loss is not uniform. For example, in the SN, DA neurons that occupy the ventral two tiers (ventral SN) are lost first, with relative sparing of those in the dorsal tier and VTA. This differential vulnerability to injury may derive from extrinsic factors such as different afferences or from

intrinsic neurochemical makeup. CB has been suggested as a marker of neuronal survival in PD but its functional role remains unknown.

Early studies showed that the majority of CB is preferentially distributed in the midbrain DA neurons that are less vulnerable to degeneration in PD animal models (i.e. CB is present mostly in nuclei A10 rather than A8 and A9) (German et al., 1992; Rogers, 1992; Liang et al., 1996b). Moreover, Graybiel and colleagues' earlier work on chemical compartmentalisation of the striatum demonstrated that the CB-poor nigrosome 1 (the largest cluster in the ventrolateral pars compacta) was the most severely depleted of neurons in PD, compared to the CB-rich background of the SNC, the "matrix" (Damier et al., 1999a, b). Many researchers suggested that CB might confer resistance to excitotoxicity by means of calcium homeostasis (Yamada et al., 1990; Lavoie and Parent, 1991) but knockout of CB did not alter developmental survival of midbrain DA neurons nor increase susceptibility to MPTP (Airaksinen et al., 1997). Hence, CB might have alternative functions other than the survival of DA neurons. ***In Chapter 3 and 4, the effects of 6-OHDA and MPTP/p on CB+ and CB- neurons were investigated. In Chapter 5, the inputs to the CB+ and CB- DA neurons were elucidated, which might shed light on the contribution of CB to the differential vulnerability of DA neurons.***

1.5 Neuroprotective Strategies for Parkinson's Disease

The current symptomatic therapy for PD consists mainly of dopamine replacement such as the use of levodopa and adjuvant surgical therapy such as deep brain stimulation that relieves motoric symptoms (Lang and Lozano, 1998a, b). However, there is no proven neuroprotective or neuro-restorative therapy to prevent cell death (Dawson and Dawson, 2002). The US National Institute of Neurological Disorders and Stroke has initiated one of its largest neuroprotective trials ever in an attempt to identify therapeutic opportunities for PD

(Ravina et al., 2004). Two areas that are under extensive exploration are anti-oxidative and anti-inflammatory agents.

In PD, and some neurodegenerative diseases such as Alzheimer's disease (AD), susceptibility to oxidative stress may be genetically influenced but environmentally activated, for example, by exposure to toxins, heavy metals, viruses or hypoxia (Potashkin and Meredith, 2006). Post-mortem brain tissues from PD and AD patients clearly display increased indices of reactive oxygen species (Andersen, 2004): markers for lipid peroxidation, including 4-hydroxynonenal and malondialdehyde, have been identified in the cortex and hippocampus of AD patients, the SN of PD patients and in spinal fluid from patients with amyotrophic lateral sclerosis (Dexter et al., 1989; Hensley et al., 1998; Pedersen et al., 1998; Butterfield et al., 2002). Clinical features also show that oxidative stress plays an important role in both familial and sporadic PD. For example, one of the earliest changes in patients with PD and incidental Lewy body disease is the loss of glutathione (Sian et al., 1994; Owen et al., 1996).

In familial PD, the intracellular inclusions termed Lewy bodies and contain α-synuclein. This protein may be toxic during the intermediate formation steps of small aggregates called protofibrils (Volles et al., 2001), but their accumulation inside Lewy bodies may not be toxic (Tanaka et al., 2004). α-synuclein has been suggested to bind to and permeabilize synaptic vesicles, thereby increasing the amount of dopamine present in the relatively acidic environment of the cytoplasm, where it is more likely to be oxidized (Conway et al., 2001; Volles et al., 2001; Lotharius and Brundin, 2002). Dopamine metabolism yields oxidative by-products such as superoxide, hydrogen peroxide and dopaminergic quinines (Andersen, 2004), which might increase the rate at which tyrosine is modified in the α-synuclein protein (Przedborski et al., 2001; Saito et al., 2003). Nitrated, hyperphosphorylated, or

phosphorylated α-synuclein will have an altered hydrophobicity and conformation from a natively unfolded molecule to an insoluble β-sheet aggregate (Clayton and George, 1999), which might subsequently become unrecognisable by the ubiquitin-proteasome protein degradation system, resulting in its build-up in the cell (Jha et al., 2002). Abnormal protein phosphorylation may also modify its ability to bind lipids and affect triglyceride turnover (Ellis et al., 2001). It is also possible that the proteins that are involved in protofibril formation self-induce oxidative stress – transfection of cells with mutant human A53T α-synuclein or *parkin* genes results in increased oxidation of both proteins and lipids (Hsu et al., 2000; Ostrerova-Golts et al., 2000; Hyun et al., 2002).

In sporadic PD, glial cells may be activated in response to cellular damage such as oxidative injury. The downstream cascade involves the production of more free radicals, such as nitric oxide and hydrogen peroxide, and cytokines. Glial iNOS (inducible nitric oxide synthase) concentrations are increased in the midbrain of PD patients (Knott et al., 2000). In addition, cylooxygenase-2 (COX-2, which is induced during pathophysiological responses to inflammatory stimuli) has been proposed to mediate microglial activation through the generation of reactive oxygen species (Czlonkowska et al., 2002), which perpetuates the chronic inflammatory response seen in MPTP-induced mouse models (Vijitruth et al., 2006).

Under normal circumstances, a response by microglia is protective in combating pathogens. However, under pathological conditions induced by insults such as oxidative stress, excitotoxicity and trauma, microglia can be over-stimulated and produce excessive cytotoxic agents that damage neurons. Subsequently, neuronal and/or microglial COX-2 could be overexpressed, leading to secondary injury (Vijitruth et al., 2006). In a 6-OHDA-lesion rat model, microglial activation was initially focal, then widespread at striatal and nigral levels at 4 weeks post-treatment (Cicchetti et al., 2002). In chronic MPTP- and 6-OHDA-induced

PD rodent models, microarray analyses showed that the expression of genes associated with oxidative stress, inflammation and apoptosis are significantly altered in toxin-treated animals compared to controls (Grunblatt et al., 2001; Mandel et al., 2002). Based on earlier studies, microglial activation precedes massive death of the DA neurons (Sugama et al., 2003b). Microarray-based gene expression profiling studies have been used by several labs to determine the effects induced by Parkinsonism, which suggest that alterations of several genes associated with the cell cycle and apoptosis are linked to dopaminergic neuronal degeneration (Bonin et al., 2004; Bassilana et al., 2005; Duke et al., 2006; Anantharam et al., 2007). Thus, pharmacological intervention to stop the positive feedback loop between the production of reactive oxygen species and microglial activation may prevent DA cell death.

In several epidemiological studies, non-steroidal anti-inflammatory drugs (NSAIDs) have shown protective effects in reducing the risk of PD (Chen et al., 2005). NSAIDs are competitive inhibitors at the cyclooxygenase (COX) active site. Their neuroprotective mechanisms involve prostaglandin-dependent and prostaglandin-independent suppressions, and may also interact with other proteins such as transcription factors and transporters (FitzGerald, 2003). ***In Chapter 6, the anti-oxidant and anti-inflammatory effects of the most prominent NSAID, salicylic acid (aspirin), were examined in the MPTP/p-treated PD model. The effect of MPTP/p-induced oxidative stress on CB+ and CB- DA neurons was also assessed.***

1.6 Environmental Risks in Parkinson's Disease

The ecogenetic theory suggests that most cases of PD result from the actions of environmental factors in genetically susceptible individuals on a background of normal ageing. Epidemiologic data supported this idea by showing family history of PD and exposures to environmental toxins (e.g. pesticides) increase risk (Mellick, 2006), while

cigarette smoking reduces risk (Quik, 2004). In fact, the discovery of MPTP when a group of drug addicts in California developed subacute onset of severe PD in 1982 (Langston et al., 1984) subsequently provided information about the genetic factors determining cell susceptibility to xenobiotic insults (Corsini G.U., 2002). As a result, polymorphic genes that code for metabolic enzymes have been considered as candidates for conferring differential risk for PD (Mellick, 2006).

Drug metabolising enzymes (DME) are widely distributed in the body, but the majority are found in the liver in vertebrates. They can be classified as either phase I or phase II enzymes with phase I DME responsible for introducing functional groups to xenobiotics (e.g. by oxidation, reduction, hydrolysis), thereby increasing the reactivity of the compound while phase II DME conjugate small molecules onto phase I metabolites or the parent molecules (e.g. by glucuronidation, sulfation, acetylation and methylation), usually leading to detoxification and elimination of the xenobiotics from the body. On the other hand, in addition to exerting detoxifying effects, DME can activate pro-carcinogens and pro-mutagens (Guengerich, 1992). There are over 30 families of DME in humans (Evans and Relling, 1999) and most have genetic variations, which result in different levels of expression and enzymatic efficiencies. Individuals therefore have different profiles of xenobiotic metabolism.

Given their prominence in xenobiotic metabolism, cytochrome P450 (CYP) has been studied extensively. These phase I DME are expressed in the brain and in DA neurons (Warner and Gustafsson, 1994). If CYP is preferentially expressed in subpopulations of neurons, those neurons which do not contain CYP or other DME may be more susceptible to xenobiotic insults. Moreover, if the activity of a certain CYP gene, determined by genetic variability, leads to a poor-metaboliser phenotype, neurons may be more prone to degeneration when toxic compounds are not eliminated soon enough. Indeed, when the CYP2E1 isozyme was

inhibited by diethyldithiocarbamate, ethanol or acetaldehyde, the retention time of intraneuronal MPP^+ in the affected area was increased, potentiating MPTP toxicity in mice (Corsini et al., 1985; Zuddas et al., 1989).

Arylamine *N*-acetyltransferases (NAT) are examples of phase II DME. They play an important role in detoxification and metabolic activation of xenobiotics by catalysing the conjugation of an acetyl group from acetyl coenzyme A to the terminal nitrogen of aromatic and heterocyclic amines, arylhydrazines and hydroxyarylamines. In humans, NATs are highly polymorphic, with single nucleotide polymorphisms giving rise to fast and slow acetylator phenotypes. Epidemiological studies suggested that various NAT alleles are linked to increased susceptibility to drug toxicity and diseases which are caused by arylamine exposure. Therefore, NATs have attracted much attention in the pharmacogenomics and pharmacokinetics field.

Three *NAT* loci are located on human chromosome 8 (Blum et al., 1990; Hickman et al., 1994) – *PNAT, NAT1, NAT2*. *PNAT* is a pseudogene which contains premature stop codons (Blum et al., 1990), whereas *NAT1* and *NAT2* encode functionally active 34 kDa proteins (Blum et al., 1990; Ohsako and Deguchi, 1990). *NAT1* and *NAT2* differ in tissue distribution, substrate specificity and expression levels during development and in adults – NAT1 activity is detected in many human tissues, both early in development (Pacifici et al., 1986) and in adults (Stanley et al., 1996), while NAT2 activity is predominantly observed in the liver and intestinal epithelium (Jenne, 1965; Hickman et al., 1998).

In mouse, there are also three *Nat* genes, *Nat1*, *Nat2* and *Nat3*. No distinct substrate or role for murine NAT3 has yet been identified. Historically, mouse *Nat2* was designated because, like human *NAT2*, it encodes a protein that demonstrates polymorphism. However, it is now

known that mouse *Nat2* encodes the functional equivalent of the human NAT1 isozyme; and mouse *Nat1* is functionally equivalent to human NAT2 (Hein et al., 2000a). NATs in humans and mice overlap in expression patterns and substrate specificities, which reinforce the notion that genetic duplication of the *NAT* genes occurred before the divergence of mice and humans (Upton et al., 2001a).

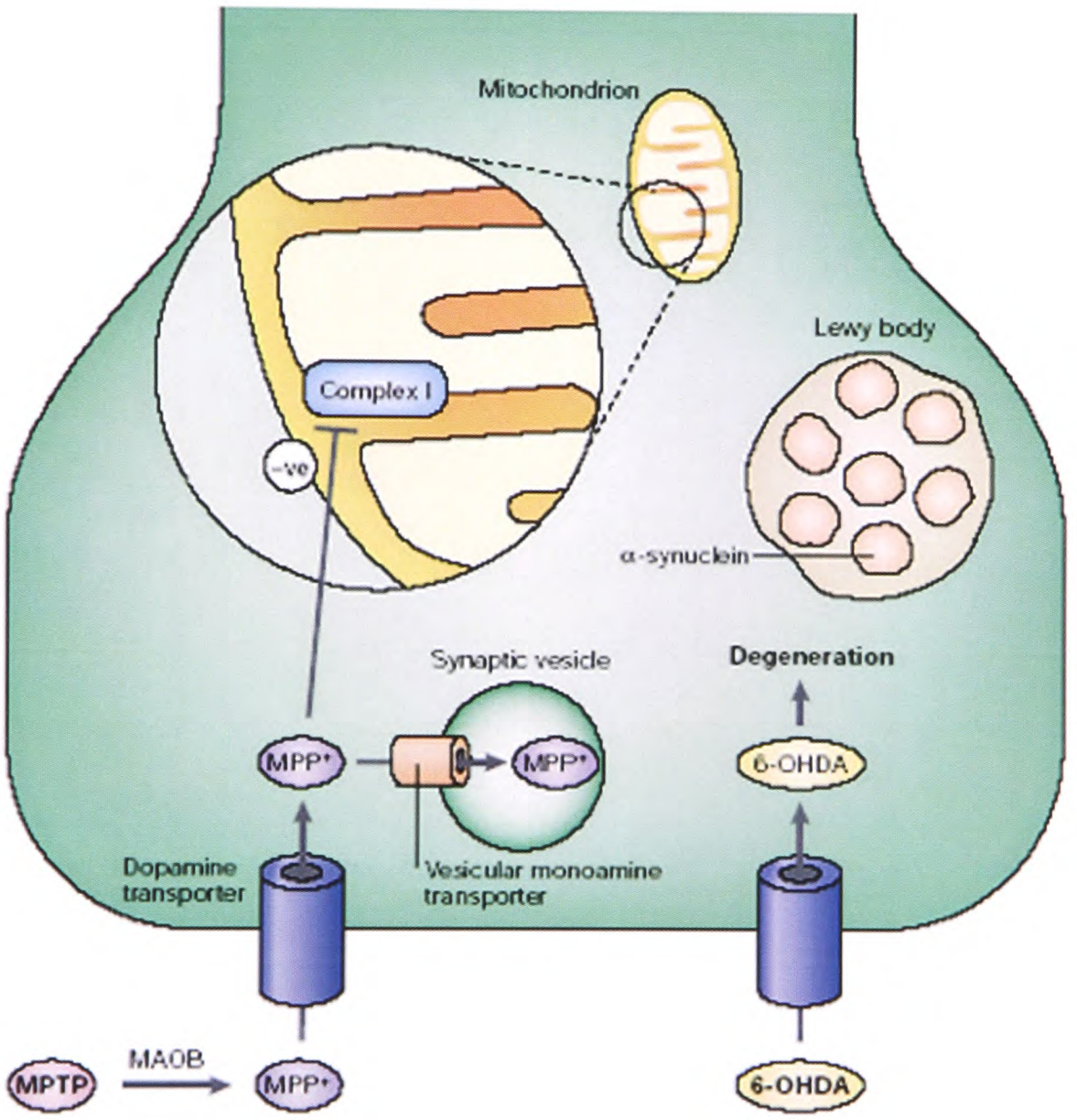
In Chapter 7, the expression of mouse NAT2 in the brain was investigated in the wildtype and Nat2-/- knockout mice. Furthermore, potential mouse NAT2 substrates were screened in order to understand the endogenous role of NAT in the brain. Finally, primary behavioural tests were used to assess the motor functions of the Nat2 wildtype and transgenic mice. Together, the data could be used when both genetic and environmental factors (and their interactions) are considered in the pathology of PD.

Figure 1.2

Schematic illustration showing the pathogenesis of neuronal dysfunction produced by neurotoxins that affect DA neurons.

The mechanisms by which neurotoxins kill DA neurons involve mitochondrial dysfunction and oxidative damage. 1-methyl-4-phenyl-1,2,3,6-tetrahydropyridine (MPTP) is converted by monoamine oxidase B (MAOB) to 1-methyl-4-phenylpyridinium (MPP^+). MPP^+ is taken up by the dopamine transporter and can then be accumulated by mitochondria, leading to complex I inhibition and the generation of free radicals, or by the vesicular monoamine transporter, thus reducing toxicity. Chronic MPTP treatment increases the expression of α-synuclein and might produce Lewy bodies. 6-hydroxydopamine (6-OHDA) is taken up by the dopamine transporter and it then generates free radicals.

[Figure adapted from Beal, 2001]


Mitochondrion
Lewy body
Complex I
-ve
α-synuclein
Synaptic vesicle
Degeneration
MPP+
MPP+
6-OHDA
Dopamine transporter
Vesicular monoamine transporter
MPTP
MAOB
MPP+
6-OHDA

2 General Materials and Methods

This chapter contains general methodological information. Specific information pertinent to only one experimental chapter is included in a brief section on the experimental design used in the relevant chapters.

2.1 Animal models

All experiments were carried out either according to the UK Animals (Scientific Procedures) Act 1986 or with appropriate ethical approval from the Rosalind Franklin University, North Chicago, USA and were designed to respect animal welfare and to minimise suffering. Mice were housed with food pellets and water available *ad libitum*. The room was maintained at constant temperature and humidity on a 12-h light/dark cycle.

Expression profiling by cDNA array technology revealed that subpopulation of C57BL/6J mice, namely the C57BL/6JOlaHsd supplied out of Blackthorn barriers from Harlan has a chromosomal deletion of the α-synuclein locus in the C57BL/6J inbred strain used for backcrossing (Specht and Schoepfer, 2001). Although this strain has been used as the 6-hydroxydopamine model, the α-synuclein status was not the aim of the study and no direct comparison was made with the MPTP/p-treated mice (which were from Charles River, US, expressing α-synuclein).

2.1.1 6-hydroxydopamine-lesioned mouse model

For the investigations using 6-hydroxydopamine (6-OHDA) and anterograde tracers, male C57Bl/6 mice (Harlan) were used, weighing between 22 to 26 g at the beginning of the study. The post-operative care is of note here: the animals were injected with 1 ml of sterile sucrose/saline solution subcutaneously (s.c.) immediately after surgery to inject 6-OHDA. They were then housed singly with a palatable mash, milk and water and were kept warm for 48 hours. Subsequently, they were closely monitored and weighed every day for at least two

weeks. Where the mice failed to thrive, small quantities of condensed milk were offered and further sucrose/saline solution was injected in some circumstances. They were monitored daily such that their body weight did not reduce to below 80% of their pre-operation weight.

2.1.2 MPTP/probenecid-lesioned mouse model

Treatments with MPTP and probenecid (MPTP/p) were carried out at the Department of Cellular and Molecular Pharmacology, Rosalind Franklin University, Chicago, by the group of Professor GE Meredith. Male C57Bl/6 mice (Charles River Laboratories, Wilmington, MA, USA), aged 8-10 weeks and weighing 18-22 g at the beginning of the study, were housed two to four animals per cage with food pellets and water *ad libitum*. All experiments were performed in accordance with the Guide for the Care and Use of Laboratory Animals as promulgated by the National Institutes of Health and approved by the Institutional Animal Care and Use Committees (IACUC) of University of Washington and the Chicago Medical School.

2.1.3 GAD65-GFP mouse model

Transgenic mice expressing green fluorescent protein (GFP) under the control of the GABA decarboxylase-65 (GAD_{65}) promoter were bred in the Department of Pharmacology, Oxford, from animals originally developed by Dr. Szabo at the Department of Functional Neuroanatomy at the Institute of Experimental Medicine in Budapest, Hungary. Animals were genotyped two days after birth using specifically designed spectacles with light source and filters for identifying GFP *in vivo* (GFsp-5 Model, BLS, Biological Laboratory Equipment Service Ltd; Budapest, Hungary). GAD_{65}-GFP mice were identified as having fluorescent green brains and spinal cords when observed using the spectacles. Non-GAD_{65}-

GFP mice were removed from the litter and culled. Animals were weaned at 4-5 weeks and group-housed in single sexes until used for experiments or as breeders.

The generation and analysis of the transgenic mice were described in detail elsewhere (Erdélyi et al., in preparation; (Erdélyi F, 2002; Bali et al., 2005). In brief, a genomic clone of the mouse GAD_{65} gene, isolated from a genomic library, contained the 5.5 kb upstream region and the first six exons of the mouse GAD_{65} gene. The GFP marker, with its translational start site (ATG) removed, was fused into the GAD_{65} gene, to the first or third exon. This construct was injected into fertilized mouse eggs of the CBA/C57Bl6F2 background. One of the transgenic lines, on a C57Bl/6 background showed GFP expression that corresponded well with the pattern of endogenous GAD_{65}. In this case a 6.5 kb segment (which includes the 5.5 kb upstream region) drives the expression of GFP.

2.1.4 Arylamine N-acetyltransferase (Nat) transgenic mice

The generation of a stable Nat2 knockout line of mice by targeted insertion of a *lacZ*-containing cassette has been described (Cornish et al., 2003) (See Figure 7.1). Essentially, a TAG3/IRES/lacZ/loxP/neo/loxP reporter ablation cassette was inserted into the BglII site in the Nat2 coding region, an MCl-thymidine kinase dimer-negative selection cassette was appended, and the construct used to generate a null allele of mouse *Nat2* by homologous recombination in 129/Ola embryonic stem cells. The mutant gene was maintained in the heterozygote state on a rapid acetylator (C57Bl/6) background by backcrossing Nat2+/- males to C57Bl/6 mice obtained from Harlan (Bicester, Oxfordshire, UK). Nat2+/+, Nat2+/- and Nat2 -/- animals used for analysis were generated by inter-crossing. Routine genotyping of adult mice was by PCR using DNA isolated from ear clips as described in Cornish *et al.* (Cornish et al., 2003). Primers used for genotyping were mNat2-1, mNat2-10 (Estrada et al., 2000), and Neo-T (Cornish et al., 2003).

2.2 Stereotaxic surgery

The stereotaxic coordinates for surgery were calculated from The Mouse Brain in stereotaxic coordinates (Paxinos and Franklin, 2004). The point of fusion of four skull plates – Bregma – was taken as the reference coordinate for the anterior/posterior and medial/lateral axes, whilst the brain surface acted as the reference point for the dorsal/ventral axis.

Micropipettes for the introduction of neurotoxin or tracers into the mouse brain were made on a vertical pipette puller (Sutter Instruments). Glass capillary tubes of 0.69 mm internal diameter (Clark Electromedical Instruments) were used. Temperature was set at 850 and pull strength at 90, such that tips at least 1 cm long and approximately 20-30 μm internal diameter were produced. The extremity of the tip usually sealed and required breaking open under a dissection microscope with a pair of fine forceps. Tips diameters were measured using an eye-piece graticule.

Mice were anaesthetized with an i.p. injection of a 1:1:2 solution of hypnorm/hypnovel/sterile water at a dose of 10 ml/kg, and were placed into a stereotactic frame. Suitable level of anaesthesia was reached when the animal showed slowing of heart rate, breathing rate and finally, the absence of eye reflex or response to a toe pinch. Excess fur overlying the skull region was trimmed. The ventral edges of tissue surrounding the ear canal were cut with fine scissors to allow unrestrained access of the stereotaxic frame. The head of the mouse was then secured to the frame via bars inserted into the ear canals and a nose and upper jaw clamp.

Using a scalpel blade, an incision was made along the midline of the skull rostrocaudally, and the skin retracted. The underlying bone was exposed by removing any attached connective tissue, the electrode positioned over Bregma and the zero coordinates recorded.

Using injection site coordinates derived from the atlas (Paxinos and Franklin, 2004), the micropipette was lowered to the surface of the skull, to locate the rostro-caudal and lateral location and the overlying skull was removed by drilling above the area of interest. Any remaining bone fragments were peeled away using fine-tipped forceps and the micropipette lowered to the surface of the dura and the ventral zero coordinate noted for the adjustment of the dorsoventral coordinate. The micropipette was then lowered, breaking the dura and descended to the desired injection site.

2.2.1 Lesion injections

To achieve unilateral lesions of the nigrostriatal system, mice received 6-OHDA injections into the right medial forebrain bundle (MFB). 6-OHDA (Sigma, USA) was dissolved at a concentration of 50 µg/µl in 0.1% ascorbic acid to prevent 6-OHDA from being oxidized (Song et al., 1999). Two different volumes (60nl and 30nl) were tried, resulting in final dosages 3 or 1.5 µg respectively. The toxin was placed using a glass pipette at the following coordinates: AP: -1.4 mm; ML: ±1.1 mm; DV: -4.9 mm with respect to Bregma and brain surface. The injection was conducted at a rate of 60 nl/min and the pipette was left in place for another 5 minutes before being slowly withdrawn. The wound was cleaned and rehydrated with saline, and sutured with Vicryl (Size 5, Ethicon). Mice were kept 1 (Chapter 3) or 3 months (Chapter 4) following drug treatment under normal husbandry conditions. They were anesthetized with 0.2–0.4 ml sodium pentobarbital (Sagatal, Rhône Mérieux, i.p.) followed by transcardial perfusion with 0.9% saline and fixative (4% paraformaldehyde and 0.05% glutaraldehyde in phosphate buffer (PB), pH 7.4, see below "*Tissue Fixation*"); brains were removed and post-fixed in the same fixative for 2 h or were washed in several changes of phosphate buffer saline (PBS).

Animals which received MPTP and probenecid were treated with a protocol published previously (Meredith et al., 2002; Jin et al., 2005). Briefly, mice received 10 doses of MPTP hydrochloride (25 mg/kg in saline, s.c.) and probenecid (250 mg/kg in dimethyl sulfoxide (DMSO), i.p.) administered twice a week for 5 weeks. This procedure was done exclusively in the USA under the US animal licence. Neither DMSO nor probenecid produce an effect *per se* on nigrostriatal dopaminergic neurons (Lau et al., 1990). Also, DMSO did not appear to cause inflammation at the injection site (Pitner J., Rosalind Franklin University, personal communication). Animals treated with probenecid or saline alone formed the primary control groups, each of which matched a MPTP/p groups in age and survival time. An earlier investigation had already demonstrated that vehicle alone at the concentration used in these studies produced no effects on striatal dopamine contents or function over a 6-month period after treatment (Lau et al., 1990). Animals were kept 1 (Chapter 3) or 3 months (Chapter 4) following drug treatment and then anesthetized with pentobarbital (135 mg/kg, i.p.) followed by transcardial perfusion with PBS (0.1 M) and fixative (4% paraformaldehyde and 0.05% glutaraldehyde in PB). Their brains were removed and immersed overnight in the same fixative at 4°C, and then transported in PBS by courier to Oxford.

2.2.2 Anterograde tracer injections

Anterograde tracing was carried out (Chapter 6) with the neuronal tracer Biotinylated Dextran Amine (BDA). The suitability of BDA as a neuroanatomical tracer has been compared to alternatives such as the lectin Phaseolus vulgaris-leucoagglutinin (PHA-L) particularly for electron microscopy (Wouterlood and Jorritsma-Byham, 1993). It was shown that the ultrastructural details of BDA-labelled neurons were generally better preserved than in PHA-L-labelled material and penetration of the reagent into the sections was complete. The detection method for transported BDA is fast and less complicated than that for PHA-L, which requires a 2- or 3-step immunohistochemical procedure (Gerfen and Sawchenko,

1984), and therefore suited to study "point-to-point" connectivity (Ding and Elberger, 1995). It has the advantage over other tracers such as biocytin and neurobiotin, in that the latter two tracers appear to be quickly catabolised and are effective only over short survival times (i.e. 2-3 days) (King et al., 1989; Izzo, 1991; Kita and Armstrong, 1991; Vercelli et al., 2000). As for wheat-germ agglutinin conjugated HRP (WGA-HRP), the disadvantage is that trans-synaptic labelling can result with high concentrations and long survival times (Apkarian and Hodge, 1989). Thus, WGA-HRP, biocytin and neurobiotin might not be very effective and reliable for tracing long-projecting axons such as those in this study. One limitation of BDA is it might be retrogradely transported into local collaterals of axons that intermingle with anterogradely labelled axons. The areas of interest in the thesis were both descending pathways and thus this limitation would not become problematic.

BDA is a charged molecule and can therefore be administered by iontophoresis. This technique was preferred over pressure ejection as it achieves a more discrete site of deposit and minimises the amount of tracer taken up by fibers passing through the region (Bacon, 2002). Injections were made by passing a current of 7 μA, on a cycle of 7 secs on-5 secs off for 10 min (Gerfen and Sawchenko, 1984). This was reported to prevent tracer being deposited in the pipette track and contaminating other neuronal populations. The micropipette was slowly retracted after a further 5 min and the skin sutured using Vicryl (Size 5).

2.2.3 Tissue fixation

There are three main purposes for fixation: First, it is to preserve the tissue in its near-*in vivo* state and prevent further enzyme degradation. Second, it is to retain tissue integrity for subsequent processing, storage and examination. Third, it is to strengthen the tissue to aid sectioning. Insufficiently fixed tissue will have limited anatomical detail at the electron

microscopic level. Excessively fixed material will prevent antibody penetration, limiting the amount of immunolabelling, although this might be reversed by increasing the number of buffer washes and by penetration enhancement methods (Section 2.3.7).

Paraformaldehyde and glutaraldehyde used in light and electron microscopy studies react mainly with proteins by cross-linkage. Preliminary studies showed 4% paraformaldehyde (TAAB) and 0.05% glutaraldehyde (from a 25% stock solution, TAAB) in 0.1 M sodium phosphate buffer (pH 7.4) gave good fixation without much reduction in antigenicity. These concentrations were therefore used in all immunohistochemical experiments (except in Chapter 7 where no glutaraldehyde was used in fixation). Additional fixation methods using picric acid and frozen sections were performed and will be described in Chapters 3 and 7.

The tissue was exposed to the fixative by perfusion-fixation and by a 2-hour post-fixation if necessary. Perfusion-fixation allows the flushing of peroxidase-containing blood cells out of the brain and gives a rapid and even infiltration of the fixative. Mice were deeply anaesthetized with sodium pentobarbital, Sagatal (0.2 ml/25 g mouse, i.p.) and perfused transcardially by pressure with ~20 ml of 0.9% saline followed by ~60 ml of fixative per mouse. Good perfusion is characterised by fasciculation of the forelimbs followed by rapid hardening of the body. The skull bones, the meninges and connective tissues were then removed and the brains were taken into 0.1 M PBS.

2.3 Tissue preparation prior to immunohistochemistry

2.3.1 Sectioning of the brain

Perfusion-fixed mouse brains were washed three times in 0.1 M PBS. Coronal blocks (Chapter 3 to 6) containing the forebrain to the midbrain were cut with a razor blade. They

were attached to the cutting stage of a vibratome (Leica, Milton Keynes, UK) with a thin layer of cyanoacrylate glue (Loctite) applied to one of the coronal surfaces. 50 μm thickness were cut with the blade set at a low speed of advance (up to 1) and a high frequency of vibration (10). In Chapter 7, horizontal sections of 30 μm were cut through the whole brain. Free-floating sections were transferred to a series of glass vials containing 0.1 M PBS using a paintbrush. They were then processed either directly for immunohistochemistry or were stored at -20°C after equilibration in anti-freeze solution for use at a later date.

2.3.2 Penetration enhancement

Tissue fixed as described above will not allow large molecules such as antibodies (150-200 kDa) to penetrate deep into the tissue. Immunostaining can often be weak or restricted to the surfaces of the sections. Penetration was enhanced using chemical or mechanical disruption of the tissue, depending on whether it was to be analysed in the light or electron microscope.

In most experiments for light microscope studies, detergent was used for penetration enhancement. It acts by dissolving the lipid layers of membranes, thereby allowing the entry of immunoreagents, although compromise of the ultrastructure makes tissue unsuitable for electron microscope studies. Triton X-100 (BDH) in a final concentration of 0.1% in PBS was used with the primary antibody.

In the case of GAD immunostaining (Chapter 3 and 4) for light microscopy and all electron microscopic studies, mechanical disruption was used for penetration enhancement. The process of freeze-thaw is thought to cause the formation of ice crystals in the tissue and results in holes being formed in the membranes when thawed. The ice crystals formed are kept small by freezing in cryoprotectant solution, which allow for ultrastructural integrity.

The sections were first equilibrated in cryoprotectant solution (25% sucrose, 10% glycerol in 0.05 M phosphate buffer (pH 7.4)) until they sank. This can be achieved either by shaking at room temperature for at least 2 h, or at 4°C overnight. Isopentane (BDH, Poole, UK) was pre-cooled with liquid nitrogen for 30 min. The sections were transferred from the glass vials to a mesh basket immersed in cyroprotectant. They were flattened with a paintbrush and excess cryoprotectant blotted. The basket was placed into the beaker containing the chilled isopentane for 1 min. The sections turned white upon freezing and were then submerged in a beaker of liquid nitrogen for 30 sec. Finally, the basket was taken out, the sections thawed in the cryoprotectant and were transferred to glass vials with PBS (Figure 2.3.2).

In further processes where washing was required, three 10-minute changes of 0.05 M PBS (pH 7.4) were used. This is to remove excess reagent or antibodies before proceeding to the next incubation. All incubations and washings were performed with shaking.

2.4 Immunohistochemistry

Antibodies used in immunohistochemistry can be categorised as two classes. Polyclonal antibodies are a mixed population of antibodies produced by an animal in reaction to the introduction of purified antigen into their system. Many peptide sequences of the antigen can act as an epitope, leading to antibodies with affinities and avidities for different parts of the antigen. These can provide amplification of signal when detecting large antigens and are relatively easy to produce, but increase the chances of cross-reactivity and artefact staining (Richard A. Goldsby, 2000). In contrast, a monoclonal antibody, which is derived from a single plasma cell, is specific for one epitope on a complex antigen. Its production involves creating hybrids between the spleen cells that produce antibodies and myeloma cell lines (Kohler and Milstein, 1975). These hybrids produce a single antibody species which has immortal-growth properties.

Immunohistochemistry takes advantage of the antibody-antigen recognition to reveal the proteins in the cell. The two basic methods involve either directly binding a chromogen to the primary antibody, or indirectly using a secondary antibody (labelled or unlabelled) which binds to the primary. The latter multi-step method allows for relatively inexpensive antibodies, as only the generic secondary antibodies need labelling, as well as an amplification of the signal. It involves the use of a primary antibody raised against the epitope of interest in a particular species. The primary antibodies, usually of the IgG family, can then act as antigens for a secondary antibody raised in a third species. Hence, the multi-step method also allows any combination of antigens to be revealed using antibodies against the neurochemical markers raised in different species.

The optimal concentrations of primary and secondary antibodies used in these studies have been determined in the preliminary studies (Table 2.1). Most of the antibodies (tyrosine hydroxylase, calbindin, $GAD_{65/67}$ and MAC) are commercially available and well-characterised. Further control experiments testing the specificities were performed in the preliminary study (data not shown). For example, sections incubated with fluorescein-conjugated or biotinylated secondary antibodies only did not yield any immunoreactivity, showing that they do not bind to the mouse tissue directly; sections reacted with a polyclonal rabbit anti-mouse primary antibody showed no immunoreactivity when incubated with a goat anti-mouse secondary antibody, showing that the secondary antibody was species specific.

2.4.1 Immunofluorescence

Immunofluorescence (IHF) was used to demonstrate the co-localisation of two or more proteins. Free-floating sections were taken either directly after sectioning or following storage in antifreeze at -20°C. They were washed in PBS and incubated in primary antibodies over 48 h at 4°C. It was customary to incubate the sections in both primary antibodies

simultaneously, and likewise for the secondary antibodies. The only exception was with the use of NAT and TH primary antibodies where sequential incubations were performed (Chapter 7). Unbound antibodies were then washed away in PBS, followed by incubation of sections in two different fluorescein-conjugated secondary antibodies against NAT or TH for 2 h at room temperature. The sections were washed and mounted onto gelatin-coated slides (Bolam, 1992) with fluorescent mounting medium (VectaShield mounting medium with DAPI, Hard-Set, Vector Laboratories). Slides stored in the dark at 4°C can be examined under the fluorescent microscope for up to a year. Note that no blocking serum was used – in the preliminary studies, sections were pre-incubated with or without 4% normal goat serum in PBS for 30 min at room temperature, followed by incubation of primary antibody with or without 1% normal goat serum respectively. No difference was observed. Furthermore, background immunostaining was negligible even in the absence of blocking steps. Hence this process was not performed to better preserve the physiological state of the tissues.

2.4.2 Immunohistochemistry for light microscopy

After washing, free-floating sections were incubated with 0.3% hydrogen peroxide (Sigma) and 10% methanol in PBS for 10 min. After this "quenching" of endogenous peroxidase activity, the sections were washed and incubated with the primary antibody for 48 h at 4°C. The sections were then incubated with biotinylated secondary antibodies for 2 h at room temperature. During the washings, the ABC solution (Vector Laboratories) was prepared and equilibrated for 30 min. The sections were incubated in the ABC solution for 1 h at room temperature. After washings, the sections were reacted with 3,3'-diaminobenzidine tetrahydrochloride (DAB, SK-4100, Vector Laboratories) using a modified dilution (See 2.4.3.1) for 1 to 10 min until the sections become moderately brown. The sections were washed briefly in PBS and mounted on gelatin-coated slides to dry overnight.

For microscopic analysis, it is necessary to "fill" the spaces within the tissue so that there is an equal refractive index to light throughout the tissue. This involves the use of a mounting medium, preferably ones that are not miscible with water, thereby giving rise to the need for dehydration. The reaction products of DAB and SG (for EM) are stable through the dehydration processes.

The sections on slides were washed briefly in distilled water before dehydrating through an ascending series of aqueous alcohols. The slides were immersed in each ethanol solution for 10 min in this order: 50%, 70%, 80%, 90% and 15 min in 100% (twice) and xylene (twice). Xylene is a link reagent that allows both alcohol and the mounting medium to dissolve, as well as a clearing agent that gives similar refractive index as proteins. As a result, the tissue became translucent when completely infiltrated with xylene. Sections were immediately mounted in XAM mounting medium (BDH) and coverslips applied. Once the xylene and the solvent of XAM were evaporated and XAM hardened, the sections could be examined under the light microscope.

2.4.3 Immunohistochemistry for electron microscopy

In Chapter 6, the anterogradely-labelled projections had to be revealed with a chromogen prior to the immunostaining of the midbrain neurons. Dual immunoperoxidase labelling was used to distinguish between the projections and the neurons for the EM. Avidin-biotin-peroxidase complex (ABC) and the peroxidase anti-peroxidase (PAP) techniques can allow two signals to be localised without any cross-reactivity (Ramos-Vara, 2005) (Figure 2.4.3).

2.4.3.1 Use of the Avidin-Biotin-Peroxidase Complex (ABC) bridge method

Avidin, a 68 kD protein from egg white, binds to the small vitamin molecule biotin with a supernormal affinity and can therefore be used to increase amplification of the signal. A complex of biotinylated horseradish peroxidase (HRP) molecules and avidin is allowed to form 30 min before incubation with the biotinylated antibody (hence prepared during the washings). The manufacturers have determined the optimal ratio of the HRP and avidin to provide the right amount of amplification without losing any sensitivity. This results in a lattice-like complex of many bound HRP molecules but still with free biotin-binding sites available on the avidin molecules to detect the biotinylated antibody. When the chromogen is added, the antigen can be detected at sites where the bound peroxidase molecules catalyse the reduction of the chromogen.

As an example, sections prepared for LM described in Section 2.4.2 involve the use of biotinylated secondary antibody (which has been directed against the already bound primary antibody). A commercially available ABC kit (Vector Laboratories, Peterborough, UK) was used: two drop of solution A (avidin) and two drop of solution B (biotinylated HRP) were mixed in 5 ml of PBS for 30 min before incubation.

The ABC method also has a great advantage in revealing the injected BDA for EM because it uses relatively small molecules and they are able to penetrate deep into tissues. Bearing in mind that tissues used for EM can only be treated with freeze-thaw for penetration enhancement, tissues were taken from this process (Section 2.3.2) to be quenched with hydrogen peroxide and methanol (Section 2.4.2). After washings, the sections were incubated with the ABC solution for 4 h at room temperature. Unbound reagents were washed out. The BDA-labelled projections were then revealed with the introduction of DAB.

For single marker immunohistochemistry, the ABC method and the chromogen DAB were used. The dilution of DAB used was modified (1 drop buffer, 2 drops DAB and 1 drop hydrogen peroxide, ABC Standard Elite Kit, Vector Laboratories) which was half the concentration according to the manufacturer's instructions. This gives a less robust reaction which allows the sections to be incubated for longer and more easily monitored. For dual immunohistochemistry for EM, the PAP method and the chromogen slate grey (SG, Vector Laboratories) were used to label the second marker.

2.4.3.2 Use of the Peroxidase Anti-Peroxidase (PAP) method

The PAP method works by using a secondary antibody in excess so that it will bind to the primary antibody with only one of the two antigen binding fragments. This allows the second binding site to be used in the next stage of the reaction which involves the addition of the PAP complex, consisting of an antibody raised against HRP and then reacted with HRP to form an antibody-antigen complex. This antibody is raised in the same species as the primary antibody so it will be recognized by the secondary antibody.

Sections with the BDA-labelled projections revealed were further processed for dual-labelling. The sections were washed and quenched for 10 min to remove excess ABC solution. After washings, one series of sections was incubated with monoclonal mouse anti-TH (1:1000, Diasorin) antibody, another series with monoclonal mouse anti-calbindin (1:1000, Swant) antibody for 24 h at 4°C. On the following day, the primary antibodies were washed out, followed by incubation of the rabbit anti-mouse IgG secondary antibody (1:50, DAKO) for 24 h at 4°C. After washings, the sections were incubated with the mouse PAP complex (1:100, DAKO) for 2 h at room temperature. The excess reagents were washed out and the sections reacted with SG (3 drops chromogen and 3 drops hydrogen peroxide in 5 ml

PBS, Vector Laboratories) until the sections became moderately grey, usually about 10 minutes.

2.4.4 Electron microscopy

2.4.4.1 Post-fixation, dehydration and resin embedding

After the chromogen reaction, sections were washed in PBS and in 0.1 M PB. They were then transferred to a watch glass and flattened in a solution of 1% osmium tetroxide and 5% β (D)+ glucose (Sigma) in 0.1 M PB for 30 min. The osmium tetroxide acts to post-fix the tissue and is a powerful oxidizing agent, which can make distinguishing the brown DAB and grey/black SG colour difficult under EM. The addition of glucose helps to maintain colour differentiation between the two chromogens (Duque A., 2006). Osmium solution was removed and the reaction stopped with two brief washes in distilled water. This is important as any residual phosphate from the buffer may form electron-dense uranyl phosphate precipitates on the tissue in subsequent steps.

The sections were dehydrated in ascending alcohol concentrations as follows: 50% ethanol (twice) for 10 min; 40 min in the dark with 70% ethanol and 1% uranyl acetate, which increases electron scattering and hence greatly increase the contrast and visibility of the specimen under EM, and a brief 90% ethanol rinse. Sections were transferred back in glass vials with 90% ethanol for 20 min and finally immersed twice in dry 100% ethanol for 10 min. Since the embedding resins are not miscible with water, dehydration is particularly important to ensure the resin infiltrates the tissue completely. Sections were then washed for 20 min in propylene oxide, a link reagent miscible with both ethanol and the epoxy resin.

Durcupan ACM (Fluka) epoxy resin was made up according to the manufacturer's instructions, namely the components A:B:C:D were mixed in the ratio 10:10:0.3:0.2 by weight, and allowed to stand for a few minutes after stirring to allow small bubbles to rise to the surface. This resin mixture was also used to make the stub for ultrathin sectioning (Section 2.4.4.3). The sections were transferred to aluminium foil boats filled with resin overnight. The foil boats were warmed on a hotplate until the resin had become fluid, allowing the sections to be transferred with a pair of forceps onto slides. A coverslip was applied and the sections were gently pressed to remove bubbles from under the glass. Excess resin was blotted and the slides were placed in an oven at 60°C for 48 h.

2.4.4.2 Correlated light and electron microscopy

The location of the dual-immunolabelled profile can be documented under LM and areas of interest specifically selected for EM investigation. Since the immunolabelled neurons and the BDA-labelled projections were in brown and grey/black colour respectively, they could be distinguished under LM and be used under EM to identify potential synaptic connections. Areas of interest were photographed under LM.

2.4.4.3 Ultrathin sectioning

The coverslip was removed from the slides using a double-edged razor blade and the tissue excised using a scalpel blade. The tissue was then glued (cyanoacrylate glue Loctite) to a pre-formed resin stub and dried overnight. The block was fixed in the specimen holder of an Ultracut-E microtome (Leica, UK) and excess glue and resin was trimmed away with a razor blade under a stereo-microscope. The block face was cut to a trapezium, with the top and bottom edges parallel, so to produce serial sections and to orient them after cutting. The distance between the block surface and the region of interest was estimated under LM.

A glass knife was prepared from Leica glass and cut on a knife maker (7701B; LKB). This was inserted in the knife holder at a clearance angle of 4°. The block was repositioned, such that its bottom edge was parallel to the knife edge to produce ribbons of sections and the block surface parallel to the tilt of the knife. The knife was used to cut sections of 1 to 2 μm from the block surface until the region of interest was almost reached, as assessed under LM. The glass knife was then replaced with a diamond knife (45° cutting, Diatome) and the clearance angle changed to 6°. Once the block was re-positioned, the knife boat was filled with filtered de-ionised water to a level which was flat against the knife edge. Silver-coloured sections of 60-70 nm were cut through the area of interest with the automated cutting. They were then collected serially onto pioloform-coated, single slot, copper grids, dried and stored in grid boxes.

Ultrathin sections were stained using Reynolds' lead citrate (Reynolds, 1963) to enhance contrast and examined under EM. The alkaline lead stain enhances the electron-scattering properties of biological tissues by combining with cytoplasmic membranes, ribosomes, glycogen and nuclear material. Small drops of lead stain were placed on the uncovered side of Parafilm in a Petri-dish. The grids were floated on the drops with the tissue side down for 2 min. The grids were then washed in a stream of distilled water, dipped in 90% ethanol and dried using filter paper and warm air from a hair-dryer. The sections were returned to the grid box for EM examination.

2.5 Image capture

All LM micrographs were taken with a microscope (Leica Diaplan) with the QImaging CCD cameras (interchangeable for fluorescent and light microscopies), except for the triple immunofluorescent experiments (See Chapter 6). The micrographs were digitalised with the accompanied QCapture Pro software (Version 5.0.1.26, QImaging Corporation) and their

contrast, levels, sharpness and positions optimised with Adobe Photoshop CS. All EM micrographs were taken using the electron microscope (EM410, Philips) with a Gatan Multiscan digital camera and Digital Micrograph software.

2.6 Statistical analysis

All statistics were performed with PRISM and SPSS version 10.0 statistics package.

Table 2.1 Summary of antibodies used in these studies

Chapter	Epitope	Dilution	Penetration enhancement	Secondary antibody	Dilution	Experiment
3, 4, 5	Tyrosine hydroxylase (Polyclonal rabbit, *BioMol*)	1:1000	Triton X-100	Alexa Fluor 488 (Goat anti-rabbit, *Molecular Probes*)	1:500	IHF
	Calbindin (Monoclonal mouse, *Swant*)	1:1000	Triton X-100	Alexa Fluor 568 (Goat anti-mouse, *Molecular Probes*)	1:500	IHF
	Tyrosine hydroxylase (Monoclonal mouse, *DiaSorin*)	1:1000	Triton X-100	Biotinylated goat anti-mouse (*Vector Laboratories*)	1:500	IHC for LM
	Calbindin (Monoclonal mouse, *Swant*)	1:1000	Triton X-100	Biotinylated goat anti-mouse (*Vector Laboratories*)	1:500	IHC for LM
	GAD-65/67 (Rabbit polyclonal, *Chemicon*)	1:2000	Freeze-thaw	Biotinylated goat anti-rabbit (*Vector Laboratories*)	1:200	IHC for LM
5	MAC-1 (Rat polyclonal, *Boehringer Mannheim*)	1:500	Triton X-100	Biotinylated goat anti-rat (*Vector Laboratories*)	1:300	IHC for LM
6	Tyrosine hydroxylase (Polyclonal rabbit, *BioMol*)	1:1000	Triton X-100	Cy5-conjugated (Goat anti-rabbit, *Jackson Laboratory*)	1:400	IHF
	Calbindin (Monoclonal mouse, *Swant*)	1:1000	Triton X-100	Alexa Fluor 488 (Goat anti-mouse, *Molecular Probes*)	1:500	IHF
	Tyrosine hydroxylase (Monoclonal mouse, DiaSorin)	1:1000	Freeze-thaw	Rabbit anti-mouse IgG (*DAKO*); Mouse PAP (*DAKO*)	1:50 1:100	IHC for EM
	Calbindin (Monoclonal mouse, *Swant*)	1:1000	Freeze-thaw	Rabbit anti-mouse IgG (*DAKO*); Mouse PAP (*DAKO*)	1:50 1:100	IHC for EM
7	Mouse NAT2 (Polyclonal rabbit)	1:300	Triton X-100	Alexa Fluor 488 (Goat anti-rabbit, *Molecular Probes*)	1:500	IHF

Methods Appendix

A. Chemicals

0.2 M Phosphate buffer (PB)

35.598 g of di-sodium hydrogen orthophosphate di-hydrate (Na_2HPO_4, pH 9, BDH) in 1 liter (Solution A) and 31.202 g of sodium di-hydrogen orthophosphate de-hydrate (NaH_2PO_4, BDH) in 1 liter (Solution B). The two solutions were mixed in a ratio of 4:1 to produce PB, and adjusted to pH 7.4 using more di-sodium salt to produce a more alkaline solution or more di-hydrogen salt to make it more acidic.

4% paraformaldehyde (PFA) with 0.05% glutaraldehyde

8% PFA (TAAB) was added into distilled water which had been heated to 56-58°C. A few drops of 0.5 M sodium hydroxide was added to help dissolving the PFA. They were mixed thoroughly on a magnetic stirring hot plate until the solution was clear. It was filtered and mixed with equal amount of 0.2 M phosphate buffer (PB, pH 7.4) and allowed to cool to room temperature. A final concentration of 0.05% glutaraldehyde was added from a 25% stock (TAAB, EM grade).

Phosphate buffered saline (PBS)

50 ml of 0.2 M PB (pH 7.4), 8.76 g sodium chloride and 0.2 g potassium chloride in 1 litre distilled water.

Antifreeze

24.96g of NaH_2PO_4 and 28.48g of Na_2HPO_4 in 160 ml distilled water. 120 ml of ethylene glycol and the same volume of glycerol were then added and dissolved.

Cyroprotectant

25 g of sucrose in 25 ml of 0.2 M PB and 10 ml of glycerol. The solution was made up to 100 ml with distilled water.

Lead citrate staining solution

0.266 g lead nitrate in 9.6 ml distilled water with 0.354 g tri-sodium citrate added. The resulting white solution was shaken thoroughly and 0.4 ml of 4 M sodium hydroxide was added. The solution was stored in a tightly-stoppered vial to ensure that atmospheric carbon dioxide did not react with the highly alkaline solution to precipitate lead carbonate. The solution was sterile-filtered before use.

0.05 M Tris-HCl pH 7.6

6.05 g of 0.05 M Tris was added and dissolved in 1 litre distilled water. The pH was bought down to 7.6 by adding 5M HCl drop-wise.

B. Materials

Pioloform coating of copper grids

Single slot copper grids were cleaned in chloroform, dried on filter paper and stored in glass vial for use. 1% solution of Pioloform (1 g of pioloform powder in 100 ml of chloroform) was used to fill the reservoir of the grid coating apparatus, and a clean microscope slide placed upright in the solution. The tap at the base of the apparatus was then slowly opened to allow the solution to flow out, leaving a thin coating on the slide. The slower the solution travels, the thicker the layer of coating. The coated slide was removed and a single edge razor blade was used to score the bottom edge. The slide was then lowered gently at ~45° into a dish of distilled water, and the pioloform film separated from the slide. Single slot copper grids (shiny side up) were placed individually onto the film. When the film was covered with

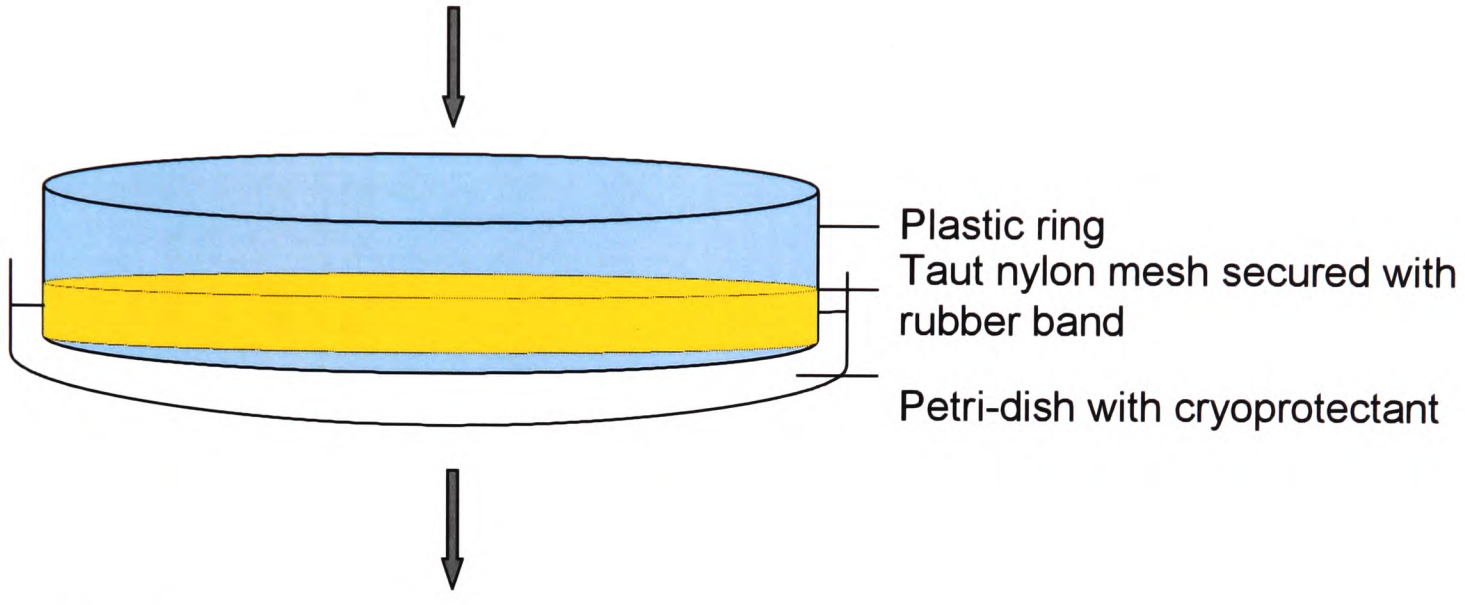
grids, a piece of Parafilm was placed over them and the coated grids were removed from the water. The Parafilm with coated grids was then stored in a clean Petri-dish.

Gelatin-coated slides

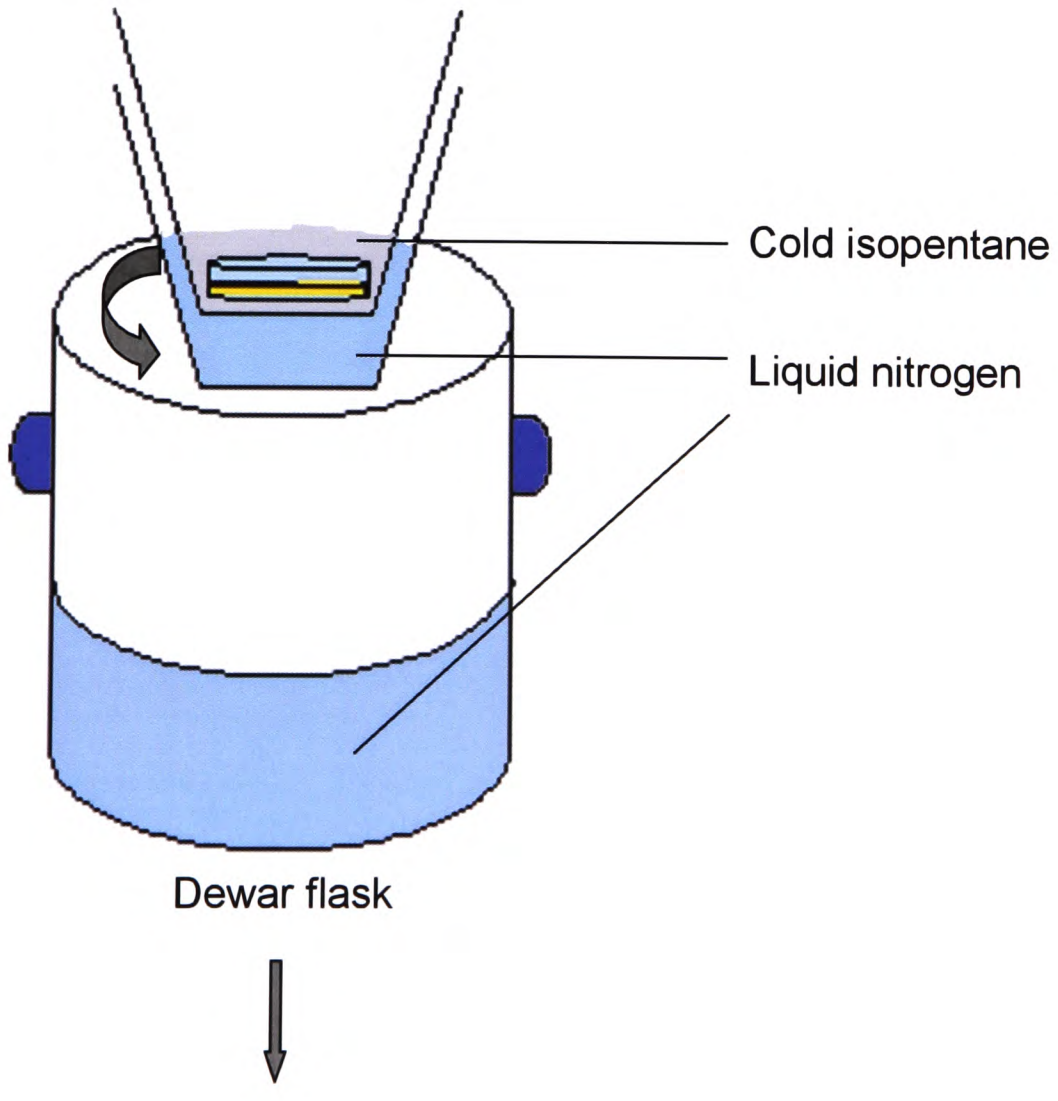
Slide coating medium was prepared by dissolving 0.1 g chrome alum (to prevent bacterial growth), 1.0 g gelatin and 200 ml distilled water. The glass slides were individually put into the cold coating solution and dried upright in a dust-free environment. They were then stored in slide boxes for use.

Figure 2.3.2
Freeze-Thaw

1. Cryoprotected sections transferred from glass vial to nylon mesh and flattened with a paintbrush



2. Mesh basket containing the sections is immersed in liquid nitrogen-cooled isopentane for 1 min. Then transferred to the liquid nitrogen beaker underneath for 30 seconds



3. Sections thawed in petri-dish with cryoprotectant

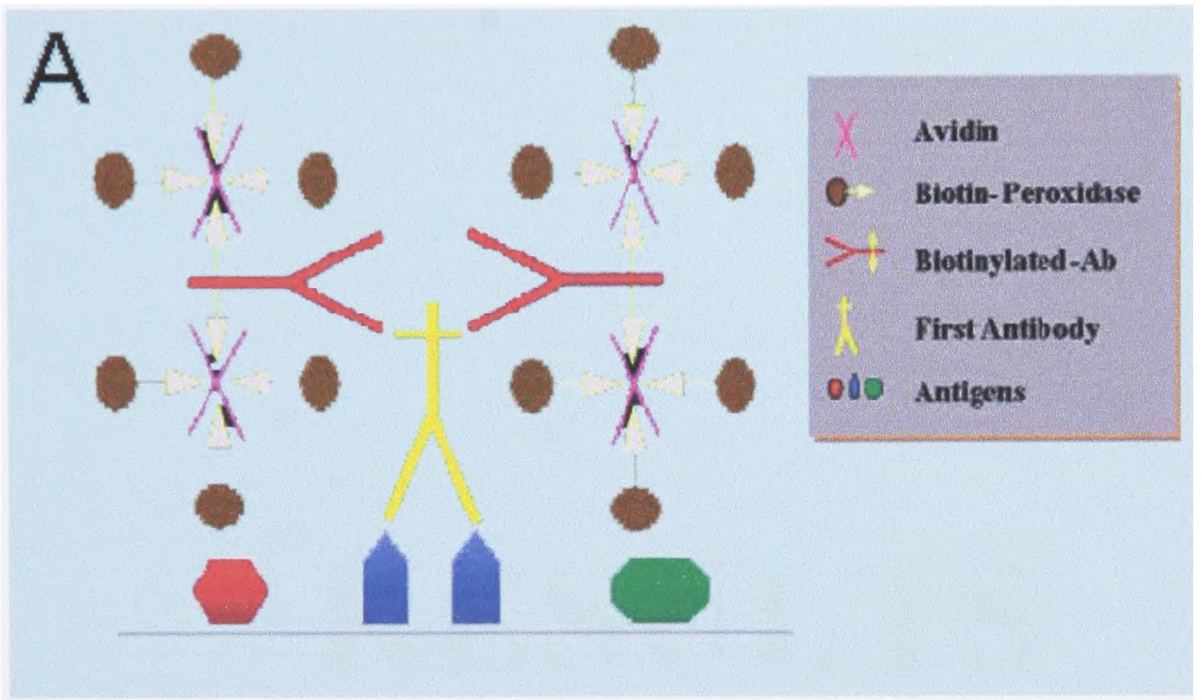
Figure 2.4.3

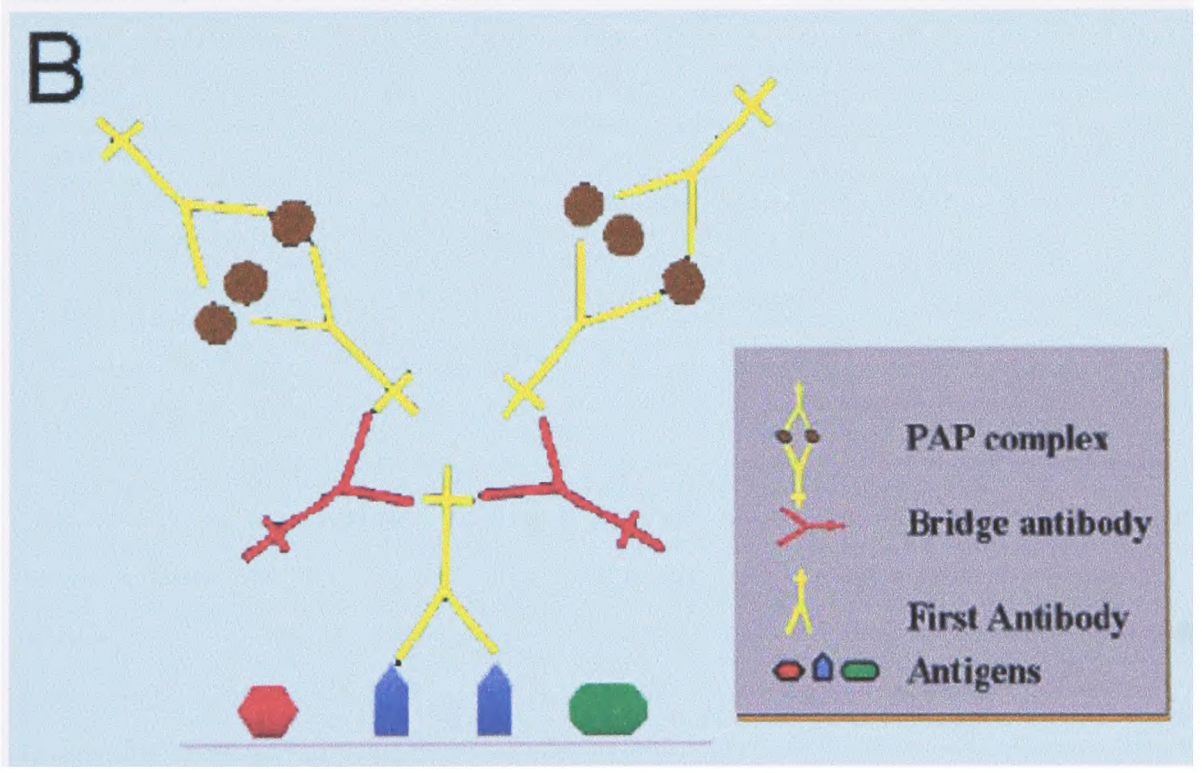
Comparison between the avidin-biotin complex (ABC) method and the peroxidase anti-peroxidase (PAP) method.

(A) In the ABC method, the second antibody is biotinylated and the third reagent is a complex of avidin mixed with biotin linked with peroxidase. The avidin and labelled biotin are allowed to react together prior to application, resulting in the formation of a large complex with numerous molecules of peroxidases. The proportion of avidin to labelled biotin must be such that some binding sites of avidin to labelled biotin are left free to attach to the biotin on the secondary antibody.

(B) The PAP method is another indirect immuno-detection method. The mouse monoclonal primary antibody binds to the antigen (tyrosine hydroxylase or calbindin), followed by subsequent binding of a second (bridge) layer of rabbit anti-mouse Igs. The secondary antibody is in excess so as to bind both the primary antibody through one antibody binding site and the PAP complex through the other binding site. A third layer is an antiperoxidase raised in mouse (the same host species as the primary antibody) coupled with peroxidase. This stable complex (peroxidase-antiperoxidase) is therefore composed of two mouse IgG molecules and three peroxidase molecules, one of which they share.

[Figure adapted from Ramos-Vara, 2005]


A
Avidin
Biotin-Peroxidase
Biotinylated-Ab
First Antibody
Antigens


B
PAP complex
Bridge antibody
First Antibody
Antigens

RESULTS

3 Viability of Midbrain Neurons in the 6-hydroxydopamine and MPTP/probenecid Mouse Models of Parkinson's Disease

3.1 Introduction

Loss of DA neurons in the SNC leads to the major clinical symptoms of PD, but there is widespread neuropathology and the SNC only becomes involved toward the middle stages of the disease (Braak et al., 2003; Dawson and Dawson, 2003). Moreover, it is considered that the loss of DA neurons in SN is higher than in the VTA in PD pathology (Rodriguez et al., 2001) and this pattern of cell loss is desirable in animal models. Neuronal subpopulations within VTA and SN are also divergent with multiple electrophysiological properties and projection patterns (Fallon and Loughlin, 1995; Wolfart et al., 2001; Neuhoff et al., 2002; Korotkova et al., 2004; Korotkova et al., 2005). These differences might be related to developmental gene regulation and expression of neuroprotective markers such as the calcium-binding protein CB (Yamada et al., 1990; Liang et al., 1996b; Neuhoff et al., 2002; Korotkova et al., 2004).

Calbindin is an intracellular protein that is abundantly expressed in various subpopulations of neurons in the mammalian brain (Jande et al., 1981; Celio, 1990; Baimbridge et al., 1992). Its proposed functions include intracellular calcium buffering (Mattson et al., 1991; Baimbridge et al., 1992), enzyme activation (Morgan et al., 1986; Reisner et al., 1992), ion channel modulation (Kohr et al., 1991) and facilitation of intracellular calcium diffusion (Feher, 1983). In PD and in animals treated with the neurotoxin 1-methyl-4-phenyl-1,2,3,6-tetrahydropyridine (MPTP), there is a preferential loss of those midbrain DA neurons that lack CB (Yamada et al., 1990; Lavoie and Parent, 1991; German et al., 1992; Iacopino et al., 1992; Liang et al., 1996a). Cell lines and primary neuronal cultures that overexpress CB have shown to be more resistant to degeneration induced by Ca^{2+} ionophores and dexamethasone (Dowd et al., 1992). These *in vivo* and *in vitro* studies suggest a neuroprotective role for CB (Heizmann and Braun, 1992). However, there is no evidence for a neuroprotective role of endogenous CB in CB null-mutant mice treated with MPTP or in a CB-deficient weaver

strain (Airaksinen et al., 1997). Because MPTP produces alterations in intracellular Ca^{2+} as one component of its toxicity (Liang et al., 1996a), this study aims to explore further Airaksinen's finding by investigating the expression of CB in neurons following treatment with 6-hydroxydopamine or MPTP/probenecid (MPTP/p) as PD models.

The major class of inhibitory neurons in the SN and VTA are GABAergic neurons. By inhibiting DA neurons they play an important role in mesocorticolimbic circuitry: About 58% of mesoprefrontal and 20% of mesoaccumbal neurons are GABAergic (Carr and Sesack, 2000). The control of motor activity requires a complex interaction between the different pathways of the basal ganglia, namely between DA and the striatonigral GABAergic (GABA) direct and indirect systems. In essence, dopamine activates the direct striatonigral GABA pathway via D1 receptors or inhibits the indirect striatopallidal GABA pathway via D2 receptors (Floran et al., 1990; Aceves et al., 1992; Robertson et al., 1992). Two subpopulations of nigrostriatal neurons that use or may use GABA as the neurotransmitter have been identified: one formed by neurons localised in the SNR that contain GABA, GAD67 and possibly GAD65 (the two GAD isoforms), and the calcium binding protein parvalbumin (PV) (Celio, 1990; Gerfen, 1992; Lee and Tepper, 2007), and another formed by a subset of DA neurons lying in the SNC and VTA that, under normal conditions, contains GAD65 mRNA but not GAD67 mRNA and is not immunoreactive for GABA, either GAD isoform or PV (Gonzalez-Hernandez et al., 2001). Therefore, the nigrostriatal pathway is likely to include at least three components: (1) tyrosine hydroxylase-immunoreactive DA cells; (2) DA/GABA cells coexpressing tyrosine hydroxylase and GAD65 mRNA (constituting around 8-9% of the nigrostriatal projection); and (3) GABA cells expressing GAD67 and PV (constituting around 6-7% of the nigrostriatal projection) (Gonzalez-Hernandez et al., 2004).

Because of the heterogeneity of the GABAergic population in the midbrain, there is a complex regulation of nigral GABAergic activity after nigrostriatal DA degeneration which might involve local mechanisms, the nigro-striato-nigral loop, and interhemispheric mechanisms whose anatomical basis remains unstudied (Diaz et al., 2003). In neurotoxin-based lesion models of PD, GAD isoforms are upregulated (Soghomonian et al., 1992; Laprade and Soghomonian, 1999; Gonzalez-Hernandez et al., 2004). In MPTP-treated monkeys, GAD65 and GAD67 mRNA levels increase in striatopallidal neurons and in neurons of the internal (the entopenduncular nucleus in rodents) segment of the pallidum (Pedneault and Soghomonian, 1994; Soghomonian et al., 1994; Soghomonian and Laprade, 1997), consistent with an involvement of GAD65 and GAD67 in the expression of motor disorders in Parkinsonism (Gerfen and Wilson, 1996). Increases in DA cell firing after a lesion (Gonzalez-Hernandez et al., 2004) might be a regulatory mechanism in which the brain attempts to restore the nigro-striatal-nigral balance. This finding could in part explain why after unilateral lesion, the motor asymmetry observed in animals (Diaz Palarea et al., 1987; Castellano et al., 1989; Rodriguez et al., 1992) and humans (Morrish et al., 1995; Poewe and Wenning, 1998) is much lower than that expected when only DA asymmetry is taken into account. The two GAD isoforms, however, might subserve different roles in the modulation of motor activity. For example, GAD67 but not GAD65 mRNA levels are increased in the globus pallidus of MPTP-treated Parkinsonian monkeys (Pedneault and Soghomonian, 1994; Soghomonian et al., 1994; Stephenson et al., 2005). Although alterations of GAD isoforms after neurotoxic lesions have been investigated in the globus pallidus and striatum, little is known about changes in the midbrain. Here, I have investigated the changes in GAD expression in the SN and VTA.

3.2 Aims

- To elucidate the change in expression patterns of TH and CB immunoreactivity in midbrain DA neurons in the 6-OHDA and MPTP/p-treated mice one month after treatment
- To investigate GAD expression in the midbrain using GFP-tagged GAD65 transgenic mice and GAD65/67-immunoreactivity in 6-OHDA-treated mice
- To investigate the extent of cell loss in the midbrain in 6-OHDA and MPTP/p-treated mice using unbiased stereology
- To compare the 6-OHDA and MPTP/p treatments as Parkinson's disease models

3.3 Methods

3.3.1 Animals and lesions

Experiments were carried out on male C57Bl/6 mice as described in Section 2.1. To achieve unilateral lesions of the nigrostriatal system, mice received either 3 or 1.5 μg of 6-OHDA injected into the right medial forebrain bundle (n=4) at AP: -1.4 mm; ML: ±1.1 mm; DV: -4.9 mm (Paxinos and Franklin, 2004). They were killed by perfusion-fixation 1 month post-treatment.

For MPTP/probenecid treatment, mice were treated twice weekly for 5 weeks and then had a further 1 month survival time. The MPTP/p mice (n=4) were injected with 250 mg/kg i.p of probenecid followed by 25 mg/kg s.c. MPTP hydrochloride injection. The probenecid controls (n=4) were given 250 mg/kg i.p. of probenecid. The control animals (n=4) were given 25 mg/kg saline.

[Future work in the understanding of probenecid action on MPTP could involve the measurements of MPTP level in the cerebrospinal fluid (CSF), in order to compare the efficiency of probenecid blockade of MPTP at the brain and at the kidney level.]

3.3.2 Immunohistochemistry and immunofluorescence

Immunohistochemical detection was performed as previously described (Section 2.2.3, 2.3, 2.4) in order to show (1) the extent of the neurotoxic lesions in the striatum (2) expression patterns of immunoreactivity for TH, CB and GAD in the midbrain. Briefly, after inhibition of endogenous peroxidase activity, brain sections from the 6-OHDA- or MPTP/p-treatments were washed in PBS. Striatal and midbrain sections were immunostained for TH (1:1000, mouse monoclonal anti-TH, DiaSorin) and another series of midbrain sections for CB (mouse monoclonal anti-CB, Swant) with 0.3% Triton X-100 overnight at 4°C. The sections were incubated with biotinylated anti-mouse IgG secondary antibody (1:500, Vector Laboratories) for 2 h at room temperature and then with avidin-biotin peroxidase complex (Vector Laboratories) for 1 h at room temperature. Immunoreactions were visualized using diaminobenzidine. The sections were mounted onto gelatin-coated slides, dried, dehydrated in an ethanol gradient, lipid clearance in xylene, and coverslips applied.

The conditions for GAD immunostaining have been optimised. It was found that routine perfusion conditions (4% paraformaldehyde, 0.05% glutaraldehyde) or with the addition of 0.4% picric acid produced only limited GAD immunostaining. Penetration enhancement using freeze-thaw significantly improved the quality of staining (see Section 2.3.2). After one freeze-thaw cycle, sections were washed, then immersed for 10 minutes in 0.3% hydrogen peroxide and 10% methanol to inhibit endogenous peroxidase activity. After further washes, sections were immunostained overnight at 4°C for GAD (rabbit polyclonal anti-GAD65/67, 1:2000, Chemicon). Thereafter, they were incubated for 2 hours at room temperature with

biotinylated goat anti-rabbit antiserum (1:200, Vector Laboratories). Immunolabelling was visualised by incubation for 1 hour in ABC solution and for 10 minutes in DAB/H_2O_2. After several rinses in PBS, sections were mounted on gelatinized slides, dehydrated, cleared in xylene, and cover-slipped with XAM as described previously.

For immunofluorescence, rabbit polyclonal anti-TH antibody (1:1000, BioMol) and mouse monoclonal anti-CB antibody (1:1000, Swant) were used with 0.3% Triton-X. Immunolabelling was visible after incubation for 2 hours in 1:500 goat anti-rabbit Alexa Fluor 488 (for TH) or goat anti-mouse Alexa Fluor 568 (for CB). After several rinses, sections were mounted onto gelatinized slides, air-dried, cover-slipped with Vectashield (Vector).

3.3.3 Nissl staining

Midbrain sections (50 μm) were counterstained with cresyl violet prior to stereological analysis. They were mounted onto coated slides and allowed to dry, as described previously (Bolam, 1992). They were delipidated by passing through graded dilutions of ethanol (70%, 90%, 100%) for 4 minutes each, after which they are rehydrated by passing back through decreasing concentrations of ethanol (90%, 70%, 50%) and finally back into water. The sections were placed in cresyl violet solution for 20 minutes (15 ml of 1 M sodium acetate, 75 ml of 0.2 M formic acid, 150 ml of 0.5% aqueous cresyl violet). Once the sections had an overall purple appearance, they were dehydrated and differentiated with acidified (with acetic acid) 70% ethanol for 3 minutes, followed by increasing concentrations of ethanol (70%, 90%, 100%, 100%) and xylene (twice) for 1 minute each and finally cover-slipped with XAM.

3.3.4 Stereological Analysis

Quantitative analysis of cell numbers in brain sections using stereology after immunolabelling has been hampered by the problem of poor antibody penetration to tissue. If penetration problems go undetected, they will lead to underestimation in the structure counts (Miettinen et al., 2002). Torres *et al.* has reported that a two-layered distribution of staining is seen in standard methods of fixing, processing, and immunohistochemical staining, in which the supper and lower thicknesses of the section are stained but not the central thickness of the section (Torres et al., 2006). Nevertheless, cresyl violet (and other histochemical stains) gives full thickness staining, possibly because the cresyl violet molecules are smaller relative to the immunoglobulins used in immunohistochemistry. Therefore, the number of immunolabelled neurons (TH+, CB+, TH/CB+) was counted manually, whereas the cresyl violet-stained cells were counted by stereology.

The mean thickness of sections used in each animal was estimated from measurements of the thickness of each section (about 5 – 6 midbrain sections per animal). The software (StereoInvestigator, version 5.0, MicroBrightField, Brattleboro, VT, USA) was linked to drive a motorized stage in three axes (x, y, z) on a Leica DIALUX microscope. Under the 100x oil objective, the distance between the upper and lower surfaces of the sections can be measured using the z-axis.

With the aid of a stereotaxic brain atlas (Paxinos and Franklin, 2004), the borders of the neuron-containing layers of the substantia nigra and VTA were defined on a relatively small number of sections (~5) taken systematically along the entire length of the midbrain. On these sections the Cavalieri estimator (Cavalieri, 1966) was used to estimate the reference volume from the areas of the sectional profiles of the layers and the known distance between the sections under 40x magnification.

A sampling grid was positioned above the SN or VTA. This grid was divided into counting frames that were equidistant from each other and their spacing set so that only 100-200 neurons were sampled within each brain (West and Gundersen, 1990). The optimal dimensions of each grid size were established following a restricted pilot study, in which 20 sampling sites were used in the SN and 30 sites in the VTA. A neuron was only counted if it lay within the disector area; i.e. came into focus as the optical plane moved through the disector height (14 μm with 2 μm guard zone) and did not intersect the forbidden lines. The precision of each estimate was expressed as the coefficient of error.

The three-dimensional disector probe, with its unbiased counting rule, was used systematically within the delineated regions to estimate the numerical density of neurons. Such random systematic sampling (i.e. with a fixed and known periodicity from a random starting point) was carried out in all three dimensions at all levels of the sampling scheme (sections, disectors, and points). The product of the reference volume and the numerical density is an unbiased estimate of the total number of neurons (West and Gundersen, 1990). At the same time, an unbiased estimate of the SN or VTA volume can be obtained from the sum of the section areas positioned parallel through the midbrain, separated by a known constant distance.

3.3.5 Electron microscopy

Brain sections taken from mice after 5 weeks MPTP/p post-treatment were further processed for electron microscopy as described in Section 2.4.4.

3.3.6 Image analysis

All light microscopy was visualised and captured with a microscope (Zeiss) with the QImaging CCD cameras (interchangeable for fluorescent and light microscopies) as

described in Section 2.4.5. The micrographs were digitised with the accompanied QCapture Pro softwave and their qualities optimised with Adobe Photoshop CS. Several micrographs were merged using Canon PhotoStitch (version 3.1) in order to generate full pictures of the SN or VTA region.

3.3.7 Quantitative and statistical analysis

The number of TH+, CB+ and TH+/CB+ neurons was counted manually from the immunofluorescence images for the reason elaborated in Section 3.3.4. The one-month post-lesion data were part of a global study with the additional aspect of time (Chapter 4) and therefore must be analysed statistically as a whole to minimise the possibility of obtaining false positives. For the 6-OHDA-treated mice, differences in immunopositive neurons (TH+ or CB+ or TH+/CB+) between ipsi and contralateral SN and VTA were analysed using repeated measures general linear models with cell count and lesion treatment as the within-subjects variable (because the ipsi- and contralateral sides were in the same animal), and time (1- vs. 3-month post-treatment) as the between-subject variable (SPSS, 1999). If there was a significant cell count, treatment or cell count-treatment interaction effect, then the *post-hoc* Fisher's *t*-test (also called least significant difference (LSD) multiple comparison) were performed to determine where the differences lay, with $P<0.05$ considered significant. For GAD immunoreactivity, a two-tailed Student's *t*-test (Mann-Whitney test) was used to compare the ipsi and contralateral sides. For the MPTP/p-treated mice, repeated measures general linear modelling was also undertaken but with only cell count as the within-subject factors, and lesion treatments and time as the between-subjects factors (because the treatments were done on different animals), followed by *post-hoc* Fisher's *t*-test.

3.4 Results

3.4.1 Normal expression of TH and CB in mouse

DA neurons in the SN and VTA were identified using TH as the neuronal marker and this was co-localised with CB. Based on the computer-generated map by Liang *et al.* (Liang et al., 1996a), the midbrain can be divided into four rostrocaudal levels: Level 1 is at the middle portion of the mammillary nucleus, which contains the DA neurons in the substantia nigra pars compacta (SNC), substantia nigra pars reticulata (SNR) and rostral VTA. Level 2 is at the level of the caudal portion of the mammillary nucleus, which contains the same regions as in level 1, and also the interfascicular nucleus just medial to the fasciculus retroflexus. Level 3 is at the rostral interpenduncular nucleus level which contains the substantia nigra pars lateralis (SNL) and nucleus paranigralis. Level 4 is at the caudal interpeduncular nucleus level; and contains the caudal extent of nucleus A10, the central linear nucleus and the retrorubral field.

The pattern of co-localisation of TH with CB in the C57/Bl6 mouse was region-specific. Intense immunostaining for TH, CB, or TH+/CB+ was found mostly in levels 2 (Figure 3.1 A-C) and 3 (Figure 3.1 D-F). The TH+ or CB+ neurons were round to oval and TH+ neurons usually had unstained nuclei whereas both nucleus and cytoplasm of the CB+ neurons were usually immunostained.

By the appearance in the SNC, more DA cell bodies (Figure 3.1 A) were observed compared to the CB+ ones (Figure 3.1 B): not all of the TH+ neurons contain CB, or vice versa (Figure 3.1 A-C, arrows). TH-immunostaining was particularly intense in the ventrolateral portion of the SNC whereas most CB+ neurons were found in the dorsomedial portion and in small patches in the SNL (data not shown). The VTA contained numerous double-immunostained neurons (Figure 3.1 F) though some TH+ neurons did not contain CB (double arrows).

3.4.2 Effects of 6-OHDA in the striatum one month post-treatment

In our preliminary study, the dosage of the 6-OHDA was determined in order to create a unilateral, partial lesion in mouse. This was determined to be 1.5-3 μg per mouse. After the 6-OHDA injections, mice initially showed a notable impairment in gait and a lack of motivation for food, though these behavioural deficits gradually disappeared over the 1-month post-treatment survival period.

Mice striata were immunoreacted for TH so that the extent of the lesion could be assessed. DA denervation in the striatum was not quantified by densitometric or immunoblotting analyses, since no correlation was being made between the loss of striatal fibers and loss of midbrain dopaminergic neurons; fibre loss in the striatum provided a qualitative assessment of the completeness of the lesion.

No differences in DA fiber loss were observed in mice between which received 1.5 or 3 μg OHDA. In the rostral striatum (Fig. 3.2 A), DA cell fibers are apparently intact on the contralateral side (Fig. 3.2 C) but only remnants of the DA fibers were observed on the ipsilateral side (Fig. 3.2 E). This pattern and distribution of DA fibers applied to both caudate putamen and the nucleus accumbens. In the caudal striatum (Fig. 3.2 B), a marked decrease in TH+ fibers was also observed on the ipsilateral side (Fig. 3.2 F) compared to that on the contralateral side (Fig. 3.2 D). The higher intensity of TH immunostaining on the contralateral sides compared to the ipsilateral sides also reflected the larger number of TH+ fibers in the former.

3.4.3 Effects of 6-OHDA in midbrain neural degeneration one month post-treatment

3.4.3.1 Dopaminergic neurons

Sections of midbrain were subjected to single label peroxidase immunohistochemistry to reveal the morphology and fate of TH+ and CB+ neurons. There was a substantial loss of TH+ neurons in the SNC, SNR, SNL on the ipsilateral side (Figure 3.3 A) although, as previously reported, on the contralateral side, cells in the dorsal tier of the SN had long TH-positive processes oriented along the medio-lateral axis of the SNC, whereas those in the ventral tier had dendrites that penetrated the SNR. On the contralateral side TH-positive neurons were distributed throughout both the dorsal and ventral tiers of the SNC (Fig. 3.3 C), but on the ipsilateral side only some dorsal tier TH-positive neurons were present (Fig. 3.3 E). Similarly, in the dorsolateral region of the SN, TH+ neurons on the contralateral side are absent from the ipsilateral side (Fig. 3.3 B). A less pronounced loss was seen in the VTA (Fig. 3.3 D, F), though the decrease was still evident on the ipsilateral side (Fig. 3.3 F).

Profiles of CB+ and TH+ neuronal loss were similar. In the SNC (Figure 3.4 A, arrowheads), CB immunoreactivity is present in the neuronal cell bodies of various sizes and shapes (Figure 3.4 C), as well as in their processes (Figure 3.4 C, inset). However, few CB+ neurons were found on the ipsilateral side (Figure 3.4 E). In the VTA (Figure 3.4 B), there were fewer CB+ neurons on the ipsilateral side (Figure 3.4 F) compared to the contralateral side (Figure 3.4 D).

Immunolabelling with fluorescent tags did not differ significantly from the data with permanent markers (Figure 3.5, 3.6). In the SN, TH+ neurons were found along the whole length of the SNC to SNL on the contralateral side (Figure 3.5 A), but there were very few TH+ neurons on the ipsilateral side (Figure 3.5 B). CB+ neurons were confined to the ventral-medial portion of the SNC on the contralateral side (Figure 3.5 C), but again, almost

none was found on the ipsilateral side (Figure 3.5 D). Most of the CB+ neurons were co-localised with TH+ neurons on the contralateral side (Figure 3.5 E) but not on the ipsilateral side (Figure 3.5 F), presumably due to the lesion.

In the VTA (Figure 3.6), TH+ immunostaining was abundant on the contralateral side (Figure 3.6 A). On the ipsilateral side, TH+ neurons were evidently lost along the SN but with less pronounced loss in the VTA (Figure 3.6 B). CB+ neurons were present in the VTA and SNL, but not in the medial portion of the SNC (Figure 3.6 C). The number of CB+ neurons was reduced on the ipsilateral side (Figure 3.6 D). Most of the CB+ neurons were co-localised with TH on the contralateral side (Figure 3.6 E), as well as those that remained post-lesion on the ipsilateral side (Figure 3.6 F).

Unbiased stereological quantification has been proposed as the most efficient and accurate estimate of neuronal numbers (Sterio, 1984; West, 1993). However, these estimates require a minimum number of 'hits' to achieve statistical power and too few immunostained neurons remained on the ipsilateral side of the SN and VTA for me to apply this method. Thus, the total number of midbrain immunoreactive neurons on each side was counted according to an established method (Petroske et al., 2001).

Statistical analyses using the general linear model procedures of ANOVA showed three characteristics (Figure 3.7): First, the numbers of neurons in the three populations differ significantly from each other in both the contralateral and ipsilateral hemispheres (***$P <$ 0.0001) and the *post-hoc t*-test confirmed this. Second, the 6-OHDA lesion caused significant changes in all three neuronal populations (***$P < 0.0001$). Third, there was a significant cell count x treatment interaction (***$P < 0.0001$) such that midbrain TH+ and CB+ neurons were preferentially affected (loss of 78% and 77%, respectively) but the TH+/CB+

population was less affected by the lesion (loss of 69%). Moreover, double-immunostaining showed that 28% of TH+ cells were TH+/CB+ in the midbrain on the contralateral side, but 40% of TH+ cells were TH+/CB+ in the ipsilateral side.

3.4.3.2 GABAergic neurons

In addition to the neurodegeneration observed in TH+ dopaminergic neurons, the effect of 6-OHDA was also investigated in the other major type of midbrain inhibitory neuron, GABAergic neurons. Originally, transgenic mice expressing the GFP-tagged GAD65 construct were used. GAD65 was found in the lateral habenular nucleus (Figure 3.8 A) in areas that were almost devoid of TH (Figure 3.8 B, C). However, although GAD65 was also present in the prefrontal cortex, as expected (data not shown), none was found in the midbrain (Figure 3.8 D-F) cell bodies.

To further study GABAergic neurons, an antibody that recognises both isoforms (GAD65/67) was used. In the absence of GAD65-immunopositive cells, it is assumed that this is labelling only GAD67 containing neurons. GAD65/67 immunolabelling was found mostly in the SNR, on both the contralateral and ipsilateral sides (Figure 3.9 A, B), localised in the neuronal cytosol. Few immunoreactive neurons were found in the VTA on either side (Figure 3.9 C, D). Statistical analyses showed a small but significant reduction of GAD65/67+ neurons of 21% (*$P = 0.0286$, Figure 3.10) on the injected side. (See Table 3.1 for detailed cell count and statistical data)

3.4.3.3 Total neuronal number and total volume of the midbrain

It is possible that the reduction in neuronal numbers for dopaminergic neurons (with or without CB) and GABAergic neurons was accompanied by a decrease in midbrain size,

thereby maintaining the cell density constant. Unbiased stereology was used to quantify the total number of neurons, regardless of chemical phenotype, in the SN and VTA separately (Figure 3.11). Estimates showed that the ipsilateral side has a significant loss of 14% total number of SN neurons (*$P = 0.029$, Figure 3.12 A) but an insignificant loss in VTA neurons ($P = 0.686$). Moreover, there was no significant reduction in the total SN volume ($P = 0.886$, Figure 3.12 B) nor in the VTA ($P = 0.686$).

3.4.4 Effects of MPTP/probenecid in the striatum one month post-treatment

MPTP/probenecid injection into mice produced bilateral brain lesions. In the rostral striatum of the saline control, a large mass of intact TH+ fibers was observed (Figure 3.13 A). This resembles to the pattern seen in mice with probenecid only injections (Figure 3.13 C). At mid-striatal levels, MPTP/probenecid (MPTP/p) treated mice showed apparent reductions in TH+ fibers (Figure. 3.13 E). In the caudal striatum, saline and probenecid controls both displayed prominent TH+ processes (Figure 3.13 B, D), while a decrease of TH+ fibers was observed in the MPTP/p mouse (Figure 3.13 F).

3.4.5 Effects of MPTP/probenecid in midbrain neural degeneration one month post-treatment

3.4.5.1 Inclusion formation

Lewy bodies have been identified in both idiopathic and familial PD. However, not all animal models of PD reproduce this pathology. Under electron microscopy, dense filamentous inclusions with variable shapes and sizes were found in the cytoplasm of neurons (Figure 3.14 A, high magnification in B). Further immunohistochemistry with antibodies against α-synuclein and TH will be required to identify if the inclusion bodies were α-

synuclein-immunoreactive and if they were localised in the dopaminergic neurons respectively.

3.4.5.2 DA neurons

Accompanying the reduction in TH+ fibres the striata was an apparent loss of TH+ neurons in the SN. In both the saline (Figure 3.15 A) and probenecid (Figure 3.15 C) controls, TH+ was found throughout the SNC, SNR and SNL. In the MPTP/p mice, there was a marked decrease of TH+ neurons, although some remained in the dorsal tier of SNC and SNL (Figure 3.15 E). Both saline and probenecid treated mice had numerous TH+ neurons in the VTA, as well as in the adjacent SNC (Figure 3.15 B, D). An apparent reduction of TH+ neurons was found in the MPTP/p-treated VTA and dorsolateral part of SN (Figure 3.15 F) but most of the TH+ neurons in the mid-level of the SNC did not survive.

CB+ cell bodies were found in the SNC and small islands of SNL in both saline and probenecid control animals (Figure 3.16 A, C). The MPTP/p-treated mice showed some loss of CB+ neurons in the middle of the SNC and in the SNL (Figure 3.16E). In the VTA, CB+ neurons were distributed throughout the region and the adjacent SN (Figure 3.16 B, D). Although CB+ neurons seemed to be spared in the VTA in MPTP/p-treated mice, few were observed in the SN post-treatment (Figure 3.16 F).

Double immunofluorescence showed very similar expression patterns of TH and CB as in the immunohistochemistry: In the SN, TH+ neurons were abundant in the saline and probenecid controls in the SNC (Figure 3.17 A, D) but there were fewer after MPTP/p treatment (Figure 3.17 G). In both controls, CB+ neurons were found along the length of SNC and SNL (Figure 3.17 B, E) but only in the ventral part of SNC in the MPTP/p-treated mice (Figure 3.17 H). Most CB+ neurons in the SNC, but not in the most lateral part of SNL, were TH+

also (Figure 3.17 C, F, I). In the VTA and along the border of the SNC and SNR (Figure 3.18), TH+ neurons were quite numerous in the saline and probenecid controls (Figure 3.18 A, D). After MPTP/p-treatment, TH+ neurons were still quite numerous in the VTA but were substantially reduced in other midbrain regions (Figure 3.18 G). As for CB+ neurons, they were found in the VTA and SNL of both controls (Figure 3.18 B, E) but only in the VTA in the MPTP/p-treated mice (Figure 3.18 H). Again, most CB+ neurons were TH+ (Figure 3.18 C, F, I).

Statistical analyses showed three characteristics: First, all three neuronal populations have significantly different cell numbers (Figure 3.19) and MPTP/p counts differed significantly from the saline and from probenecid in all three populations. *Post-hoc t*-test further identified that, in the saline and probenecid controls, the paired significance lay in all three populations (TH+ vs CB+, TH+ vs TH+/CB+ and CB+ vs TH+/CB+, all $***P < 0.0001$). However, in the MPTP/p-treated mice, the number of TH+ and CB+ cell counts were comparable. Second, the treatment caused significant changes ($***P < 0.0001$). *Post-hoc t*-test further identified: a) In the TH+ population (Figure 3.19 A), there was no significance between the saline and probenecid treatment, but significant differences between the saline vs MPTP ($***P < 0.0001$) and probenecid vs MPTP ($***P < 0.0001$) treatments; b) In the CB+ population (Figure 3.19 B), there were paired significances among the three treatments (saline vs probenecid, saline vs MPTP/p and probenecid vs MPTP/p, $***P < 0.0001$ in each case) and c) In the TH+/CB+ population (Figure 3.19 C), there were also paired significance among the treatments (each pair $***P < 0.0001$).

The reason behind the significant decreases of CB+ and TH+/CB+ neurons between the probenecid- vs. saline control groups is unknown. Previous studies have shown that probenecid administration does not differ from saline treatment in relations to DA cell

number and dopamine function (Lau et al., 1990; Petroske et al., 2001; Dervan et al., 2004). Probenecid was used to inhibit the rapid clearance and excretion of MPTP from the brain and kidney following each injection. It is possible that, as a result of renal blockade by probenecid, that there are higher levels of acid metabolites such as homovanillic acid (HVA, the major metabolite of dopamine found in lumbar CSF derived mainly from brain rather than spinal cord (Curzon et al., 1971; Goodwin et al., 1973; Young et al., 1973)) and 3-methoxy-4-hydroxyphenyl-glycol (MHPG, the major metabolite of noradrenaline in brain) in blood, which may affect CSF levels of these acids (Gordon et al., 1975). Another study also showed an increase in 3,4-dihydroxyphenylacetic acid (DOPAC, a dopamine metabolite) in rat brain after probenecid treatment (Gordon et al., 1976). Perhaps the midbrain neurons could detect and respond to the higher metabolite levels and hence here shows a decrease in the number of CB+ and TH+/CB+ neurons. Further study on the action of probenecid on MPTP-treated mice using a larger number of animals should clarify this result.

Finally, there was a significant cell count x treatment interaction – there was a 59% decrease in TH+ neurons comparing the MPTP/p cell counts to the saline control, but only 37% decrease in CB+ neurons and 37% decrease in TH+/CB+ neurons. Moreover, the proportion of TH+ neurons which were TH+/CB+ was similar in the saline and probenecid controls (35% and 32% respectively) but higher in the MPTP/p-treated mice (54%), a trend similar to that seen in the 6-OHDA-treated mice.

3.5 Discussion

My experiments showed that both 6-OHDA and MPTP/p treatment caused substantial loss of DA innervation in the striatum. The remaining fibres did not show a patch or matrix preference. Immunolabelling of midbrain neurons illustrated that neuronal loss was most severe in the SN but with relative sparing in the VTA. When neurons were quantified as a

whole in the SN and VTA, both TH+ and CB+ neurons were lost but there may be some evidence for the spared neurons to be more likely to be TH+ with CB+. Furthermore, 6-OHDA lesion caused a small but significant reduction in GAD65/67+ neurons in the midbrain. The total neuronal loss in the midbrain was only significant in the SN between the lesioned and un-lesioned sides, without causing a significant change in the total midbrain volume.

Calbindin has been used as a marker for the compartmental organization of dopaminergic neurons in the midbrain in human (McRitchie and Halliday, 1995; Damier et al., 1999a), monkeys (Gaspar et al., 1993; Haber et al., 1995) and rodents (Liang et al., 1996a; Liang et al., 1996b; Nemoto et al., 1999). Immunological results here showed that CB was restricted in the dorsal tier of the rostral SNC, the SNL and the VTA. This is in agreement with the CB expression pattern seen in mouse (Liang et al., 1996a), where the organization of midbrain DA neurons is reportedly similar to that in humans. Thus, in the mouse SN there are three tiers of cells, beginning dorsally with the SNC DA neurons that contain the calcium-binding proteins, then the SNC DA neurons that lack both CB and calretinin, and finally the SNR DA neurons that lack the calcium-binding proteins. This is similar to the τ, β and σ tiers of the human SN as described by Olszewski and Baxter (Olszewski J., 1954). Therefore, deciphering the heterogeneity and the distribution of CB-containing DA neurons in mice is potentially important in the understanding loss of DA neurons in human PD pathology.

In the 6-OHDA and MPTP/p mouse models, TH+ striatal fibers were stained to reveal the severity of the lesion. Marked reductions were found on the ipsilateral side of the 6-OHDA-treated mice and in the MPTP/p-treated striata. There were no apparent differences in the TH+ loss in different parts of the striatum. This is important since the DA neurons that contain CB in the dorsal tier of the SNC and the VTA correspond to the DA neurons that

project to the striatal matrix compartment, whereas DA neurons that do not express CB, in the ventral tier of the SNC and SNR, correspond to the DA projection to the striatal patches; this topology is also found in rat (Gerfen et al., 1987). Such distinct features of cytoarchitecture may have functional significance.

In a study by Kirik *et al.*, 6-OHDA was injected at one, two, three, or four sites into the lateral sector of the right striatum, compared with the complete nigrostriatal bundle lesion. Results showed that the functional effects induced by 6-OHDA lesions depend not only on the total dose of the toxin injected, but also on the site of toxin injected (Kirik et al., 1998). Injection of 6-OHDA into the medial forebrain bundle (MFB) reproduces some features of late-stage PD with extensive denervation and loss of DA neurons (Deumens et al., 2002; Sajadi et al., 2004). The extensive neuropathology and profound loss of sensorimotor function may be analogous to a severely rigid-akinetic terminal stage of the human disease (Kirik et al., 1998), or to the most severe cases of MPTP-induced parkinsonism (Ballard et al., 1985).

Although 6-OHDA administered unilaterally along the nigrostriatal pathway is largely uncrossed (Reader and Dewar, 1999), a bilateral lesion could be induced and that the un-injected side of the brain may still show some abnormalities, given the one month survival period. Nonetheless, the effect of 6-OHDA was compared on the ipsilateral and contralateral (control) sides in the same mouse in this study, therefore the potential neuronal losses bilateral should not affect the comparison. Such reduction in the variability among animals is one of the advantage of the unilateral lesion. Fewer animals can be used in each experimental group compared to the MPTP/p regimen.

In both the 6-OHDA and MPTP/p mouse models, the numbers of TH+, CB+ and TH+/CB+ neurons differ, with the exception of TH+ and CB+ cells in the MPTP/p-treated mice. This is likely to be the effect of the MPTP/p treatment, in which the numbers of spared TH+ and CB+ neurons were approximately the same. Furthermore, the lesion treatments caused substantial cell loss in all three neuronal populations. Surprisingly, in the MPTP/p model, there were significant differences between the saline and probenecid controls, although only in the CB+ and TH+/CB+ populations. No report to date has shown that probenecid might adversely affect neuronal survival and repeated experiments, using larger numbers of mice, would give a higher statistical power to confirm this observation.

There was a neuronal cell count x treatment interaction, i.e. the extent of cell loss in each neuronal population was different in response to the lesion. From the immunolabelling, the reduction was particularly pronounced in the ventral tier of SNC and SNL, but less severe in the dorsal tier of SNC and VTA. Moreover, CB+ neurons were reduced in the SNC and SNL, but less so in the VTA. In the 6-OHDA model, TH+ and CB+ neurons were lost to a similar extent (78% and 77% respectively, comparing ipsilateral and contralateral counts) whilst the reduction was lower (69%) for TH+/CB+ neurons. In the MPTP/p model, the same trend was observed, showing a 59% TH+ cell loss but only 37% in both CB+ and TH+/CB+ populations. Although this seems to imply a more toxic effect on all three cell types from 6-OHDA compared to MPTP/p, the administration protocol (delivery route, dosage and so on) for both were different and cannot be compared directly. If we hypothesise that the presence of CB is neuroprotective for TH+ dopaminergic neurons, one would expect a lower reduction in the number of TH+/CB+ neurons after lesion, which was indeed the case here. However, CB+ neurons were also vulnerable to the neurotoxins, which implies that CB could not be the only determinant in the sparing of neurons; it may only confer resistance to the lesion when it is present in TH+ dopaminergic neurons.

My data show that about one third of TH+ neurons also contain CB. Thus on the contralateral side of the 6-OHDA-treated mice 28% of TH+ neurons were TH+/CB+ while in the MPTP/p model, the proportions were 35% in the saline and 32% in the probenecid controls, respectively. These neuronal numbers are from estimates for the whole nigral/VTA complex but previous reports showed that the proportion of TH+/CB+ neurons varies hugely between regions. For example, by using computer-imaging procedures (German et al., 1988; German et al., 1989) and a semi-quantitative method, it was found that 21.7% of DA neurons were TH+/CB+ in the SNC but 100% in the SNL and 55% in the VTA (Liang et al., 1996a). Nevertheless, colocalisation of CB (and calretinin) has been reported in <35% of the TH+ in mouse VTA (Airaksinen et al., 1997), which is in the same order of magnitude as the present finding. Importantly, there was a higher percentage of TH+/CB+ neurons on the ipsilateral side of the 6-OHDA-treated mice and in the MPTP/p-treated mice. This would imply that there was a greater reduction in TH+ only neurons, or that there was an up-regulation of CB. The latter explanation is unlikely because, despite reports of short term changes in CB content after 6-OHDA lesions (Ng et al., 1996), such increases have not been seen with a post-treatment survival period of one month. Further experiments using more animals should reduce the variability between groups and subsequently, neuronal numbers could be estimated separately in SN and VTA.

From the two neurotoxin-based models, the VTA neurons indeed appeared to suffer less pronounced neuronal loss relative to the SN. MPTP damages the DA pathways in a pattern similar to that seen in PD, including relatively greater cell loss in the SNC than the VTA and a preferential loss of neurons in the ventral and lateral segments of the SNC (Sirinathsinghji et al., 1992; Varastet et al., 1994; Dauer and Przedborski, 2003). It is of note that, the neurodegeneration in PD extends well beyond DA neurons (reviewed by (Hornykiewicz and Kish, 1987)). Neurodegeneration and LB formation are found in noradrenergic (locus

coeruleus), serotonergic (raphe), and cholinergic (nucleus basalis of Meynert, dorsal motor nucleus of vagus) systems, as well as in the cerebral cortex (especially cingulated and entorhinal cortices), olfactory bulb, and autonomic nervous system. Degeneration of hippocampal structures and cholinergic cortical inputs contribute to the high rate of dementia that accompanies PD, particularly in older patients. However, the clinical correlates of lesions to the serotonergic and noradrenergic pathways are not as clearly characterized as are those in the DA systems (reviewed by (Dauer and Przedborski, 2003)).

The contribution of CB as a neuroprotective factor in PD remains a subject of controversy. There are data demonstrating that the presence of CB in midbrain DA neurons identifies a population of cells in the mouse that are less vulnerable to MPTP-induced degeneration, possibly due to its calcium-buffering capability (Yamada et al., 1990; Gaspar et al., 1994; Liang et al., 1996b; Parent et al., 1996) and a recent gene profiling study shows a differential CB expression in the midbrain DA neurons (Chung et al., 2005). On the other hand, there is neither evidence for a neuroprotective role of CB in MPTP-treated and CB-deficient *weaver* mice, nor for a compensatory mechanism by calretinin (Airaksinen et al., 1997). The present study does not provide direct evidence of a neuroprotective role of endogenous CB, though it is still plausible that it plays a role in the differential vulnerability of DA neurons. For example, single-cell RT-multiplex PCR experiments demonstrated that differential midbrain CB expression is associated with differential I_h channel densities (Neuhoff et al., 2002) – by having a lower density of I_h channel and a weak rebound activation, neurons might be less susceptible to glutamatergic input (Beal, 2000) and the potential excitotoxicity. Recently, Korotkova *et al.* reported a higher expression level of Pitx3, the transcription factor that regulates the differentiation and survival of DA neurons (Korotkova et al., 2005). *Pitx3* is only expressed in the ventral tier of the SNC and about half of the VTA DA neurons in mice (Semina et al., 1997; Smidt et al., 1997; van den Munckhof et al., 2003). CB has been linked

with the co-localisation of neuropeptides such as neurotensin and cholecystokinin (German and Liang, 1993), as well as a low dopamine transporter mRNA level (Sanghera et al., 1994). Thus, CB might be a marker for the less vulnerable neurons in midbrain, rather than the explanation for their resistance. In addition, the development of CB+ neurons could play a role in its subsequent effect on DA neurons. Cell counting in the adult mice or in transgenic knockouts (such as the *weaver* mice used by Airaksinen *et al.*) might not represent the full effect of CB in a progressive neurological disease. Further studies at different developmental stages may be useful to understand the role of CB in a disease state. Alternatively, immunohistochemistry using Pitx3 and Sonic hedgehog (Shh) as markers may provide clues to subpopulations of neurons less vulnerable to neurodegeneration.

Accompanying the loss of TH+/CB+ neurons, stereological data show a significant reduction in total neuronal number in the SN. There was no significant difference in the SN or the VTA volumes on either side of the 6-OHDA-lesioned mice, which could be due to an increase in microglia. This is in agreement with previous studies in the MPTP/p model which showed no shrinkage in the SN/VTA volumes (Petroske et al., 2001). From the examination of GAD expression in the 6-OHDA-treated mice, it can be concluded that both the loss in DA neurons (with or without CB) and GABAergic neurons contributed to the total cell loss in the SN. The reduction of GABAergic cells was not found in the SNR in paraquat-treated mice (McCormack et al., 2002), indicating variation between animal models.

Moreover, my results show that the main form of GABA expressed in midbrain somata appears to be GAD67. Using the same C57Bl/6 mouse strain as the PD models, transgenic mice expressing GFP-tagged GAD65 did not show any fluorescent signal in the midbrain. Because GAD65 mRNA was found in the nigral GABAergic cell population (Gonzalez-Hernandez et al., 2001), the lack of GAD65 signal in this experiment was likely to be due to

the rapid transport to axon terminals in an inactive form that is post-transcriptionally regulated by binding pyridoxal phosphate (Miller et al., 1978; Denner and Wu, 1985; Erlander et al., 1991; Erlander and Tobin, 1991; Kaufman et al., 1991; Martin et al., 1991). The results demonstrated that there are subpopulations of GABAergic neurons involved in PD, and that GAD65 and GAD67 could be differentially altered following lesion, as reported by Diaz *et al.* using electrophysiological and histochemical studies. Further experiments using different monoclonal antibodies or *in situ* hybridisation against GAD65 or GAD67 on the neurotoxin-treated brain sections would be able to distinguish their different roles. Alternatively, the role of GAD65 might be illustrated by making neurotoxic lesions in the transgenic GFP-GAD65 mice, since both GAD65 and GAD 67 mRNA are reportedly upregulated following 6-OHDA lesions (Lindefors et al., 1989; Soghomonian et al., 1992; Diaz et al., 2003; Gonzalez-Hernandez et al., 2004), which could change the dynamics of the basal ganglia.

As seen under electron microscopy, inclusion bodies were formed one month after MPTP/p treatment. These landmarks in PD pathology are rarely observed in other acute neurotoxic models (Meredith et al., 2004) and there is no report showing inclusion bodies in the 6-OHDA mouse model. Although this is a major difference between the 6-OHDA and MPTP/p models, the observations on midbrain cell loss were similar. The two toxins has highlighted the similarities and differences between the models and this has produced greater insight into the process of neurodegeneration.

Figure 3.1

Double Immunofluorescent labelling of TH and CB in C57Bl/6 mice.

(A-C) In the SN, TH+ neurons (green) were mostly located in the SNC. CB+ neurons (red) were also observed, with many of them co-localised with TH+ neurons (yellow), though some of them were TH-/CB+ (arrows).

(D-F) In the VTA, there were numerous cells that were TH+/CB+. Some neurons were TH+/CB- (arrowheads).

Scale bar = 100 μm

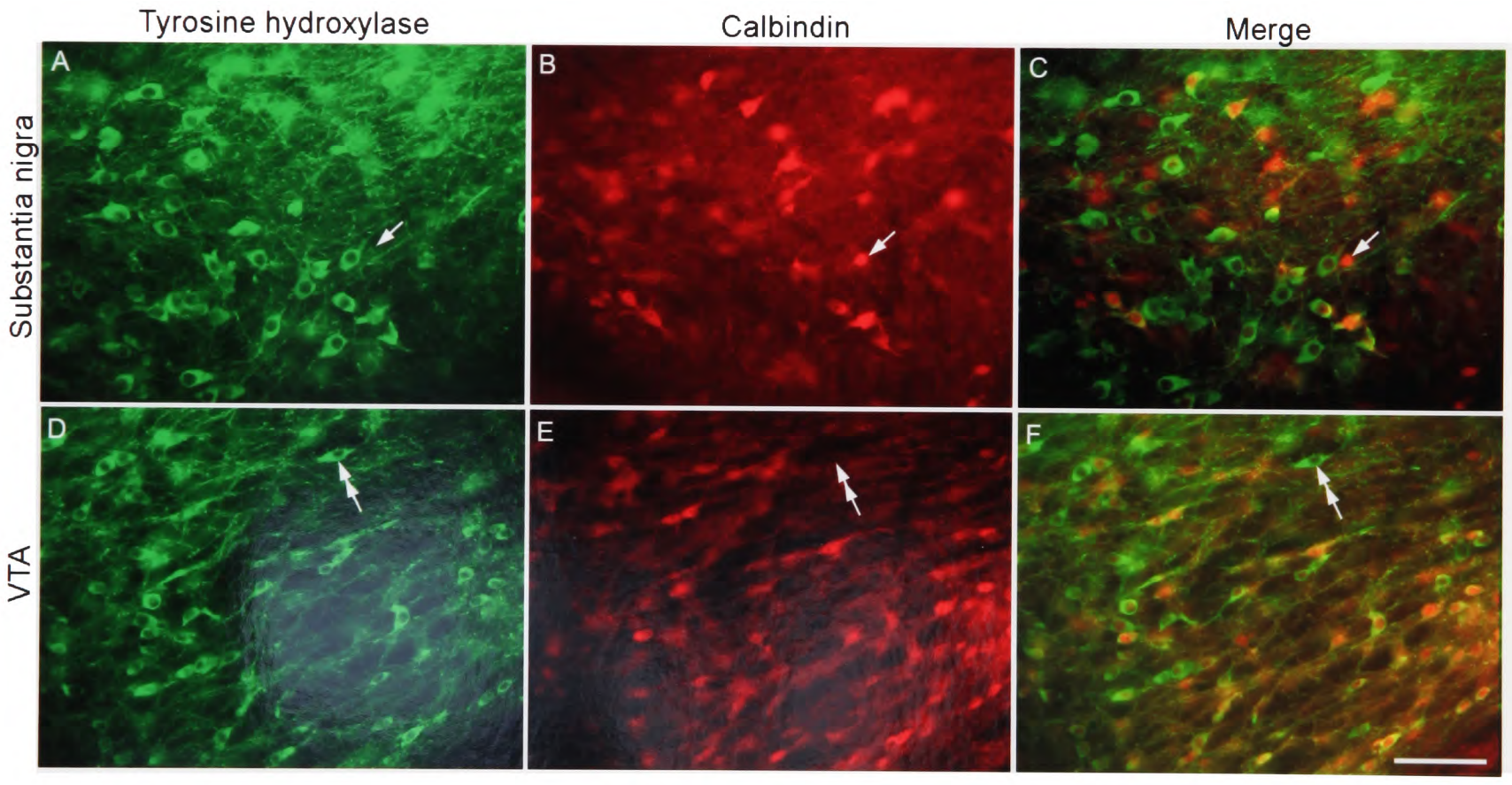

Tyrosine hydroxylase
Calbindin
Merge
Substantia nigra
VTA
A
B
C
D
E
F

Figure 3.2

Representative microphotographs demonstrating TH+ fibers in the rostral striatum (A) and caudal striatum (B) one month after 6-OHDA treatment.

(A, B) One month after 6-OHDA treatment, striata in the hemisphere ipsilateral to the injection (on the right) showed an apparent loss of TH+ fibers compared to the contralateral sides.

At higher magnification, in both rostral (C, E) and caudal (D, F) striatum, there was a substantial loss of TH+ fibers (compare C & E and D & F).

Scale bars: A, B = 1mm; C-F = 50 μm

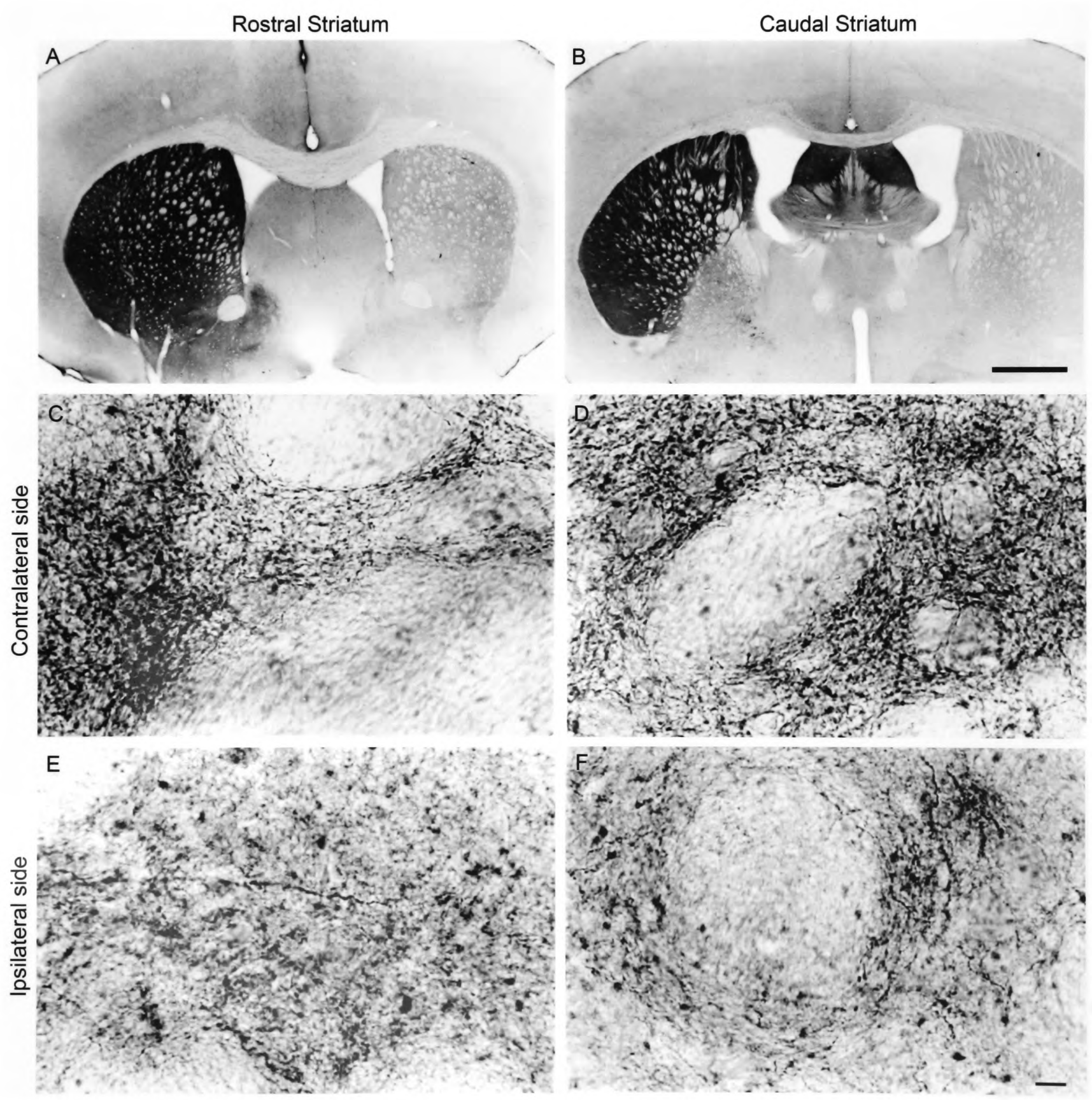

Rostral Striatum
Caudal Striatum
A
B
C
D
E
F
Contralateral side
Ipsilateral side

Figure 3.3

TH-immunolabelling in midbrain one month after unilateral (right side) injection of 6-OHDA.

Immunoreactive neurons were lost from SN (A) and VTA (B).

TH+ neurons in the intact SN (C) have cell bodies in the SNC and dendrites extending into the SNR. There was a substantial loss of TH+ neurons in the ipsilateral side (compare C & D with E & F) particularly in the medial SN, adjacent to the VTA (F).

Scale bars: A, B = 1 mm; C- F = 100 μm

Ipsilateral side

Contralateral side

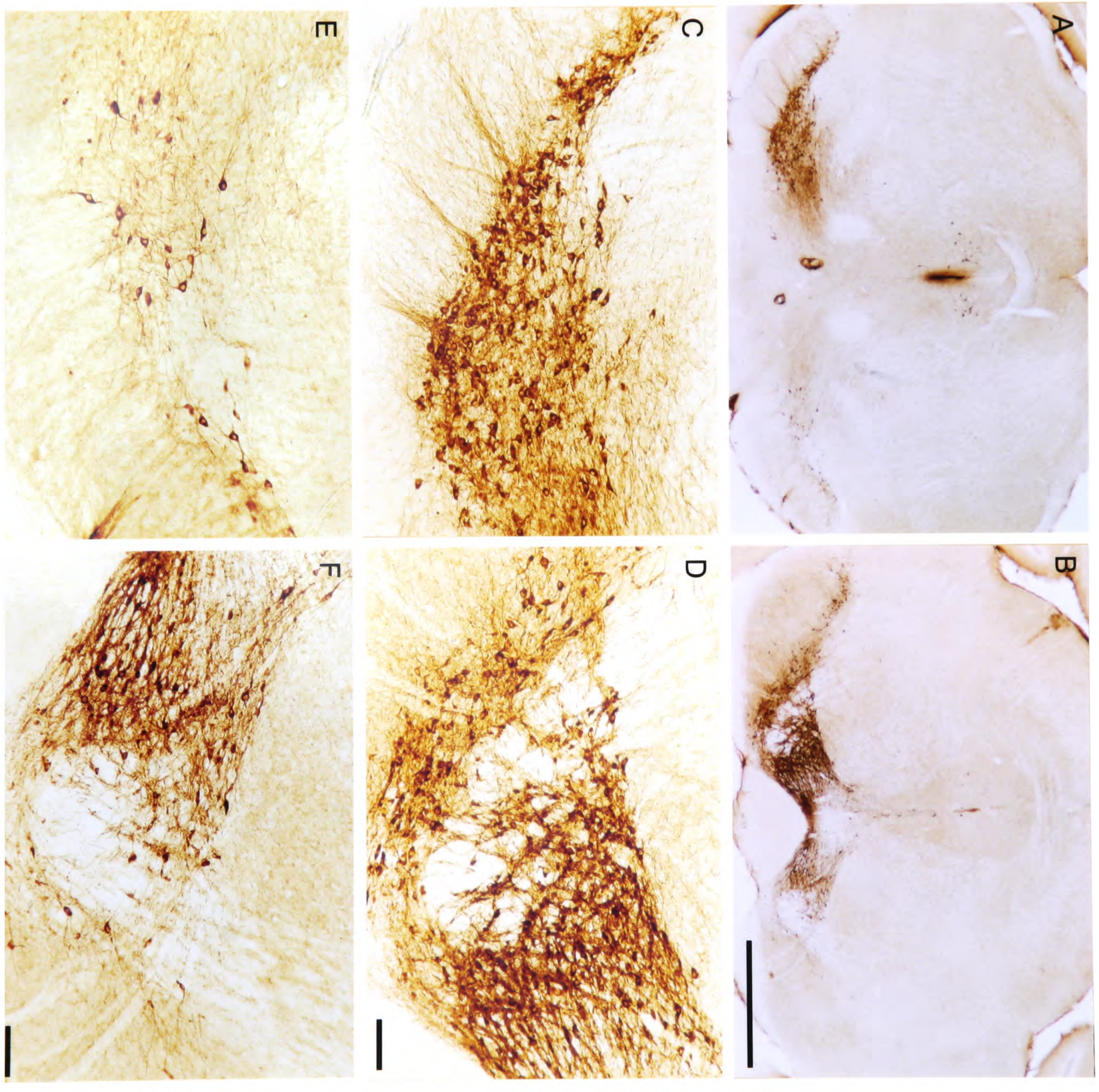


Figure 3.4

CB+ neurons in the midbrain one month after 6-OHDA treatment.

CB+ neurons were present in both the SN (A) and VTA (B). At higher magnification, in the SN of the uninjected side (C), neurons were located in the SNC adjacent to the fasiculus retroflexus (arrowheads) but absent from the SNR. CB-immunoreactivity was found in the neuronal cell body as well as in the processes (C, inset). In the VTA (D), CB+ neurons were fairly evenly distributed. Toxin treatment resulted in an apparent loss of CB+ neurons from the SN (compare C & E) and from the VTA (compare D & F).

Scale bars: A, B = 1 mm; C- F = 100 μm; C inset = 10 μm

Ipsilateral side

Contralateral side

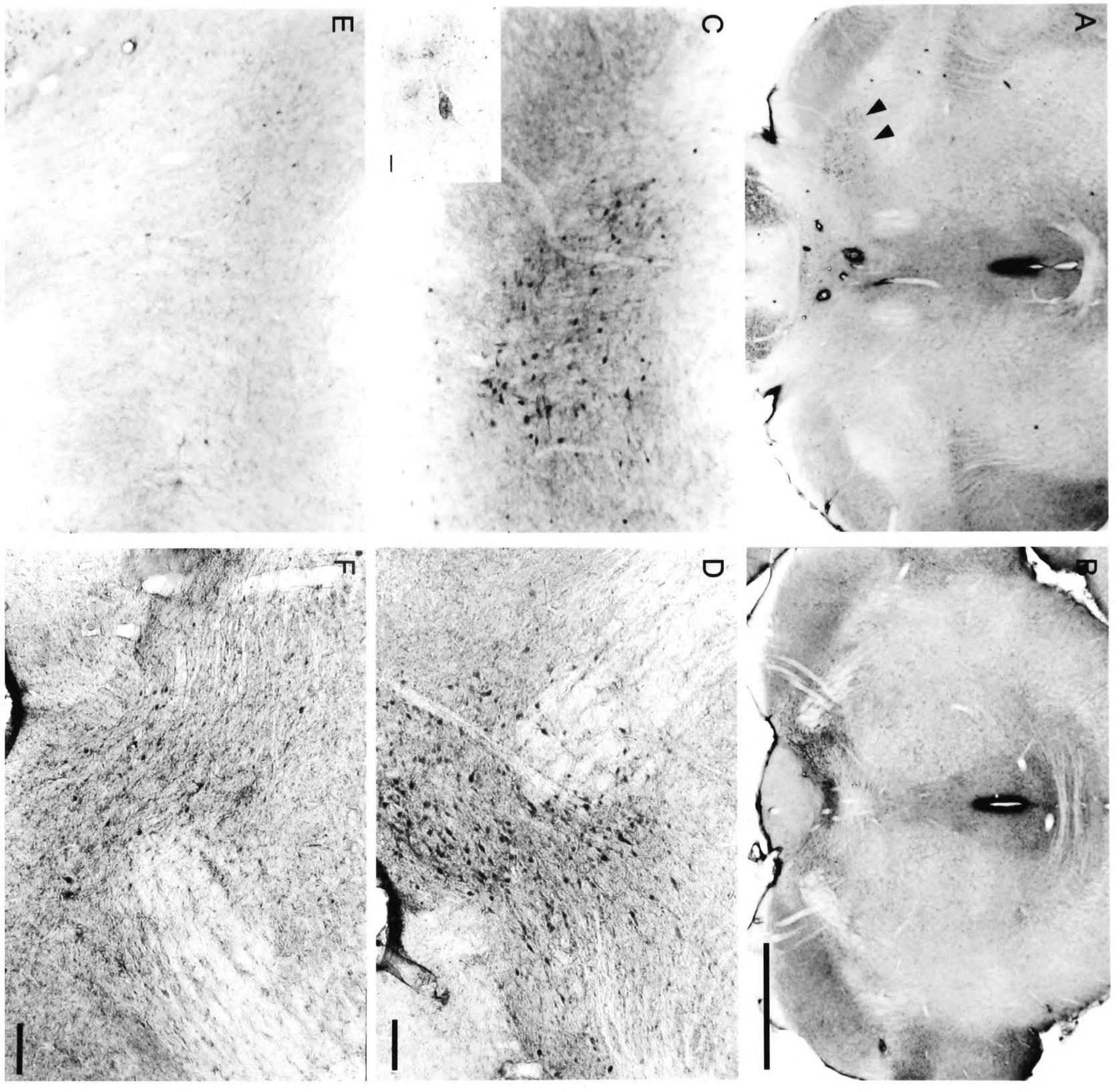


Figure 3.5

Double immunofluorescent labelling of TH and CB in the SN one month after 6-OHDA treatment.

Coronal sections through the midbrain at the level of the SN comparing TH and CB immunoreactivity on the side contralateral (A) and ipsilateral (B) to the injection of toxin. CB was mostly present in the SNC near the midline on the contralateral side (C). Very few CB+ neurons were found on the ipsilateral side (D). Some of the neurons co-localised with both TH and CB on the contralateral side (E, arrows) but not on the ipsilateral side (F).

Scale bars = 100 μm

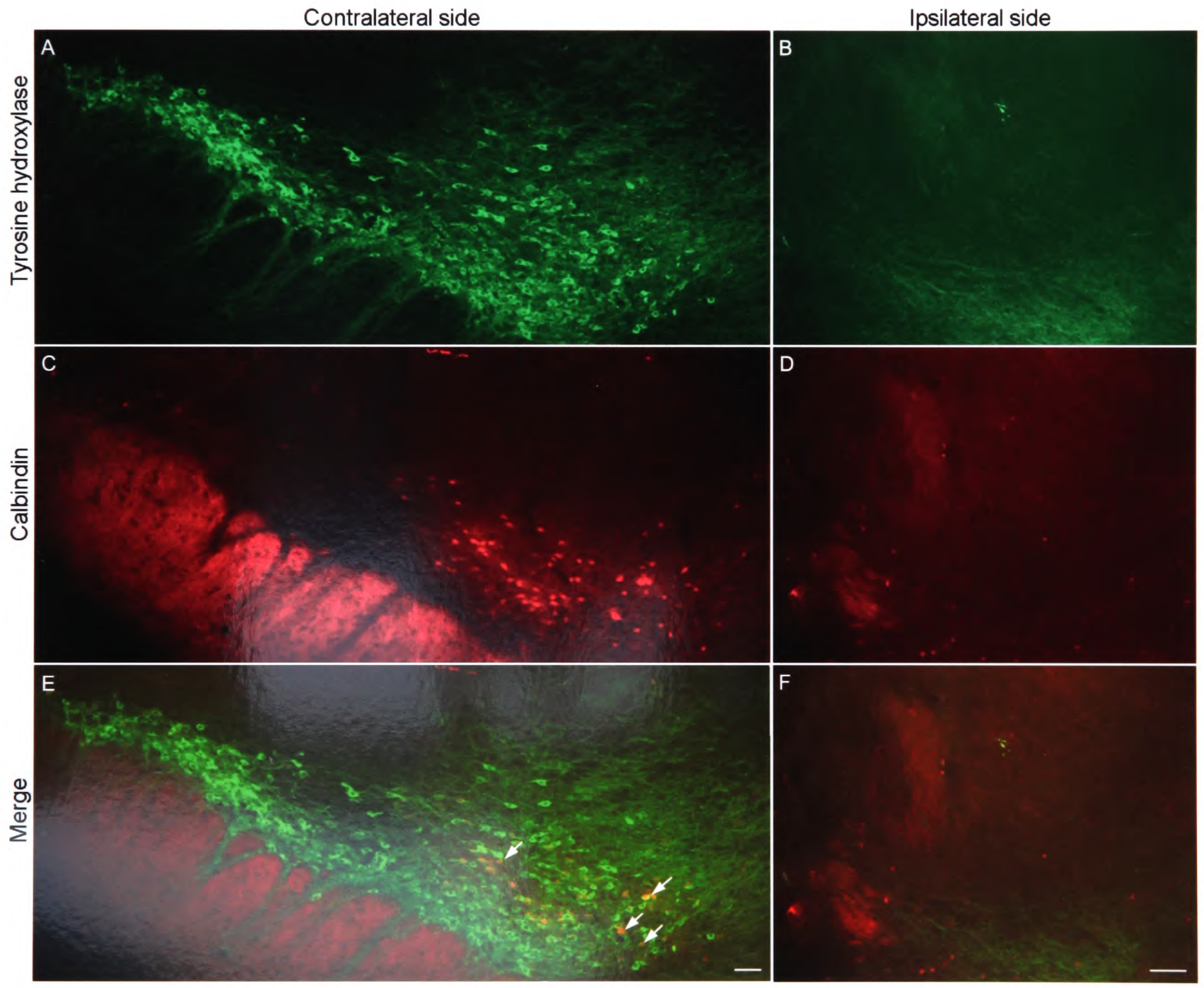

Contralateral side
Ipsilateral side
Tyrosine hydroxylase
Calbindin
Merge
A
B
C
D
E
F

Figure 3.6

Double immunofluorescent labelling of TH and CB in the VTA one month after 6-OHDA treatment.

Coronal sections through the midbrain comparing TH and CB immunoreactivity on the side contralateral (A, C, E) and ipsilateral (B, D, F) to the injection of toxin. TH neurons were widely distributed in the VTA (A) and were substantially reduced on the toxin-treated side (B). CB+ neurons were also reduced by the toxin treatment (compare C & D). Nevertheless, some neurons were both TH+ and CB+ (arrows), both in the contralateral (E) and ipsilateral hemispheres (F).

Scale bars = 100 μm

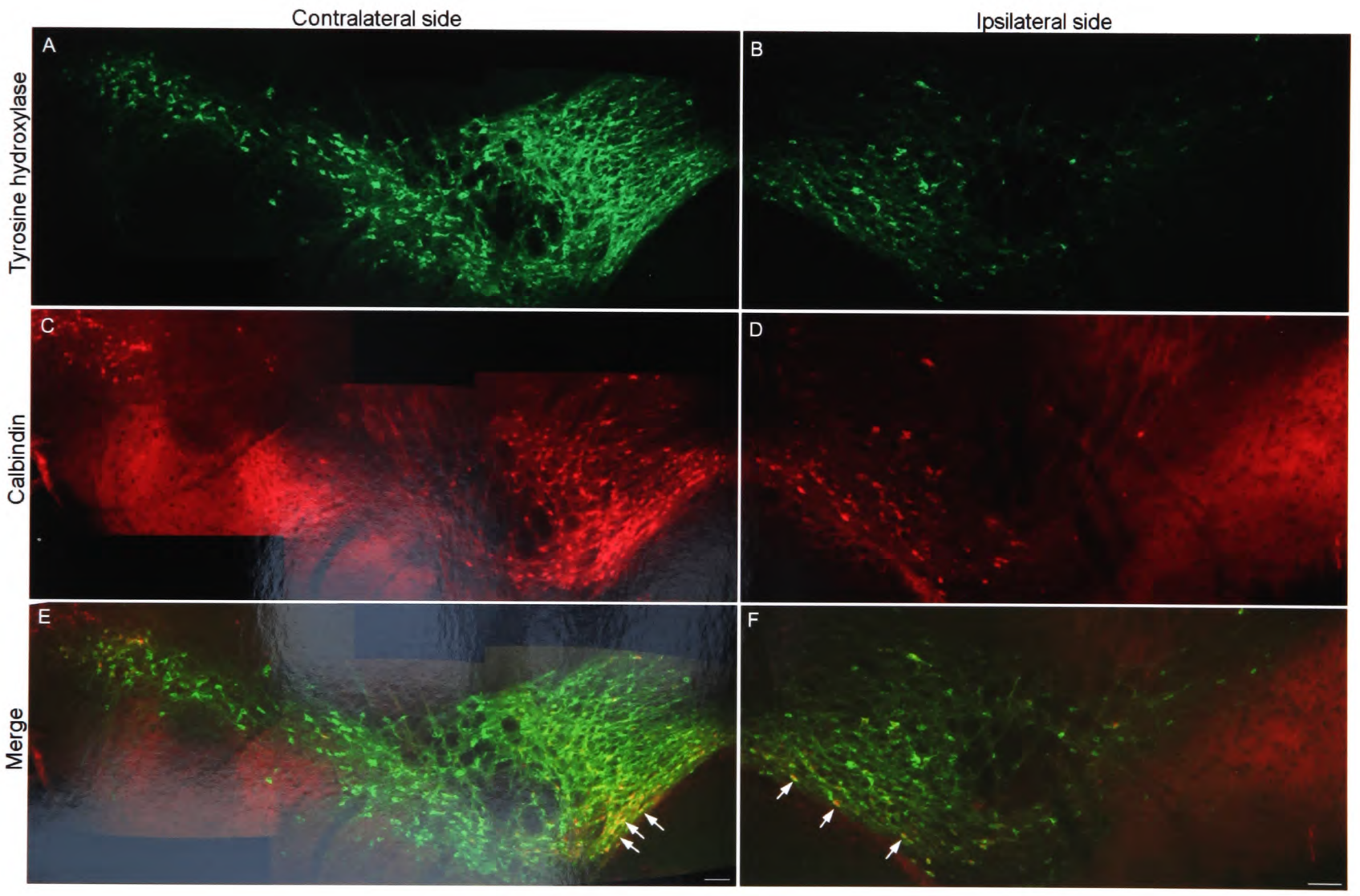

Contralateral side
Ipsilateral side
Tyrosine hydroxylase
Calbindin
Merge
A
B
C
D
E
F

Figure 3.7

Mean number of tyrosine hydroxylase (TH+) and/or calbindin (CB+) neurons in the substantia nigra and VTA in 6-OHDA model. (Not assessed stereologically)

Immunopositive neurons in each 1 in 3 sections were counted and then multiplied to obtain the total neuronal number representing the injected or uninjected hemisphere. Statistical analyses were performed showing that there was a significant difference in all three types of neurons ($F_{(2,12)} = 131.556$; $P < 0.0001$). The lesion caused significant cell loss in all three neuronal populations ($F_{(1,6)} = 688.588$; $P < 0.0001$). Moreover, one or more neuronal population responded significantly differently to lesion ($F_{(2,12)} = 288.319$; $P < 0.0001$). The error bars mark SEM.

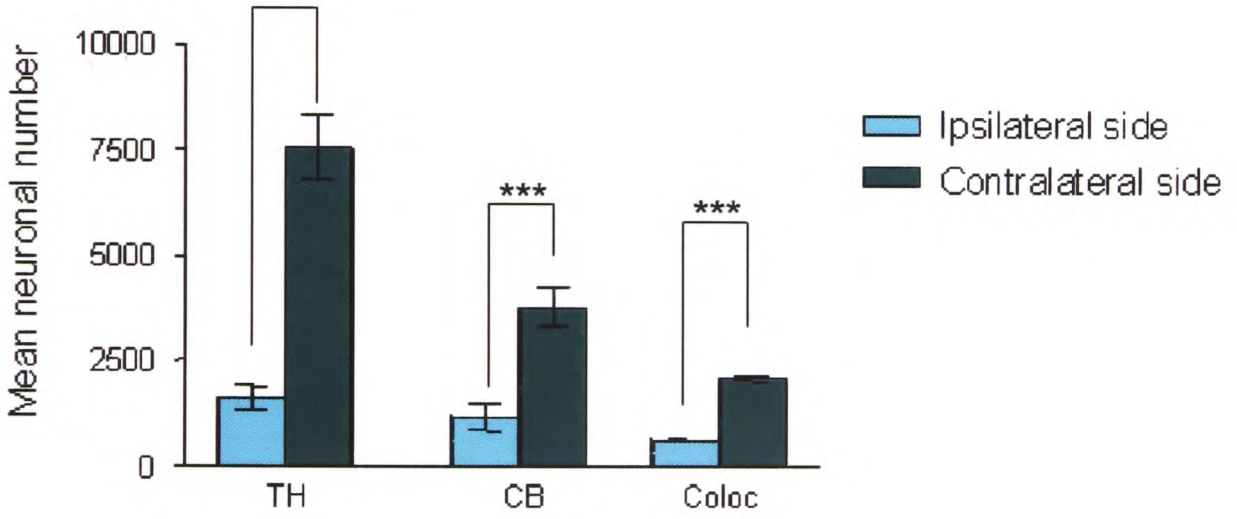


Figure 3.8

Expression of GFP-GAD65 and TH-immunoreactivity in C57Bl/6.

GFP-tagged GAD65-containing neurons were found in the lateral habenular nucleus (A, green), whereas TH+ neurons were mostly localised in the fasciculus retroflexus (B, red). There was little or no colocalisation of GAD65 and TH (C).

In the midbrain, there was no GFP-GAD65 (D) although there was a normal pattern of TH+ (E). There were, therefore, no double-labelled neurons (F).

Scale bar = 1 mm

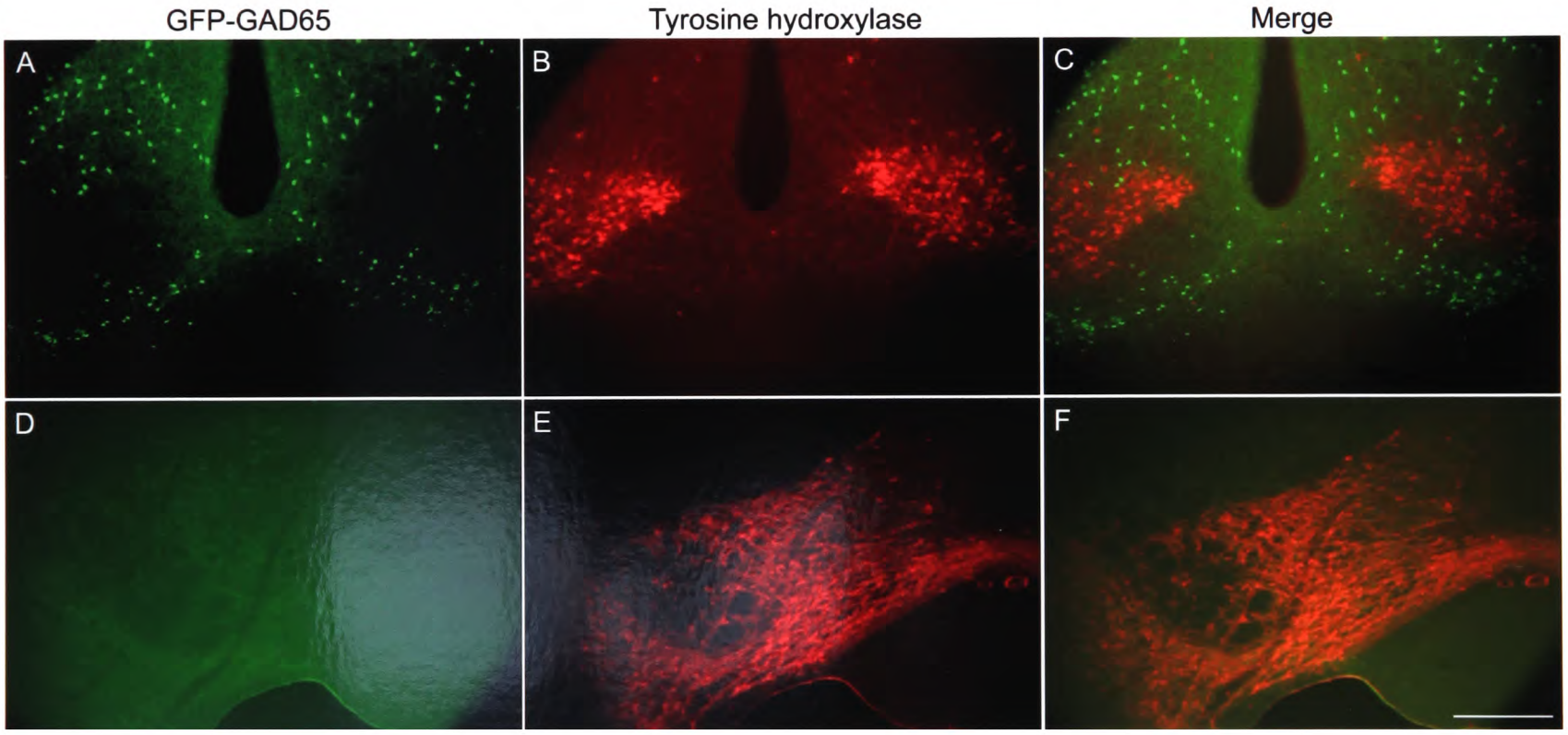

GFP-GAD65
Tyrosine hydroxylase
Merge
A
B
C
D
E
F

Figure 3.9

GAD65/67 immunoreacitivy in the SN and VTA one month after 6-OHDA treatment.

In the SN, GAD was expressed primarily in the SNR on both the side contralateral (A) and ipsilateral (B) to the toxin injection.

In the VTA, there were very few GAD+ neurons on either the contralateral (C) or ipsilateral sides (D).

Scale bar = 100 μm

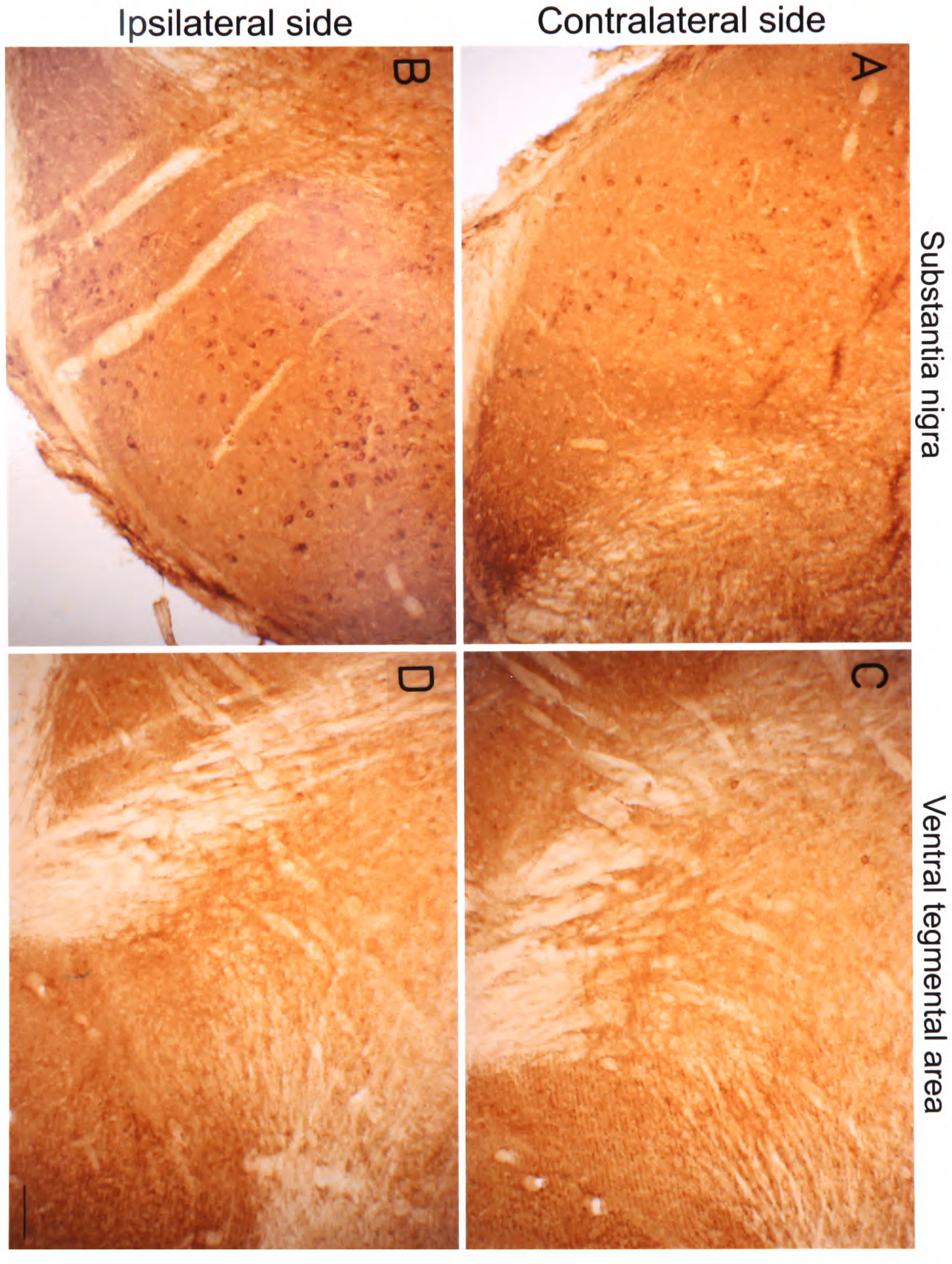

Ipsilateral side
Contralateral side
B
A
Substantia nigra
C
D
Ventral tegmental area

Figure 3.10

Mean number of GAD65/67-immunoreactive neurons in the substantia nigra and VTA one month after 6-OHDA treatment. (Not assessed stereologically)

Immunopositive neurons in each 1 in 3 sections were counted and then multiplied to obtain the total neuronal number representing the injected or uninjected hemisphere. On the contralateral side, there was an average of 1782 GAD65/67+ neurons (SEM ± 239.6) compared to 1400 on the ipsilateral side (SEM ± 125.6), meaning a 21% cell loss. This reduction was significant according to the general linear modelling of variance and *post hoc* Fisher's *t*-test. The error bars mark SEM.

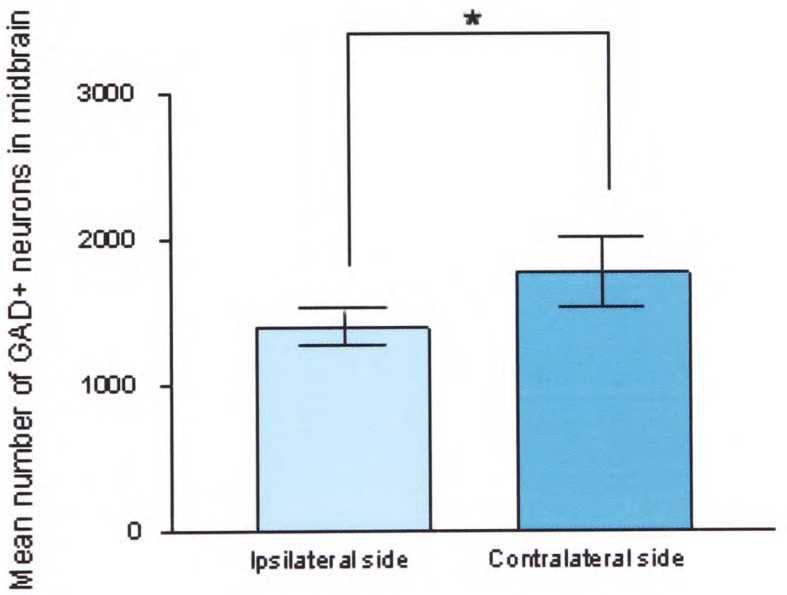
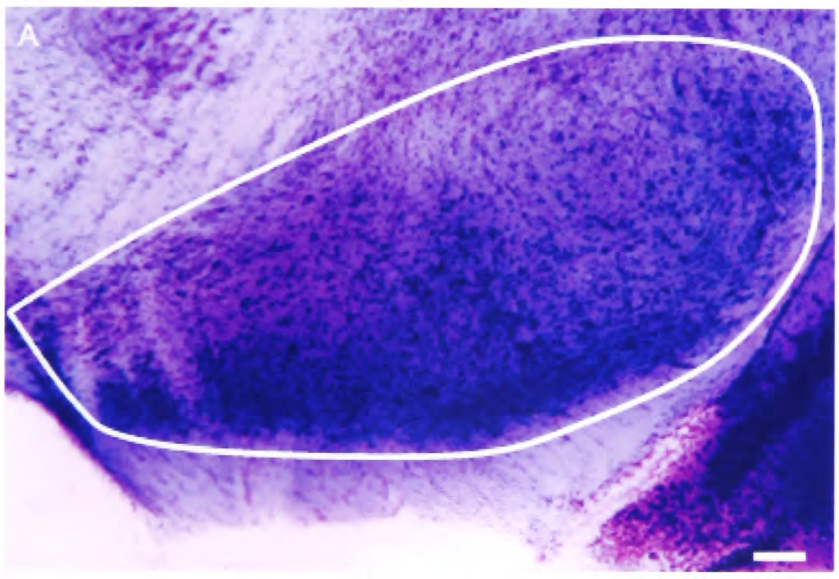


Figure 3.11

Light micrographs illustrating the stereological counting frame. The midbrain region to be counted was defined (white line) at a low magnification (A, scale bar = 100 μm). Neurons were counted at high magnification (B, scale bar = 10 μm). Neurons can be distinguished from glia by being generally larger with larger nuclei; the nuclear membrane should be visible in at least a few of the focal planes which pass through the nucleus, whereas glial cells are usually much smaller with smaller, darker and/or granular nuclei. Only cells that lay within the volume of the frame and/or touched the dashed white lines were counted (asterisks) and those that crossed the solid white lines were excluded from analysis.


A

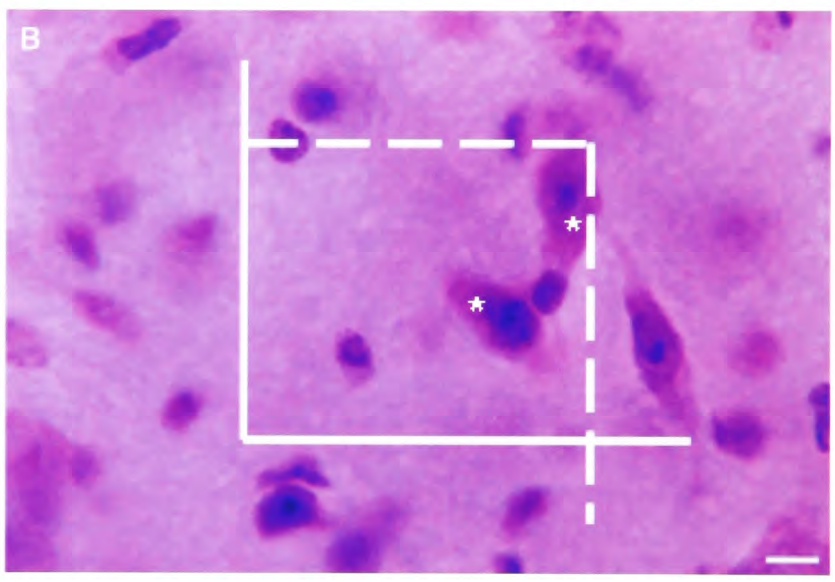

B

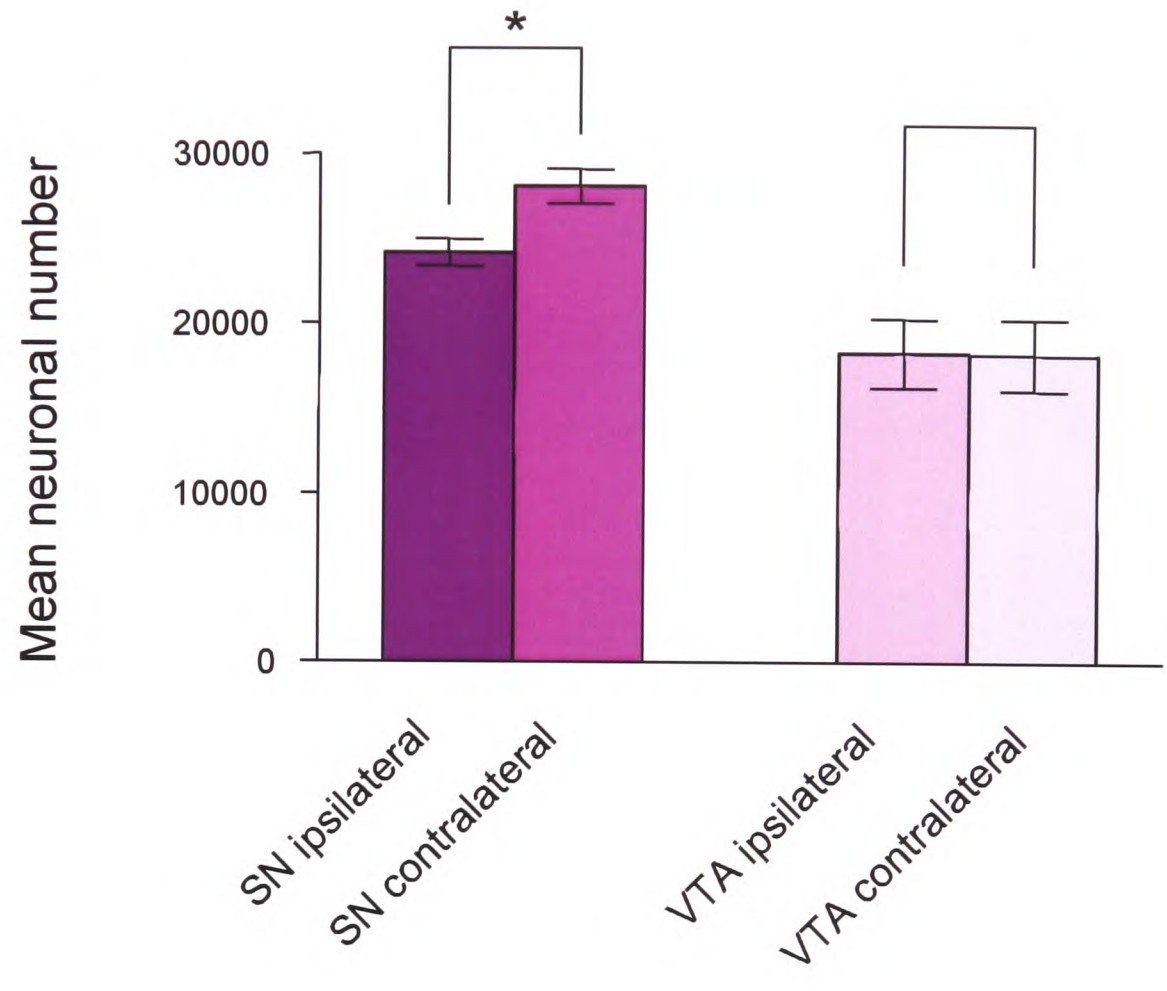
Figure 3.12

Stereological estimation of the total neuronal number and total volumes of the SN and VTA one month after 6-OHDA treatment.

(A) The mean neuronal numbers in the SN and VTA were analysed independently. A significant loss of 14% was found in the SN (Student's *t*-test, two tails, $*P = 0.029$), but there was no significant difference in the VTA (Student's *t*-test, two tails, $P = 0.686$).

(B) There was no significant change in volume in either the SN (Student's *t*-test, two tails, $P = 0.889$) or in the VTA (Student's *t*-test, two tails, $P = 0.886$).

A


*
30000
20000
10000
0
Mean neuronal number
SN ipsilateral
SN contralateral
VTA ipsilateral
VTA contralateral

B

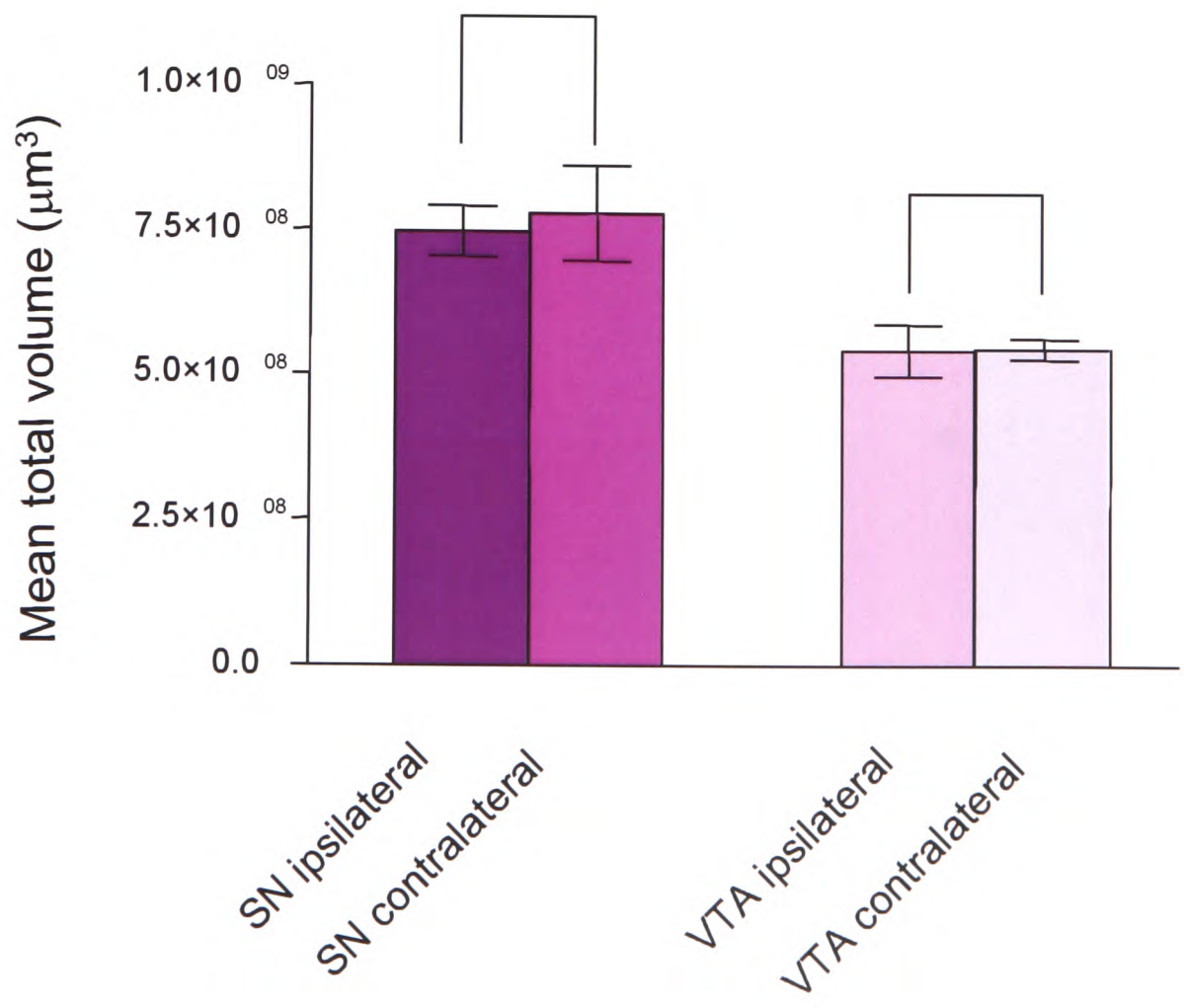

1.0×10 09
7.5×10 08
5.0×10 08
2.5×10 08
0.0
Mean total volume (μm3)
SN ipsilateral
SN contralateral
VTA ipsilateral
VTA contralateral

Figure 3.13

TH immunoreactivity in the rostral and caudal striata one month following MPTP/p treatment.

Mice were treated with saline (A, B), probenecid (C, D) or MPTP/p (E, F).

In the rostral (A, C) and caudal (B, D) striatum, TH+ fibers appeared intact in both saline (A, B) and probenecid (C, D) controls.

Treatment with MPTP/p resulted in a large decrease in TH+ fibers (white arrows) in both rostral (E) and caudal (F) striatum.

Scale bar = 10 μm

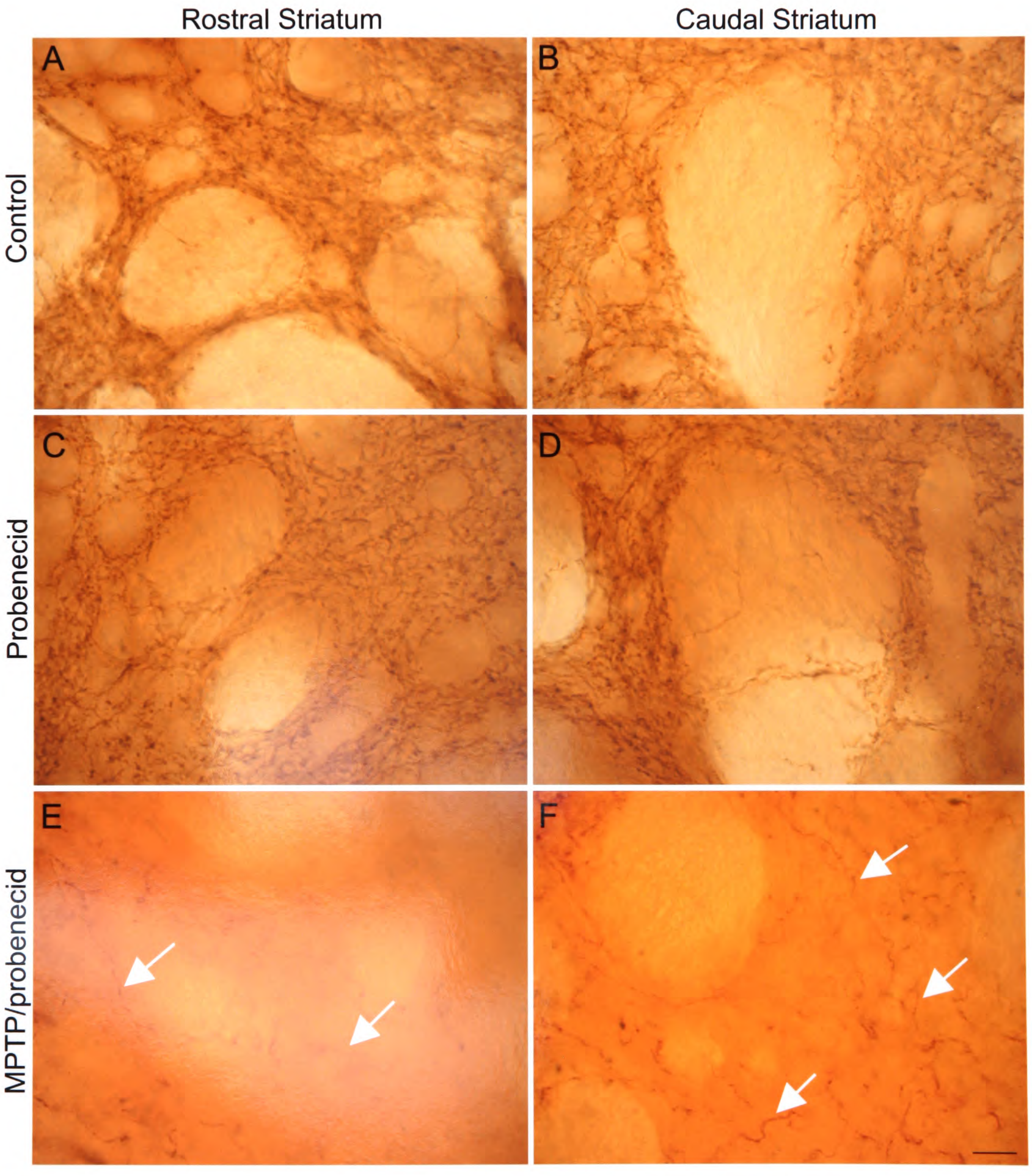

Rostral Striatum
Caudal Striatum
Control
Probenecid
MPTP/probenecid
A
B
C
D
E
F

Figure 3.14

Electron micrograph showing the presence of inclusion bodies one month after MPTP/probenecid treatment.

C57Bl/6 mice were treated with MPTP (25 mg/kg) in conjunction with probenecid (250 mg/kg) administered twice weekly for five weeks. Dense inclusion bodies were found in neurons in the SN of these mice. Scale bars are as shown.

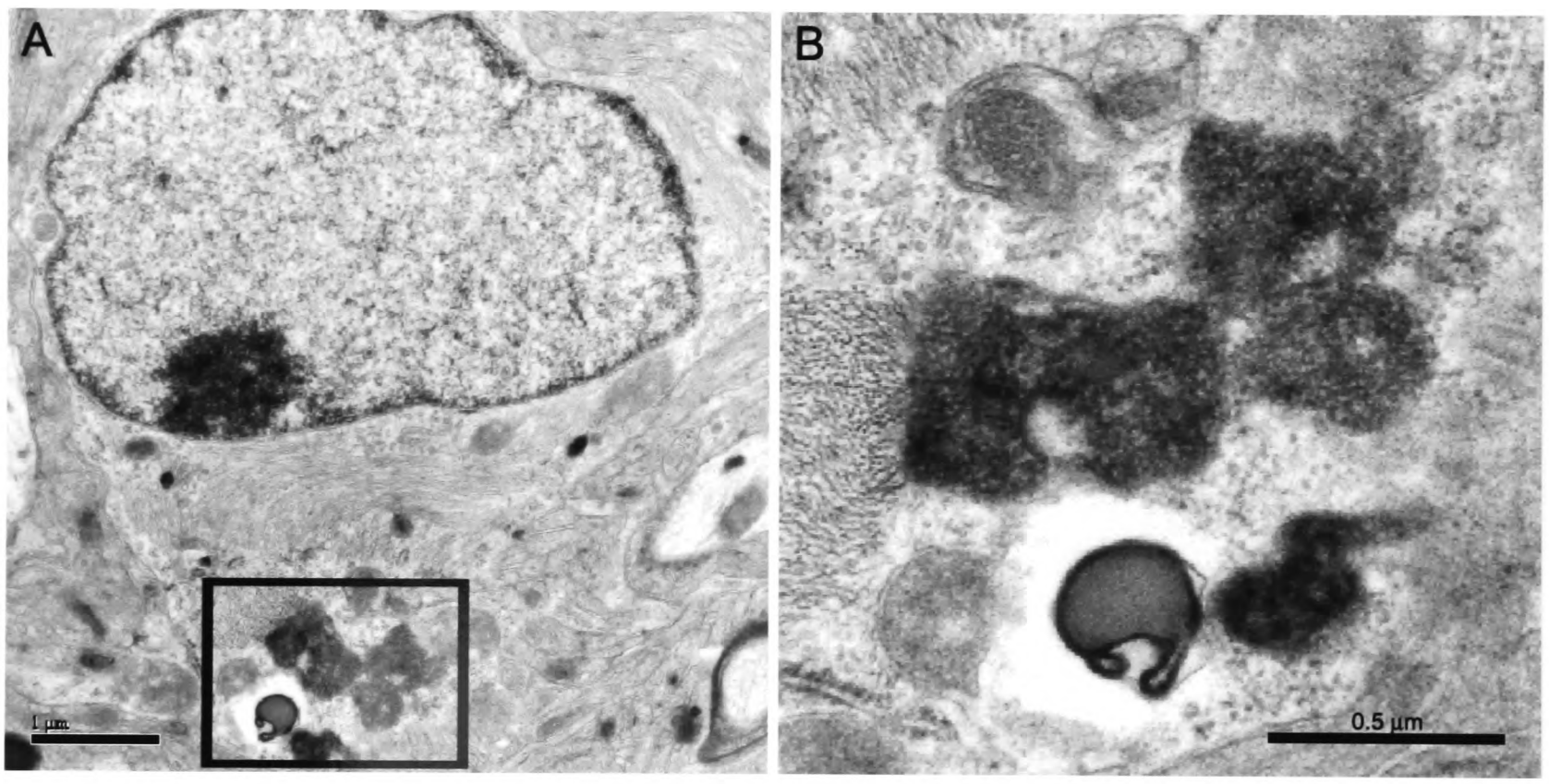

A
B
1 µm
0.5 µm

Figure 3.15

TH immunoreactivity in the midbrain in the MPTP/p mouse model.

In the SN (A, C) and VTA (B, D) of the saline (A, B) and probenecid (C, D) control mice, TH-immunostaining was intense in the cell bodies and dendrites projecting into the SNR.

At similar midbrain levels in the MPTP/p mice (E, F), there was a substantial loss of TH+ cell bodies and dendrites, particularly in the middle portion of the SNC (E). Some TH+ neurons survived in the dorsomedial region of the SNC and the SNL. Loss of TH+ neurons in the ventral tegmental area of the MPTP/p mouse was less pronounced (F).

Scale bar = 100 μm

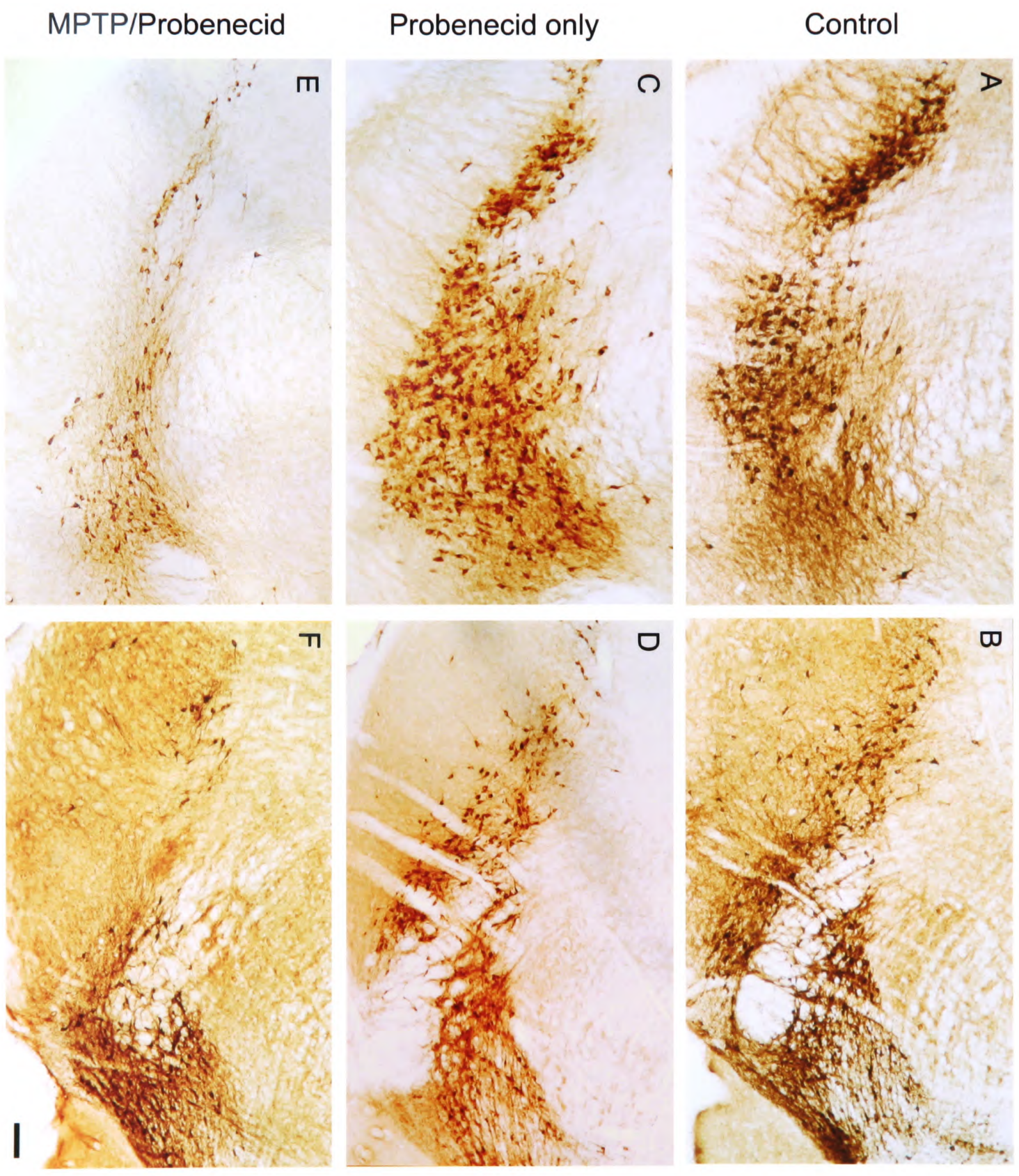

MPTP/Probenecid
Probenecid only
Control
E
C
A
B
D
F

Figure 3.16

CB immunoreactivity in the midbrain in the MPTP/p mouse model.

In the SN (A, C) of the saline (A, B) and probenecid (C, D) control mice, CB+ was mostly found in the SNC and SNL. In the MPTP/p mice (E, F), there was a substantial loss of CB+ neurons in the SNC and no immunostaining was left in the SNL. In the VTA (B, D, F), a less pronounced decrease in CB+ neurons was observed.

Scale bar = 100 μm

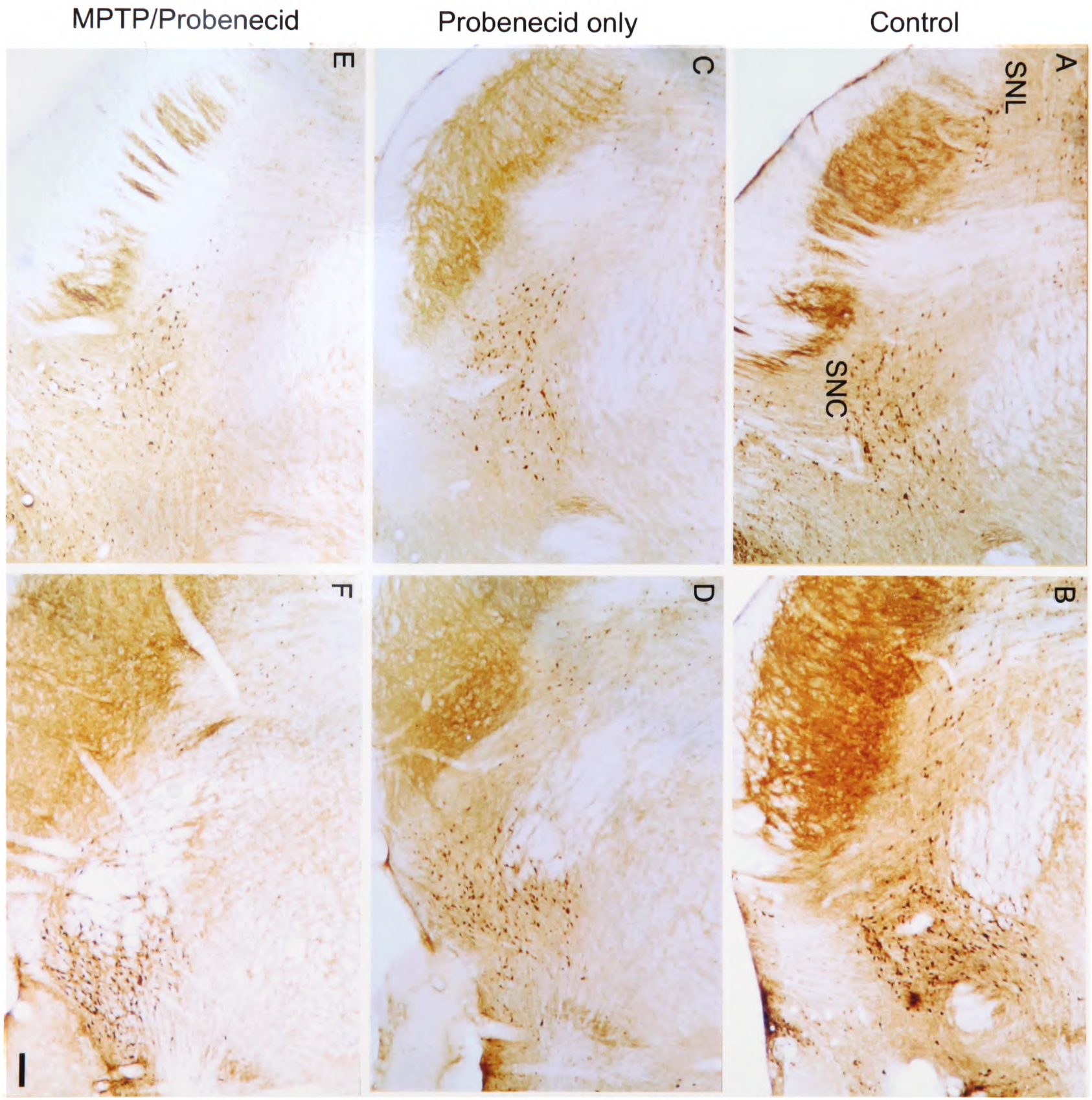

MPTP/Probenecid
Probenecid only
Control
E
C
A
SNL
SNC
F
D
B

Figure 3.17

Double immunofluorescent labelling of TH and CB in the SN one month after MPTP/probenecid treatment.

Coronal sections through the SN of saline control (A-C), probenecid control (D-F) and MPTP/probenecid-treated (G-I) mice. TH (A, D, G, green) was mostly expressed in the SNC and along the SNR, whereas CB (B, E, H, red) was found near the midline and in the SNL. Double labelled cells are indicated by arrows in C, F and I.

In MPTP/p mice (G-I), there were marked reductions in TH+ (compare G with A & D), CB+ (compare H with B & E) and in TH+/CB+ (compare I with C & F) neurons.

Scale bar = 100 μm

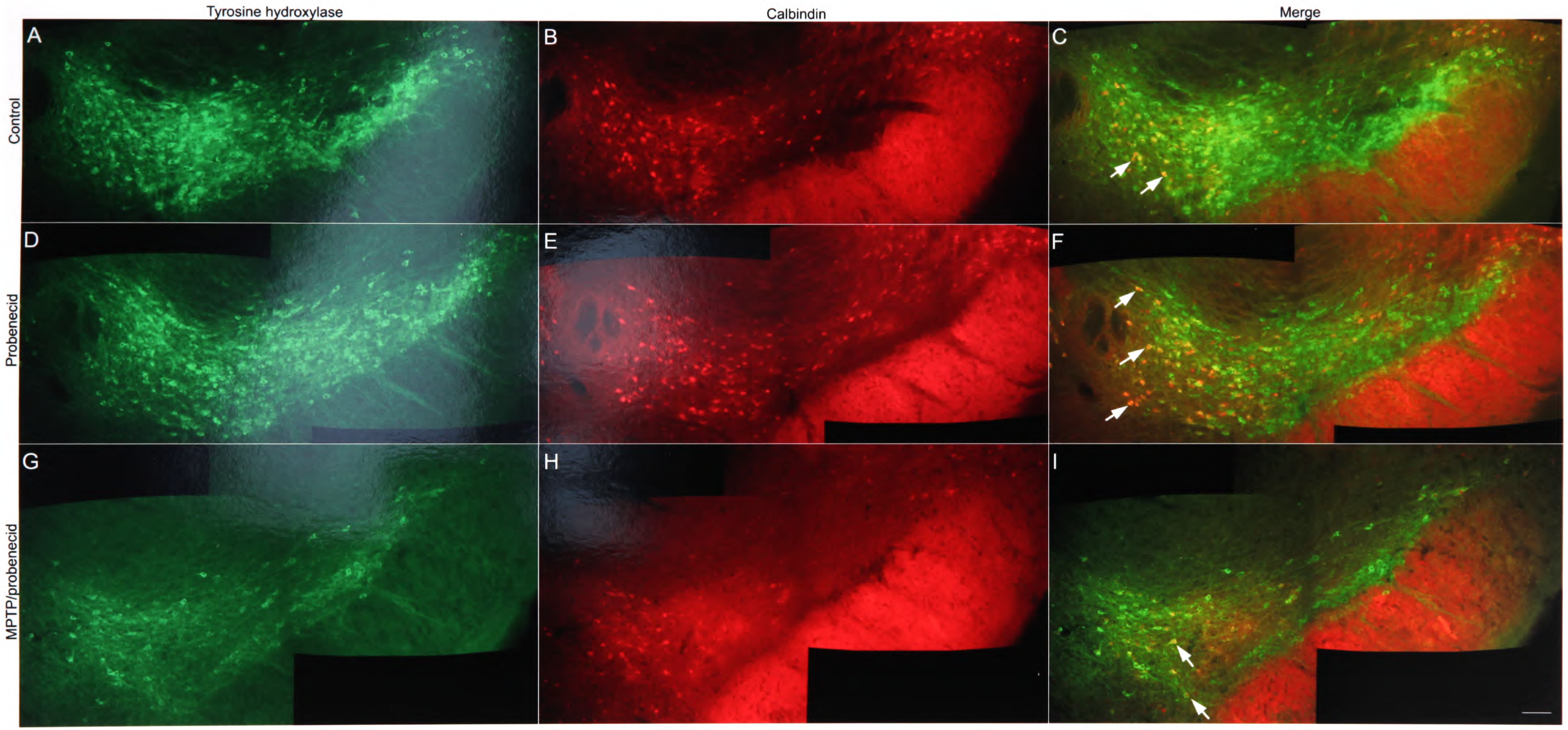

Tyrosine hydroxylase
Calbindin
Merge
Control
Probenecid
MPTP/probenecid
A
B
C
D
E
F
G
H
I

Figure 3.18

Double immunofluorescent labelling of TH and CB in the VTA one month after MPTP/probenecid treatment.

Coronal sections through the SN of saline control (A-C), probenecid control (D-F) and MPTP/probenecid-treated (G-I) mice. TH (A, D, G, green) was mostly expressed in the VTA, SNC and along the SNR and SNL, whereas CB (B, E, H, red) was found in the VTA and SNL.

In MPTP/p mice (G-I), there were marked reductions in TH+ (compare G with A & D), CB+ (compare H with B & E) and in TH+/CB+ (compare I with C & F) neurons but many remained in the VTA.

Scale bar = 100 μm

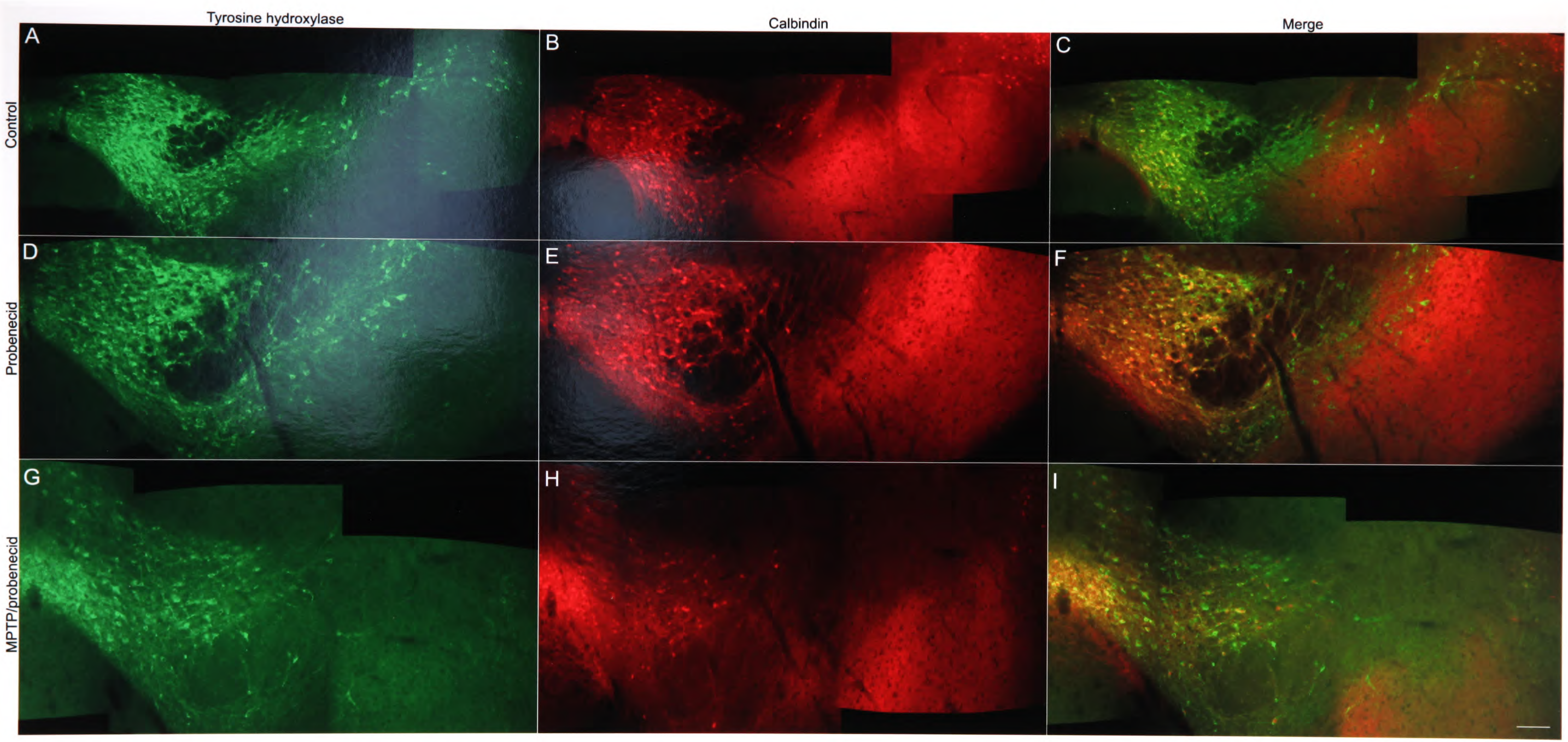

Tyrosine hydroxylase
Calbindin
Merge
Control
Probenecid
MPTP/probenecid
A
B
C
D
E
F
G
H
I

Figure 3.19

Number of TH+, CB+ and TH+/CB+ neurons in the midbrain one month after MPTP/probenecid treatment. (Not assessed stereologically)

Immunopositive neurons were counted on both hemispheres of the mice, representing bilateral counts.

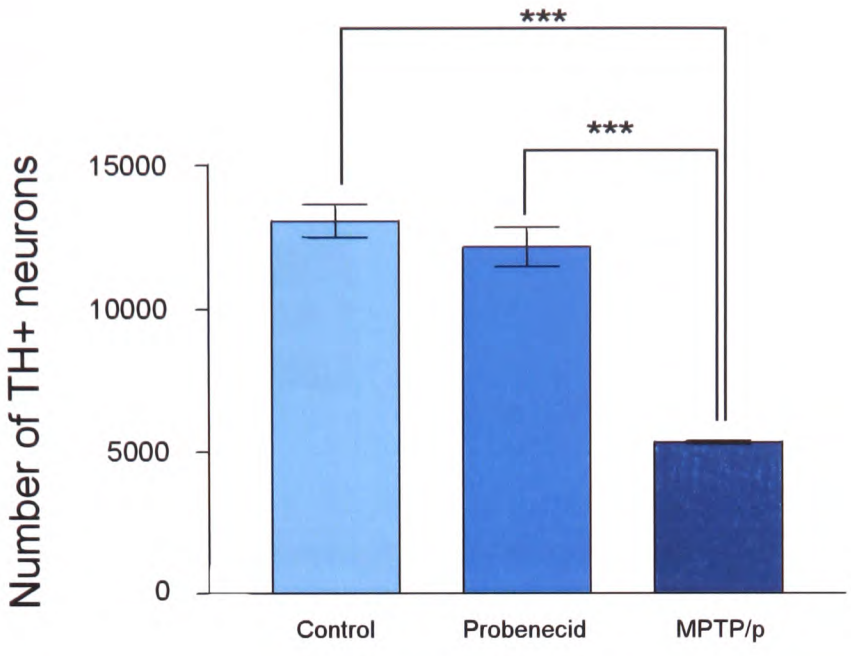
General linear model of variance showed significant differences among the three neuronal populations ($F_{(1.383,22.134)} = 350.172$; $P < 0.0001$). Saline or probenecid or MPTP/p treatment also caused significant differences ($F_{(2,16)} = 220.635$; $P < 0.0001$). The error bars mark SEM.

(A) *Post-hoc* Fisher's *t*-test showed significant reductions (59%) in TH+ neurons following MPTP/p treatment compared with saline ($P < 0.0001$) and probenecid ($P < 0.0001$) controls. There was no significant difference between TH+ neurons in saline and probenecid controls.

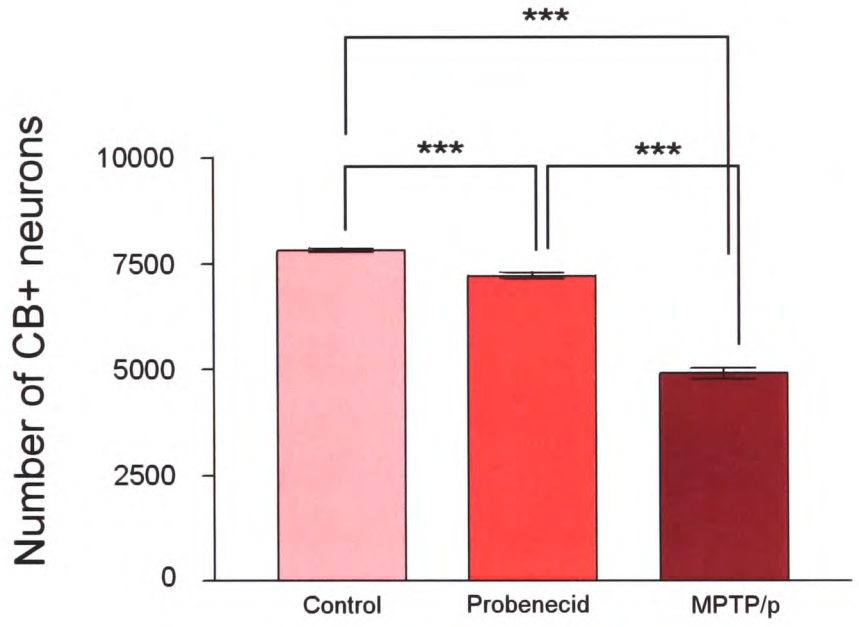
(B) There was a significant reduction in CB+ neurons (37%) following MPTP/p treatment compared with saline ($P < 0.0001$) and probenecid ($P < 0.0001$) controls. There was also significant reduction of CB+ neurons following probencid treatment ($P < 0.0001$) compared to the saline controls.

(C) There was a significant reduction in the number of TH+/CB+ co-localised neurons (37%) following MPTP/p treatment compared with saline ($P < 0.0001$) and probenecid ($P < 0.0001$) controls. There was also significant reduction of CB+ neurons following probenecid treatment ($P < 0.0001$) compared to the saline controls.

A


***
***
Number of TH+ neurons
15000
10000
5000
0
Control
Probenecid
MPTP/p

B


***
***
***
Number of CB+ neurons
10000
7500
5000
2500
0
Control
Probenecid
MPTP/p

C

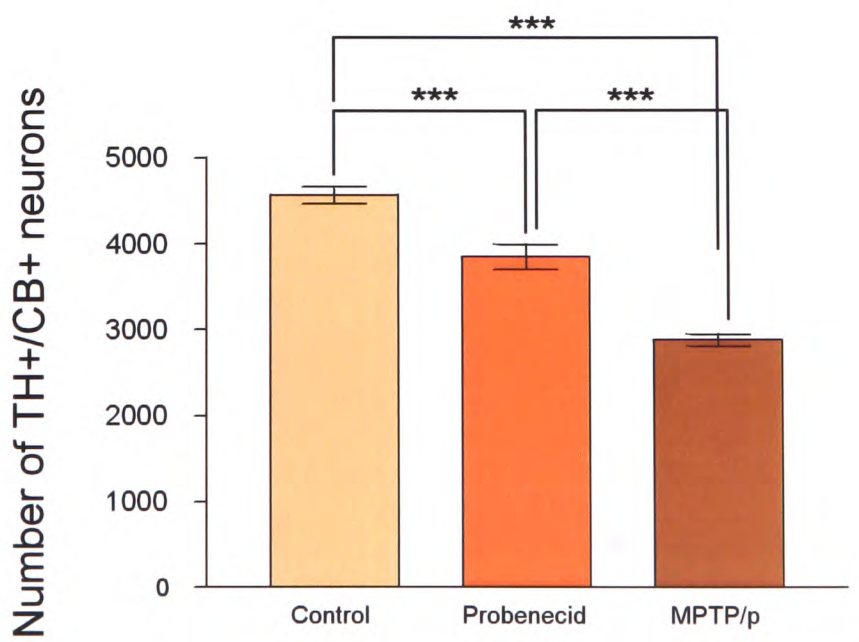

***
***
***
Number of TH+/CB+ neurons
5000
4000
3000
2000
1000
0
Control
Probenecid
MPTP/p

Table 3.1

6-OHDA 1month

	TH	SEM	CB	SEM	TH+/CB+	SEM	% TH+ that are TH+/CB
Contralateral (Unlesioned)	7550	764.6	3773	456.3	2094	55.38	28%
Ipsilateral (Lesioned)	1634	280.2	1186	312.7	647	9.211	40%
Neuronal loss	78%		77%		69%		

GAD 1 month

	GAD	SEM
Contralateral (unlesioned)	1782	239.6
Ipsilateral (Lesioned)	1400	125.6
Neuronal loss	21%	

Statistical Analyses

GLM

Within-subject factors	Sig.	
Count (TH, CB, TH+/CB+)	√	$F(2,12) = 131.556$; $P < 0.0001$
Treatment	√	$F(1,6) = 688.588$; $P < 0.0001$
Count x Treatment	√	$F(2,12) = 288.319$; $P < 0.0001$

***Post-hoc t*-test**

Cell count		Sig.	
Contralateral	TH vs CB	√	$P < 0.0001$
Contralateral	TH vs TH+/CB+	√	$P < 0.0001$
Contralateral	CB vs TH+/CB+	√	$P = 0.002$
Ipsilateral	TH vs CB	√	$P = 0.01$
Ipsilateral	TH vs TH+/CB+	√	$P = 0.003$
Ipsilateral	CB vs TH+/CB+	√	$P = 0.05$
Treatment			
TH	Contra- vs Ipsi-	√	$P < 0.0001$
CB	Contra- vs Ipsi-	√	$P < 0.0001$
TH+/CB+	Contra- vs Ipsi-	√	$P < 0.0001$

GLM (GAD)

Within-subject factor	Sig.	
Treatment	√	$F(1,6) = 76.079$; $P < 0.0001$

***Post-hoc t*-test**

		Sig.	
Treatment	Contra- vs Ipsi-	√	$P = 0.001$

MPTP 1 month

	TH	SEM	CB	SEM	TH+/CB+	SEM	% TH+ that are TH+/CB+
Saline	13065	577.4	7804	41.25	4563	100.6	35%
Probenecid control	12148	680.7	7208	68.98	3848	146.3	32%
MPTP/p	5314	55.69	4888	127.3	2878	66.05	54%
Neuronal loss	59%		37%		37%		

Statistical Analyses

GLM

Within-subject factors	Sig.	
Count (TH, CB, TH+/CB+)	√	F(1.383,22.134) = 350.172; *P* < 0.0001
Count x Treatment	√	
Between-subject factor		
Treatment	√	F(2,16) = 220.635; *P* < 0.0001

***Post-hoc t*-test**

Cell count		Sig.	
Saline	TH vs CB	√	*P* < 0.0001
Saline	TH vs TH+/CB+	√	*P* < 0.0001
Saline	CB vs TH+/CB+	√	*P* < 0.0001
Probenecid	TH vs CB	√	*P* < 0.0001
Probenecid	TH vs TH+/CB+	√	*P* < 0.0001
Probenecid	CB vs TH+/CB+	√	*P* < 0.0001
MPTP/p	TH vs CB	x	
MPTP/p	TH vs TH+/CB+	√	*P* = 0.002
MPTP/p	CB vs TH+/CB+	√	*P* < 0.0001
Treatment		Sig.	
TH	Saline vs Probenecid	x	
TH	Saline vs MPTP/p	√	*P* < 0.0001
TH	Probenecid vs MPTP/p	√	*P* < 0.0001
CB	Saline vs Probenecid	√	*P* < 0.0001
CB	Saline vs MPTP/p	√	*P* < 0.0001
CB	Probenecid vs MPTP/p	√	*P* < 0.0001
TH+/CB+	Saline vs Probenecid	√	*P* < 0.0001
TH+/CB+	Saline vs MPTP/p	√	*P* < 0.0001
TH+/CB+	Probenecid vs MPTP/p	√	*P* < 0.0001

4 Progressive Neurotoxicity to Midbrain Neurons in Mouse Models of Parkinson's disease

4.1 Introduction

In the normal human ageing process, the loss of brain weight is approximately 2-3% per decade from 50 to 90 years of age (Stark and Pakkenberg, 2004). A reduction in the overall volume of the SN with ageing is reported in many histological studies such as in monkeys (Pakkenberg et al., 1995; Emborg et al., 1998; Chen et al., 2000) and humans (Ma et al., 1999; Chen et al., 2000; Cabello et al., 2002; Chu et al., 2002). Most of the recent work was assessed stereologically with systematic sampling and disector counting to show the relationship between age and the overall SN volume plus the number and volume of neurons in the SNC and in the VTA. Siddiqi *et al.* found no significant relationship between age and the overall volume of these DA brain stem nuclei, but there was a significant loss of the total number of neurons in the SNC and the paranigral part of VTA (VTApn) (Siddiqi et al., 1999). Hence, they suggested that the age-related neuronal loss in these regions contributed to the deficits in DA innervation, resulting in impaired cognitive performance.

The reported age-related nigrostriatal changes in a population of individuals free of neurological disorders can serve as a quantitative documentation of the ageing process. Ageing has been identified as a risk factor for the sporadic form of PD, with its disease aetiology rarely diagnosed before 50 years of age. Thereafter, its incidence and prevalence increase near-exponentially (Tanner and Goldman, 1996; McCormack et al., 2004). Epidemiological studies reveal that approximately 1-2% of people over age 65 are affected with PD. Similar to PD, ageing involves a mechanism that produces a regionally specific (putamen) DA loss (Gibb and Lees, 1991; Kish et al., 1992; Stark and Pakkenberg, 2004). However, mechanisms underlying this age-related neurodegeneration remain unknown.

There are three predominant theories concerning ageing and PD (Thiruchelvam et al., 2003). The first one postulates that the ageing nigrostriatal system may be more vulnerable to the damage caused by genetic or environmental insults. Older mice (9-12 months) given MPTP

showed greater decreases in dopamine levels and TH when compared with young mice (2-3 months) (Date et al., 1990a; Sugama et al., 2003a; Ohashi et al., 2006). MPTP-treated young mice (<3 months) have a significant recovery of striatal DA levels that was not observed in older mice (8-12 months) (Ricaurte et al., 1987; Date et al., 1990a). This effect of MPTP in relation to ageing has been extensively studied using C57Bl/6 mice (Jossan et al., 1989; Walsh and Wagner, 1989; Date et al., 1990b; Irwin et al., 1992; Irwin et al., 1993).

The second theory considers interactions between ageing and toxicity (Calne and Langston, 1983). Thus, exposure to a neurotoxicant could induce a notable but limited insult to the nigrostriatal DA system in early or middle life, but compensatory mechanisms would exist to preserve normal DA function until later in life. This hypothesis assumes that ageing normally is accompanied by a decline in nigrostriatal DA system function that, when added to the earlier lesion, will accelerate the natural decline of the system to disease levels (Thiruchelvam et al., 2003).

Barbeau put forward the third theory, suggesting that an insult in early or middle life would lead to a compensatory response by increasing DA production in the remaining terminals, which would add to the stress in the DA system, followed by additional neuronal death (Barbeau, 1984; Thiruchelvam et al., 2003). To test whether neurotoxicity progressively exacerbates neuronal cell death in the brain with time, the 6-OHDA and MPTP/p-lesioned mice were allowed to survive for a 3-month post-treatment period, and then compared histologically and quantitatively with the mice with a 1-month post-treatment period from Chapter 3.

4.2 Aims

- To examine the histological alterations of midbrain TH+, CB+ and TH+/CB+ neurons in the 6-OHDA and MPTP/probenecid models 3 months post-treatment
- To examine the histological alterations of midbrain GAD65/67+ neurons in the 6-OHDA and MPTP/probenecid models 3 months post-treatment
- To compare the neuronal number of midbrain TH+, CB+, TH+/CB+ and GAD65/67+ neurons in the 1- and 3-month post-treatment mouse models

4.3 Methods

4.3.1 Animals and lesions

Experiments were carried out on male C57Bl/6 mice weighing about 22g. A final dosage of 1.5 μg of 6-OHDA in 0.1% ascorbic acid was injected into the medial forebrain bundle (n=4) with coordinates as described in Section 3.3.1. Mice were killed by perfusion fixation 3 months post-treatment. By this time the mice were about 6 months old.

For MPTP/probenecid lesion, a total of 10 mice were treated in the U.S. as described in Section 3.3.1 (MPTP/p mice, n=4; probenecid controls, n=4; saline controls, n=2*). They were killed by perfusion-fixation 3 months post-treatment.

*The number of saline controls is fewer than 3, which may skew the statistical interpretation. Future work aims to increase the number of animals used.

4.3.2 Immunohistochemistry and immunofluorescence

Striatal sections of the 6-OHDA- and MPTP/p-treated mice were immunolabelled with TH (1:1000, mouse monoclonal anti-TH, DiaSorin) to reveal the extent of the neurotoxic lesions. Double immunofluorescence using antibodies against TH and CB was performed as described in Section 3.3.2 using midbrain sections. GAD65/67 immunohistochemistry was performed using the freeze-thaw method as described in Section 3.3.2.

4.3.3 Image analysis

All light microscopy was visualised and captured with a microscope (Zeiss) with the interchangeable QImaging CCD cameras (for both light and fluorescent microscopy) as described in Section 3.3.6. The micrographs were digitised with QCapture Pro software and contrast and brightness optimised with Adobe Photoshop CS. Several micrographs were merged using Canon PhotoStitch (version 3.1) in order to generate full pictures of the SN or VTA region.

4.3.4 Quantitative and statistical analysis

The number of TH+, CB+ and TH+/CB+ neurons was counted manually from the immunofluorescent images and analysed as described in Chapter 3 as part of the study (Section 3.3.8). For the 6-OHDA-treated mice, differences in immunopositive neurons between ipsilateral and contralateral SN and VTA were analysed using repeated measures general linear models, with cell count and lesion treatment as the within-subjects factors, and time as the between-subject variable. If there was a significant cell count, treatment or cell count x treatment interaction effect, then the *post-hoc* Fisher's *t*-test were performed to determine where the differences lay, with $P < 0.05$ considered significant. For GAD immunoreactivity, the general linear model was used with lesion treatment as the within-

subject factor and time as the between-subject factor. For the MPTP/p-treated mice, repeated measures general linear modelling was also undertaken but with only cell count as the within-subject factor, and lesion treatments and time as the between-subjects factors (because the treatments were done on different animals), followed by *post-hoc* Fisher's *t*-test.

4.4 Results

4.4.1 Effects of 6-OHDA in midbrain neural degeneration 3 months post-treatment

4.4.1.1 Nigro-striatal projections in the striatum

Mice striata were immunoreacted for TH, as performed in the 1-month post-treatment 6-OHDA lesion model, such that the extent of the lesion could be assessed. Fiber loss in the striatum again provided a qualitative assessment of the completeness of the lesion rather than a quantitative comparison between the neurotoxic effects in the 1- or 3-months post-treatment regimens. Hence, it was not necessary to quantify the DA denervation in the striatum by densitometric or immunoblotting analyses.

In the rostral striatum (Figure 4.1), DA cell fibers were apparently intact on the contralateral side (Figure 4.1 A) but only remnants of the DA fibers were observed on the ipsilateral side (Figure 4.1 C, arrows). This pattern and distribution of DA fibers applied to both caudate-putamen and the nucleus accumbens. In the caudal striatum, a marked decrease in TH+ fibers was also observed on the ipsilateral side (Figure 4.1 D, arrows) compared to that on the contralateral side (Figure 4.1 B).

4.4.1.2 DA neurons in the midbrain

Immunofluorescent labelling showed dramatic reductions in the number of midbrain TH+, CB+ and TH+/CB+ neurons between the injected and un-injected brain hemispheres. In the SN contralateral to the 6OHDA injection (Figure 4.2), TH immunostaining was abundant across the whole length of the SNC and SNL (Figure 4.2 A). There were fewer CB+ than TH+ neurons, and CB+ neurons were confined to the ventral-medial portion of the SNC and the SNL (Figure 4.2 C). Most of the CB+ neurons were co-localised with TH+ neurons (Figure 4.2 E). On the side ipsilateral to the injection, very few TH+ neurons were present (Figure 4.2 B). A number of CB+ neurons were observed in the SNC only (Figure 4.2 D). Because of the small number of TH+ neurons, it was not possible to calculate the proportion of CB+ neurons co-localised with TH in a single section (Figure 4.2 F).

In the contralateral VTA (Figure 4.3), TH immunostaining was abundant, extending across the VTA, SNC and SNL (Figure 4.3 A). CB+ neurons were present mostly in the VTA (Figure 4.3 C) but not in the SNL, as observed in the 1-month model. The majority of CB+ neurons were co-localised with TH (Figure 4.3 E). On the ipsilateral side, TH+ neuron loss was evident particularly in the SN region, but not in the VTA (Figure 4.3 B). There was an apparent reduction of CB+ neurons in the VTA (Figure 4.3 D) and most of them co-localised with TH (Figure 4.3 F).

The number of immunolabelled neurons was counted in a 1 in 3 series of sections as previously described (Section 3.4.3.1). These numbers were then multiplied to obtain the total number of immunolabelled neurons for the whole midbrain (SN and VTA included). Table 4.1 summarizes the counting and statistical analyses.

In the 3-month post-treatment mice, there were significantly more TH neurons than either CB+ or TH+/CB+ in both contralateral and ipsilateral hemispheres, but no significant difference between the number of CB+ vs TH+/CB+ neurons on either side. The lesion treatment significantly reduced all three neuronal populations (***$P < 0.0001$) from the *post-hoc* *t*-test analyses. Moreover, the lesion affected the three populations differently because there was a 79% loss of the TH+ neurons (Figure 4.4 A) but only 54% loss in the CB+ neurons (Figure 4.4 B) and 59% loss in the TH+/CB+ neurons (Figure 4.4 C). In addition, on the contralateral side, only 26% of TH+ neurons were co-localised with CB (percentage TH+/CB+:TH+ neurons) whereas on the ipsilateral side this proportion rose to 52%.

When the 1- and 3-month data were compared, post-treatment time was not a significant factor to the overall neuronal populations, and no cell count x time interaction was found. There were, however, treatment x time interactions ($F_{(1,6)} = 7.332$; *$P = 0.035$) and the subtle differences were revealed by *post-hoc* *t*-test analyses. Firstly, for TH+ neurons (Figure 4.4 A), there was no significance between the 1- vs 3-month groups in either the treated or untreated hemispheres. On the other hand, there was a significant reduction (**$P = 0.0014$) of CB+ neurons (Figure 4.4 B) over this period on the contralateral side. For the TH+/CB+ neurons (Figure 4.4 C), there was a significant reduction (*$P = 0.044$) over this period on the contralateral side as well, although unexpectedly there was a significant recovery on the ipsilateral side (***$P < 0.0001$), as shown by the significant increase in neuronal number.

Future work will include unilaterally-injected saline controls in comparison with the unilaterally-injected 6-OHDA group, in order to rule out any bilateral lesion effect.

4.4.1.3 GABAergic neurons in the midbrain

GAD65/67 immunostaining was mostly found in the SNR close to the SNL, both on the contralateral and ipsilateral sides (Figure 4.5 A & B respectively). In the VTA, there were very few immunolabelled neurons on either the contralateral (Figure 4.5 C, arrows) or ipsilateral (Figure 4.5 D) sides. The GAD65/67+ neurons were counted in a 1 in 3 series of sections and multiplied to obtain the total number for the midbrain. In all, 968 neurons were calculated on the contralateral side (SEM ± 165.9) and 531 on the ipsilateral side (SEM ± 124.0), which amounts to a 45% loss. Figure 4.6 illustrates the comparison between the 1- and 3-month post-treatment data. General linear modelling showed a significant effect of lesion treatment ($F_{(1,6)} = 76.079$; $^{***}P < 0.0001$) and *post-hoc* *t*-test showed that, in the 3-month post-treated mice, there were significantly fewer immunolabelled neurons ipsilaterally than contralaterally ($^{*}P = 0.001$). Although there was no treatment x time interactions, post-treatment time did play a significant role ($F_{(1,6)} = 99.792$; $^{***}P < 0.0001$) and *post-hoc* *t*-test showed that, over time, there were significant reductions in labelled cell numbers both contralaterally ($^{***}P < 0.0001$) and ipsilaterally ($^{***}P < 0.0001$).

4.4.2 Effects of MPTP/probenecid in midbrain neural degeneration 3 months post-treatment

4.4.2.1 Nigro-striatal projections in the striatum

In the rostral striatum of the saline control, a large mass of intact TH+ fibers was observed (Figure 4.7 A). This resembles the pattern seen in mice treated with probenecid alone (Figure 4.7 C). On the other hand, in the MPTP/p-treated mice, TH+ fibers appeared as shorter, interrupted segments (Figure 4.7 E). In the caudal striatum, saline and probenecid controls both displayed prominent TH+ processes (Figure 4.7 B & D respectively), whereas that in the MPTP/p-treated mice appeared shorter and less dense (Figure 4.7 F).

4.4.2.2 DA neurons in the midbrain

In the saline controls, TH+ cell bodies were found throughout the SNC, SNR and SNL (Figure 4.8 A) and this pattern was also seen in the probenecid controls (Figure 4.8 D). In the MPTP/p mice, there was a marked decrease of TH+ neurons, although some were observed in the dorsal tier of SNC (Figure 4.8 G). CB+ neurons were found in the ventro-medial portion of SNC and SNL in both saline (Figure 4.8 B) and probenecid controls (Figure 4.8 E) and it was mainly those in the SNC that survived MPTP/p treatment (Figure 4.8 H). Merged images showed that most CB+ neurons were co-localised with TH in the saline (Figure 4.8 C), probenecid controls (Figure 4.8 F) and MPTP/p mice (Figure 4.8 I).

In the VTA and along the border of SNC and SNR, there were large numbers of TH+ neurons in the saline and probenecid controls (Figure 4.9 A & D respectively) and these were still quite numerous after MPTP/p treatment (Figure 4.9 G). In controls, CB+ neurons were found mostly in the VTA but also along the border of SNC and SNR (Figure 4.9 B & E saline and probenecid respectively) whereas in the MPTP/p-treated mice, numerous CB+ neurons remained in the VTA but not the SNC (Figure 4.9 H). Most CB+ neurons in the SNL were lost after MPTP/p treatment. Merged images showed that most CB+ neurons were co-localised with TH in the saline (Figure 4.9 C), probenecid controls (Figure 4.9 F) and MPTP/p mice (Figure 4.9 I).

Immunolabelled were neurons counted in every third section and multiplied to obtain the total number in the midbrain as previously described (Figure 4.10). Because the treatment effects are seen bilaterally, and both sides of the brain were counted, the number of immunolabelled neurons was at least double that counted in the 6-OHDA animals, where the lesion was unilateral. Similar to the trend seen in the 6-OHDA lesion, the numbers of TH+, CB+ and TH+/CB+ neurons were significantly different, except that no paired significance

was found between TH+ and CB+ population in the MPTP/p-treated mice. There was no cell count x time interaction. Nevertheless, there was a cell count x treatment interaction. Thus, there were 50% fewer TH+ neurons in the MPTP/p treated mice, compared with saline controls, but only 25% loss in the CB+ population and 21% in the TH+/CB+ populations. *Post-hoc t*-test confirmed this by showing paired significance in all groups except the saline vs probenecid controls in the TH+ population. Post-treatment time seemed to have a significant effect in this model ($F_{(1,16)} = 4.319$; $*P = 0.005$) and there was a treatment x time interaction ($F_{(2,16)} = 6.405$; $**P = 0.009$). Interestingly, only the CB+ neurons were affected by post-treatment time, with reductions of neurons over this period in the saline and probenecid controls ($***P < 0.0001$) and a small but significant recovery in the MPTP/p-treated mice ($*P = 0.005$).

4.5 Discussion

Most publications to date that relate age and neuronal loss have exposed animals of different ages to a neurotoxin. This study, however, sought to determine whether neurotoxic insults relatively early in life could produce an ongoing cell loss over time. My experiments showed that 6-OHDA and MPTP/p treatment with a 3-month survival period produced similar trends of midbrain neuronal death compared to 1-month post-treatment. There were reductions and shortening of DA striatal fibers in the striatum, reductions of TH+, CB+ and TH+/CB+ neurons in the midbrain, particularly in the SN, but less severe in the VTA, and a reduction in midbrain GAD65/67+ neurons. However, the effects of survival time on neuronal survival seemed differ subtly between the two animal models and between cell populations.

The consequence of post-treatment survival time is first compared in the 6-OHDA model. In both time-points, lesions produced different extents of neuronal loss among the three cell types. The percentage cell loss showed a more pronounced loss in the TH+ population

compared to the CB+ and TH+/CB+ populations. Furthermore, most of the TH+ loss was in the ventral tier of SNC and SNL but less severe in the dorsal tier of SNC and VTA, as seen in the 1-month post-treatment (Chapter 3) and consistent with previous reports (German et al., 1989; Liang et al., 1996b; Airaksinen et al., 1997; Petroske et al., 2001). In addition, the proportion of TH+ neurons which were also co-localised with CB+ was higher on the lesioned hemisphere, giving some evidence that TH+/CB+ neurons were more likely to be retained after lesion.

My data also illustrate that TH-/CB+ neurons respond differently from TH+/CB- neurons. General linear modelling showed that post-treatment survival period was not a significant factor in the TH+ population in the 6-OHDA-treated mice, implying that there was an irreversible, but not progressive, cell death over the period examined. Moreover, there was no cell count x time interaction, meaning that the proportions of neuronal populations did not change significantly over this period. This is surprising because *post-hoc* *t*-test revealed a treatment x time interaction that only affected the CB+ and TH+/CB+ subtypes – TH-/CB+ and TH+/CB+ neurons were reduced on the contralateral side over time but the number of TH+/CB+ neurons increased, or recovered, on the ipsilateral side. This suggests that the cell count x time interaction was not statistically powerful enough to show a time difference, as confirmed by the *P* value. As a consequence of the changes in TH-/CB+ and TH+/CB+ neurons with respect to time, three months after lesion, the numbers of TH-/CB+ and TH+/CB+ neurons did not differ between treated or untreated sides (in contrast to the 1-month post-treatment finding). It is plausible that TH+/CB- neurons, by increasing the co-expression of CB, attempted to confer some resistance to the lesion over time, thereby more TH+/CB+ remained on the ipsilateral side in the 3-month post-treated mice.

There was also GABAergic cell loss, presumably from the SNR, where GAD65/67 immunostaining was most abundant. Statistical analyses showed that GAD65/67+ neurons were progressively lost from 1 to 3 months after 6-OHDA lesion from both treated and untreated hemispheres, while the lack of treatment x time interactions suggests that this reduction was not exacerbated by the lesion. The significant GAD65/67+ cell loss in the contralateral hemisphere suggests that a bilateral lesion induced by 6-OHDA may have taken place; unilaterally-injected saline controls in future study may be able to justify this result.

In contrast to this finding, striatal GAD levels in the C57Bl/6 paraquat and maneb mouse model showed no significant difference between the 2 weeks and 3 months post-treatments (Thiruchelvam et al., 2003). Tomas-Camardiel *et al.* also found no decrease in GAD mRNA levels in the striatum following manganese treatment in aged rats (Tomas-Camardiel et al., 2002). This is likely to be due to the different mechanism of paraquat and 6-OHDA: whereas 6-OHDA involve the generation of hydrogen peroxide and causes irreversible nigrostriatal lesion, the toxicity of paraquat appears to be mediated by the formation of superoxide radicals (Day et al., 1999; Dauer and Przedborski, 2003). Moreover, it was found that the initial paraquat insult to rodents does not itself induce any neuronal loss by predisposes to the toxic consequences of subsequent challenges (McCormack et al., 2005; Purisai et al., 2007). Since the paraquat mouse model may involve multiple injections, and that its "priming" effect results in microglial activation, its effect on GABAergic neurons may be different from this 6-OHDA-induced neurodegeneration.

Comparing 1- to 3-month post-treatments in the MPTP/p model, there were several similar trends: first, the loss of TH+ neurons was proportionately greater than the loss of CB+ cells at both time points as expected; second, more TH+/CB+ neurons were found in the MPTP/p-treated mice compared to the controls, which supported the 6-OHDA data that there could be

an increase in CB+ expression to confer resistance in response to the neurotoxin; third, the cell counts were all significantly different among the three neuronal populations and treatment groups, except that the number of TH+ vs CB+ neurons in the MPTP/p-treated mice which could be due to the lesion. Surprisingly, the saline and probenecid controls significantly differ in the CB+ and TH+/CB+ populations, which suggest that the CB-containing populations have different characteristics to the TH+ only neurons.

Post-treatment survival period was a significant factor in the MPTP/p model. The most striking finding was that CB+ neurons were progressively lost in the uninjected hemisphere (6-OHDA model) and in the control mice in the MPTP/p model. If CB+ neurons are also progressively lost in the human brain, the proportion of TH+/CB- neurons would increase and may become more vulnerable to insults. This might be the underlying cause of PD pathogenesis in old age. On the other hand, there was an increase, or recovery, of CB+ neurons in the MPTP/p mice. There could be an increase in TH+ and CB+ co-expression in order to confer neuroprotection during lesion. Taken together, my experiments showed that only the loss of GABAergic neurons was exacerbated with time. Future work could include injecting a low dose of MPTP/p at a young age but only sacrifice after 1-2 years (normal expected longevity of mice) to test an age effect, to mimic the human PD characteristics.

It is difficult to be definitive about the relationship between progressive neuronal loss and PD pathogenesis because even studies of the normal nigrostriatal degeneration process gave conflicting results – some groups reported that in human, there was a reduction in the overall volume of SN with time (Ma et al., 1999; Chen et al., 2000; Cabello et al., 2002; Chu et al., 2002) and a decrease in SN neuronal number (McGeer et al., 1977; Mann et al., 1984; Fearnley and Lees, 1991; Stark and Pakkenberg, 2004). On the other hand, a few non-stereological studies have reported no cell loss in SN with age (Muthane et al., 1998; Kubis

et al., 2000; Uchida et al., 2003). These contrasting results may be due to differences in staining methods, differences in the delineation of the SN region or the use of stereology. In non-human models of Parkinsonism, the type of animal model is obviously the major variable. For C57Bl/6 mouse models, some report age-related changes in the nigrostriatal system (Ricaurte et al., 1987; McNeill and Koek, 1990; Tatton et al., 1992), but others suggest no age-related reductions in nigral DA neurons (McNeill et al., 1988; McNeill and Koek, 1990). In this study, the 6-OHDA and chronic MPTP/p models have shown to be good representative models of PD pathology because they both produced persistent neuronal loss in the midbrain from the 1-month to the 3-month post-treatment. The present data also suggest that there may be a gradual loss of CB+ neurons and/or TH+/CB+ neurons over time, unrelated to toxin treatment; the major loss of neurons due to progressive neurotoxicity was GABAergic. It is possible that the mice used in this study were not old enough, or that the post-treatment survival time could be longer, in order to elicit a similar ageing effect in the DA neurons. If this is the case, our data would suggest that neurodegeneration and ageing have a more complicated interaction than previously thought. If CB-containing and GABAergic neurons were indeed preferentially affected with respect to age and lesion, assessing the number of midbrain neurons after 6 or 12 months post-treatment might produce a greater change. Such future work is made possible by the 6-OHDA and the chronic MPTP/p mouse models.

The results so far have shown that PD pathology involves multiple factors, which also interact in a complex network. The increased vulnerability of the DA neurons with age is considered to be a result of oxidative stress caused by the increased generation of reactive oxygen species (Knapowski et al., 2002; Giovannelli et al., 2003; Stark and Pakkenberg, 2004) and a reduced capacity of the anti-oxidant components (Itoh et al., 1996; Naoi and Maruyama, 1999). However, the lack of a relationship between striatal areas with higher

dopamine content and striatal areas and vulnerability to PD, suggests that the oxidative stress hypothesis is not an explanation for DA cell loss (Kish et al., 1992). On the other hand, accumulating evidence shows that subsets of microglia in the brain become activated with the advancement of ageing (Mrak et al., 1997; Mrak and Griffin, 1997; Rozovsky et al., 1998; Sugama et al., 2003a). Sugama *et al.* showed massive microglial activation surrounded DA neurons in the SN in older mice at 7 days, contrast to the lack of microglial activation in young mice after MPTP treatment in C57BL/6 mice (Sugama et al., 2003a). The role of oxidative stress and the effect of salicylic acid as an anti-oxidant and anti-inflammatory agent will be examined in the Chapter 6, and would compliment on the findings in this chapter.

Figure 4.1

Representative microphotographs demonstrating TH+ fibers in the rostral striatum (A) and caudal striatum (B) 3 months after 6-OHDA treatment.

At high magnification, in both rostral (A, C) and caudal (B, D) striatum, there was a substantial loss of TH+ fibers (compare A & C and B and D).

Scale bar = 50 μm

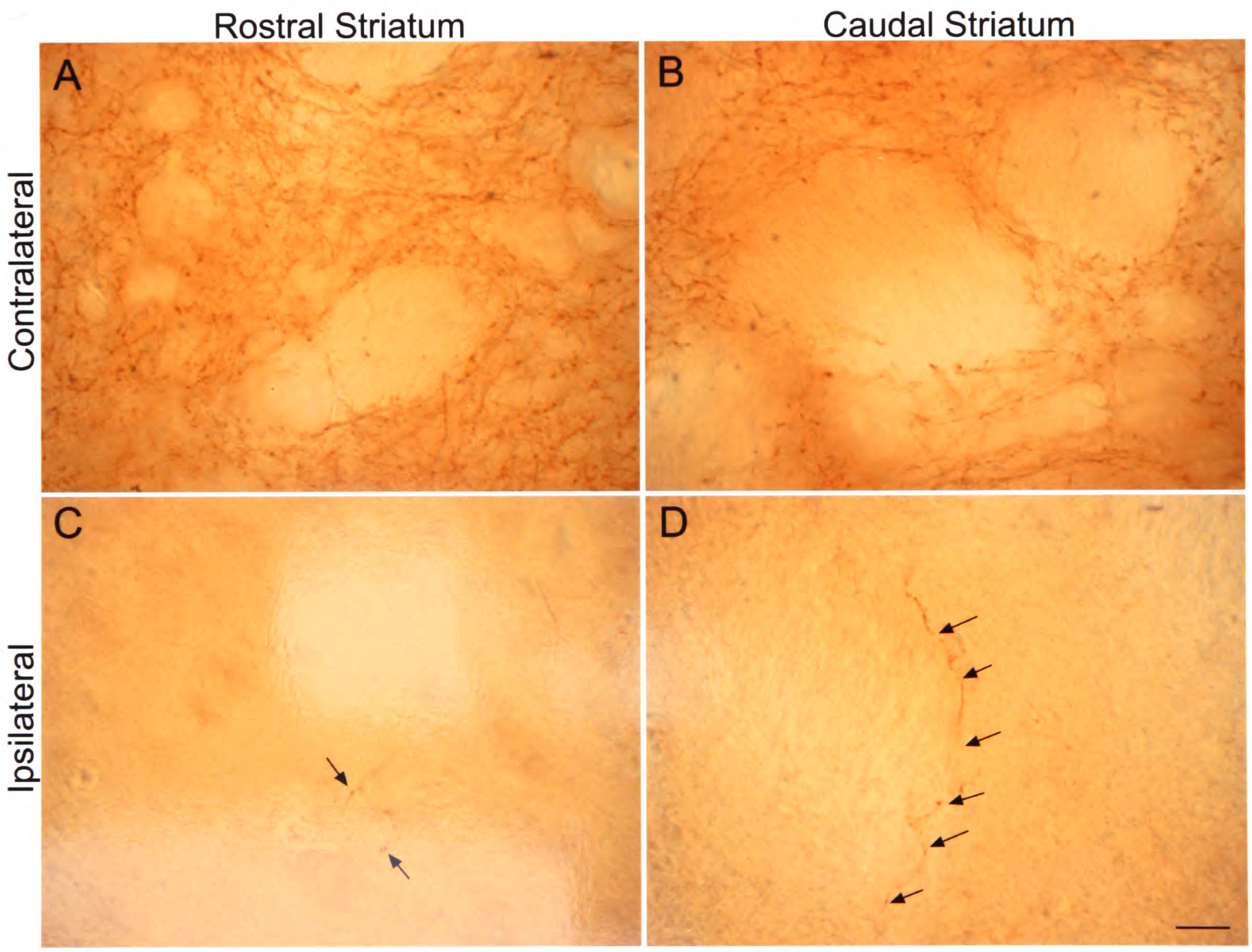

Rostral Striatum
Caudal Striatum
Contralateral
Ipsilateral
A
B
C
D

Figure 4.2

Double immunoflourescent labelling of TH and CB in the SN 3 months after 6-OHDA treatment.

Coronal sections through the midbrain at the level of the SN comparing TH and CB immunoreativity on the side contralateral (A, C, E) and ipsilateral (B, D, F) to the injection of toxin. TH+ neurons were widely distributed in the SN (A) but were substantially reduced on the toxin-treated side (B). CB+ neurons were also found along the SNC and SNL (C) but its number was reduced on the toxin-treated side (D). Some neurons were both TH+ and CB+, both in the contralateral (E) and ipsilateral hemispheres (F).

Scale bar = 100 μm

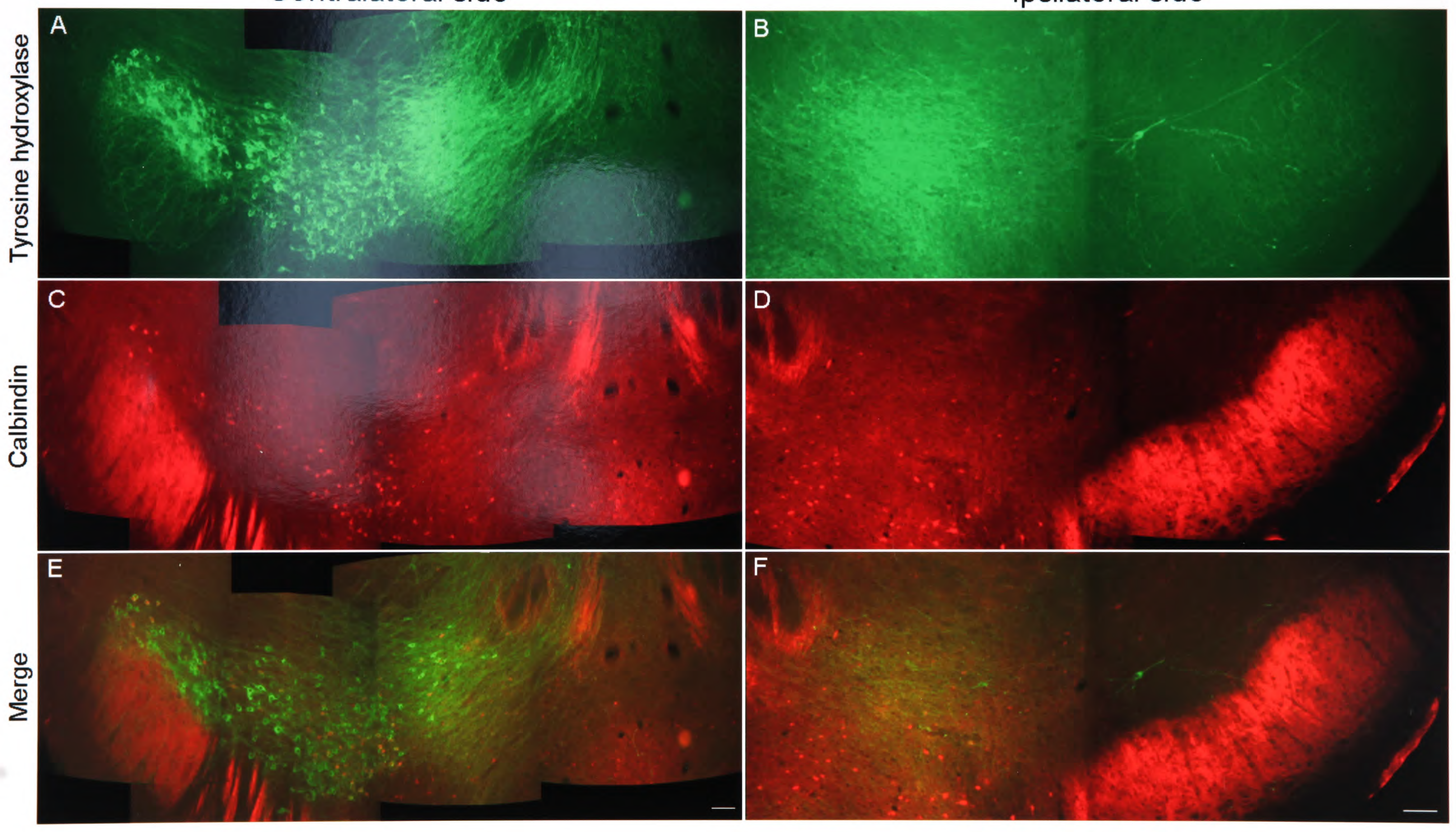

Contralateral side
Ipsilateral side
Tyrosine hydroxylase
Calbindin
Merge
A
B
C
D
E
F

Figure 4.3

Double immunoflourescent labelling of TH and CB in the VTA 3 months after 6-OHDA treatment.

Coronal sections through the midbrain at the level of the VTA comparing TH and CB immunoreativity on the side contralateral (A, C, E) and ipsilateral (B, D, F) to the injection of toxin. TH+ neurons were widely distributed in the VTA (A) but were substantially reduced on the toxin-treated side especially in the SNC and SNL (B). CB+ neurons were also reduced by the toxin treatment (compare C & D). Nevertheless, some neurons were both TH+ and CB+, both in the contralateral (E) and ipsilateral hemispheres (F).

Scale bar = 100 μm

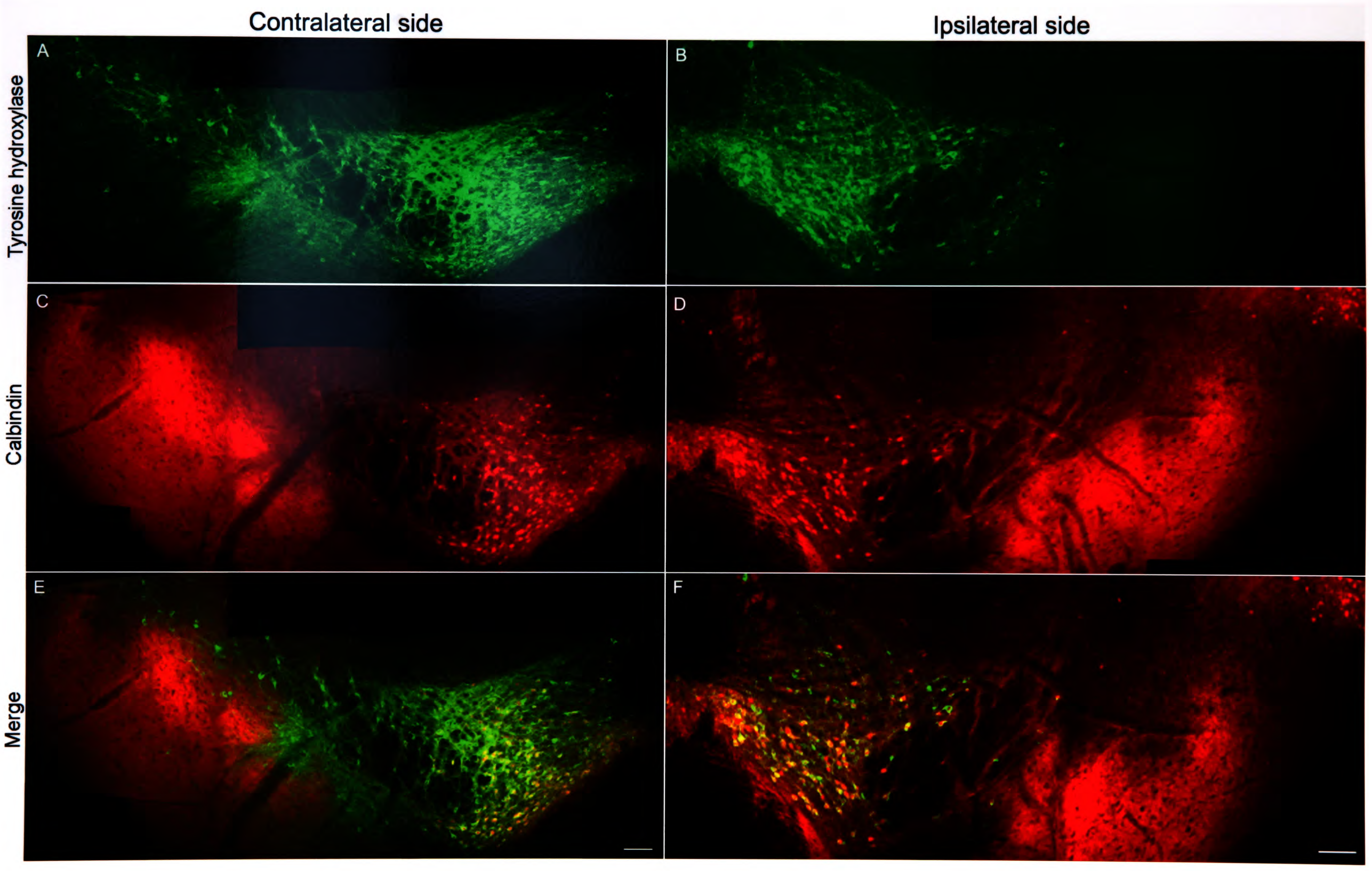

Contralateral side
Ipsilateral side
Tyrosine hydroxylase
Calbindin
Merge
A
B
C
D
E
F

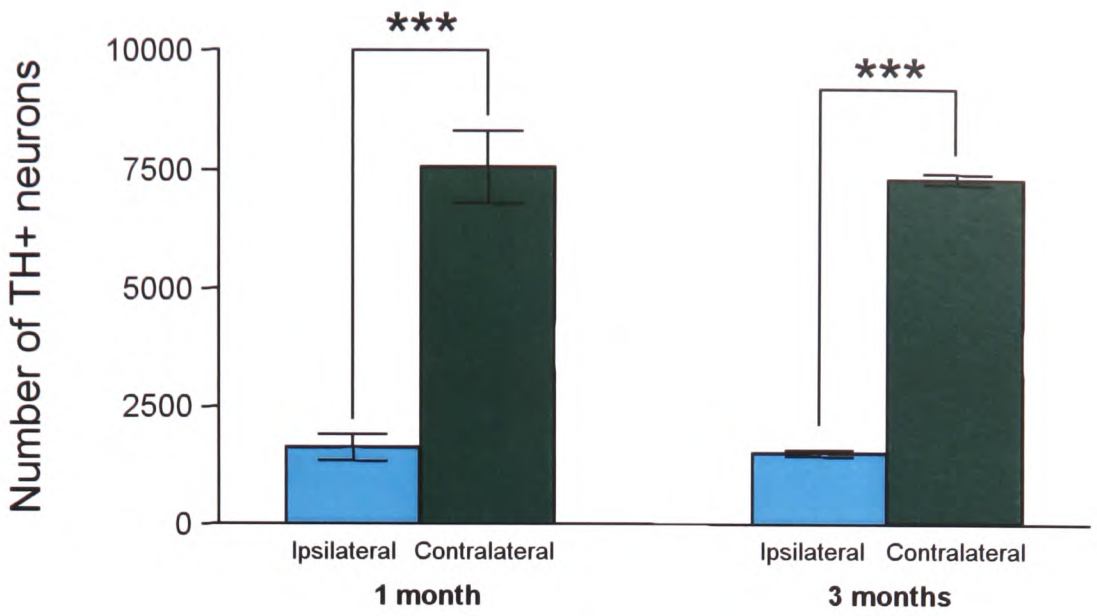
Figure 4.4

Comparison between the 1-month and 3-month post-treatment on the TH+, CB+ and TH+/CB+ neurons in the 6-OHDA model. (Not assessed stereologically)

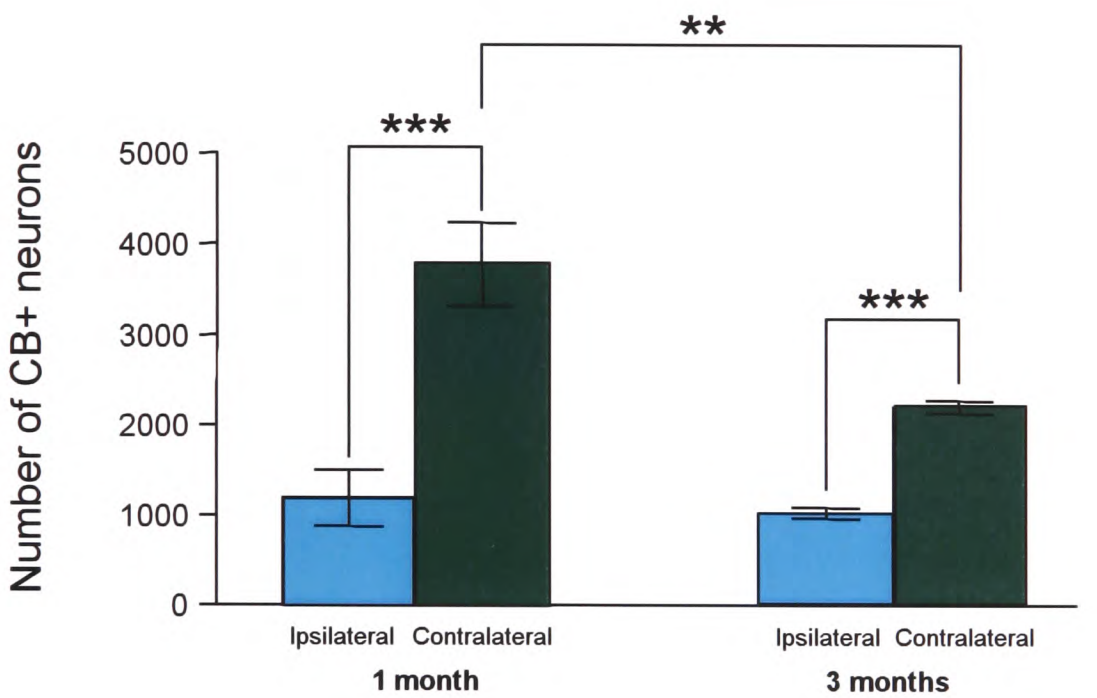
The lesion treatment showed a significantly different effect with respect to time ($F_{(1,6)} = 7.332$; $^{*}P = 0.035$). When compared the one- and three-month post-treatment data, time did not play a significant role and there was no cell count x time interaction.

Post hoc *t*-test further identified the differences: In the 3-month post-treatment data comparing the neuronal counts, there were significant differences on the contralateral side between the TH+ and CB+ ($^{***}P < 0.0001$); TH+ and TH+/CB+ neurons ($^{***}P < 0.0001$), but not between CB+ and TH+/CB+ neurons. On the ipsilateral side, the pattern is the same: there were significant differences on the contralateral side between the TH+ and CB+ ($^{**}P = 0.008$); TH+ and TH+/CB+ neurons ($^{**}P = 0.012$), but not between CB+ and TH+/CB+ neurons. (A) In the TH+ population, there was a paired significance between the contra- and ipsilateral sides in the 3-month post-treated mice ($^{***}P < 0.0001$). When compared with the 1-month data, time had no significant effect on either contra- or ipsilateral sides (B) In the CB+ population, there was a paired significance between the contra- and ipsilateral sides in the 3-month post-treated mice ($^{***}P < 0.0001$). When compared with 1-month post-treatment, there was a significance on the contralateral side ($^{**}P = 0.014$) with respect to time but no significance on the ipsilateral side. (C) In the TH+/CB+ population, there was a paired significance between the contra- and ipsilateral sides in the 3-month post-treated mice ($^{***}P < 0.0001$). When compared with 1-month post-treatment, both the contralateral and ipsilateral sides showed significant differences with respect to time ($^{*}P = 0.044$ and $^{***}P < 0.0001$ respectively).

A


Number of TH+ neurons
10000
7500
5000
2500
0
***
***
Ipsilateral
Contralateral
1 month
Ipsilateral
Contralateral
3 months

B


Number of CB+ neurons
5000
4000
3000
2000
1000
0
**
***
***
Ipsilateral
Contralateral
1 month
Ipsilateral
Contralateral
3 months

C

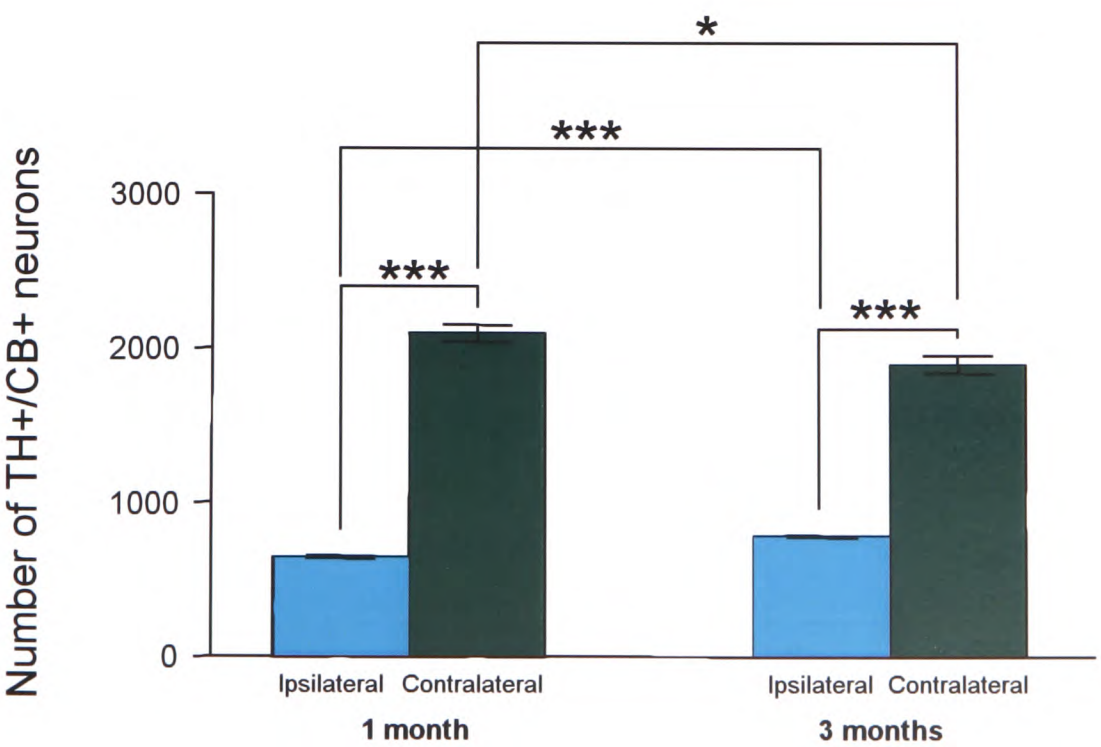

Number of TH+/CB+ neurons
3000
2000
1000
0
*
***
***
***
Ipsilateral
Contralateral
1 month
Ipsilateral
Contralateral
3 months

Figure 4.5

GAD65/67 immunoreactivity in the SN and VTA 3 month after 6-OHDA treatment.

In the substantia nigra, GAD was expressed primarily in the SNR on both the sides contralateral (A) and ipsilateral (B) to the toxin injection.

In the VTA, there are very few GAD+ neurons on either the contralateral (C, arrows) or ipsilateral (D) sides.

Scale bar = 100 μm

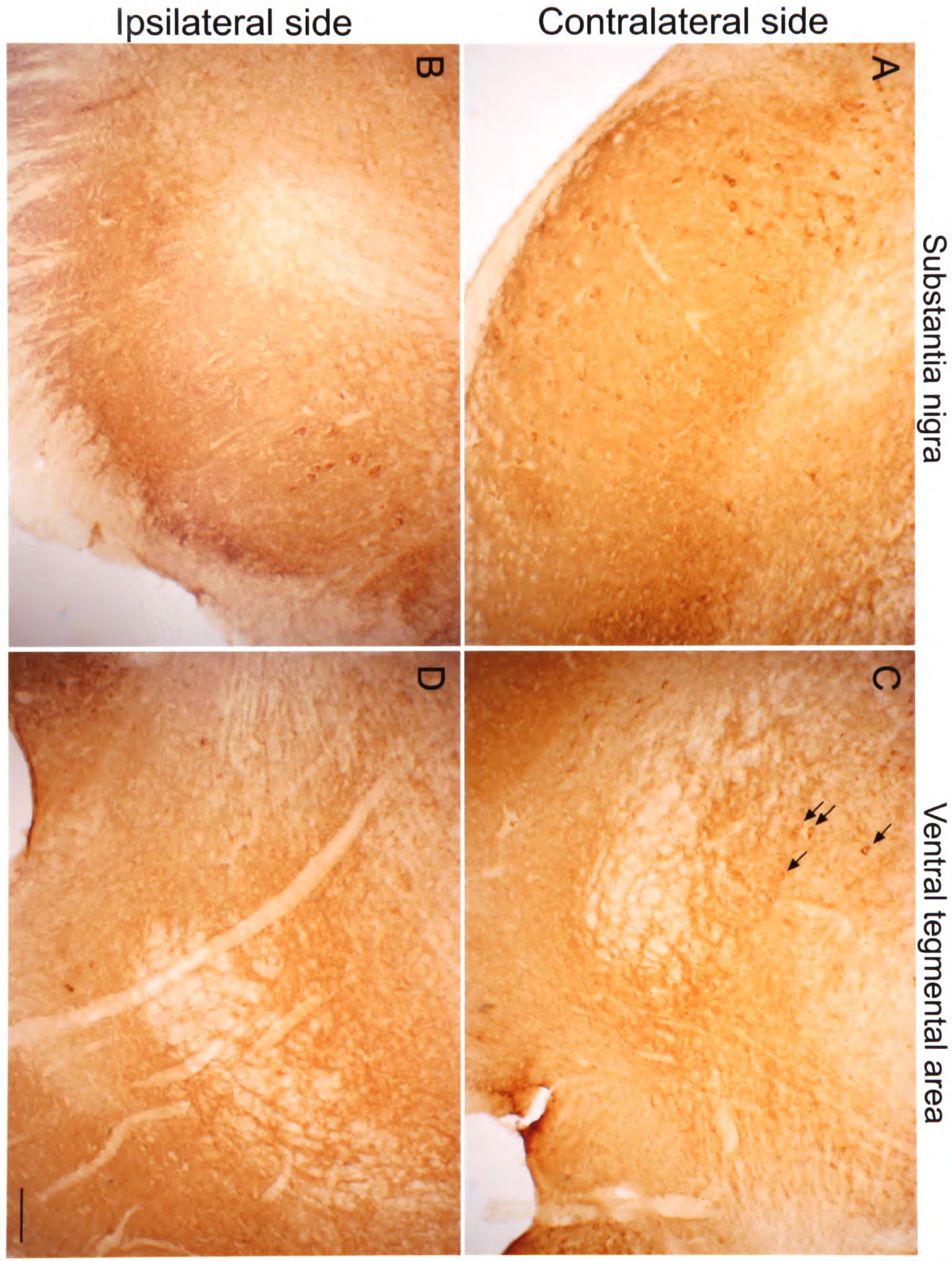

Ipsilateral side
Contralateral side
B
A
Substantia nigra
C
D
Ventral tegmental area

Figure 4.6

Comparison between the 1-month and 3-month post-treatment on the GAD65/67+ neurons in the 6-OHDA model.

The number of immunolabelled neurons were counted in every 1 in 3 sections, then multiplied to obtain the mean neuronal number. In the 3-month post-treated mice, there was a significant difference between the contralateral and ipsilateral side (**$P = 0.001$) but not treatment x time interaction. Post-treatment time significantly affected the GAD65/67+ population ($F_{(1,6)} = 99.792$; $P < 0.0001$) on both contralateral and ipsilateral side (***$P < 0.0001$). The error bars mark SEM.

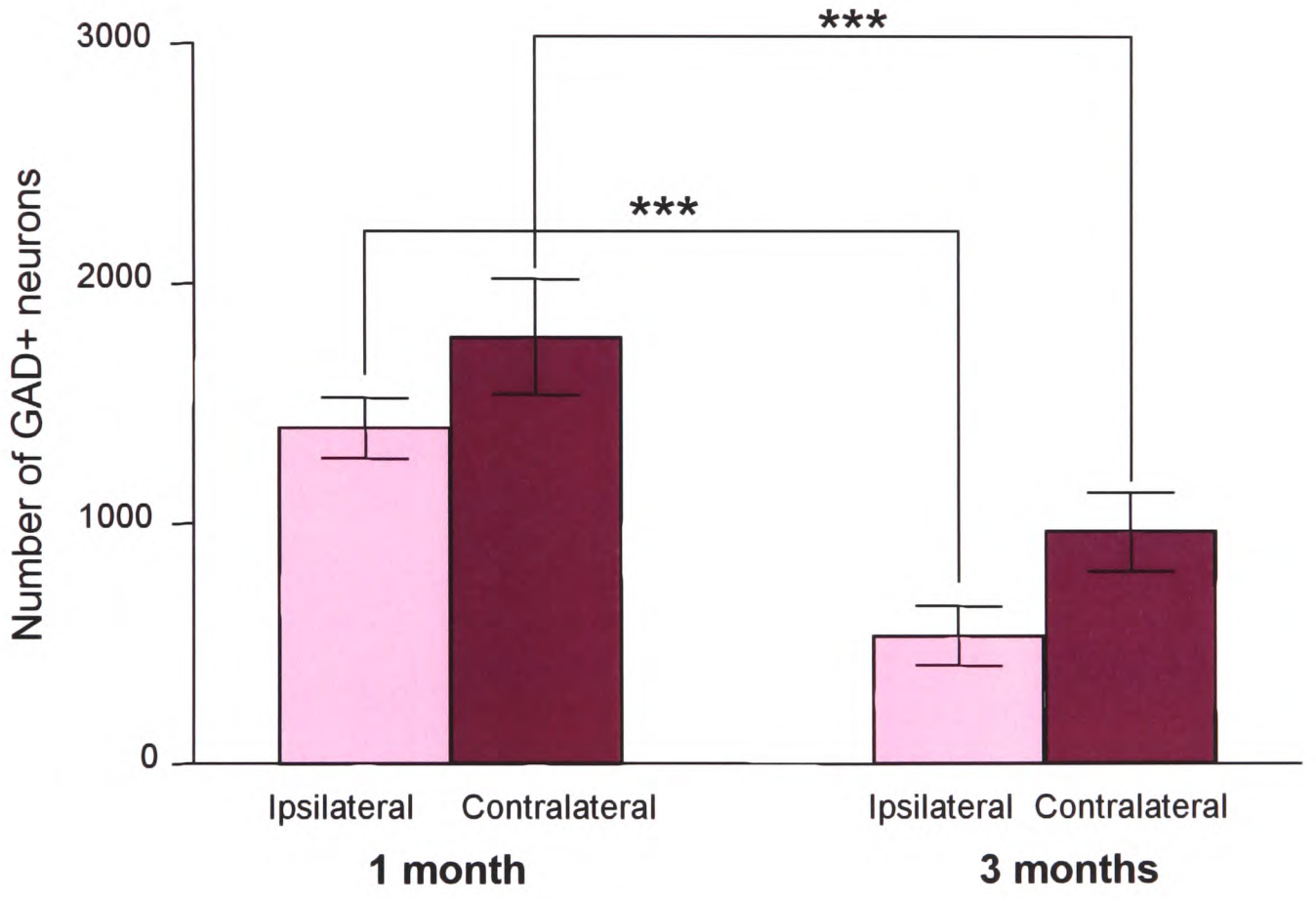

***
***
3000
2000
1000
0
Number of GAD+ neurons
Ipsilateral
Contralateral
Ipsilateral
Contralateral
1 month
3 months

Figure 4.7

TH immunoreactivity in the rostral and caudal striata 3 month following MPTP/p treatment.

Mice were treated with saline (A, B), probenecid (C, D) or MPTP and probenecid (E, F). In the rostral (A, C) and caudal (B, D) striatum at high magnification, TH+ fibers appeared intact in both saline (A, B) and probenecid (C, D) controls. Treatment with MPTP/p results in a large decrease in TH+ fibers in both rostral (E) and caudal (F) striatum.

Scale bar = 10 μm

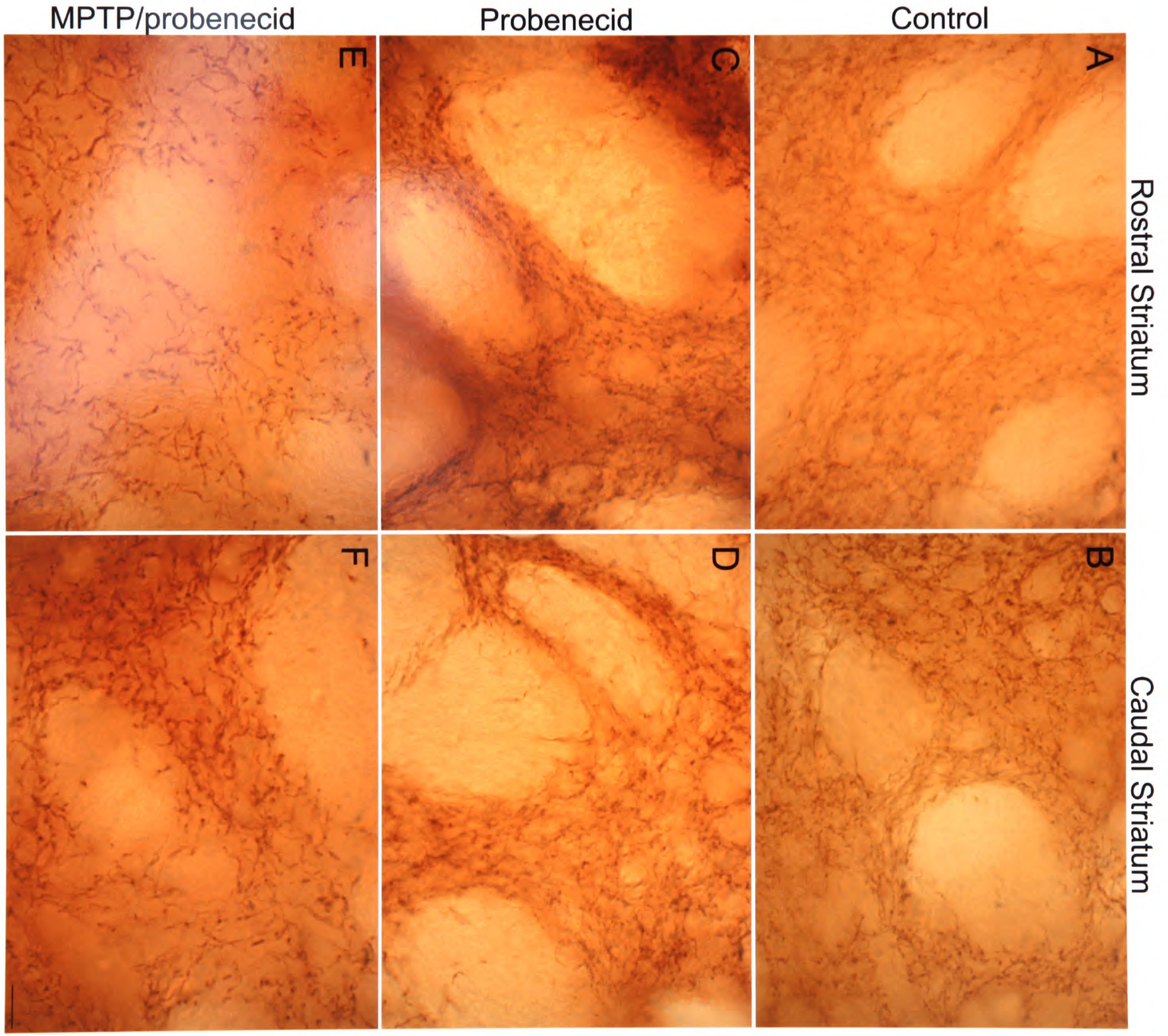

MPTP/probenecid
Probenecid
Control
E
C
A
Rostral Striatum
B
D
F
Caudal Striatum

Figure 4.8

Double immunofluorescent labelling of TH and CB in the SN 3 months after MPTP/probenecid treatment.

Coronal sections through the midbrain of saline control (A-C), probenecid control (D-F) and MPTP/probenecid-treated (G-I) mice. TH (A, D, G) was mostly expressed in the SNC and along the SNR, whereas CB (B, E, H) was found in the SNC near the midline and SNL. In MPTP/probenecid mice there were marked reductions in TH+ (compare G with A and D), CB+ (compare H with B and E) and in TH+/CB+ (compare I with C and F) neurons.

Scale bars = 100 μm

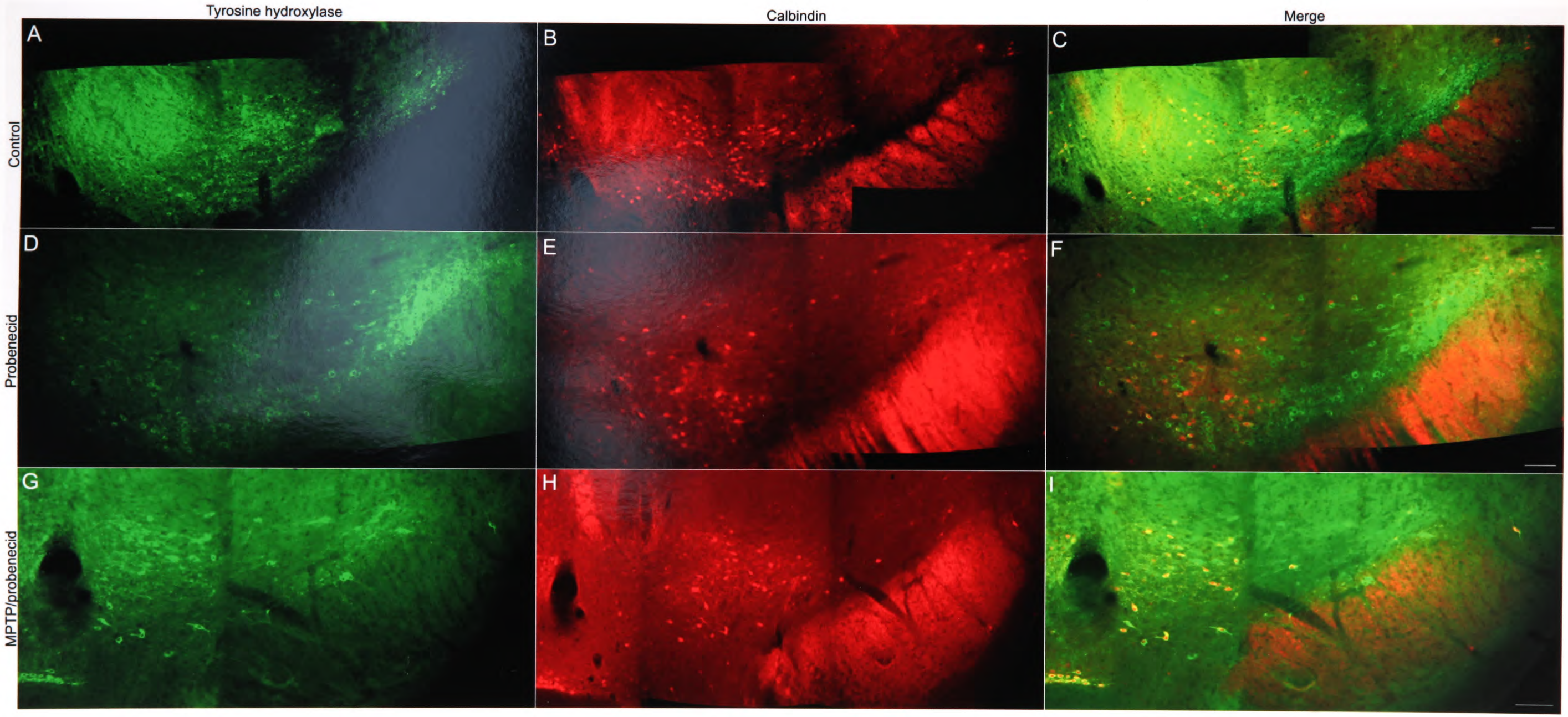

Tyrosine hydroxylase
Calbindin
Merge
A
B
C
D
E
F
G
H
I
Control
Probenecid
MPTP/probenecid

Figure 4.9

Double immunofluorescent labelling of TH and CB in the VTA 3 months after MPTP/probenecid treatment.

Coronal sections through the midbrain of saline control (A-C), probenecid control (D-F) and MPTP/probenecid-treated (G-I) mice. TH (A, D, G) was mostly expressed in the VTA and along the SNC. CB (B, E, H) was mostly found in the VTA. In MPTP/probenecid mice, neuronal loss was predominantly found in the SNC rather than in the VTA amongst the TH+ (compare G with A and D), CB+ (compare H with B and E) and TH+/CB+ (compare I with C and F) populations.

Scale bar = 100 μm

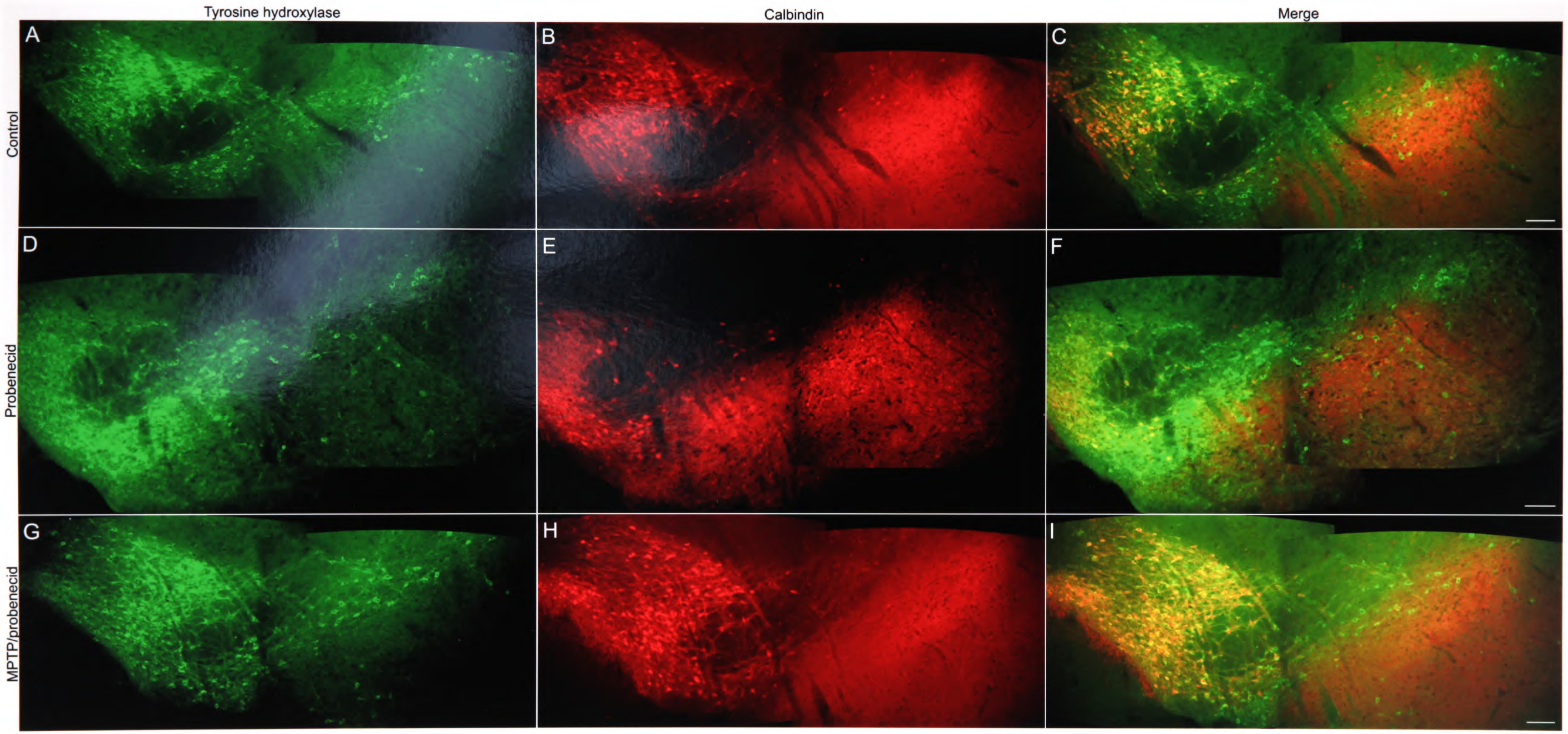

Tyrosine hydroxylase
Calbindin
Merge
A
B
C
Control
D
E
F
Probenecid
G
H
I
MPTP/probenecid

Figure 4.10

Comparison between the 1-month and 3-month post-treatment on the TH+, CB+ and TH+/CB+ neurons in the MPTP/p model. (Not assessed stereologically)

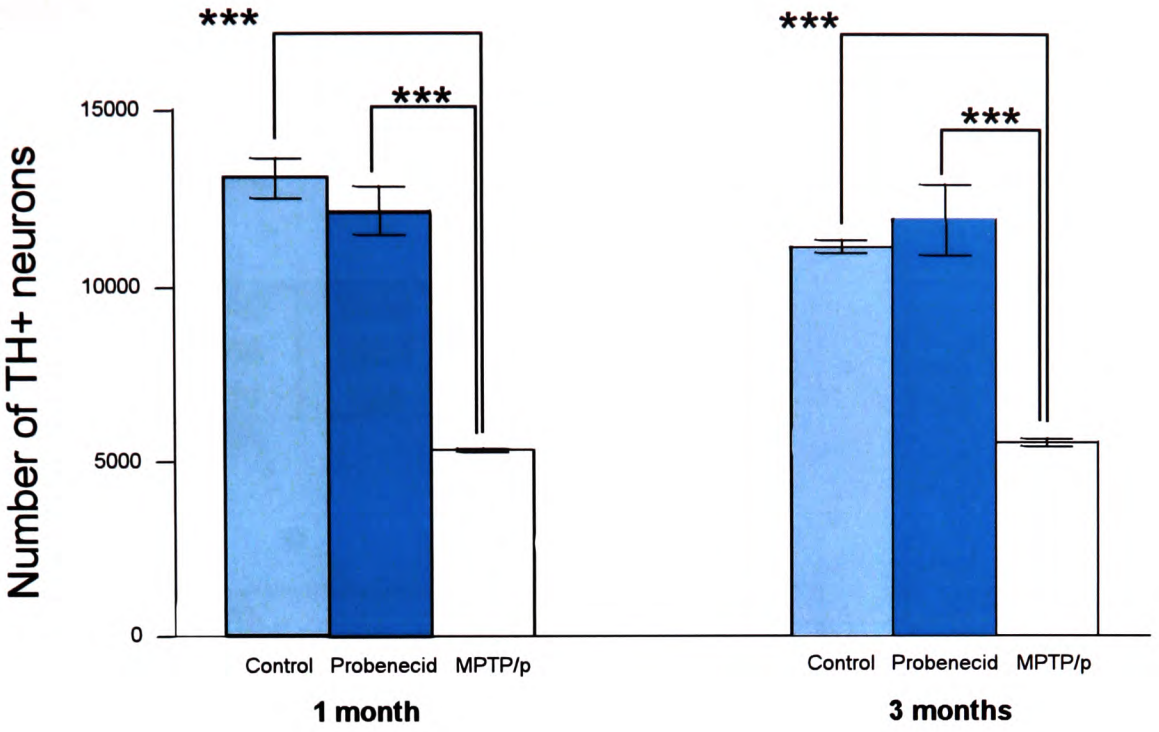
Immunopositive neurons were counted on both hemispheres of the mice, representing bilateral counts. The error bars mark SEM.

When compared the 1- and 3-month post-treatment data, there was no cell count x time interaction. Time played a significant role ($F_{(1,16)} = 4.319$; $*P = 0.05$) and there was a significant treatment x time interaction ($F_{(2,16)} = 6.405$; $**P = 0.009$).

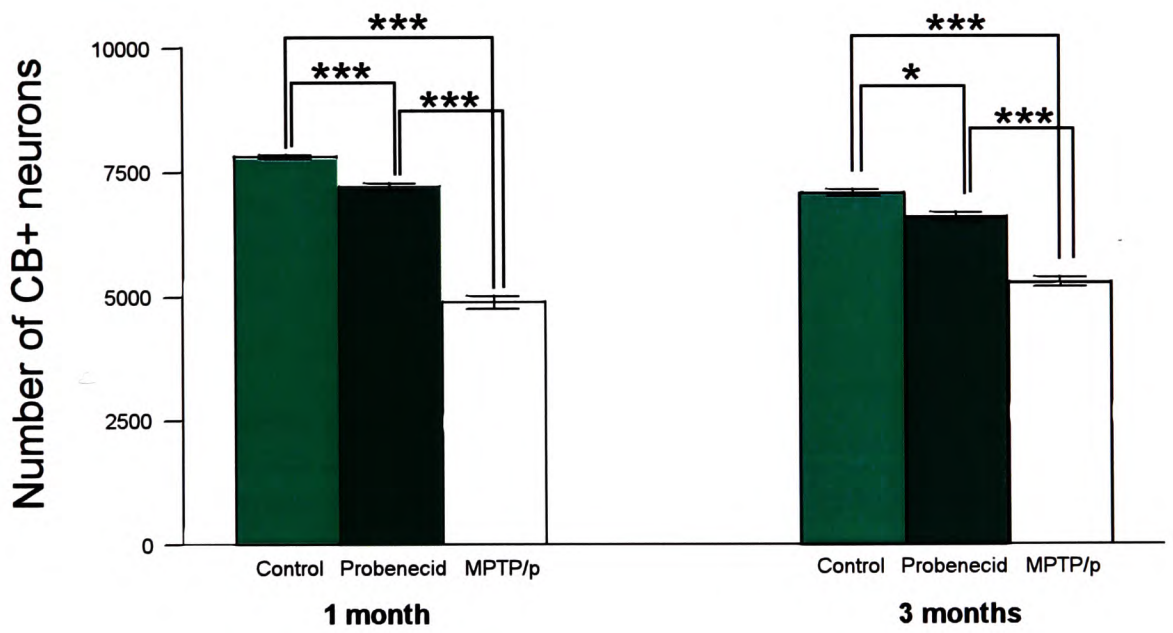
Post hoc *t*-test further identified the differences: In the 3-month post-treatment data comparing the neuronal counts, there were paired significant differences among the number of TH+, CB+ and TH+ and TH+/CB+ neurons in both saline and probenecid controls ($***P < 0.0001$). In the MPTP/p mice, there was no difference between the number of TH+ and CB+ neurons but significant differences between TH+ vs TH+/CB+ ($*P = 0.005$) and CB+ vs TH+/CB+ cell counts ($***P < 0.0001$).

(A) In the 3-month post-treated mice in the TH+ population, significant difference was absent between the saline and probenecid controls, but present between saline vs MPTP/p ($***P < 0.0001$) and probenecid vs MPTP/p ($***P < 0.0001$). (B) In the CB+ population, there were significant differences between saline vs probenecid ($***P = 0.005$), saline vs MPTP/p ($***P < 0.0001$) and probenecid vs MPTP/p ($***P < 0.0001$). (C) In the TH+/CB+ population, all three treatments gave paired significance (saline vs probenecid, $**P = 0.0017$; saline vs MPTP/p, $***P < 0.0001$; probenecid vs MPTP/p, $*P = 0.03$). Post-treatment time only had significant effect on CB+ neurons, in the saline ($***P < 0.0001$), probenecid ($***P < 0.0001$) and MPTP/p-treated mice ($***P = 0.005$).

A


***
***
***
***
15000
10000
5000
0
Number of TH+ neurons
Control
Probenecid
MPTP/p
1 month
Control
Probenecid
MPTP/p
3 months

B


***
***
***
***
*
***
10000
7500
5000
2500
0
Number of CB+ neurons
Control
Probenecid
MPTP/p
1 month
Control
Probenecid
MPTP/p
3 months

C

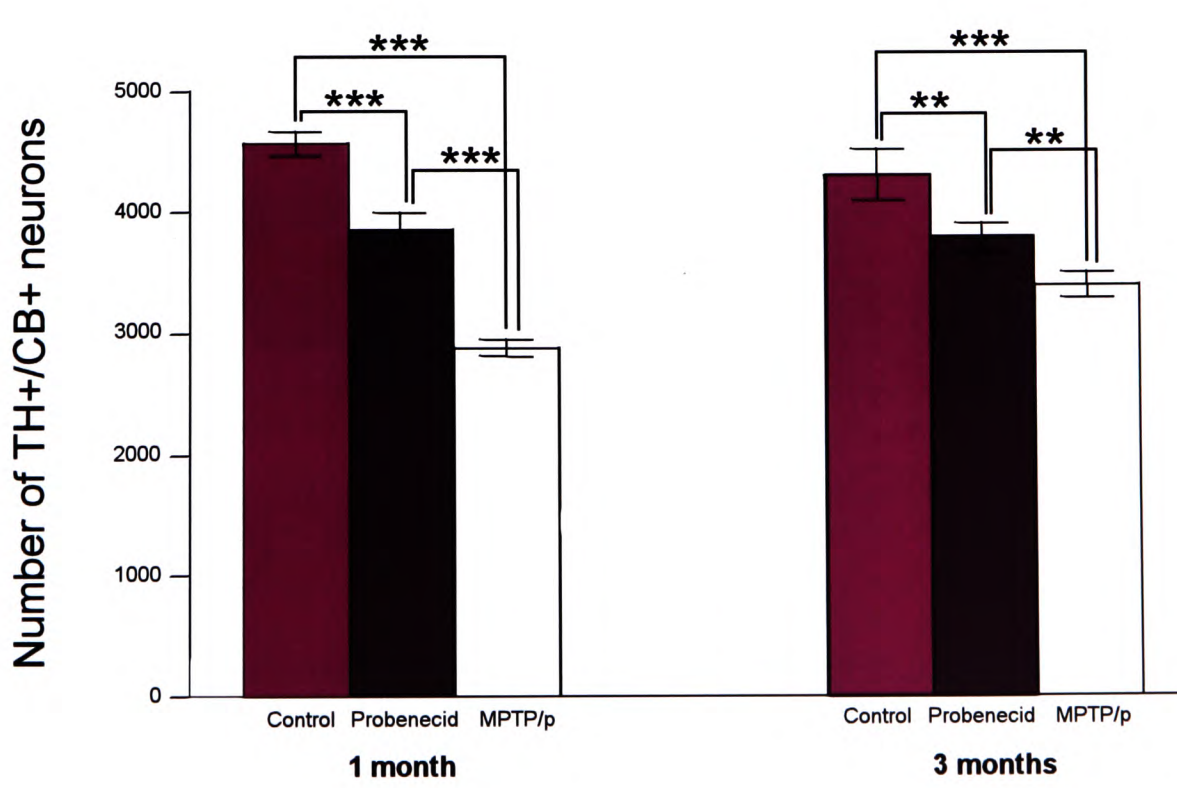

***
***
***
***
**
**
5000
4000
3000
2000
1000
0
Number of TH+/CB+ neurons
Control
Probenecid
MPTP/p
1 month
Control
Probenecid
MPTP/p
3 months

Table 4.1

6OHDA 3 months

	TH	SEM	CB	SEM	Coloc	SEM	% TH+ that are TH+/CB+
Contralateral (unlesioned)	7298	115.1	2202	69.59	1892	56.74	26%
Ipsilateral (Lesioned)	1500	62.2	1020	60.62	783	6.964	52%
Neuronal loss	79%		54%		59%		

GAD 3 months

	GAD	SEM
Contralateral (unlesioned)	968	165.9
Ipsilateral (Lesioned)	531	124
Neuronal loss	45%	

Statistical Analyses

GLM

Within-subject factors	Sig.	
Count x time	x	
Treatment x time	√	F(1,6) = 7.332; *P* = 0.035
Between-subject factor		
Time	x	

***Post-hoc t*-test**

Cell count		Sig.	
Contralateral	TH vs CB	√	*P* < 0.0001
Contralateral	TH vs TH+/CB+	√	*P* < 0.0001
Contralateral	CB vs TH+/CB+	x	
Ipsilateral	TH vs CB	√	*P* = 0.008
Ipsilateral	TH vs TH+/CB+	√	*P* = 0.0012
Ipsilateral	CB vs TH+/CB+	x	
Treatment			
TH	Contra- vs Ipsi-	√	*P* < 0.0001
CB	Contra- vs Ipsi-	√	*P* < 0.0001
TH+/CB+	Contra- vs Ipsi-	√	*P* < 0.0001
Time (1- vs 3-month)			
TH	Contralateral	x	
	Ipsilateral	x	
CB	Contralateral	√	*P* = 0.014
	Ipsilateral	x	
TH+/CB+	Contralateral	√	*P* = 0.044
	Ipsilateral	√	*P* < 0.0001

GLM (GAD)

Within-subject factor	Sig.	
Treatment	√	F(1,6) = 76.079; *P* < 0.0001
Treatment x time	x	
Between-subject factors		
Time	√	F(1,6) = 99.792; *P* < 0.0001

***Post-hoc t*-test**

Treatment (3 month)	Sig.	
Contra- vs Ipsi-	√	*P* = 0.001
Time		
Contralateral side	√	*P* < 0.0001
Ipsilateral side	√	*P* < 0.0001

MPTP 3 months

	TH	SEM	CB	SEM	Coloc	SEM	% TH+ that are TH+/CB+
Saline	11108	183	7068	75	4304	215	39%
Probenecid control	11866	988.1	6589	88.7	3774	123.9	32%
MPTP/p	5520	113.4	5281	90.1	3388	104.2	61%
Neuronal loss	50%		25%		21%		

Statistical Analyses

GLM

Within-subject factors	Sig.	
Count (TH, CB, TH+/CB+)	√	$F(1.383,22.134) = 350.172$; $P < 0.0001$
Count-Treatment	√	
Count-Time	x	
Between-subject factor		
Treatment	√	$F(2,16) = 220.635$; $P < 0.0001$
Time	√	$F(1,16) = 4.319$; $P = 0.05$
Treatment x Time	√	$F(2,16) = 6.405$; $P = 0.009$

***Post-hoc t*-test**

Cell count		Sig.	
Saline	TH vs CB	√	$P < 0.0001$
Saline	TH vs TH+/CB+	√	$P < 0.0001$
Saline	CB vs TH+/CB+	√	$P < 0.0001$
Probenecid	TH vs CB	√	$P < 0.0001$
Probenecid	TH vs TH+/CB+	√	$P < 0.0001$
Probenecid	CB vs TH+/CB+	√	$P < 0.0001$
MPTP/p	TH vs CB	x	
MPTP/p	TH vs TH+/CB+	√	$P = 0.005$
MPTP/p	CB vs TH+/CB+	√	$P < 0.0001$

Treatment		Sig.	
TH	Saline vs Probenecid	x	
TH	Saline vs MPTP/p	√	$P < 0.0001$
TH	Probenecid vs MPTP/p	√	$P < 0.0001$
CB	Saline vs Probenecid	√	$P = 0.005$
CB	Saline vs MPTP/p	√	$P < 0.0001$
CB	Probenecid vs MPTP/p	√	$P < 0.0001$
TH+/CB+	Saline vs Probenecid	√	$P = 0.0017$
TH+/CB+	Saline vs MPTP/p	√	$P < 0.0001$
TH+/CB+	Probenecid vs MPTP/p	√	$P = 0.03$

Time (1- vs 3- month)		Sig.	
Saline	TH	x	
Saline	CB	√	$P < 0.0001$
Saline	TH+/CB+	x	
Probenecid	TH	x	
Probenecid	CB	√	$P < 0.0001$
Probenecid	TH+/CB+	x	
MPTP/p	TH	x	
MPTP/p	CB	√	$P = 0.005$
MPTP/p	TH+/CB+	x	

5 Anatomical and morphological evidence that striatal and dorsal raphe afferents innervate TH+ and CB+ neurons in the mouse midbrain

5.1 Introduction

In the previous chapters, I have illustrated that genetic expression and protein profiles of different neurons may contribute to their differential vulnerability in Parkinson's disease. In particular, CB may have to work in synergy with other genetic or protein partners. Given that the basal ganglia are made up of neuronal circuits, the key to understanding CB's role in the DA neurons could lie in their connections with other neurons, i.e. how they are regulated. The differential inputs to DA cell bodies and dendrites located in the midbrain are mirrored by differential ion conductances in these various sectors of DA neurons (Fallon and Loughlin, 1995). These characteristics may underpin their complex physiological properties. I therefore took an anatomical and morphological approach.

I focused on two innervations: the striato-nigral and the raphe-nigral pathways. Firstly, the striatal projection neurons are studied because the striatum is a major contributor of basal ganglia input to the dopamine system and the major recipient of dopamine input (Joel and Weiner, 2000). They play critical roles not only in Parkinson's disease, but in other major neurological and psychiatric disorders (DeLong, 1990; Albin et al., 1995; Rogers et al., 1998; Graybiel and Rauch, 2000; Meyer-Lindenberg et al., 2002; Saka and Graybiel, 2003; Wichmann and DeLong, 2003; Chao and Nestler, 2004), as well as in motor control and habit and reward learning (Gerfen, 1992; Graybiel, 2000; Packard and Knowlton, 2002). Secondly, the raphe-nigral pathway has been of great interest because of its implications in stress, anxiety and depression. Much functional data indicate that this pathway and the major neurotransmitter it releases, 5-HT, affect nigral function (Blackburn et al., 1980; Blackburn et al., 1982b; Blackburn et al., 1982a; Corvaja et al., 1993).

The most detailed analysis on the DA circuits with the striatum was reviewed by Joel and Weiner (Figure 5.1) (Joel and Weiner, 2000) using rat and primate models. In rats, the striatal

projections to DA cell bodies and proximal dendrites arise mainly from the limbic striatum, which projects to both the dorsal and ventral tiers, with the exception of the group of DA cells in the SNR. In contrast, the projections of the associative and motor striatum to DA cell bodies and proximal dendrites are restricted to the ventral tier, to its medial and lateral aspects, respectively. The reverse is true with regard to striatal projections to the ventrally extending dendrites of DA cells. Most of these projections arise from the matrix of the associative and motor striatum, and are directed to the medial and lateral SNR, respectively, whereas limbic striatal projections are restricted to the most medial SNR. In the three striatal subdivisions, different sets of neurons project to the DA cell bodies and proximal dendrites or to the ventrally extending DA dendrites. In the motor and associative striatum, these sets correspond to the patch and matrix compartments, respectively. Similarly, in primates, the main striatal input to the DA cell bodies arises from the limbic striatum, which projects to most of the DA system (except for the more lateral and ventral parts of the SN), with some contribution from a specific set of neurons in the motor and associative striatum, which projects to subregions within the main horizontal band and to the DA columns.

The present study focuses on striato-nigral connections of the mouse. To date, the majority of such studies have concentrated on the core-shell projections (Bolam et al., 1979; Somogyi et al., 1981a; Somogyi et al., 1981b), in the context of in drug addiction-related studies (Zocchi et al., 2003) and very few address species differences suggesting that comparisons between mice and other species should be made with caution.

Another challenge in studying striatal outputs is that, despite their functional and clinical importance, the molecular basis for the differential function of these striatal projection neuron pathways remains largely unknown. A recent attempt using fluorescent activated cell sorting (FACS)-array profiling in juvenile and adult mouse brains has identified a new set of

genes (e.g. transcription factors) with restricted expression in the striato-nigral and striato-pallidal neurons (Lobo et al., 2006). These results underscore the need to assess specific input-neuron interactions using anatomical and morphological experiments.

Studies of the raphe-nigral pathway have mostly focused on 5-HT-containing neurons, which provide a major input to the SN from the dorsal raphe nucleus (DRN) (Corvaja et al., 1993). Injections of retrograde tracer into the SN showed neuronal cell bodies in the DRN but not the median raphe nucleus (MRN) (Miller et al., 1975; Bunney and Aghajanian, 1976; Dray et al., 1976; Imai et al., 1986; Wirtshafter et al., 1987). However, similar injections into the VTA revealed neuronal cell bodies within both the DRN and MRN (Simon et al., 1979). Injection of anterograde tracers into the DRN resulted in labelled axon varicosities in the cat and rat SNC and SNR (Bobillier et al., 1976; Vertes, 1991; Corvaja et al., 1993) as well as the VTA (Vertes, 1991). The axon terminals from the DRN form asymmetrical synapses with dendrites and spines in the SN, some of which displayed TH-immunoreactivity (Corvaja et al., 1993) and some dorsal raphe inputs project to the VTA where they form both symmetrical and asymmetrical synapses (Van Bockstaele et al., 1993; Bacon, 2002)

5.2 Aims

- To examine the synaptic targets of the striato-nigral and raphe-nigral projections in the mouse
- To determine whether TH+ and CB+ neurons in the VTA are postsynaptic targets of the striato-nigral and/or the raphe-nigral terminals in an attempt to shed light on the differences between three types of neurons (TH+, CB+ or TH+/CB+). This was studied using triple fluorescent-labelling and will provide the immunocytochemical evidence.

- TH+ or CB+ neurons were independently examined under electron microscopy to provide the ultrastructural evidence.
- To compare the ultrastructural characteristics of the striato-nigral terminals with those of the raphe-nigral terminals onto TH+ or CB+ neurons.

5.3 Methods

A total of four male, C57/Bl6 mice (Harlan) weighing an average of 25 g were used for anterograde neuronal tracing with BDA (see Chapter 2.2.2). The coordinates for stereotactic surgery were taken from 'The Mouse Brain in stereotaxic coordinates' (Paxinos and Franklin, 2004). For the striatal injection (n=1): -0.2 mm posterior from Bregma, 2.0 mm lateral from Bregma, and 2.5 mm ventrally from the brain surface. For the dorsal raphe injection (n=2): 4.36 mm posterior from the Bregma, 0 mm lateral from Bregma, and 2.5 mm ventrally from the brain surface.

The BDA tracer injection sites were first revealed with ABC and DAB to determine their precise locations and the extent of the injections. Subsequently, three sets of serial midbrain sections were processed for a) triple immunofluorescence; b) electron microscopy (EM) for TH+ neurons and c) EM for CB+ neurons.

5.3.1 Triple Immunofluorescence

Brain sections, 50 μm thick, taken from the striatal and dorsal raphe injections were processed respectively to reveal the anterogradely labelled fibres and for immunofluorescence as described (see Chapter 2.4.2). Sections were incubated over 48 hours at 4°C, using a polyclonal rabbit antibody against TH (BioMol; 1:1000) and a mouse monoclonal antibody against CB (Swant; 1:1000) in a solution containing 0.1% Triton-X in

PBS. Sections were then washed in PBS. Preliminary studies demonstrated almost identical immunostaining patterns regardless whether the sections were incubated sequentially or simultaneously with the three secondary antibodies. Hence, sections were incubated with all three secondary antibodies for 2 hours at room temperature: using Cy3-coupled streptavidin (Jackson ImmunoResearch; 1:1000) to reveal the BDA fibres, goat anti-mouse Alexa Fluor 488 (Molecular Probes; 1:500) for CB and Cy5-coupled goat-anti-rabbit antibody (Jackson ImmunoResearch, 1:400) for TH, all in PBS. Triple-labelled sections were observed under a DMRB fluorescent microscope (Leitz, Wetzlar, Germany) with epifluorescence illumination equipped with three filter blocks: L5 (excitation filter BP, 480/40 nm; reflection short-pass filter, 505 nm; suppression filter BP, 527/30 nm), Y3 (excitation filter BP, 545/30 nm; reflection short-pass filter, 565 nm; suppression filter BP, 610/75 nm), and Y5 (excitation filter BP, 620/60 nm; reflection short-pass filter, 660 nm; suppression filter BP, 700/75 nm). They were used for the excitation of Alexa Fluor 488 (peak excitation at 488nm), Cy3 (peak excitation at 543 nm) and Cy5 (peak excitation at 633nm) respectively. Images recorded through a CCD camera (model C4742-95, Hamamatsu, UK) were analysed and displayed using the OpenLab software (version 3.1.4, Improvision, UK). Since the excitation and emission spectra of the three secondary antibodies has little overlap with each other, no "bleed-through" has been observed.

5.3.2 Electron microscopy

The BDA tracer was revealed with ABC and DAB as the chromogen, while monoclonal TH (DiaSorin; 1:1000) or CB (Swant; 1:1000) primary antibodies were revealed with the PAP protocol and SG as the chromogen (see Chaper 2.4.3). After the neurons of interest had been documented under light microscopy, the sections were processed for EM, and series of 70 nm sections examined in the electron microscope. .

5.4 Results

5.4.1 Anterograde tracing into the striatum – injection site and projections to the VTA observed under fluorescence

An injection was made into the right dorsal striatum. The injection site spread along the rostrocaudal direction of the dorsal striatum but the maximal deposition of the anterograde tracer was at approximately 0.2 mm caudal of Bregma, adjacent to the lateral ventricle (Figure 5.2). Many BDA-labelled cell bodies were found at the injection sites and the tracer was distributed throughout the dendritic tree. Although the striatum is a relatively large structure, the tracer deposition did not seem to have contaminated other regions such as the overlying cortex, indicated by the lack of BDA reaction-products.

Striatal BDA-labelled fibers innervated the SN and the VTA (Figure 5.3 & 5.4), mostly ipsilateral to the injection, although a few were found in the left hemisphere. All of the neurons shown with innervations of the striatal fibers were ipsilateral side to the injection. Although most BDA-labelled fibers were found along the rostrocaudal extent of the SNR (Figure 5.3 C & 5.4 C), very few cell bodies containing TH and an almost negligible number of CB+ neurons were located in this region.

As seen in Chapter 3 and 4, triple immunofluroscence showed typical TH immunostaining pattern in the SN (Figure 5.3 A). CB+ neurons could be found in the whole perikarya and dendrites labelled (Figure 5.3 B). These neurons did not distribute evenly along the whole SNC but were confined close to the ventral SNC adjoining the VTA. Smaller CB+ neurons were observed in the supramammillary nucleus (SuM). Close appositions were found between TH+/CB+ neurons and the BDA-labelled fibers at the interface between SNR and medial SNC (Figure 5.3 A-D, box). When the boxed region was observed under high magnification (Figure 5.3 E-H), many striatal fibers appeared to branch out into several

shorter fibers with axonal swellings along their length, some of which were in close apposition with TH+ cell bodies, as well as their proximal and distal dendrites (Figure 5.3 G & H, arrows).

Close to the VTA, some TH+ perikarya were also found in the SNR and the dorsal part of SNC (Figure 5.4 A). In contrast, CB+ neurons were mostly in the VTA (Figure 5.4 B), clearly separated from the SNC by the medial lemniscus (ml). The morphology of BDA-labelled fibers differed between the SNR and VTA (Figure 5.4 C). In the former, they appeared as varicose strings but in the latter as numerous punctate terminals. These terminals were seen alongside dendrites and cell bodies of TH+, CB+ and TH+/CB+ cells in the VTA (Figure 5.4 D, box). At higher magnification, a striatal fiber was closely apposed to a TH+/CB+ neuron perikaryon (Figure 5.4 E-H, arrowhead) while a TH+/CB- neuron was close to two striatal terminals at its cell body (Figure 5.4 E-H, arrows) and another terminal was seen on a TH-/CB+ dendrite (Figure 5.4 E-H, double arrowheads).

Although the triple immunofluorescence data suggest that BDA-labelled striatal fibers come into close apposition with TH+, CB+ and TH+/CB+ neurons in the midbrain, these can only be confirmed as synaptic contacts by examination at the ultrastructural level, a technique that is not compatible with fluorescence techniques. Tissue was therefore prepared for EM.

5.4.2 Striatal terminals forming synaptic junctions with TH+ and CB+ neurons in the VTA

In the absence of three suitable chromogens that can be adequately distinguished in the electron microscope, it was not possible to immunolabel the TH+/CB+ neurons together with the afferent fibres. Hence, midbrain sections were processed *separately* to reveal TH+ and CB+ neurons. The TH+ or CB+ neurons were identified by the grey-black SG reaction-product, whereas the anterogradely labelled terminals contained brown DAB reaction-

product under light microscopy (Figure 5.5 B & C, 5.6 B). Under light microscopy, TH- and CB- immunostaining showed similar expression patterns in SN and VTA to that observed in the triple-labelling experiments. Thereafter, TH+ and CB+ sections from approximately the same level in the VTA were compared. Neurons identified in the light microscope were further processed using a correlated light and electron microscopical examination procedure described previously (Bolam, 1992).

The VTA was chosen for the EM study because, from the previous chapters, most TH+/CB+ neurons are located here. Therefore, if synaptic inputs are observed onto a CB+ cell under EM, it is likely that it is also TH+.

One example for each TH+ and CB+ neuron were shown here. Ultrastructural examination revealed that TH-immunolabelling was present in the cytoplasm and organelles (Figure 5.5 D & E) of cell bodies and dendrites (arrowheads). BDA-labelled striatal fibres made axo-somatic synapses with TH+ neurons which correlated to the close fiber-to-somata apposition found under light microscopy. The synaptic specialisation appeared to be asymmetric (Colonnier, 1968) (Figure 5.5 F, arrows) with thick, complex postsynaptic densities and subjunctional bodies. The axon terminal (Figure 5.5 F, asterisk) contained two mitochondria and round synaptic vesicles near the active zone. In the BDA-labelled afferents, synaptic vesicles were coated with reaction-product, appearing darker than unlabelled terminals (Figure 5.5 G, double arrowheads). Puncta adherentia were observed at the contact area (Figure 5.5 H), suggesting that it may not be a true synaptic junction.

Light microscopic examination revealed CB+ neurons juxtaposed by punctate striatal terminals in the VTA (Figure 5.6 B). Ultrastructural analysis the same cell had an oval-shaped nucleus/nucleolus (Figure 5.6 C) and its soma was rich in organelles, especially

smooth and rough endoplasmic reticulum and mitochondria. A synaptic input was established on the cell body and appeared to be asymmetric (Figure 5.6 D), with thick postsynaptic densities interdigitated at the contact areas. Moreover, varicose strings of labelled striatal afferents had axonal swellings closely apposed to a dendrite of the same neuron (Figure 5.6 E & F). Asymmetric synapses were formed on either side of the dendrite (Figure 5.6 G, arrow & double arrows; H, at high magnification).

5.4.3 Anterograde tracing from the dorsal raphe – injection site and projections to the VTA observed under fluorescence

The injection site in the dorsal raphe spanned the nucleus rostrocaudally with the maximal extent at around 4.36 mm caudal of Bregma (Figure 5.7 A & B). Some BDA deposition was also observed in the ventrolateral periaqueductal gray (VLPAG). The labelled neurons were localised bilaterally along the midline and displayed extensive dendritic trees extending ventrally along, and perpendicular to, the midline.

In the SNC, TH+, CB+ and TH+/CB+ neurons were distributed in patterns similar to those described in previous chapters (Figure 5.8 A & B). Long BDA-labelled fibres were beaded with axonal swellings (Figure 5.8 C), some of which were round, and some fusiform. As the dorsal raphe injection was at the midline, BDA-labelled projections, unlike in the striatal injection, were bilateral. A small proportion of the SNC neurons were TH+/CB+ (Figure 5.8 D). Amongst these (Figure 5.8 A-D & E-H, arrows), some were found alongside at least one varicosity on the BDA-labelled fiber (Figure 5.8 H, arrow). On the other hand, the adjacent neuron in the same frame was TH+/CB- and was not close to a fiber.

Neurons singly labelled with either TH or CB immunoreactivity were also seen closely apposed by anterogradely labelled fibres from the dorsal raphe (Figure 5.9). Thus a 'beaded'

fibre climbed along a TH+/CB- cell body, where one varicosity was closely apposed to the soma (Figure 5.9 H, arrowhead) and another to its dendrite (Figure 5.9 H, double arrowheads), while a TH-/CB+ neuron received potential afferents (Figure 5.10 A-D, arrows) only on the cell soma (Figure 5.10 E-H, arrowheads).

In the SNL (Figure 5.11 A-D), CB+ neurons were confined in the dorsal part and hence, most neurons here were TH+/CB+, although examples of TH+/CB- and TH-/CB+ neurons were also observed in this frame – a BDA-labelled fiber was alongside a TH+/CB+ neuron at its distal dendrite (Figure 5.11 A-D, box; E-H, arrow); a TH+/CB- neuron was in close apposition to two BDA-labelled fibers (Figure 5.11 I-L), one at its cell body (double arrows) and one that coursed across its dendrite (arrow); and a TH-/CB+ neuron had three potential inputs onto its cell body (Figure 5.11 M-P, double arrowheads).

In the rostral VTA (Figure 5.12, A-D), BDA-labelled fibers were long, with intensely-stained varicosities (Figure 5.12 C). A TH+/CB+ neuron was in close apposition to a BDA-labelled varicosity at its cell body (Figure 5.12 E-H, arrows). Also, a TH+/CB-neuron in the same frame received a potential input at its cell body (Figure 5.12 E-H, double arrows).

The three triple-immunolabelling combinations were again found in the caudal VTA (Figure 5.13 A-D). First, a TH+/CB+ neuron was close to two neighbouring inputs at its cell body (Figure 5.13 E-H, double arrowheads/arrows). Second, a TH+/CB- neuron was close to a short fiber (Figure 5.13 I-L, arrowheads/arrows). Third, in another section, a TH-/CB+ neuron was close to a BDA-labelled fiber (Figure 5.14 A-D; at higher magnification, E-H). The neuron appeared multi-polar (Figure 5.14 E & F, arrowheads) with the contact at the tip of its cell body (Figure 5.14 G & H, arrows).

5.4.4 Dorsal raphe terminals forming synaptic junctions with TH+ and CB+ neurons in the VTA

One example for each TH+ and CB+ neuron were shown here. Independently immunostained TH+ and CB+ neurons from similar rostrocaudal levels of the VTA were selected for further processing (Figure 5.15 A & 5.16 A). The two types of neurons showed various sizes and morphology – round or with long thick dendrite like those in Figure 5.15 B, or oval-shaped with round, centred nucleus in the middle (Figure 5.16 B). Consistent with the more limited penetration of reagents into the tissue sections, anterogradely labelled fibers were mostly seen in the midbrain as small punctate terminals instead of long varicose strings described in the triple-immunolabelling experiments. When examined under EM, the TH+ and CB+ neurons did not show as intense a staining as that seen in the previous EM experiments (Figure 5.15 C). However, it could be identified by the electron-dense granules dispersed throughout the cytoplasm, formed by the SG reaction-product.

A TH+ neuron received multiple contacts from the BDA-labelled fibers including an axo-somatic contact (Figure 5.15 B, arrow; C, box). It appeared to be a symmetric synapse, with thin post-synaptic densities more resembled to the presynaptic membrane (Figure 5.15 D, arrows). Another apposition was observed on the other side of the cell body (Figure 5.15 E arrow; 5.15 F, box). This projection crossed the TH+ neuron and made a contact with one of its processes. Observations in serial sections confirmed that this synaptic contact was small and symmetric (Figure 5.15 G, arrows). The TH+ neuron also received synaptic inputs from unlabelled projections. Thus an unlabelled terminal, in a location marked with an arrow (Figure 5.15 H), and filled with round synaptic vesicles and mitochondria formed a small symmetric synapse with the TH+ neuron (Figure 5.15 J, arrows).

The CB+ neurons were also in close contact with multiple, round BDA-labelled axon terminals at the cell somata (Figure 5.16 B & E). One of these, located at the tip of the perikaryon (Figure 5.16 C, box), formed a symmetric synapse (Figure 5.16 D, arrow). The labelled bouton was filled with darkly-coated synaptic vesicles and the pre- and post-synaptic specialisations were of similar thickness. In a different plane, the same neuron was closely apposed by two further BDA-labelled fibers, one with a round varicosity (Figure 5.16 E, double arrows; 5.16 F, box) and another with a short projection (Figure 5.16 E & F, arrows). The round varicosity seemed to form a small symmetric synapse (Figure 5.16 G, arrows) whilst the short projection appeared as an axon collateral forming symmetric synapses with both the CB+ neuron (Figure 5.16 H, arrows) and an unlabelled dendrite (blue arrowheads).

5.5 Discussion

5.5.1 Striato-nigral pathway in the mouse

In the striatum, a major nucleus of the basal ganglia, 95% of the neurons are projection neurons called medium spiny neurons (MSNs). These neurons are further subdivided into two morphologically indistinguishable and mosaically distributed neuronal subtypes: striato-nigral MSNs (the direct pathway) and striato-pallidal MSNs (the indirect pathway) (Parent et al., 1984; Smith et al., 1998; Lobo et al., 2006). Current models of basal ganglia function suggest that these two projection neuron pathways provide balanced but antagonistic influences on the basal ganglia output and behaviour: the direct pathway promotes movement and the indirect pathway inhibits it (Gerfen, 1992; Albin et al., 1995; Graybiel, 2000). Imbalance of these two pathways therefore plays a key role in movement disorders such as Parkinson's disease.

The major challenge of studying the striato-nigral pathway in the mouse is that the complexity and heterogeneity of the neuronal population in the striatum significantly limits the use of genetic or cell profiling (Lobo et al., 2006). DARPP-32, a D1-receptor associated signalling protein found in striatal projection neurons in mammals, is also localised (with few exceptions) to regions that receive DA innervation. A detailed immunohistochemical study in the rat brain demonstrated that the highest levels of DARPP-32 are found in caudatoputamen, nucleus accumbens, olfactory tubercle, bed nucleus of stria terminalis, and portions of the amygdaloid complex (Ouimet et al., 1984)(reviewed by (Svenningsson et al., 2004). Hence, neuroanatomical procedures – using anterograde tracers injected into the dorsal, caudal striatum and immunostaining the midbrain neurons with neurochemical markers – have been used to confirm a striato-nigral connection.

I used fluorescence microscopy to determine whether BDA-labelled fibers from the striatum innervate the midbrain in the vicinity of TH+, CB+ and TH+/CB+ neurons in the midbrain. One could argue that confocal microscopy is a better alternative to visualise the triple immunolabelling. However, in this study, all the photomicrographs were taken at the same focal plane, with only the filters being changed. Hence, when BDA-labelled fibers were seen alongside a neuron, they were indeed in juxtapositions. Second, given that the cell bodies of midbrain neurons are about 15x30 μm, it is unlikely that there were overlapping layers of cells seen under the high magnification. Therefore, the BDA-labelled fibers could only be making contact(s) with the neuron at that focal plane or, of course, with unlabelled profiles. Third, these fluorescent data serve as a preliminary indicator in estimating the proportion of TH+ and CB+ neurons which receive potential striatal inputs; the neurons were then further studied using EM. The immunocytochemical and ultrastructural evidence would complement each other.

The results of this study are consistent with observations using BDA iontophoretic tracing in the rat central nervous system (Veenman et al., 1992; Wouterlood and Jorritsma-Byham, 1993; Bacon, 2002) and my experiments confirmed the suitability of BDA in neuronal tracing. BDA-labelled neurons deliver descending striatal projections into the midbrain, mostly to the SNR. These axons make contacts with the ventral tier DA neurons at their cell bodies and dendrites. If mouse connectivity matches that of rat and primate, these striatal projections are likely to originate from the matrix of the associative and motor striatum (arising from patches) (Joel and Weiner, 2000).

In double labelled material prepared for the electron microscope, distinguishing between the two markers is often problematic. My immunofluorescence data show that striatal fibers potentially make both axo-somatic and axo-dendritic contacts with TH+, CB+ and TH+/CB+ neurons. However, this might be difficult to confirm in the electron microscope if there are local axon collaterals of the immunolabelled neurons. Importantly for the interpretation of my study, dopaminergic midbrain neurons, despite evidence for local release of dopamine, do not have local axon collaterals. This means that, in the dual-labelled material, any labelled axon is likely to be an extrinsic input. My data also show that no striatal axons were found near CB+ or TH+/CB+ neurons in SNC due to the relative absence of CB+ neurons from this part of the nigra. Most of the anterogradely labelled fibres were located near the medial and lateral SNR. It is plausible that different regulatory mechanisms are achieved as a combination of the location of TH+, CB+ and TH+/CB+ neurons and where the striatal inputs terminate.

5.5.2 Striatal afferents terminating onto TH+ and CB+ neurons in the VTA

Most neurons in the VTA are TH+/CB+ as described in previous chapters and in the triple immunofluorescent experiments. Consequently, the singly-immunolabelled CB neurons

studied under EM were very likely to be dopaminergic. It was found that both TH+ and CB+ neurons received striatal afferents that appeared to form asymmetric synapses at the perikarya and dendrites. Synapses were distinguished from puncta adherentia, or adhesion plaques, between neuronal elements (Peters et al., 1990) which have no associated vesicles at the active zone and only a very fine, fully symmetric, thickening of the membranes. Otherwise they resemble electrochemical synapses, since there is both a widening of the interneuronal space and interneuronal material.

Asymmetric synapses are generally considered to be excitatory and likely to be glutamatergic. However, output neurons from the striatum are all GABAergic (at least in rat) and unless there is a major species difference, one would expect symmetric synapses instead of asymmetric. It was unlikely that the asymmetric synapses were from cortical inputs (which would be glutamatergic), since no BDA deposition was observed on the overlying cortex at the injection site. Apart from the cortical fibres, there are other glutamatergic inputs to the SN, forming asymmetric synapses, (Bevan et al., 1994; Charara et al., 1996) but it is highly unlikely that any of these were inadvertently labelled by my tracer injections. Nevertheless, it is possible that some of the serial sections have been lost and the observed synapse might have been symmetric and functionally inhibitory. It would be necessary to examine a much larger number of striatal terminals from more animals to fully address this question.

5.5.3 Raphe-nigral pathway in the mouse

The combination of anterograde labelling and immunocytochemistry revealed that TH+, CB+ and TH+/CB+ neurons were closely apposed by the raphe-nigral terminals. Previous studies in the rat have demonstrated that the cells of the rostral dorsal raphe project mainly to the dorsolateral half of the SN and that cells originating from the caudal part project mainly to the medioventral half of the SN (Vertes, 1991; Corvaja et al., 1993). However, our data show

a more global topographic organisation. Varicose strings of labelled raphe afferents were found in the SN and the VTA, making contacts with all TH+, CB+ and TH+/CB+ neurons on their cell bodies and dendrites. The difference between the rat and the mouse is more likely to be a species variation, rather than the size of the injection site, which was confined to the dorsal raphe. Nonetheless, retrograde tracing studies from the SN and VTA could be used to confirm the origin of the raphe-nigral projection in the rostro-caudal axis.

5.5.4 Dorsal raphe afferents terminating onto TH+ and CB+ neurons in the VTA

The dorsal raphe synapses on projection neurons. Anterogradely-labelled dorsal raphe terminals made direct synaptic contacts with a TH+ and a CB+ neuron in the VTA. These contacts were axo-somatic or axo-dendritic and appeared to be symmetrical. This suggests inhibitory inputs that might use GABA as a transmitter, although serial sections would have to be examined to confirm the synaptic specialisation. Certainly a small number of symmetrical synaptic boutons have been reported in this projection (Van Bockstaele et al., 1994). It is possible that the VTA receives GABAergic input from the raphe nucleus, which has both a high activity of GAD and a specific high-affinity uptake mechanism for GABA, although these are generally thought to be associated with raphe interneurons (Nanopoulos et al., 1982). However, the synapse found here has pre- and post-synaptic membrane specialisations which are greater than on the classical symmetric synapses. These are sometimes described as a dense-symmetric synapses and are associated with 5-HT acting as an inhibitory neurotransmitter (Gervais and Rouillard, 2000). The prominence of asymmetric junctions formed by 5-HT-labeled terminals on neurons projecting to the nucleus accumbens and those containing TH in the VTA suggests a cellular function for serotonergic excitation of mesoaccumbens DA neurons. Also, the multiplicity of junctions formed by 5-HT terminals on targets is consistent with known diverse physiological actions of 5-HT in the VTA (Van Bockstaele et al., 1994). For example, the antipsychotic drug, clozapine, has the

effect of modulating dopamine and 5-HT release (Meltzer, 1995) and is used to treat drug-induced hallucinations and psychosis in PD (Molho and Factor, 2001; Kulisevsky and Roldan, 2004).

We also observed one example of a synaptic contact from an anterogradely-labelled terminal to both a CB+ cell body and an unlabelled dendrite simultaneously. It is possible that the dendrite was a false negative, due to limited CB antibody penetration, but it is also likely that dorsal raphe projections make synaptic contact with other types of neurons in the VTA. Indeed, some of the postsynaptic substrates to the dorsal raphe terminals had the synaptology that is characteristic of SNR output neurons of the basal ganglia (Corvaja et al., 1993).

5.5.5 Functional significance of the striato-nigral and raphe-nigral projections to the TH+ and CB+ neurons

Recent publications using tissue slice preparations, animal models and in humans with PD has demonstrated abnormally synchronized oscillatory activity at multiple levels of the BG-cortical loop (Hammond et al., 2007). Our study shows that TH+/CB-, TH-/CB+ and TH+/CB+ neurons in both SN and VTA potentially receive inputs from the striatum and the dorsal raphe, with the exception of those in the SNC, where no CB+ neurons were found to have striatal input. If the location of CB+ neurons is the predisposing determinant of the type of input(s) they receive, one can envisage an imbalance in the basal ganglia in Parkinson's disease, where most of the DA neurons are lost from specific areas. The differences in innervations could lead to a dramatic change in the "reading" of brain activity. It may also be that cells are more vulnerable if innervated by more inputs to their cell bodies, particularly if these are excitatory. Further studies to characterise the number of the number of inputs received per neuron (cell body versus dendrites), may show anatomical differences between the TH+/CB+ and TH+/CB- neurons.

The morphology of the projection fibers (fine climbing versus thick fibers) and their varicosities (ovoid, fusiform, round) may also indicate differences in their synaptic contacts. In addition, the chemical nature of the striatal and dorsal raphe inputs to the midbrain neurons could be determined using neurochemical markers. Taken together, this study provides the first step to decipher possible differences in connectivity between TH+/CB+ and TH/CB-neurons in the midbrain.

Figure 5.1

A schematic representation of the different targets in the midbrain (DA cell bodies and proximal dendrites, ventrally extending DA dendrites, SNR GABAergic neurons) of projections arising from the basal ganglia nuclei in the rat. Pink line with square ends: excitatory synapse; lines with circular ends: inhibitory synapse. Dashed lines illustrate some of the connections between the basal ganglia nuclei. Adapted from Joel and Weiner, 2000.

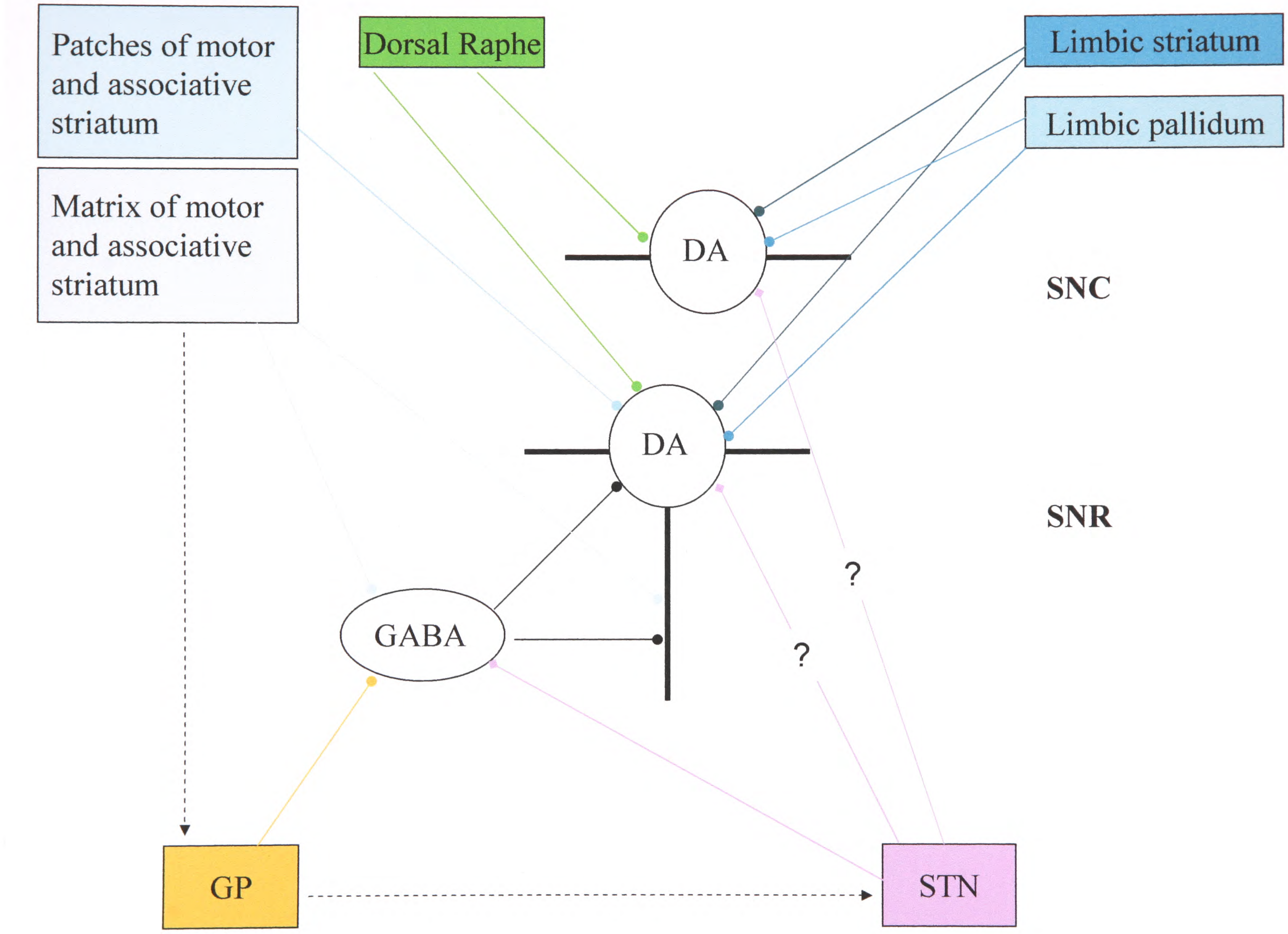

Patches of motor and associative striatum
Matrix of motor and associative striatum
Dorsal Raphe
Limbic striatum
Limbic pallidum
DA
DA
SNC
SNR
?
?
GABA
GP
STN

Figure 5.2

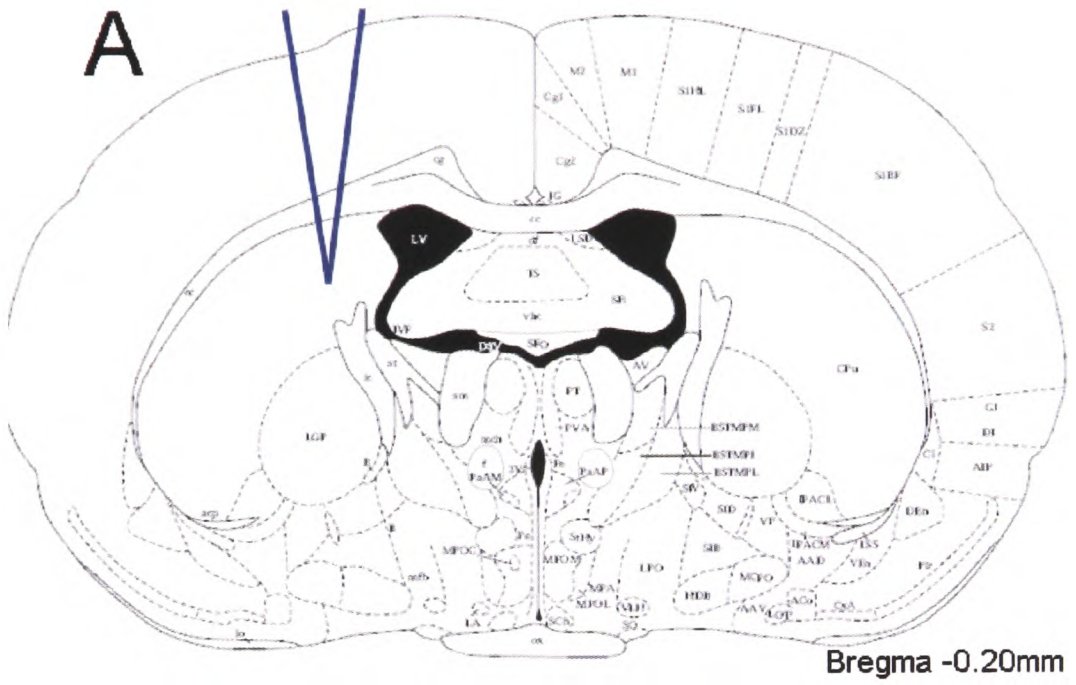
Schematic representation and light micrograph of the site of iontophoretically-deposited BDA anterograde tracer in the mouse striatum.

(A) Schematic map (adapted from the Atlas of Paxinos & Watson, 1996) of a coronal section through the dorsal striatum [Abbreviation: CPu, caudate putamen]. The blue lines indicate the approximate correlated site at which the BDA tracer was deposited.

(B) Light micrograph showing the location and the maximal extent of the BDA tracer injection amongst other serial striatal sections. The dark brown injection site shows BDA deposition into the right striatum of the mouse brain. Cells at the injection site appeared to have taken up the anterograde tracer and distributed it throughout their processes within the injected area. No deposition was observed in other brain regions (e.g. the cortex) as shown by the lack of dark brown DAB reaction product.

Scale bar: 500μm

A


M2
M1
S1HL
S1FL
S1DZ
S1BF
Cg1
Cg2
cg
ic
cc
LV
LSD
IS
SF
VDB
DVF
DPV
SHy
AV
st
sm
PT
PVA
LGP
BSTMPM
BSTMPI
BSTMPL
PaAM
PaAP
SM
SIP
VP
IPACL
DEn
SHy
IPACM
ESS
AAD
VEn
MPOC
MPOM
LPO
SI
MCPO
HDB
MPA
MPOL
VDB
AAV
ACo
SIA
LA
SCN
SO
ox
S2
CPu
GI
DI
AIP
Bregma -0.20mm

B


500µm

Figure 5.3

Fluorescent images of striatal BDA-labelled fibers projecting onto neurons in the SN.

(A & B) TH+ neurons were densely packed along the SNC, whereas the CB+ neurons were located mostly in the ventral SNC. Smaller CB+ neurons were also observed in the supramammillary nucleus (SuM).

(C) Striatal BDA-labelled fibers projected mostly into the SNR, where few TH+, CB+ and TH+/CB+ cell bodies were found.

(D) Merged image shows a small proportion of the neurons in the SNC that were TH+/CB+, but did not receive any projection from the BDA-labelled fiber. However, close contacts were made between the fibers and TH+ neurons (box).

(E-H) High magnification images of the boxed area to show TH+ **(E,** arrows), but CB- neurons **(F)**, received projections from the BDA-labelled striatal fibers **(G)** onto the dendrites.

Scale bars: A-D = 50μm, E-H = 10μm

[Note: The level at which these brain sections were taken are more rostral compared to those in previous chapters because BDA labelling was only observed here.]

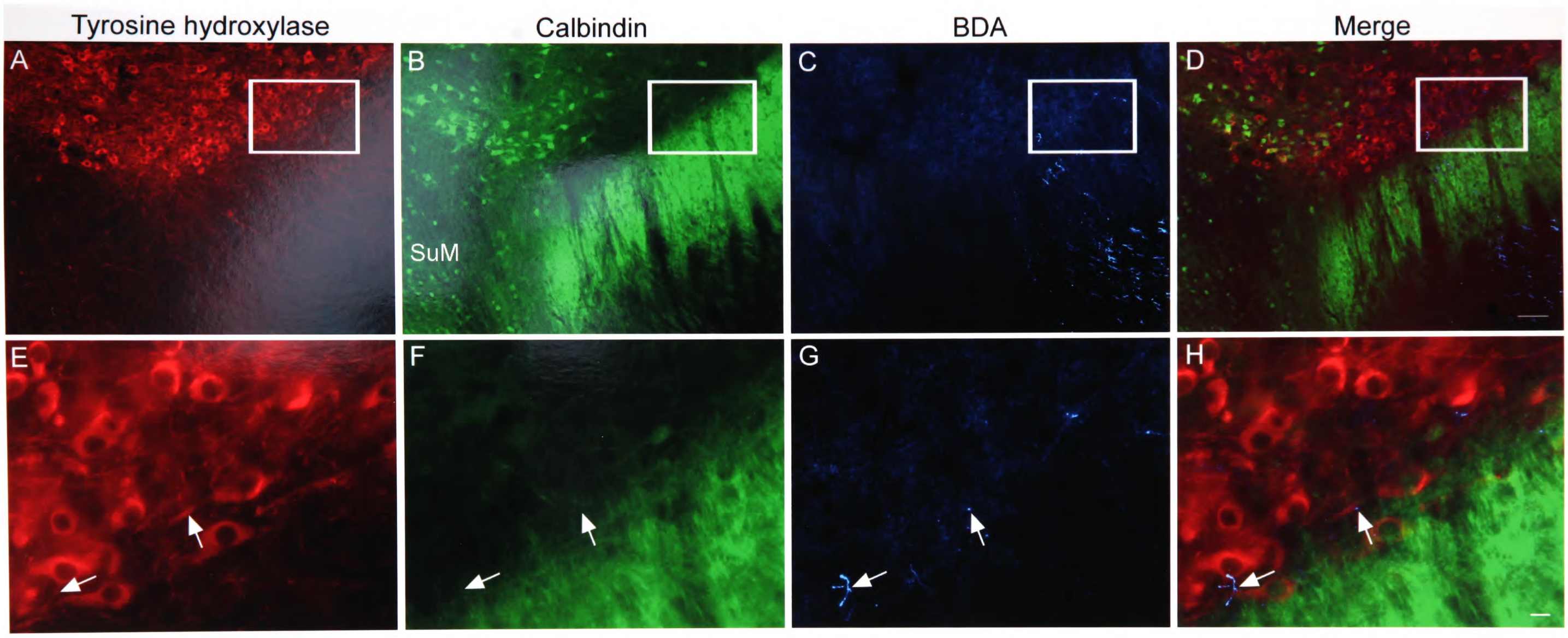

Tyrosine hydroxylase
Calbindin
BDA
Merge
A
B
C
D
SuM
E
F
G
H

Figure 5.4

Fluorescent images of striatal BDA-labelled fibers projecting onto neurons in the VTA.

(A & B) TH+ neurons were found in the VTA and the SNC adjacent to it. The majority of the CB+ neurons were in the VTA but only a few were in the SNC on the other side of the medial lemniscus (ml).

(C) Only punctuate axonal terminals from the striatal BDA-labelled fibers were found in the VTA, in contrast to the long fibers running across the SNR.

(D) Over 50% of all the immunostained neurons were TH+/CB+ in the VTA.

(E-H) High magnification images of the boxed area showing striatal BDA-labelled fibers making close contact with three types of immunolabelled neurons in the VTA: a) TH+/CB+ neuron on its cell body (arrowheads); b) TH+/CB- neuron on its cell body (arrows) and c) the dendrite of a TH-/CB+ neuron (double arrowheads).

Scale bars: A-D = 50μm, E-H = 10μm

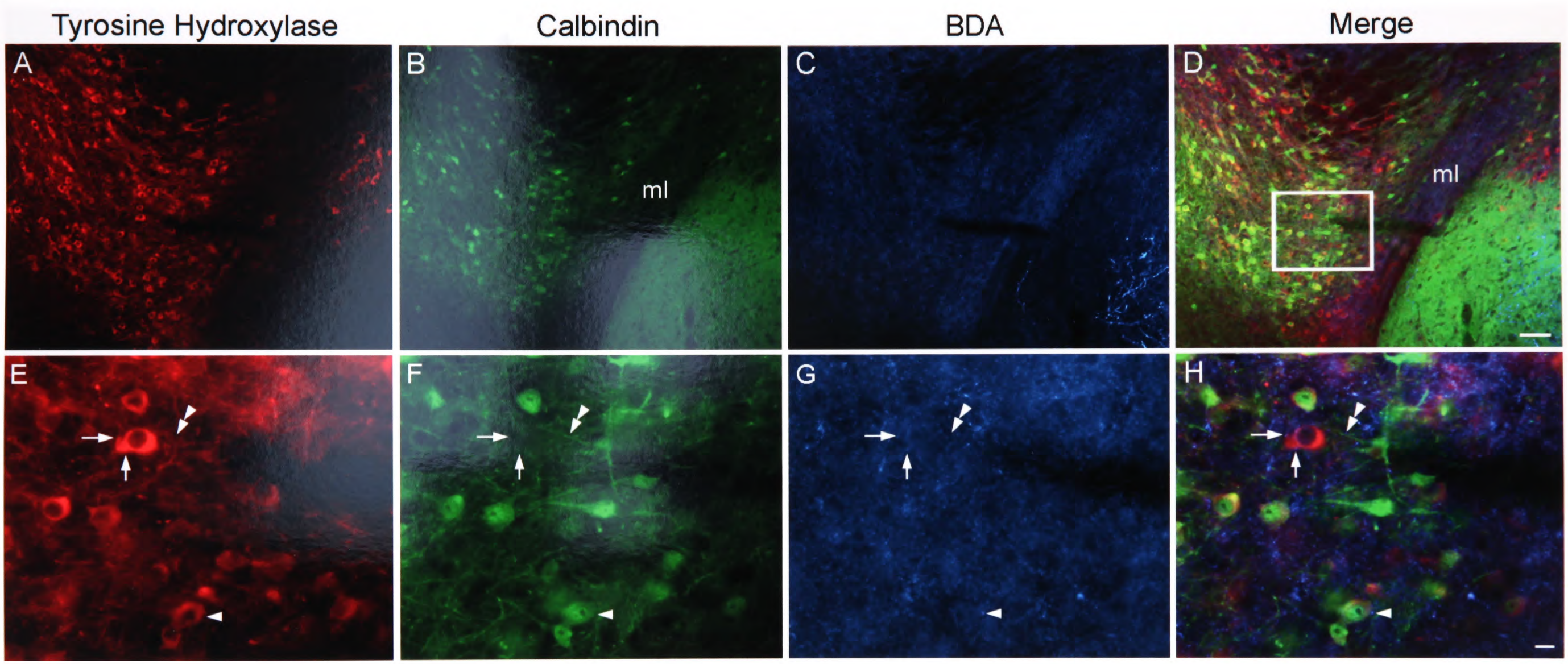

Tyrosine Hydroxylase
Calbindin
BDA
Merge
A
B
C
D
ml
ml
E
F
G
H

Figure 5.5

Synaptic contact formation between a striatal projection and a TH+ neuron in the VTA.

(A) A schematic diagram of a coronal section illustrating that the TH+ neuron investigated was taken at approximately 3.28 mm caudal to Bregma and the section was taken in the VTA (blue box).

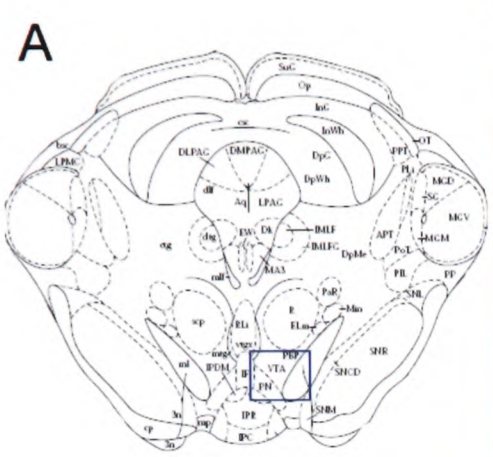
(B) Light micrograph showing the distribution of grey TH+ cell bodies and dendrites in the VTA, revealed using SG as the chromogen.

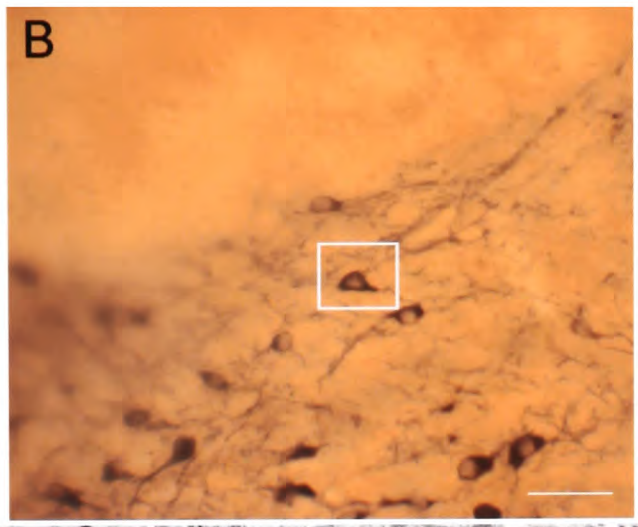
(C) Light micrograph showing a high magnification image of the TH+ neuron in the boxed region in (B). The tracer-filled axons originate from the striatum were labelled with DAB (brown). Some of the axons have varicosities in close apposition with the TH+ neuron (arrow). The DA neuron showed immunoreactivity in its cell body and proximal dendrite (grey black) and part of a TH+ dendrite (arrowhead) was used as a landmark in the tracing process under electron microscopy.

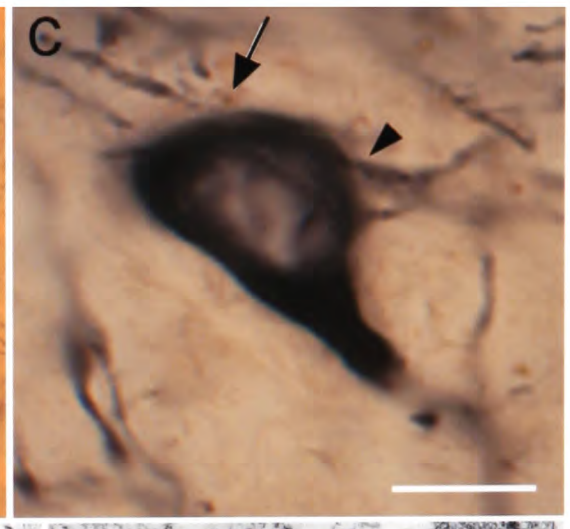
(D-F) Electron micrographs of anterogradely labelled axon terminals after injections of BDA in the striatum. The synaptic contact (D and E, arrows) correlated to that observed in the light microscopy (C, arrow). Both the cell body and the dendrite (D and E, arrowheads) were TH+. (F) The bouton appeared to form asymmetric synaptic contact (arrows) with the TH+ cell body.

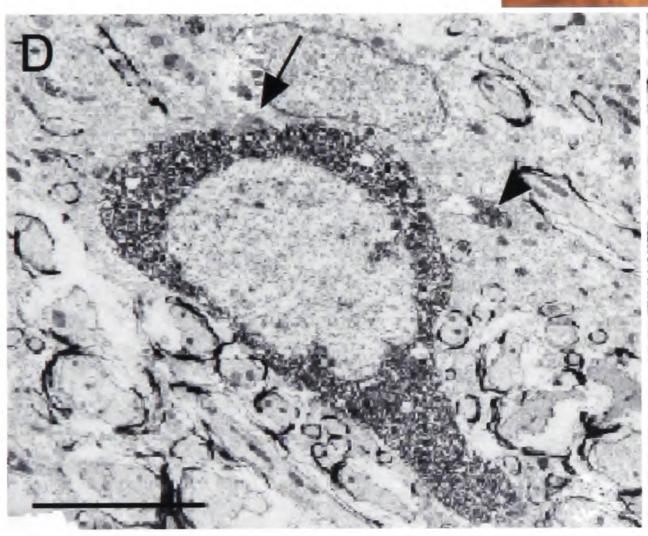
(G and H) Electron micrographs of an unlabelled axon terminal seen in close apposition with the TH+ neuron at its dendrite (double arrows). Under high magnification, the contact did not seem to form a synapse (H, arrows). [Note: H is 180° rotated from the same view in G]

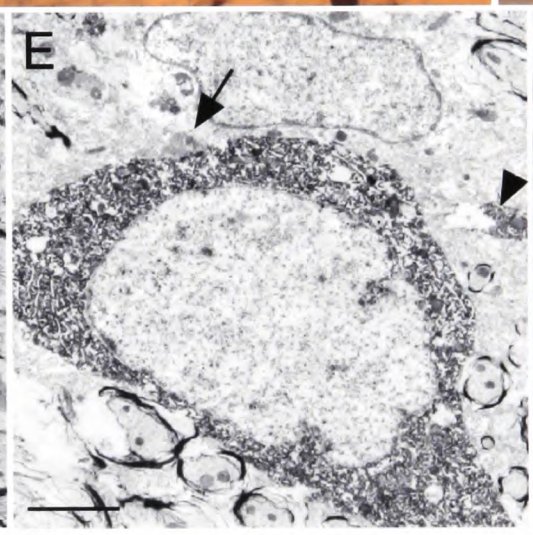
Scale bars: B = 50μm, C = 10μm, D = 5μm, E = 2μm, F = 0.5μm, G = 2μm, H = 0.5μm

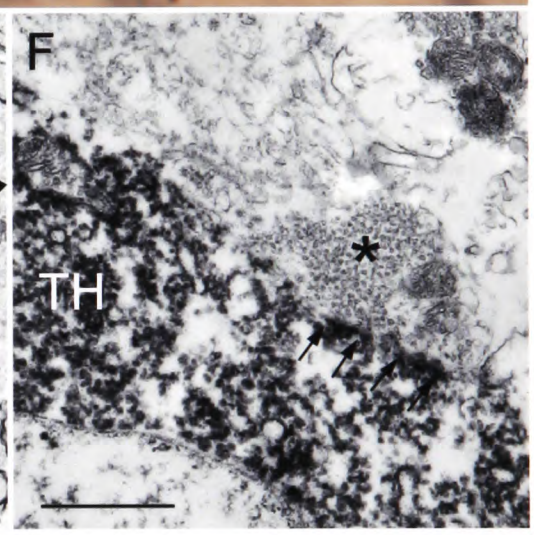

A
Bregma -3.28mm

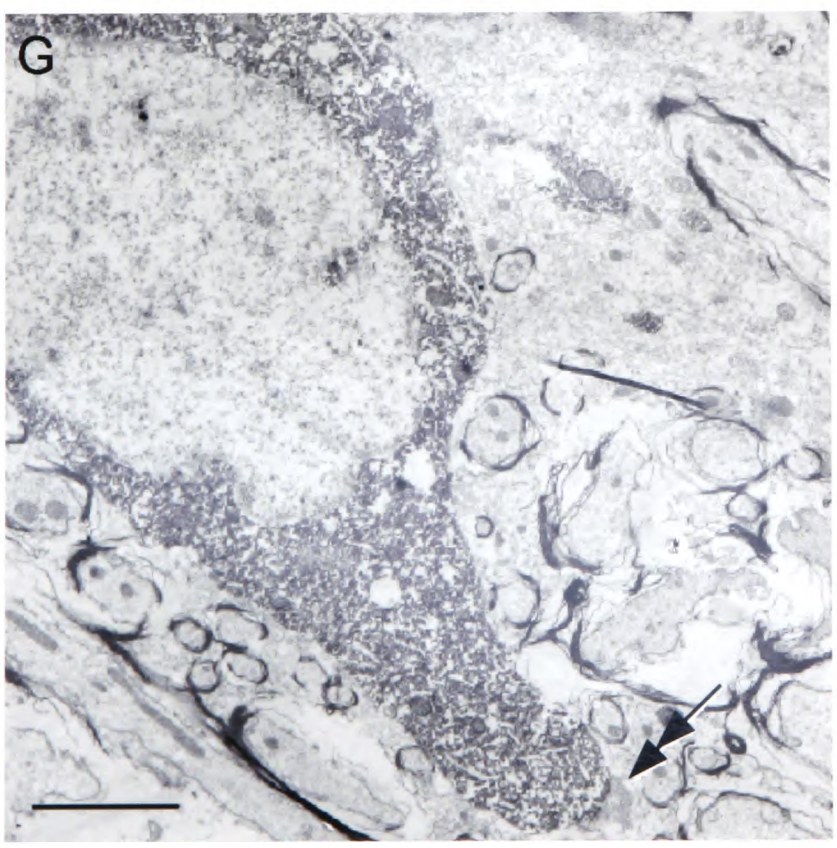

B


C


D


E


F
TH
*


G

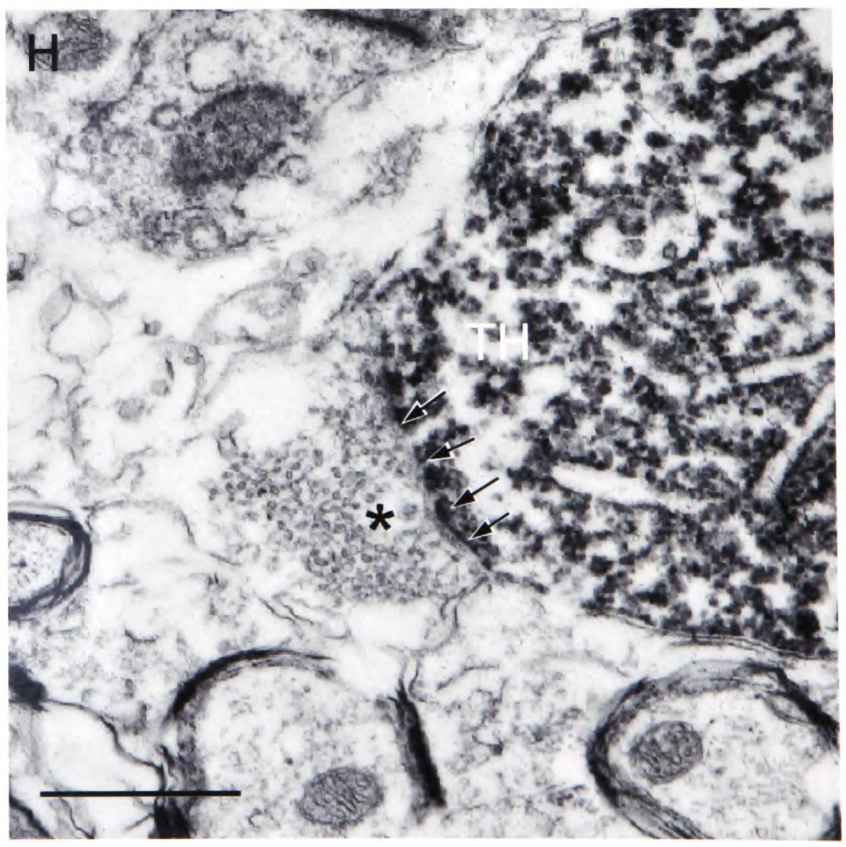

H
TH
*

Figure 5.6

Synaptic contact formation between a striatal projection and a CB+ neuron in the VTA.

(A) A schematic diagram of a coronal section illustrating that the CB+ neuron investigated was taken at approximately 3.28 mm caudal to Bregma and the section was taken in the VTA (blue box).

(B) Light micrograph showing a grey-black CB+ cell body and its long dendrite in the VTA, revealed using SG as the chromogen. Tracer-filled axon terminals were revealed with DAB (brown). The varicosities were round and were densely distributed in the region. The CB+ neuron appeared to be in close contact with several varicosities, one of which is highlighted with an arrow.

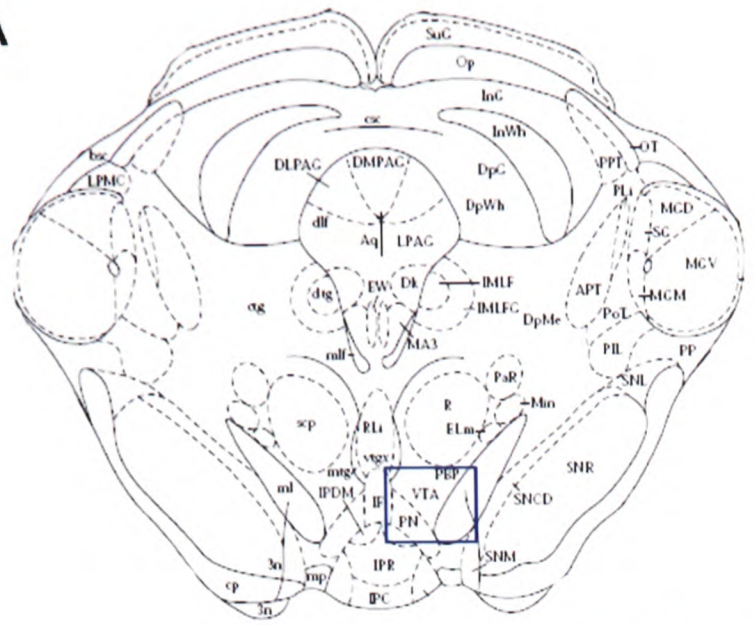
(C and D) Electron micrographs showing the CB+ neuron perikarya in synaptic contact (C, box) with a tracer-filled striatal input. There appeared to be two asymmetric contacts (D, arrows).

(E) Light micrograph showing another section of the same neuron, highlighting two opposite varicosities that made close appositions with the CB+ neuron at its distal dendrite (arrow and double arrow).

(F-H) Electron micrographs of striatal projections in contact with immunolabelled dendrite (F, box). Both synapses (G, top arrow and bottom double arrows) appeared to be asymmetric. At high magnification (H), the synaptic contact was highlighted by the double arrows showing pre- and postsynaptic specialisation. Dark synaptic vesicles and mitochondria were closely packed.

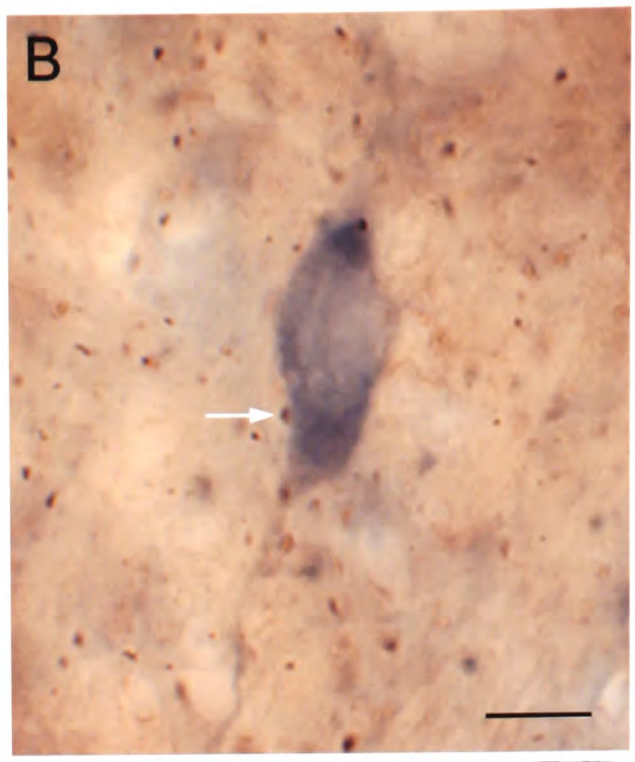
Scale bars: B = 10μm, C = 5μm, D = 0.5μm, E = 10μm, F = 5μm, G = 1μm, H = 0.5μm

A

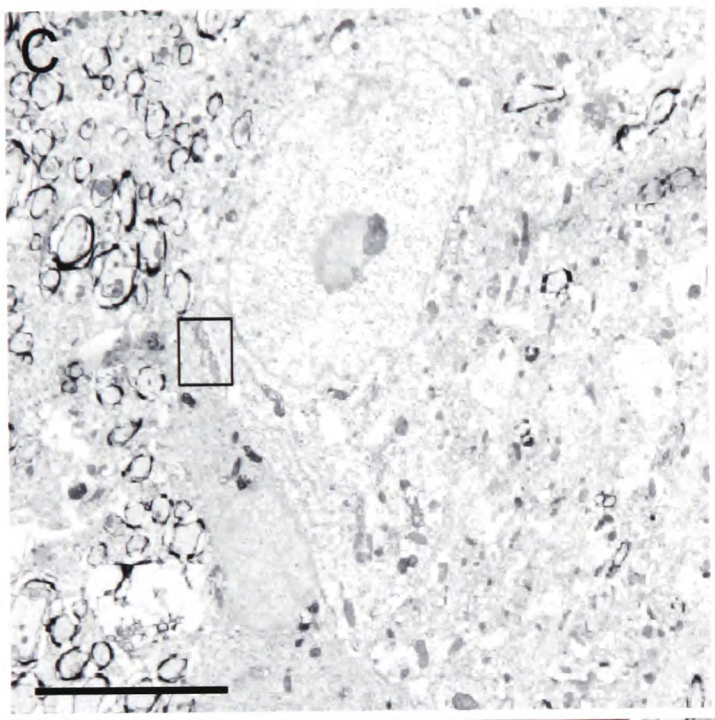


Bregma -3.28mm

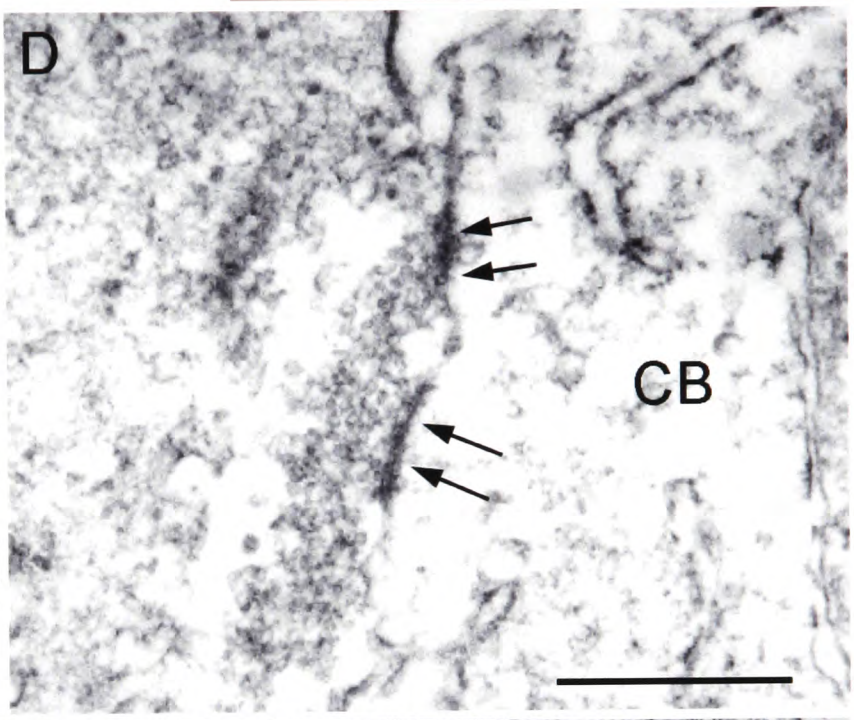
B



C

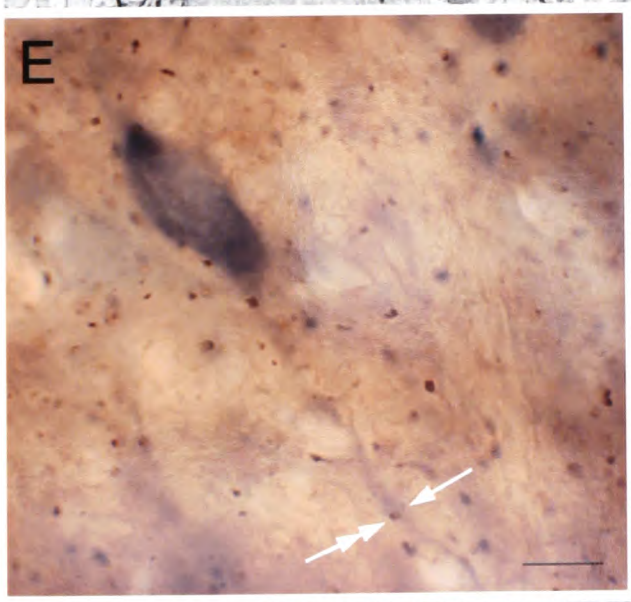


D

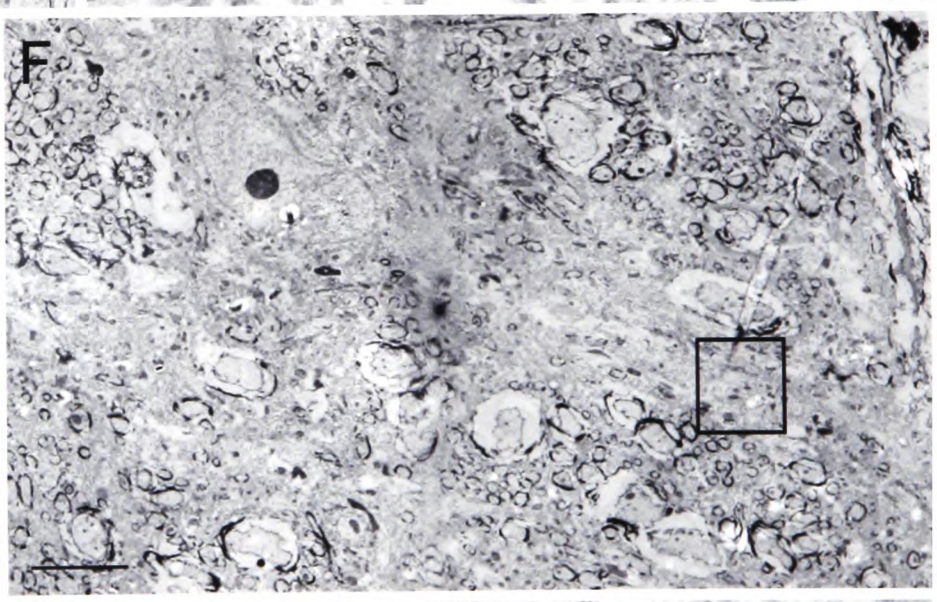




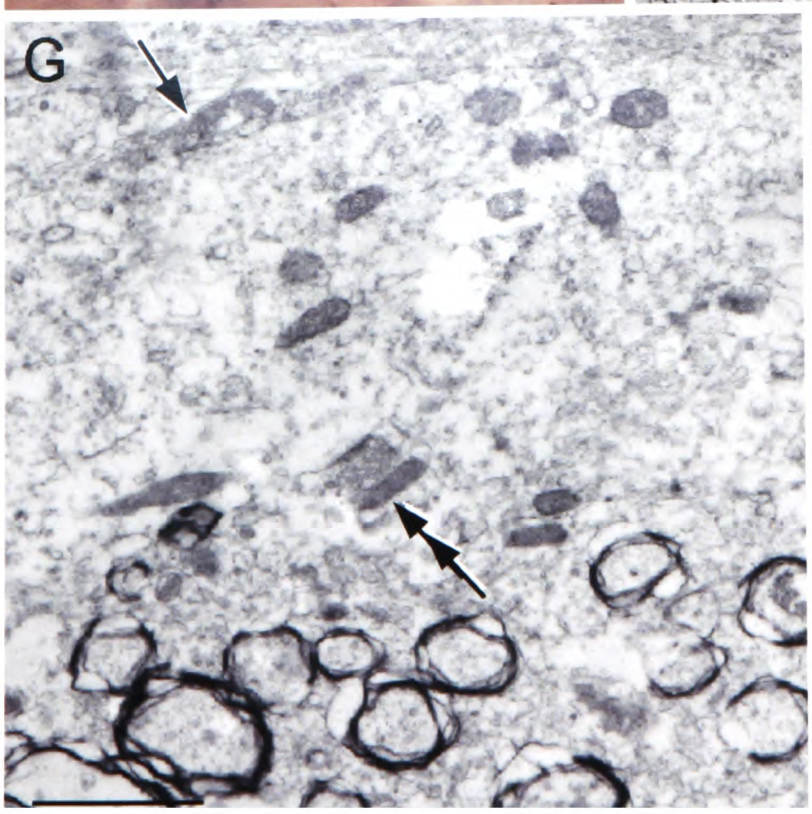
E



F



G



H

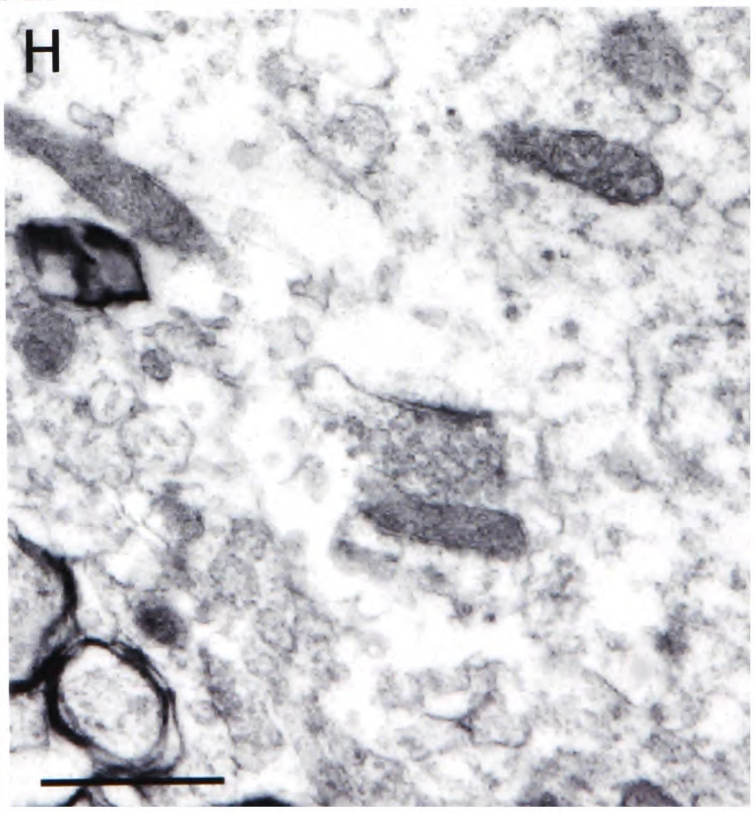


Figure 5.7

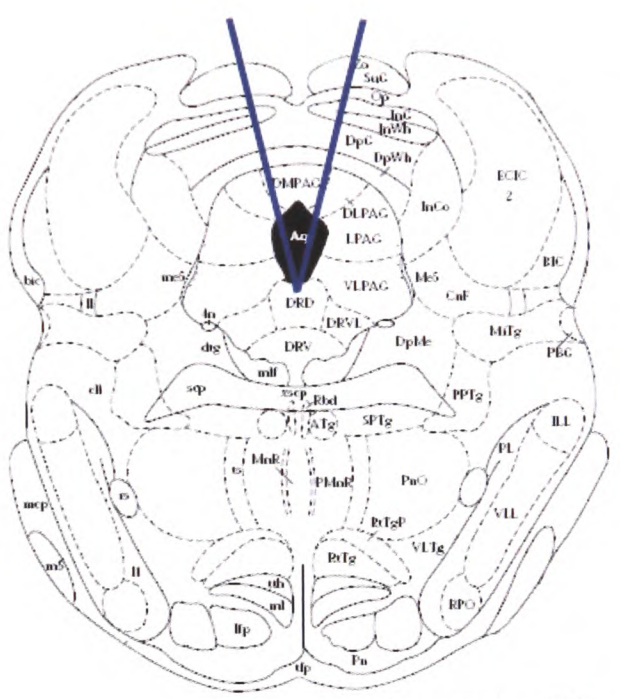
Schematic representation and light micrograph of the site of iontophoretically-deposited BDA anterograde tracer in the mouse dorsal raphe.

(A) Schematic map (adapted from the Atlas of Paxinos & Watson, 1996) of a coronal section through the dorsal raphe [Abbreviation: DRD, dorsal raphe nucleus, dorsal part]. The blue lines indicate the approximate correlated site at which the BDA tracer was deposited.

(B) Light micrograph showing the location and the maximal extent of the BDA tracer injection amongst other serial dorsal raphe sections at different rostrocaudal levels. The dark brown injection site showed BDA deposition into the dorsal raphe. Since the injection was made at the midline of the brain, BDA deposition was observed in both brain hemispheres. Cells at the injection site appeared to have taken up the anterograde tracer and distributed it throughout their processes within the injected area.

Scale bar: 500μm

A


Aq
DMPAG
DLPAG
LPAG
VLPAG
DRD
DRVL
DRV
InCo
ECIC
BIC
MiTg
PBG
DpMe
MeS
CnF
PPTg
SPTg
ATg
RtTg
PnO
PL
VLL
VLTg
RPO
Pn
LLL
scp
mcp
ml
mlf
dtg
cll
bic
III
IV
Bregma -4.36mm

B

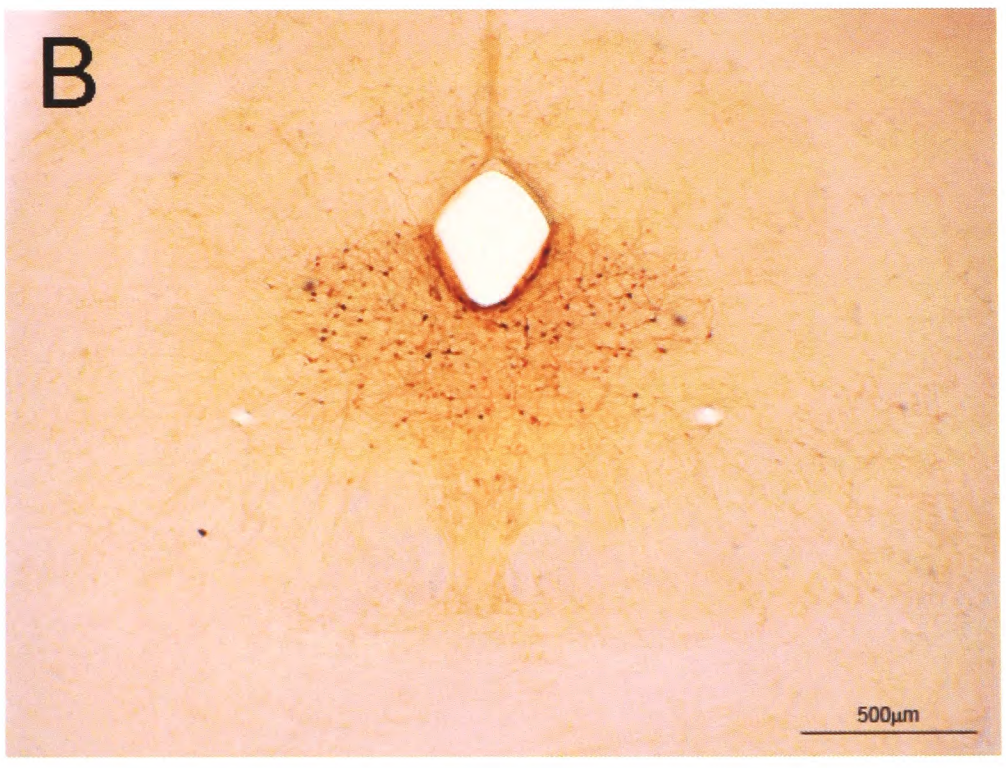

500µm

Figure 5.8

Fluorescent images of dorsal raphe fibers projecting onto TH+/CB+ neurons in the SNC.

(A & B) TH+ dopaminergic neurons were observed in the SNC, where CB+ neurons were also found.

(C) Long, thin BDA-labelled dorsal raphe projections were found in the SNC.

(D) Merged image shows a proportion of TH+/CB+ neurons. One of which had close contacts with the BDA-labelled fiber (Arrow).

(E-H) High magnification images of (A-D) respectively showing the TH+/CB+ neuron (arrow). The long BDA-labelled fiber (G) showed an array of axonal swellings along its length and can be seen as brighter spots. This suggests that the projection made *en passant* synaptic contacts with neighbouring neurons. One possible contact was onto the double-immunolabelled cell body (H, arrow).

Scale bars: A-D = 50μm, E-H = 10μm

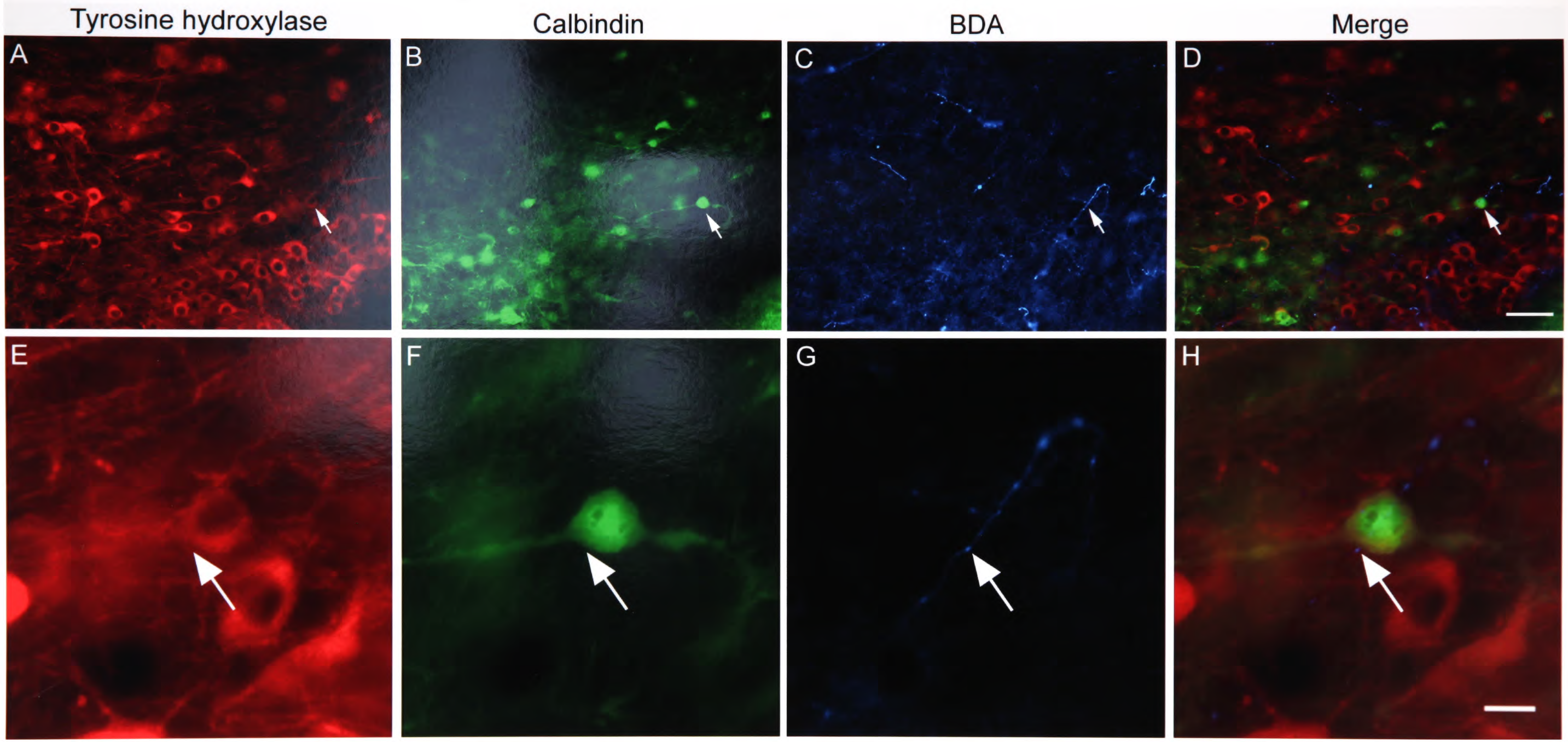

Tyrosine hydroxylase
Calbindin
BDA
Merge
A
B
C
D
E
F
G
H

Figure 5.9

Fluorescent images of dorsal raphe fibers projecting onto TH+ neurons in the SNC.

(A-D) In lateral part of the SNC (A) where CB+ neurons were sparsely located (B), BDA-labelled projections can still be observed (C). The merged image shows a TH+ neuron making close contact with a BDA-labelled fiber (arrows).

(E-H) High magnification images of (A-D) respectively. The long BDA-labelled fiber (G) made close contact with the TH+ neuron at its cell body (arrowhead) as well as on its proximal dendrite (double arrowheads).

Scale bars: A-D = 50μm, E-H = 10μm

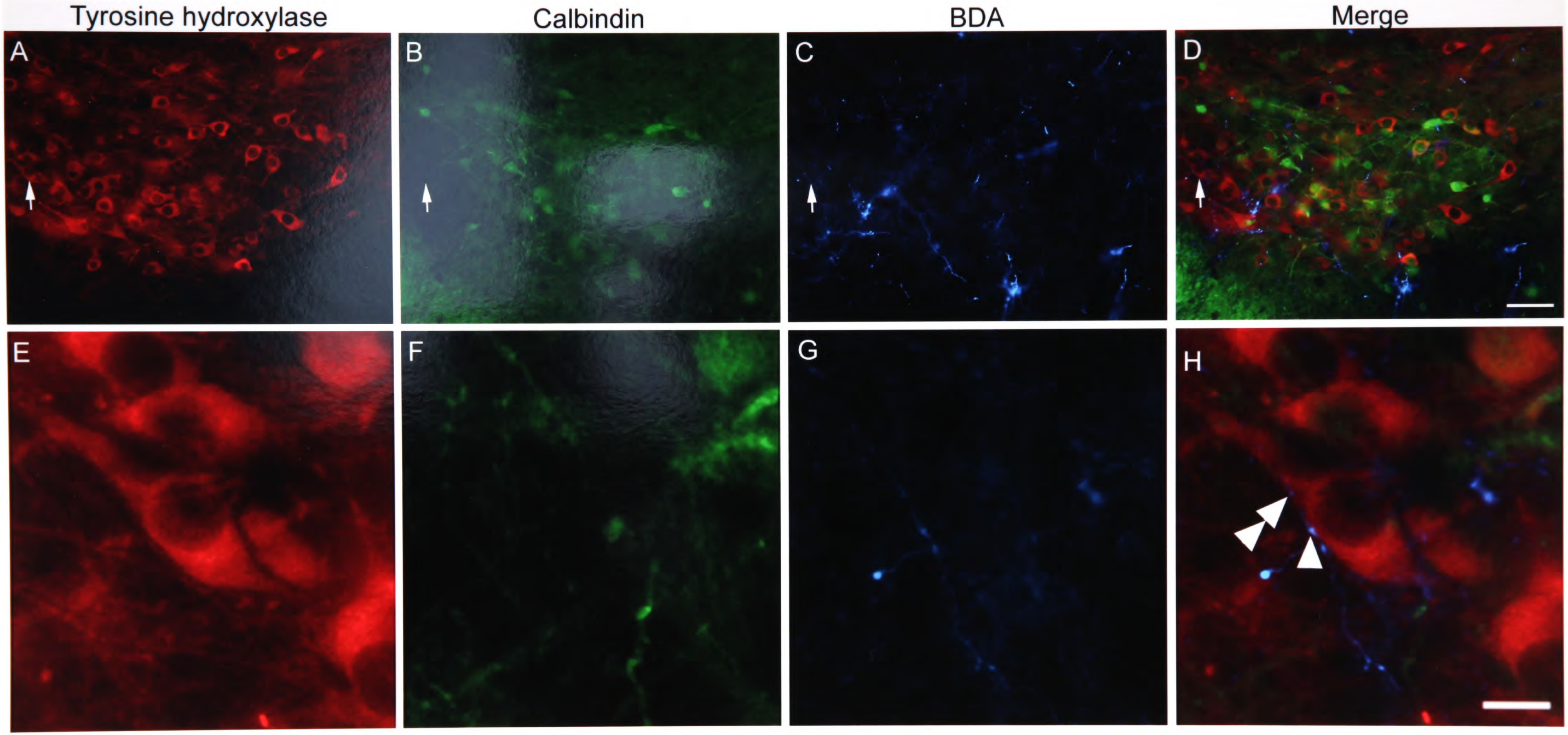

Tyrosine hydroxylase
Calbindin
BDA
Merge
A
B
C
D
E
F
G
H

Figure 5.10

Fluorescent images of dorsal raphe fibers projecting onto CB+ neurons in the SNC.

(A-D) In ventral part of the SNC where both the TH+ and CB+ neurons were sparsely located (A and B), BDA-labelled projections were present (C). The merged image shows a CB+ neuron making close contact with a BDA-labelled fiber (arrows).

(E-H) High magnification images of (A-D) respectively. The BDA-labelled fiber (G) made close contact with the CB+ neuron onto its cell body (arrowhead). On the other hand, the TH+/CB+ neuron above did not receive a projection onto its cell body.

Scale bars: A-D = 50μm, E-H = 10μm

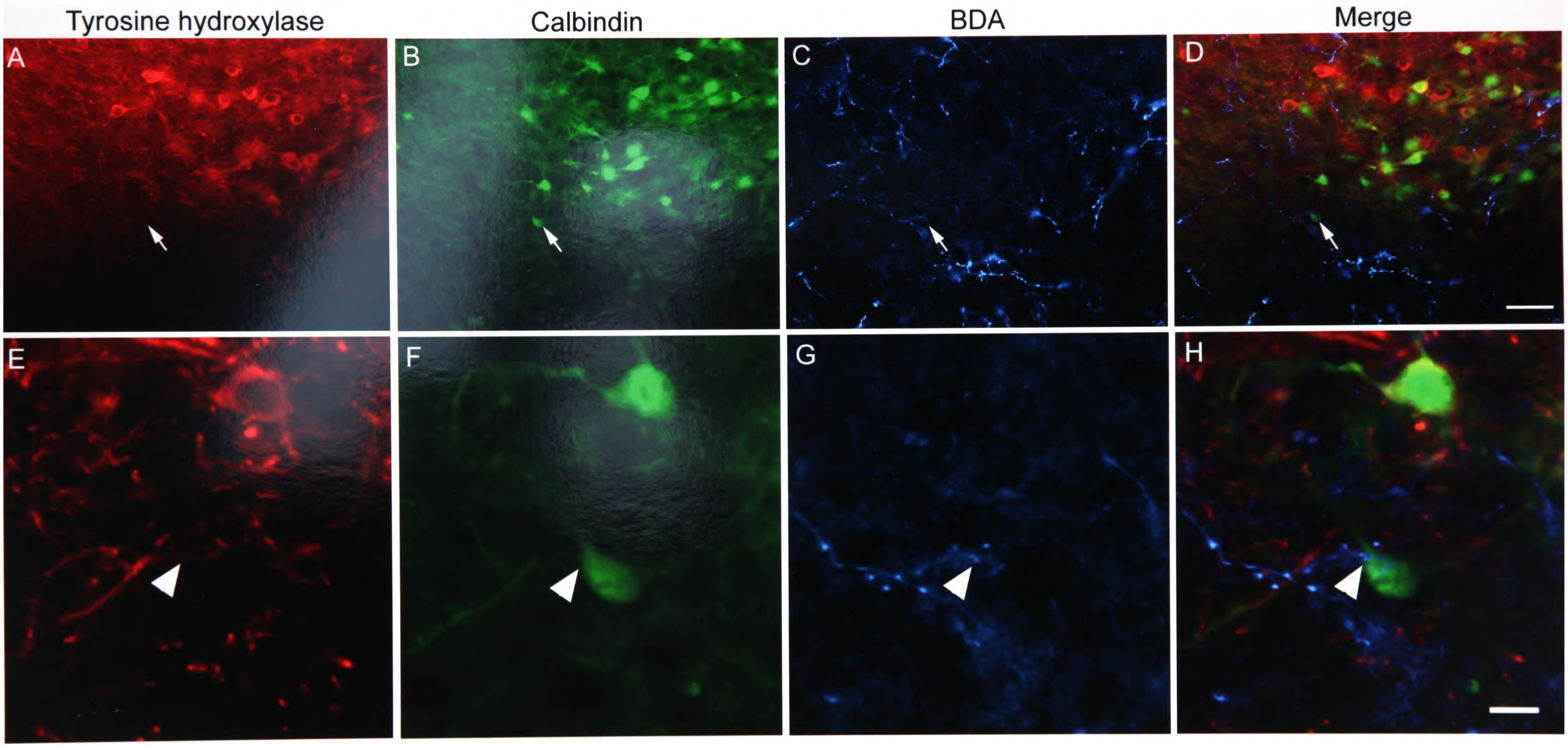

Tyrosine hydroxylase
Calbindin
BDA
Merge
A
B
C
D
E
F
G
H

Figure 5.11a

Fluorescent images of dorsal raphe fibers projecting onto neurons in the SNL.

(A-D) DA neurons showed TH-immunoreactivity along the dorsal tier of the SNC, adjoining the SNL (A), whereas the CB+ neurons were restricted to the SNL (B). BDA-labelled dorsal raphe projections were present in these regions (C). Merged image illustrates three characteristics:

a) **(E-H)** High magnification images of the boxed region showing a TH+/CB+ neuron that made close contact with a BDA-labelled dorsal raphe fiber at its distal dendrite (arrow).

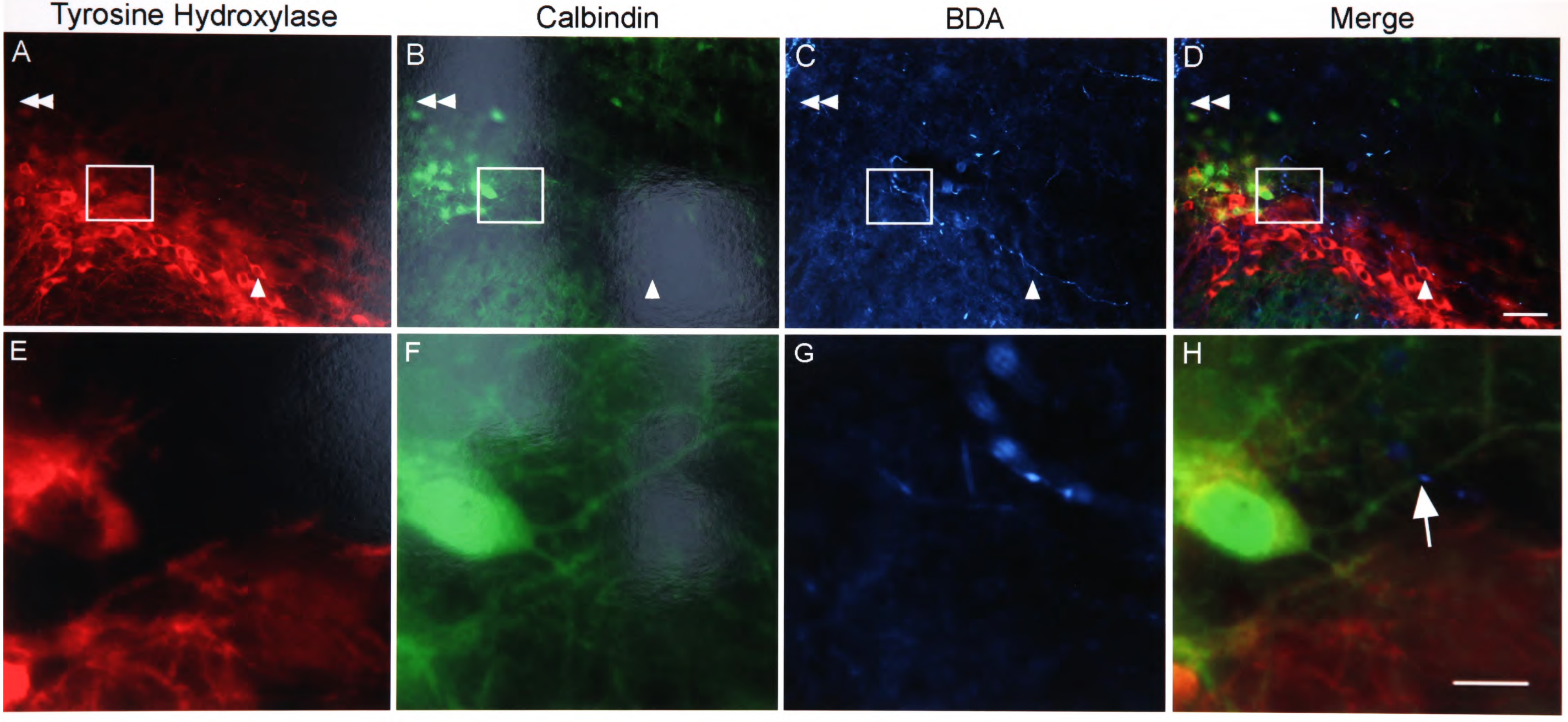

Tyrosine Hydroxylase
Calbindin
BDA
Merge
A
B
C
D
E
F
G
H

Figure 5.11b

(continue) Fluorescent images of dorsal raphe fibers projecting onto neurons in the SNL.

b) **(I-L)** High magnification images of the neuron highlighted by an arrowhead in (A-D). A TH+/CB- neuron made close contact with the BDA-labelled fiber at its distal dendrite (L, arrow) and at its cell body (L, double arrows). On the other hand, other neurons in the field (I) do not receive any projections (L).

c) **(M-P)** High magnification images of the neuron highlighted by the double arrowheads in (A-D). The neuron was not TH+ (M), but was CB+ (N). BDA-labelled projection (O) made several close contacts onto the neuronal cell body (P).

Scale bars: A-D = 50μm, E-P = 10μm

Tyrosine Hydroxylase

Calbindin

BDA

Merge

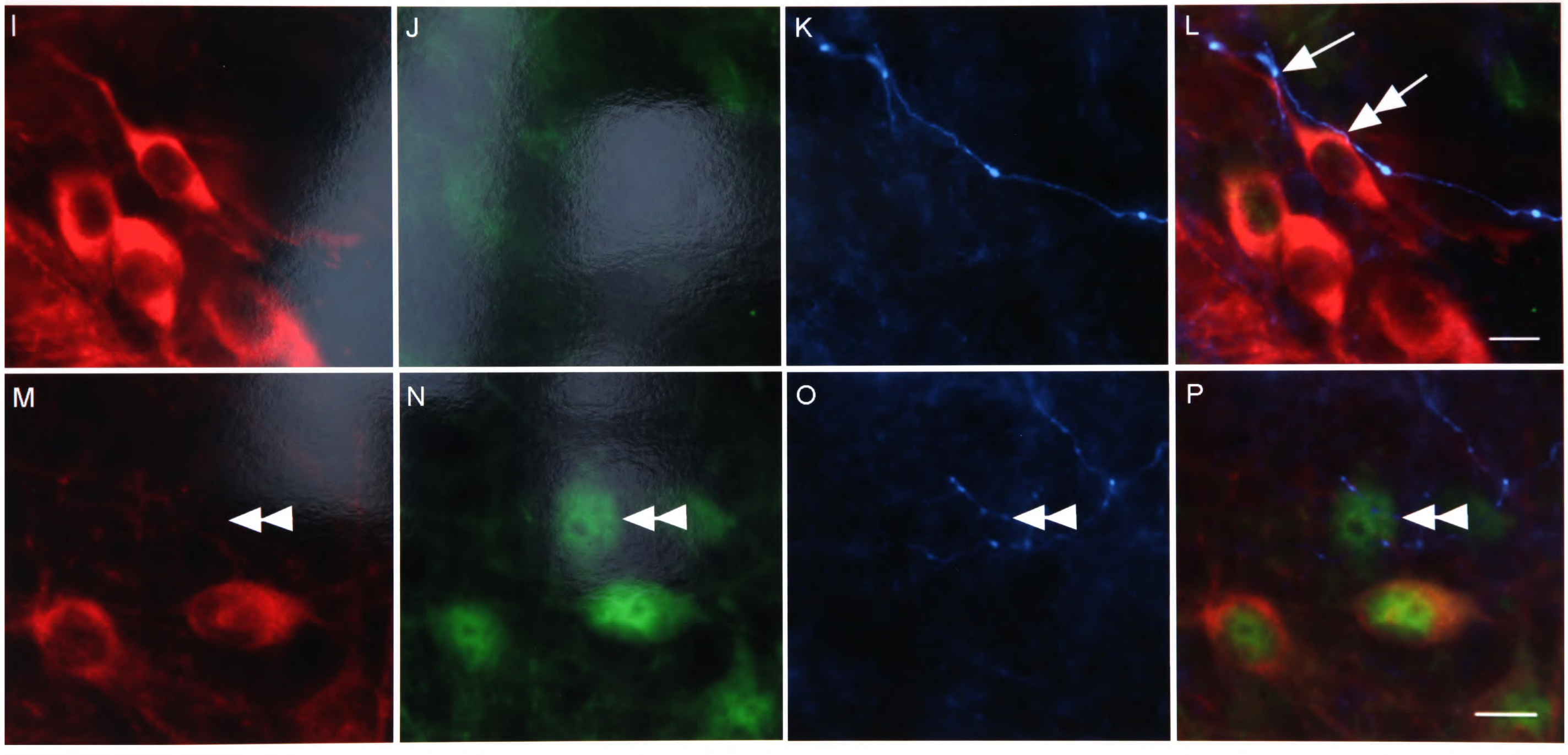


Figure 5.12

Fluorescent images of dorsal raphe fibers projecting onto DA neurons in the rostral VTA. **(A-D)** DA neurons which were TH+ were abundant in the VTA (A), as were CB+ neurons (B). Long BDA-labelled dorsal raphe fibers were observed in this region (C). Merged image shows approximately 50% of the DA neurons in the VTA were TH+/CB+ (D).

(E-H) High magnification images of (A-D) showing one of the TH+/CB+ neuron (E and F, arrowhead) which received a projection from the dorsal raphe onto its cell body (G and H, arrows). On the other hand, an adjacent neuron only showed TH-immunoreactivity (E-H, double arrows) and made close contact with the BDA-labelled fiber at its cell body (H).

Scale bar: A-D = 50μm, E-H = 10μm

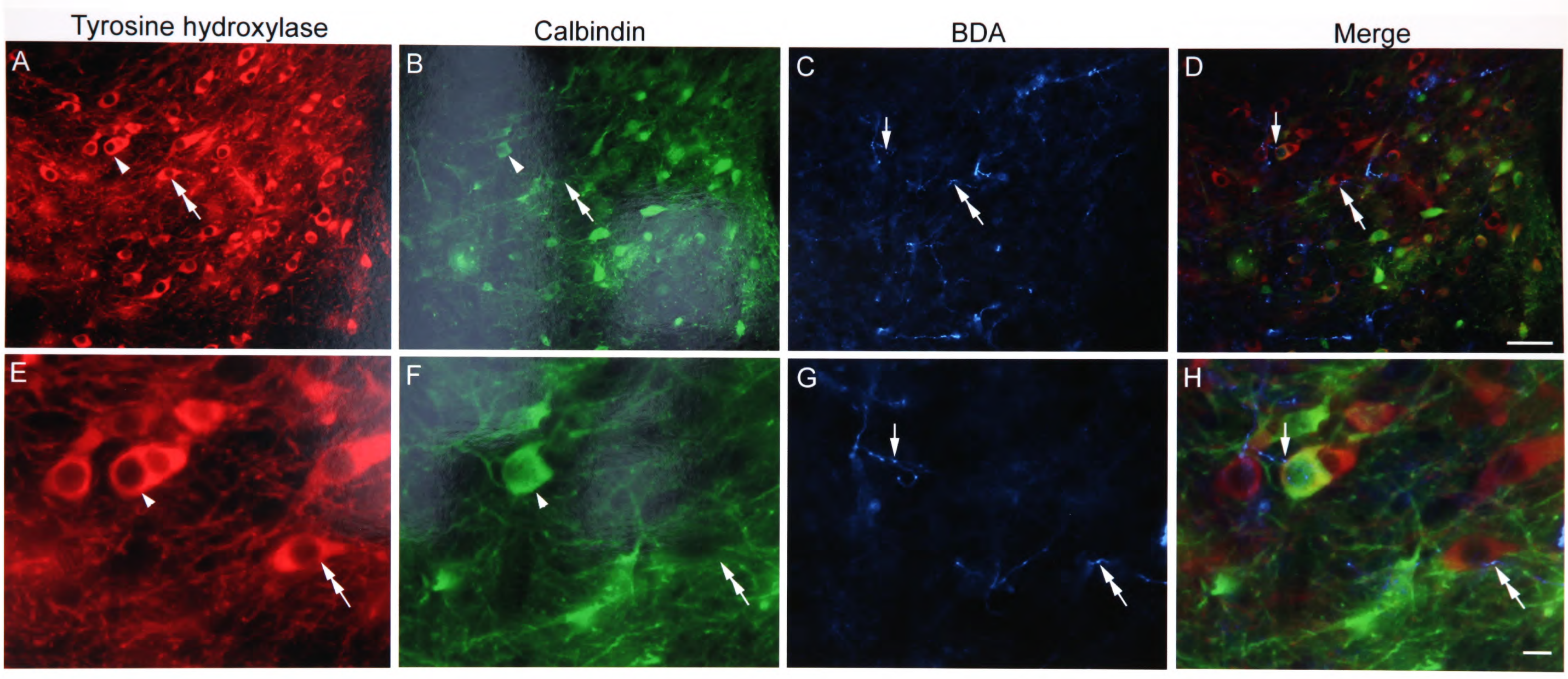

Tyrosine hydroxylase
Calbindin
BDA
Merge
A
B
C
D
E
F
G
H

Figure 5.13

Fluorescent images of dorsal raphe fibers projecting onto DA neurons in the caudal VTA.

(A-D) In the caudal VTA where its neighbouring structure includes the RRF, the number of TH+ neurons was fewer compared to that in the rostral VTA (A). Many neurons in this region were also CB+ (B) and may receive inputs from the BDA-labelled fibers (C). Merged image confirms a large proportion of TH+/CB+ neurons.

(E-H) High magnification images of a neuron located in the medial, caudal VTA (A and B, E and F, double arrowheads). It was TH+/CB+ and received two potential synaptic contacts from a BDA-labelled fiber onto its cell body (G and H, double arrows).

(I-L) High magnification images of a neuron located in the ventral, caudal VTA (A and B, I and J, arrowheads). It was TH+/CB- (I, J) and made close contact with a BDA-labelled fiber (K, arrow) at its cell body (L, arrow).

Scale bars: A-D = 50μm, E-L = 10μm

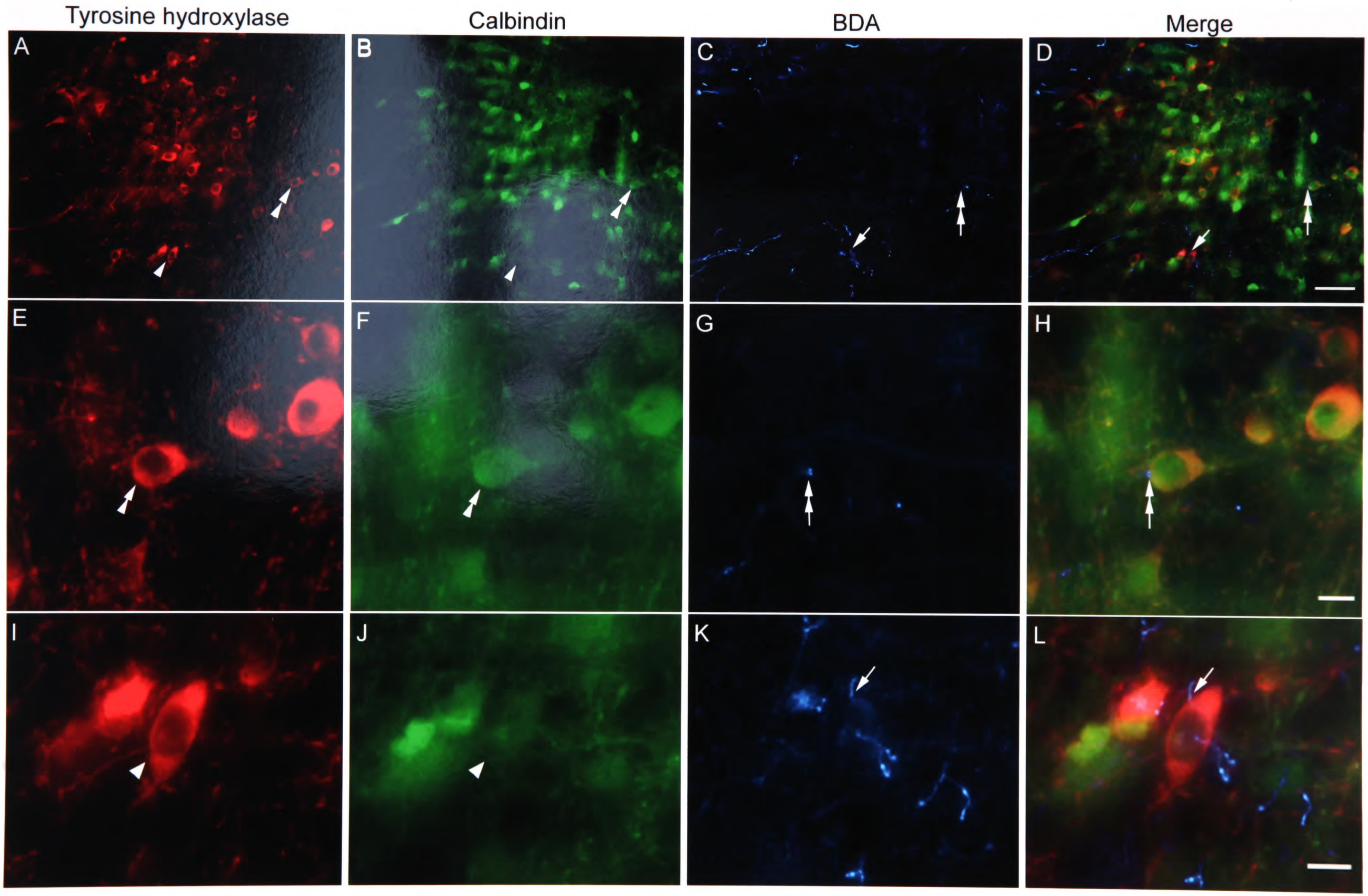

Tyrosine hydroxylase
Calbindin
BDA
Merge
A
B
C
D
E
F
G
H
I
J
K
L

Figure 5.14

Fluorescent images of dorsal raphe fibers projecting onto non-DA neurons in the VTA.

(A-D) The non-DA neurons were identified by the lack of TH-immunoreactivity (A). Some of them were CB+ (A and B, arrowheads) and made close contact with BDA-labelled fibers (C and D, arrows) at the cell body.

(E-H) High magnification images of the non-DA neuron highlighted by the arrowheads. The BDA-labelled fiber appeared to make contact onto the neuronal cell body (G and H, arrows).

Scale bars: A-D = 50μm, E-H = 10μm

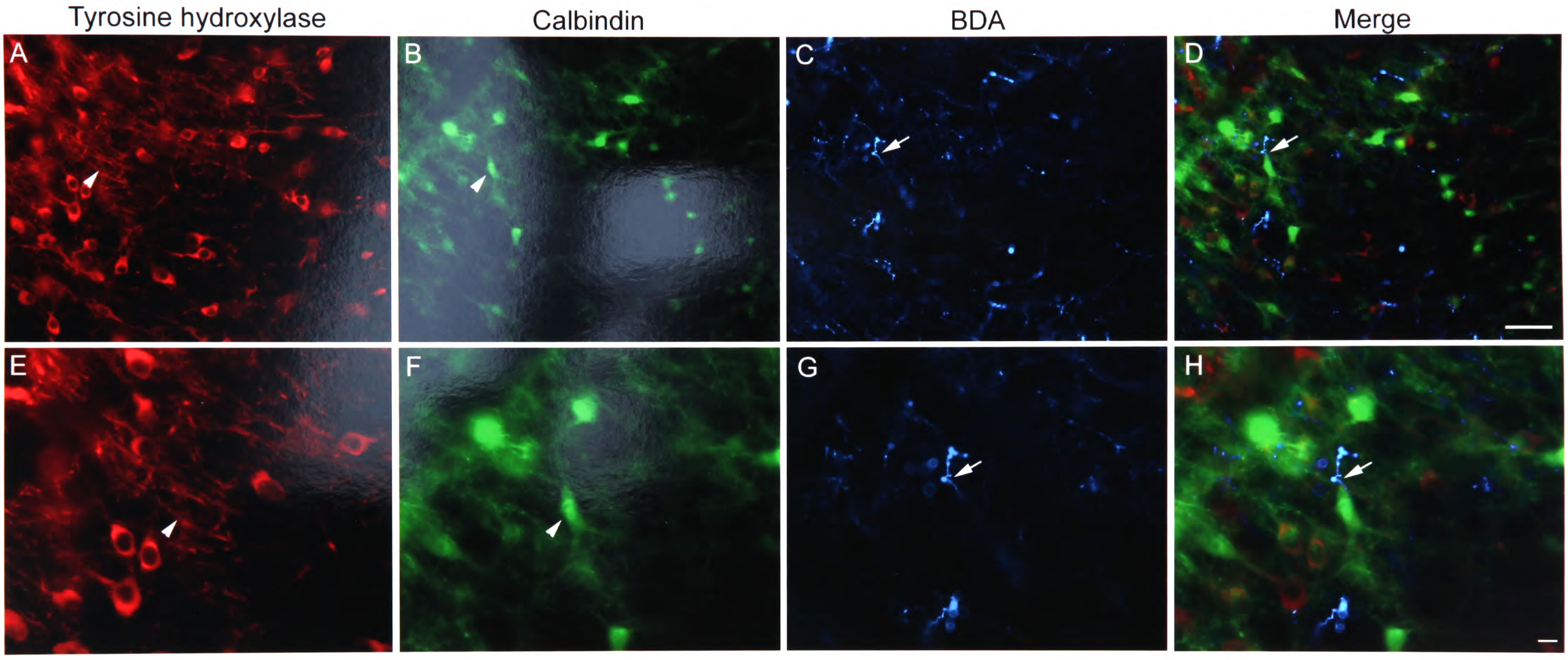

Tyrosine hydroxylase
Calbindin
BDA
Merge
A
B
C
D
E
F
G
H

Figure 5.15

Synaptic contact formation between a dorsal raphe projection and a TH+ neuron in the VTA.

(A) A schematic diagram of a coronal section illustrating that the TH+ neuron investigated was taken at approximately 3.28 mm caudal to Bregma and the section was taken in the VTA (blue box).

(B) Light micrograph showing grey-black TH+ cell bodies and dendrites in the VTA, revealed using SG as the chromogen. Tracer-filled axon terminals were revealed with DAB (brown). The varicosities were round and varied in sizes. The TH+ neuron appeared to be in close contact with one of the axon varicosities (arrow).

(C and D) Electron micrographs showing the TH+ neuron perikarya in synaptic contact (C, box) with a tracer-filled raphe-nigral input. The thickening of the pre- and postsynaptic membrane suggests a symmetric synaptic contact (D, arrows).

(E) Light micrograph showing another section of the same neuron. A long tracer-filled axon (arrow) ran across the neuron and one of its large varicosities appeared to be in close apposition with the neuronal cell body.

(F and G) Electron micrographs of a dorsal raphe projection in contact with a TH+ perikarya (F, box). The whole length of the neuron and its adjacent neuron were clearly correlated in this frame. The synapse (G, arrows) appeared to be symmetric.

(H-J) Light micrograph showing another section of the same neuron, where no varicosity was made onto the neuron (arrow). However, under electron microscopy (I), the correlated location on the immunolabelled cell body (box) did receive a symmetrical input from an unlabelled axon (J, arrows). This suggests potential synaptic regulation(s) by input(s) other than from the dorsal raphe. Scale bars: B = 10μm, C = 5μm, D = 0.5μm, E = 10μm, F = 5μm, G = 0.5μm, H = 10μm, I = 5μm, J = 0.5μm

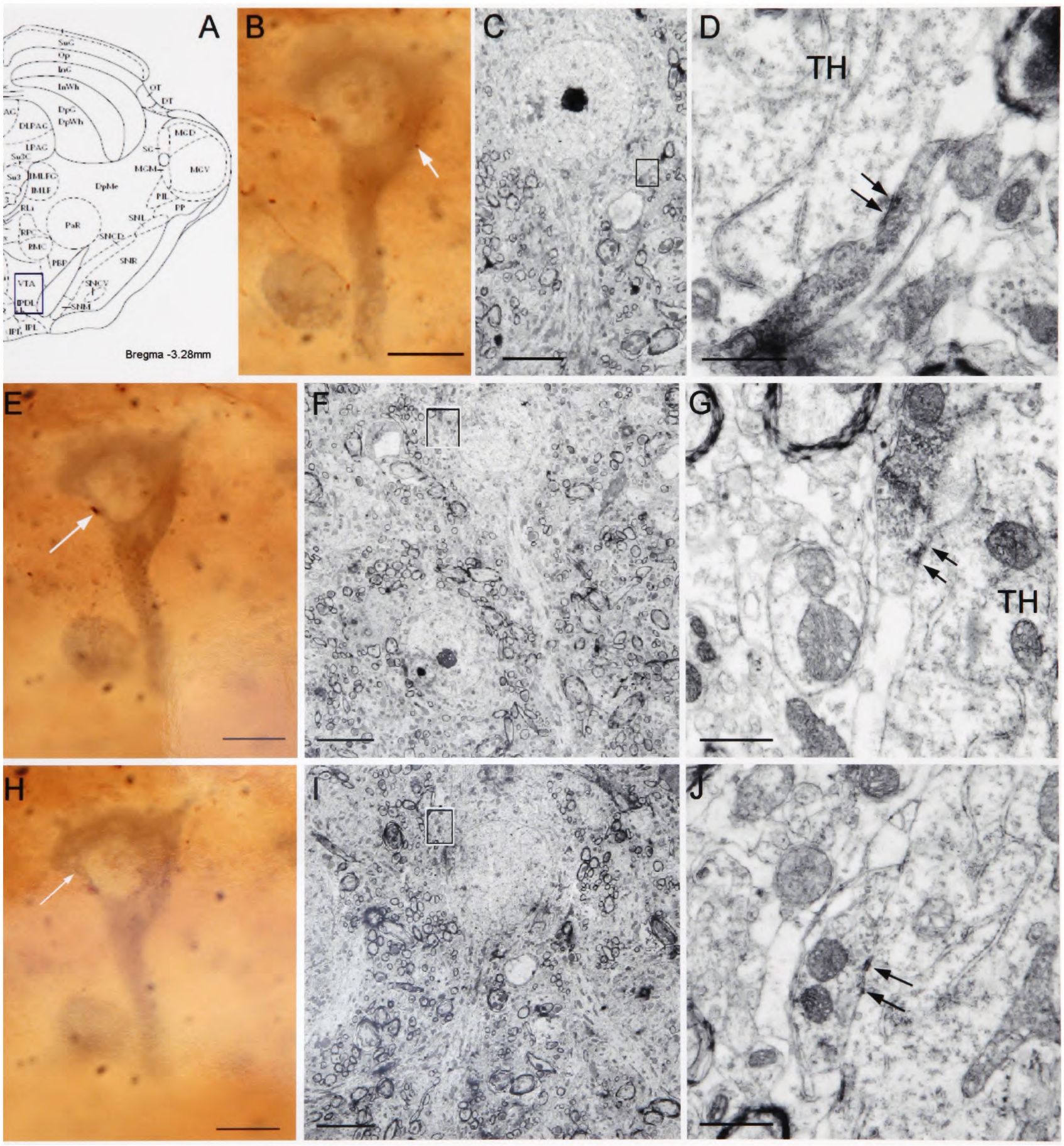

A
B
C
D
TH
SuG
Op
InG
InWh
OT
DT
DpC
DpWh
DLPAG
MGD
LPAG
SG
Su3C
Su3
IMLFC
IMLF
MGM
MGV
DpMe
PIL
RLi
PP
SNL
PaR
RPC
RMC
SNCD
PBP
SNR
VTA
PDL
SNCV
SNM
IPL
Bregma -3.28mm
E
F
G
TH
H
I
J

Figure 5.16

Synaptic contact formation between a dorsal raphe projection and a CB+ neuron in the VTA.

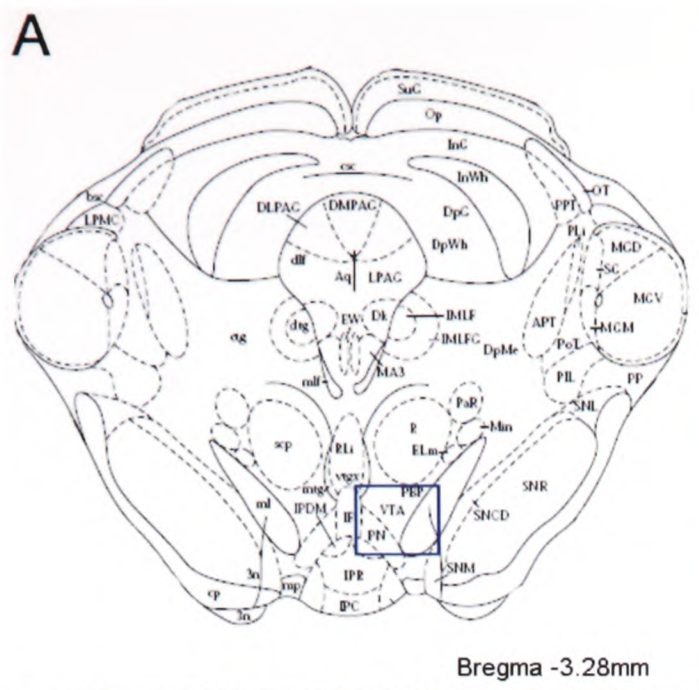
(A) A schematic diagram of a coronal section illustrating that the CB+ neuron investigated was taken at approximately 3.28 mm caudal to Bregma and the section was taken in the VTA (blue box).

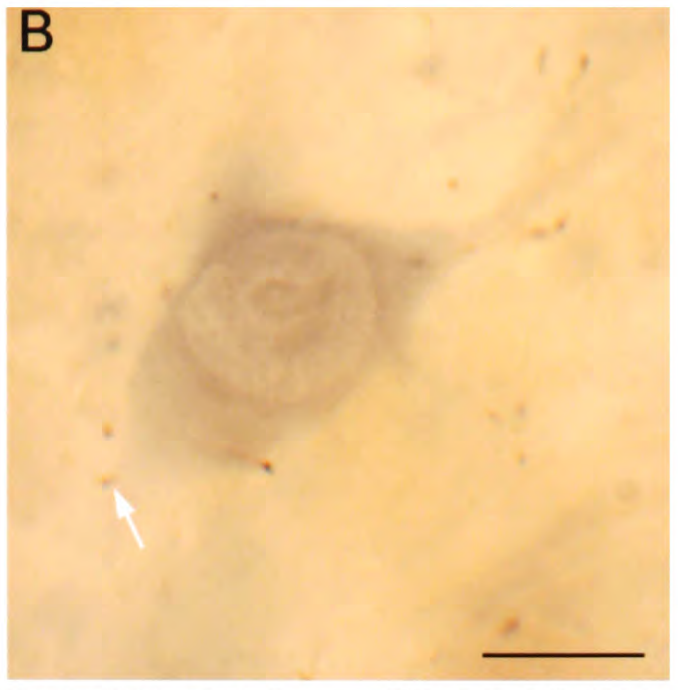
(B) Light micrograph showing a grey-black CB+ cell body in the VTA, revealed using SG as the chromogen. Tracer-filled axon terminals were revealed with DAB (brown). The varicosities were mostly large and round. The CB+ neuron appeared to be in close contact with several varicosities, one of which is highlighted with an arrow.

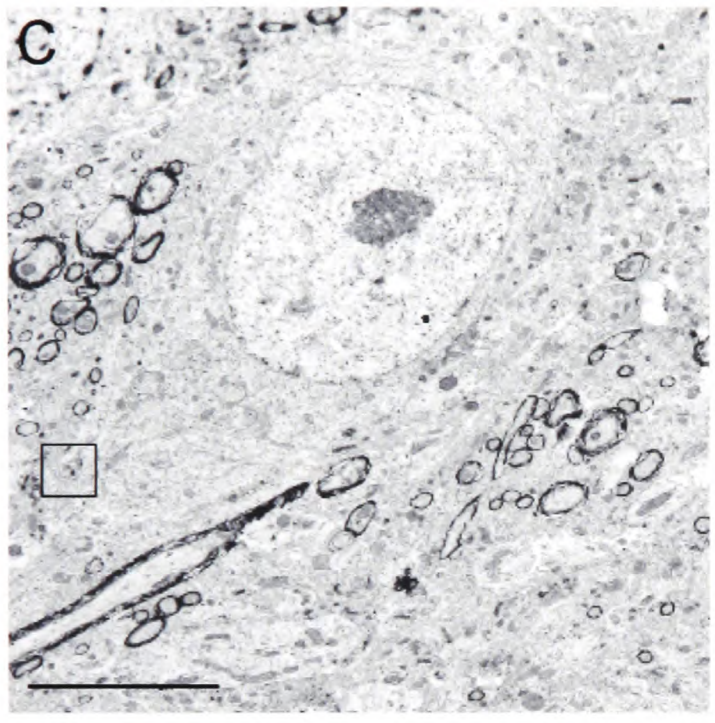
(C and D) Electron micrographs showing the CB+ neuron perikarya in synaptic contact (C, box) with a tracer-filled dorsal raphe input. It appears to be a symmetric contact (D, arrows), with densely packed synaptic vesicles in the presynaptic terminal.

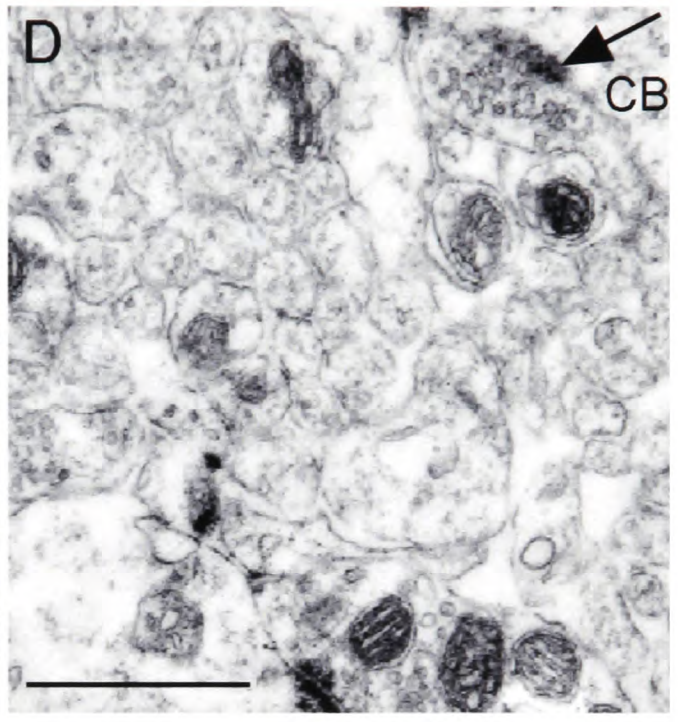
(E) Light micrograph showing another section of the same neuron. A large, round varicosity appeared to make close contact with the cell body (double arrows) whereas another tracer-filled axon seems to project across the neuron (arrow).

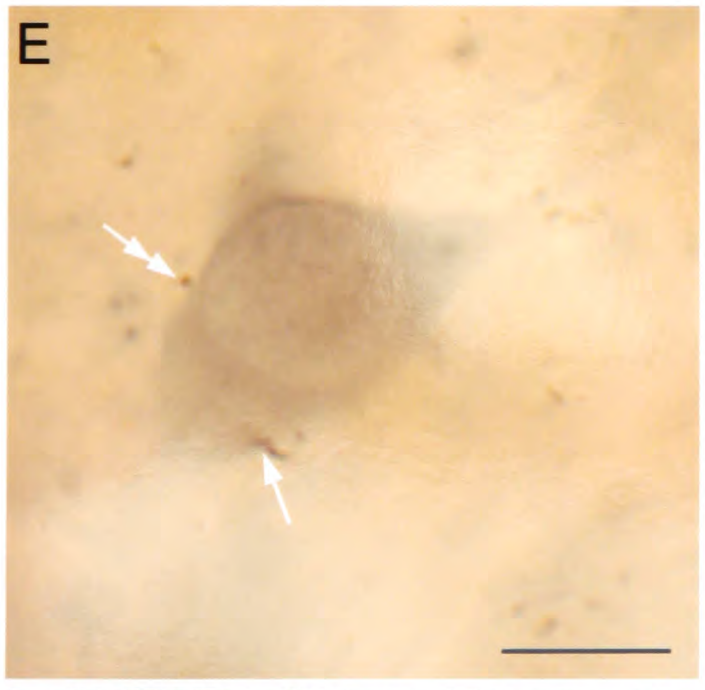
(F-H) Electron micrographs of dorsal raphe projections in contact with the CB+ perikarya (F, box and arrow). At high magnification of the boxed area, an anterogradely labelled bouton was shown making a small symmetric synaptic contact with the neuron (G, arrows). At high magnification of the area highlighted with an arrow in F, another raphe-nigral bouton made a symmetric synapse with the CB+ neuron (H, arrows) and at the same time, formed a symmetric contact with an unlabelled dendrite (H, blue arrowheads). Scale bars: B = 10μm, C = 5μm, D = 0.5μm, E = 10μm, F = 5μm, G & H = 0.5μm

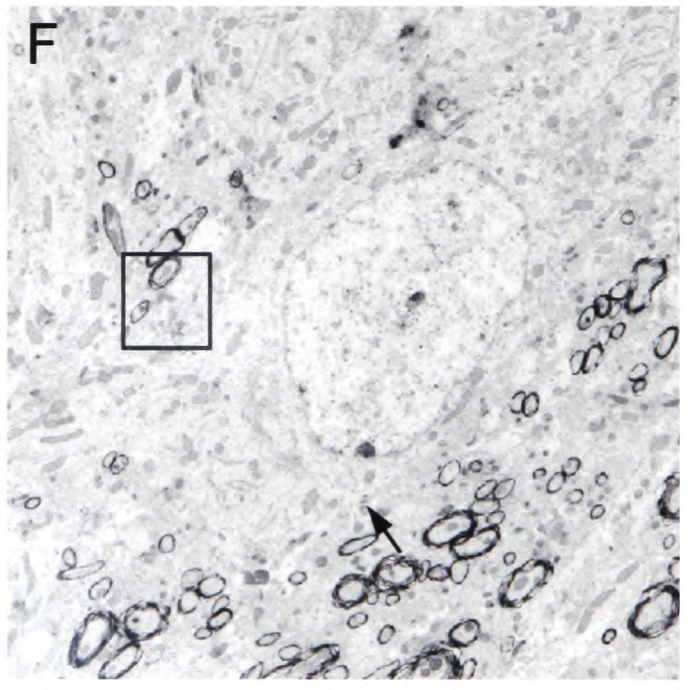

A
SuG
Op
InG
InWh
OT
LPMC
DLPAC
DMPAC
DpG
DpWh
PPT
PLi
MCD
SG
MCV
dlf
Aq
LPAG
dtg
EW
Dk
IMLF
IMLFC
APT
MCM
DpMe
PoL
mlf
MA3
PIL
PP
PaR
SNL
Mtn
scp
RLi
ELm
vtgx
SNR
mtg
ml
IPDM
IF
PBP
VTA
PN
SNCD
3n
rnp
IPR
SNM
cp
IPC
Bregma -3.28mm

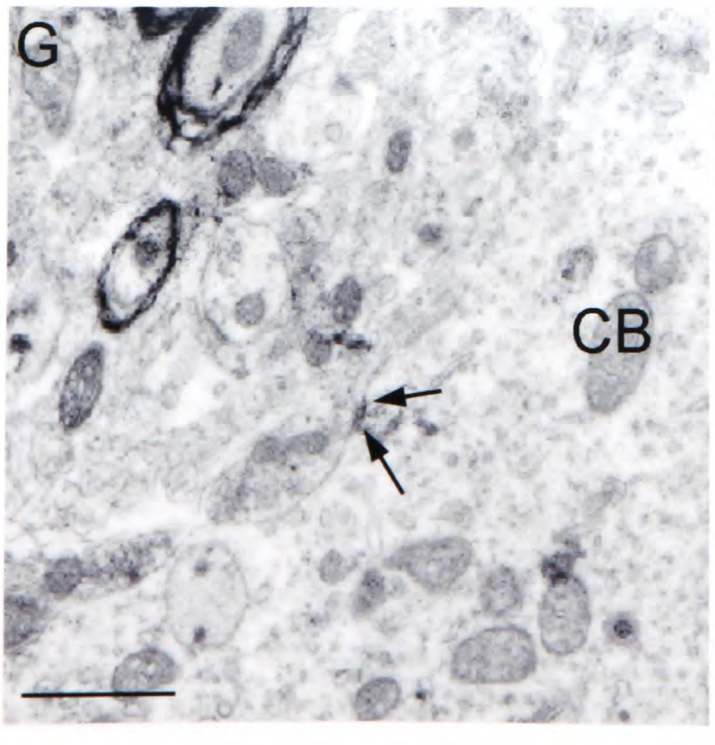

B

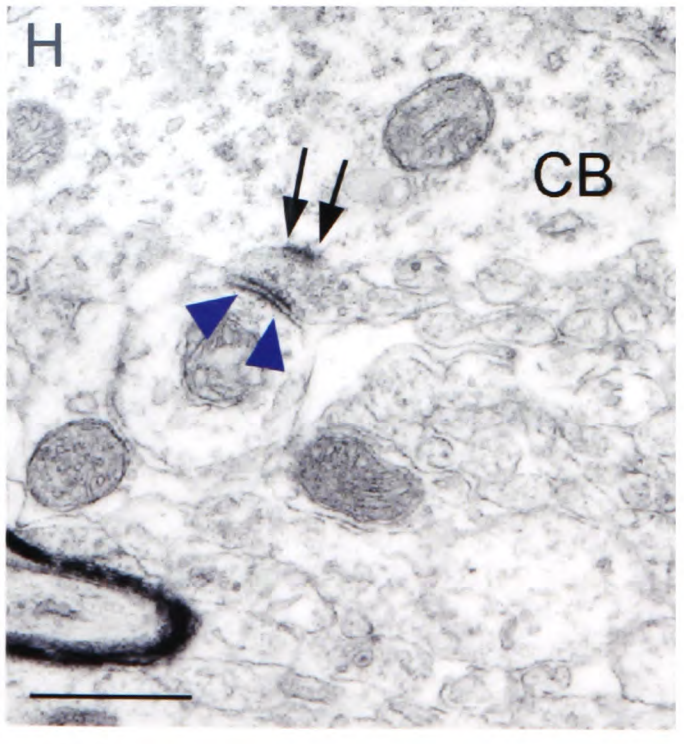

C


D
CB


E


F


G
CB


H
CB

6 Effects of Salicylic Acid on Nigral Neurons in the MPTP/probenecid Mouse Model

6.1 Introduction

The neurotoxins MPTP, and 6-OHDA have been used to induce PD-like conditions in mice. After systemic administration, MPTP, which is highly lipophilic, crosses the BBB within minutes (Markey et al., 1984). Once in the brain, the pro-toxin MPTP is oxidised to 1-methyl-4-phenyl-2,3-dihydropyridinium (MPDP+) by monoamine oxidase B (MAO-B) in glia and serotonergic neurons, the only cells that contain this enzyme. It is then converted to the reactive metabolite 1-methyl-4-phenyl pyridium, MPP^+, probably by spontaneous oxidation. MPP^+ enters DA neurons and inhibits mitochondrial complex I (Singer et al., 1987; Chiueh et al., 1992a; Chiueh et al., 1992b; Seaton et al., 1997; Grunblatt et al., 2000), thereby leading to oxidative stress and neuronal cell death (Chiueh et al., 1992a; Chiueh et al., 1992b; Chiueh and Rauhala, 1998). Since MPP+ is a polar molecule, it depends on the plasma membrane carriers to enter cells. It is a high-affinity substrate for the dopamine transporter (DAT) and for norepinephrine and serotonin transporters (Javitch et al., 1985; Mayer et al., 1986) but degeneration is most prominent in DA neurons.

DA neurons that contain neuromelanin are more susceptible to MPTP-induced degeneration (Herrero et al., 1993). Neuromelanin may contribute neurodegeneration in PD by catalysing reactive oxygen species through an interaction with iron selectively in pigmented neurons (Zecca et al., 2001). Figure 6.1 shows a diagram of dopamine metabolism to illustrate the pathways upon which neurotoxins can act.

Free radical generation is, in fact, a naturally-occurring cellular process. Most reactive oxygen species (ROS) are by-products of incomplete metabolic reduction of oxygen to water and a cascade of redox activities (Figure 6.2). The brain is particularly susceptible to the damaging affects of ROS for several reasons: its high oxygen consumption leads to a greater chance for leakage of partially reduced oxygen species; its high unsaturated fatty acid content

is particularly prone to lipid peroxidation; the presence of H_2O_2-generating enzymes such as the monoamine oxidases and the presence of readily autoxidizable substrates such as dopamine and noradrenaline (Halliwell, 1989).

Accumulating evidence suggests that oxidative stress is a feature of PD neuropathology. For example, PD is characterised by a reduction in amounts of the thiol-reducing agent glutathione (GSH) in the SN, including within DA neurons (Perry et al., 1982; Perry and Yong, 1986; Pearce et al., 1997). GSH and oxidized glutathione depletion is the earliest known biochemical indicator of nigral degeneration, and the magnitude of depletion parallels the severity of the disease (Andersen, 2004). Transgenic mouse lines that emulate the oxidative changes observed in various neurodegenerative diseases have been created. Most of them have null or partial mutations in the antioxidant enzymes such as the superoxide dismutase family (SOD), glutathione peroxidases (GSHPx-) and inducible nitric oxide synthase (NOS). Many of these mutations seem to increase sensitivities to the toxic effects of MPTP (Przedborski et al., 1992; Grunewald and Beal, 1999; Klivenyi et al., 2000b; Klivenyi et al., 2000a; Zhang et al., 2000; Kunikowska and Jenner, 2003). In chronic MPTP- and 6-OHDA-induced PD models, microarray analyses show that the expression of genes associated with oxidative stress and inflammation are significantly altered in toxin-treated animals compared to controls (Potashkin and Meredith, 2006). Hence, antioxidant enzymes, in addition to CB, may be another class of vulnerability factor contributing to differential neurodegeneration.

In order to limit oxidative stress, the antioxidant property of non-steroidal anti-inflammatory drugs (NSAIDs) have been explored in animal models of PD (Teismann and Ferger, 2001; Ton et al., 2006). Salicylic acid (SA), a metabolite produced *in vivo* following the administration of aspirin, can be hydroxylated to form 2,3- and 2,5-dihydroxybenzoic acid

(DHBA) by utilizing hydroxyl radicals (˙OH). This ˙OH scavenging action has been shown to be neuroprotective against MPTP-induced degeneration in mice (Aubin et al., 1998; Mohanakumar et al., 2000). In addition to its radical scavenging properties, aspirin's anti-inflammatory action may also work synergistically to protect neurons. However, not all NSAID treatments yield the same protective effect. In humans, although use of non-aspirin NSAIDs was inversely associated with the risk of PD in a longitudinal cohort study, no association was found between aspirin and the risk of PD (Chen et al., 2005; Ton et al., 2006). Thus, this study explores the potential of SA as a PD therapy by examining its effects on nigral cell death and its anti-inflammatory action in the MPTP/p mouse model.

6.2 Aims

- To observe the immunological differences in MPTP/probenecid mice with and without SA treatment
- To compare the numbers of TH+, CB+ and TH+/CB+ neurons in the midbrain amongst the lesioned and control groups
- To observe the microglial response amongst the lesioned and control groups as a means to demonstrate the anti-inflammatory action of SA

6.3 Methods

6.3.1 Animals and experimental protocols

MPTP/probenecid mice were treated in Professor Gloria Meredith's laboratory (Rosalind Franklin University, Chicago) as described (Chapter 2.1.2). A total of nine adult male C57Bl/6 mice weighing 22-25 g were used (Charles River Laboratories, USA): MPTP/p mice were treated with 250 mg/kg probenecid, followed by either 20 mg/kg MPTP or probenecid twice a week for 5 weeks. In cases where SA treatment was required, sodium

salicylate (Sigma Aldrich) was given from 3 days (50 mg/kg, s.c.) after the last MPTP injection to make sure the MPTP was cleared out of the mouse's system and to allow for a behavioural test. The salicylate was then given for 14 days at the same time every morning. Mice were sacrificed 5 months after MPTP treatment.

6.3.2 TH and CB immunostaining

Brains were perfused with 4% paraformaldehyde and 0.05% glutaraldehyde in PBS as described (Chapter 2.2.3). Coronal sections of 50 μm were cut. Nigral sections were immunocytochemically stained for TH (1:1000, polyclonal rabbit anti-TH, BioMol) and CB (1:1000, monoclonal anti-CB, Swant) over 48 h as described (Chapter 2.4.1). Alexa Fluor 488 (1:500, goat anti-rabbit IgG, Molecular Probes) and 568 (1:500, goat anti-mouse IgG, Molecular Probes) were incubated for 2 h as secondary antibodies to identify TH and CB respectively. The sections were then visualised under a fluorescent microscope (Leica Diaplan) and analysed with the QCapture Pro software (Version 5.0.1.26) and Adobe Photoshop. Photomicrographs showing the SN were combined using Canon PhotoStitch to show the scope of the immunostaining.

6.3.3 Macrophage antigen complex-1 (MAC-1) immunostaining

MAC-1 (also known as CD11b antibody) was used as a marker for activated microglia. Polyclonal rat anti-MAC-1 antibody (1:500, Boehringer Mannheim) with 0.1% Triton X-100 in PBS was incubated with the nigral sections for 24 h at 4°C. After washing, the sections were incubated with biotinylated goat anti-rat antibody (1:300) for 90 min at room temperature. They were then treated with ABC for 50 min at room temperature, followed by three washings in 0.05 M Tris-HCl (pH 7.6). The sections were visualised by reacting with

DAB for 10 min. They were mounted on gelatinized slides, left to dry overnight, dehydrated in ascending alcohol concentrations and mounted in XAM (BDH).

6.3.4 Cell counting and statistics

The boundaries of the SN and VTA were delineated according to a matched series of Nissl stained sections and immunolabelled neuronal cell bodies were counted using the fluorescent images under blind conditions. This procedure was carried out on four sections at a periodicity of 200 μm in the midbrain. After all immunolabelled neurons were counted, a total neuronal number was estimated by summing the number of neuron profiles and multiplying by four. Nominal values were analysed using general linear modelling procedure of ANOVA followed by *post-hoc* Fisher's *t*-test. $P < 0.05$ was used to determine statistical significance. And the results are expressed as mean cell counts ± SEM.

6.4 Results

6.4.1 Administration of SA in the MPTP/p mouse model

Four groups of mice were compared in this study: MPTP/p with SA (n=4), MPTP/p without SA (n=1), probenecid with SA (n=2) and probenecid without SA (n=2). The low number of animals used was due to an error made during perfusion, where glutaraldehyde was incorrectly not mixed into the fixation solution (Pitner J, personal communication). This could cause a difference in immunostaining results and the animals were therefore not used in the analyses. The data for MPTP/p without SA were subsequently pooled with the MPTP/p-treated mice with a 3-month survival period (Chapter 4).

The dose of salicylate used was modified from a published study (Ferger et al., 1999) as it was found that 100 mg/kg of SA caused ulcers (Meredith GE, personal communication).

Therefore a lower dose of 50 mg/kg was used. Furthermore, subcutaneous injections, as suggested by Yoshida *et al.* (Yoshida et al., 2002), were used instead of intraperitoneal because these are less invasive.

6.4.2 Effects of salicylic acid on TH+, CB+, and TH+/CB+ nigral neurons

SA was injected into the animals after MPTP/p treatment. This is to test whether SA could *rescue* the neurons which would have been undergoing neurodegeneration, rather than its ability to *prevent* neurodegeneration, so as to design a better therapy for patients who have been diagnosed with PD. To determine whether SA has any effect on nigral neurons in PD, MPTP/p-treated and probenecid-treated mice were used as test and control groups respectively. This allows a comparison between the results obtained in this experiment and previous data on the 1- and 3-month MPTP/p mice (Chapters 3 and 4). In addition to the effect of SA on the TH+ neuron number in the SN and the VTA, I also investigate any changes in CB+ and TH+/CB+ neurons, which might shed light onto the interplay of different potential vulnerability factors.

Probenecid-treated mice represent the vehicle-only control group. Without SA, control mice showed classical TH-immunoreactivity, where TH+ cell bodies were found along the SNC, SNL and with their dendritic projections into the SNR (Figure 6.3 A). CB+ neurons clustered in the SNC close to the midline, as well as in the SNL (Figure 6.3 B). Most CB+ neurons were also TH+ but only about 25% of the TH+ neuronal population was co-localised with CB (Figure 6.3 C). In the VTA, a large number of TH+ cell bodies and dendrites were observed (Figure 6.3 D), as well as abundant CB-immunoreactivity (Figure 6.3 E). Again, most CB+ neurons were co-localised with TH+ neurons and about 75% of the TH+ neurons were CB+ (Figure 6.3 F).

In the probenecid-treated mice with SA, the immunostaining pattern showed no overt difference from those without SA. TH+ and CB+ neurons were found in the same regions of the SN (Figure 6.4 A and B, respectively). From the TH+/CB+ co-localised image (Figure 6.4 C), the proportion of TH+ neurons containing CB appeared to be higher than without SA (without SA: ~25%; with SA: ~50%). This was analysed quantitatively by neuronal cell counts (Table 6.1). In the VTA, patterns of TH- and CB-immunoreactivities were similar to those without SA (Figure 6.4 D and E, respectively). The proportion of TH+ neurons containing CB also appeared to be higher here (Figure 6.4 F).

In the MPTP/p-treated mice without SA, TH-immunostaining pattern was comparable with that found in MPTP/p-treated mice with 1- and 3-months survival. Loss of TH+ neurons from the middle portion of the SNC was particularly apparent (Figure 6.5 A). As in the control mice, CB+ neurons were mostly found in the SNC close to the midline (Figure 5.5B) and a few in the SNL. Almost all CB+ neurons were TH+, whereas approximately 50% of the TH+ neuronal population was CB+ (Figure 6.5 C). In the VTA, TH+ and CB+ neurons appeared to be relatively unaffected by MPTP/p treatment, because intense immunostaining was observed (Figure 6.5 D and E). Almost all the CB+ neurons were TH+ and over 75% of the TH+ neuronal population was co-localised with CB (Figure 6.5 F).

In the MPTP/p-treated mice with SA, TH-immunostaining was found in both the SNC and VTA (Figure 6.6 A and D, respectively), where CB-immunoreactivity was also observed (Figure 6.6 B and E, respectively). The proportion of TH+/CB+ neurons in the SN and the VTA appeared to be similar to that found in MPTP/p mice with no SA treatment (Figure 6.6 C and F).

In order to evaluate quantitatively the effect of SA on neuronal populations, the numbers of TH+, CB+ and TH/CB+ were counted in the midbrain (SN and the VTA). Because only one MPTP/p-treated mouse was explicitly not treated with SA, neuronal counts from MPTP/p-treated mice (3-month survival, n=4) were pooled with this one mouse to give "MPTP/p without SA" group. The assumption that the two groups had similar TH-immunoreactivity was based on previous studies, where there no significant differences in TH-immunoreactivity between the 3-weeks and 6-month post-MPTP/p-treated mice (Petroske et al., 2001) and my own data showing no progressive loss of TH+ cells between 1 and 3 months post-lesion (Chapter 4). Results expressed in mean neuronal counts and SEM are shown in Table 6.1.

The effects of SA treatment were quite complex (Table 6.1). General linear modelling showed that, as expected, the numbers of TH+, CB+ and TH+/CB+ neurons were significantly different in the treated groups ($F_{(2,18)} = 636.084$; $^{***}P < 0.0001$). The different treatments also produced a significant effect ($F_{(3,9)} = 313.611$; $^{***}P < 0.0001$) and there was a cell count x treatment interaction ($F_{(6,18)} = 43.572$; $^{***}P < 0.0001$).

Figure 6.7 illustrates the effect of treatments on the three neuronal groups. *Post-hoc t*-test revealed that treatment with SA had no effect on any of the three cell types in the probenecid control mice. Again as expected, in (Figure 6.7 A), MPTP/p treatment caused a significant loss of TH+ neurons (Figure 6.7A) compared to the controls (MPTP/p no SA vs probenecid no SA; MPTP/p no SA vs probenecid with SA, $^{***}P < 0.0001$). SA treatment afforded a degree of protection for TH+ cells in MPTP/p treated mice, ($^{***}P < 0.0001$) although did not restore the lesioned group to the control neuronal cell counts (MPTP/p with SA vs probenecid no SA; MPTP with SA vs probenecid with SA, $^{***}P < 0.0001$).

In the CB+ population (Figure 6.7 B), MPTP/p treatment also caused a significant cell loss compared to the probenecid control (MPTP/p no SA vs probenecid no SA; MPTP/p no SA vs probenecid with SA, ***$P < 0.0001$). In this case, treatment with SA did not offer any protection to CB+ cells, such that significant reduction were seen in comparison to controls (MPTP/p with SA vs probenecid no SA; MPTP with SA vs probenecid with SA, ***$P < 0.0001$). At the same time, counts did not differ between the MPTP/p mice with or without SA treatment.

In the TH+/CB+ population (Figure 6.7 C), like CB+ neurons, there was no significant difference between the MPTP/p mice with or without SA treatment. Interestingly, although TH+/CB+ cells did not seem to be reduced by MPTP/p lesion (MPTP/p no SA vs probenecid no SA; MPTP/p no SA vs probenecid with SA) the addition of SA treatment did result in vulnerability (MPTP/p with SA vs probenecid no SA, **$P = 0.014$; MPTP with SA vs probenecid with SA, ***$P = 0.007$). In addition to the statistical analyses, the TH+/CB+ neurons were calculated as a percentage of the TH+ population. SA showed no effect in the probenecid controls (Table 6.1) but a lower percentage was found in the MPTP/p mice treated with SA.

6.4.3 Nigral microglia activation

Activated microglia have surface complement receptors that are recognised by the MAC-1 antibody. In the probenecid control mice, no immunoreactivity was observed in the SN along the border of the SNR, (Figure 6.8 A and B) or the VTA (Figure 6.8 C and D), regardless of whether or not they had been treated with SA (compare Figure 6.8 A and C with Figure 6.8 B and D). On the other hand, a large number of activated microglia which had expanded cell bodies and poorly ramified short and thick processes were seen in the MPTP/p without SA group (Figure 6.9 A and B). They were predominately in the SNR. In the SA-treated group,

MPTP/p mice there were a few non-activated microglia based on morphology described in a published literature (Cicchetti et al., 2002) in the SN (Figure 6.9 C and D). Almost no MAC-1 immunostaining was found in the VTA (Figure 6.9 E and F).

6.5 Discussion

The major findings of the present study are: (a) SA treatment was able to protect TH+ neurons but not CB+ or TH+/CB+ neurons against MPTP/p-induced loss *in vivo*, indicated by their immunostaining patterns and neuronal numbers in the midbrain and (b) that SA was able to reduce microglia activation in the MPTP/p-treated mice.

The use of SA has to be justified not only for its potential therapeutic value but also to avoid unwanted side-effects. Until recently, COX-2 inhibitors had been widely used in the prevention of cardiovascular diseases and rheumatoid arthritis; and their efficacy has been studied in large number of patients (FDA). Gastrointestinal irritation is commonly known as the major side-effect of high dose aspirin in humans, and this is apparently matched in mice, as demonstrated by the ulcer formation in the MPTP/p mice treated with 100 mg/kg SA i.p. More importantly, several COX-2 inhibitors have come under strong scrutiny because they cause an increase in heart attacks and strokes in patients taking the drugs, namely celecoxib (Celebrex, Pfizer) and rofecoxib (Vioxx, Merck). Furthermore, Kukar *et al.* found several COX-2 inhibitors increased the production of the toxic amyloid-β ($A\beta_{42}$) peptide (Kukar et al., 2005), which is widely accepted as having a key role in the progression of Alzheimer's disease (Selkoe, 2001). Since both COX-1 and COX-2 have been implicated in PD neuropathology (Figure 6.10) (Teismann and Ferger, 2001; Teismann et al., 2003; Hunot et al., 2004), this study provides important information on the suitability of SA (or aspirin) use as a neuroprotective agent.

In my experiments, SA treatment attenuated DA cell death, as has been previously reported (Aubin et al., 1998; Ferger et al., 1999; Mohanakumar et al., 2000; Sairam et al., 2003). For example, mice pre-treated with SA were protected against MPTP for at least 2 weeks post-treatment (Aubin et al., 1998) and MPTP-induced loss of TH+ nigral cell bodies was nearly completely prevented by the higher dose of sodium salicylate (Ferger et al., 1999). The different experimental procedures and PD models must be taken into consideration. First, those studies used SA prior to neurotoxin administration but here SA was given after MPTP/p. This poses an interesting implication that, whilst prophylactic use of SA may have a near-complete neuroprotective effect, its application may fail to fully rescue the DA neurons once PD degeneration progresses, although MPTP/p with SA treatment has significantly more TH+ neurons than MPTP/p without SA. The protection may be dose-dependent and further experiments will be required to test this hypothesis.

All SA studies in neurotoxin-based rodent models to this date have been acute treatments: Ferger *et al.* and Aubin *et al.* used a single dose of sodium salicylate followed by a single dose of MPTP in C57Bl/6 mice; Mohanakumar *et al.* and Sairam *et al.* used MPTP and SA twice in Balb/c mice and Sprague-Dawley rats respectively. These protocols, with fewer neurotoxin and SA administrations within a short period, may result in an acute interaction, without allowing the DA neurons to begin to degenerate before testing potential SA neuroprotection. Instead, mice used in this study received subchronic treatment of ten MPTP doses over 5 weeks and SA for 14 consecutive days, starting three days after the last toxin treatment. Moreover, the mice had a much longer survival period after MPTP/p administration (5 months) compared to the other studies (maximum of 2 weeks, possibly limited by the need to measure dopamine metabolites in the mouse brains). My data are therefore more relevant to a clinical treatment strategy and suggest at least limited efficacy for SA. Investigations on SA treatments in cardiovascular diseases have shown that its use is

time-dependent (Sobal et al., 2000; Mehta et al., 2004) and dose-dependent (Farivar et al., 1996; Brooks et al., 2003). Thus, the present model has the advantage of allowing sufficient time for MPTP to act on neurons, eliciting cell death and perhaps better replicating human PD pathology. If SA has a protective effect against MPTP/p-induced neural degeneration, such prolonged treatment should have resulted in more surviving TH+ neurons than with the toxin treatment alone, which was indeed the case.

The efficacy of SA treatment seems to be specific. In contrast to the TH+ population, the number of neither CB+ nor TH+/CB+ was significantly affected by SA treatment in the MPTP/p mice. So, the TH+/CB+ neurons shared more characteristics as CB+ neurons. If CB has a role in neuroprotection, at least when it is in DA neurons, my results showed that these CB-containing neurons cannot be "boosted" by SA and prevent cell loss. Perhaps the anti-oxidant property of SA has no obvious association with CB and these two potential vulnerability factors do not show synergistic effect in neuroprotection. It is also unexpected that the proportion of TH+/CB+ co-localised neurons in either TH+ or CB+ population was lower in the MPTP/p groups treated with SA. No report has shown a toxic effect of SA in midbrain neurons thus far. Variations in small animal groups in the "MPTP/p no SA" group may have resulted in the unexpectedly higher number of TH+/CB+ neurons compared to the "MPTP with SA" group, but misinterpretation of data was minimised by using consistent quantifying methods across the three neuronal groups. Further experiments with more animals have to be used to support these findings.

Since the mice used here were about 6 months post-MPTP/p treatment, neuronal losses in the three populations could be compared qualitatively with the 1- and 3-month post-treatment data. In the probenecid controls of all three neuronal types, cell loss was irreversible but did not seem to be progressive. In the MPTP/p-treated mice, the number of TH+ neurons showed

small increases over 6 months, which is in agreement with the recovery in striatal dopamine level and the number of midbrain TH+ cells over 6 months (Petroske et al., 2001). On the other hand, there seemed to be gradual losses in CB+ and TH+/CB+ neurons over this period. Hence, progressive neurotoxicity may indeed be exacerbated with time, in support of the findings in Chapter 4.

The limited neuroprotection of all types of midbrain neurons by SA may reflect its mechanism of action. Unlike its precursor, aspirin (acetylsalicylic acid), it does not have the acetyl- group and is therefore a weak inhibitor of COX-1 (Mitchell et al., 1993; Insel, 1996). It is more likely that the neuroprotective activity of SA is mediated through scavenging of $^{\cdot}OH$ – SA traps the highly toxic hydroxyl radical to form harmless 2,3- and 2,5-DHBA (Chiueh et al., 1992b; Obata and Chiueh, 1992; Chiueh et al., 1993) while it has been shown *in vitro* that SA is also capable of scavenging peroxynitrite ($ONOO^-$) (Kaur et al., 1997; Ferger et al., 1999). It is possible that, a mixture of reactive oxygen and nitrogen species was produced in the MPTP/p model. Although SA was effective in mopping up $^{\cdot}OH$ and $ONOO^-$ in, for example, TH+ neurons, this was not sufficient to protect all neurons from other MPTP-induced oxidative stress or further damage such as mitochondrial dysfunction.

The anti-inflammatory component of SA action was also evident against MPTP toxicity. Remarkable elimination of MAC-1-immunoreactive microglia was observed in the midbrain following SA administration in the MPTP/p-treated mice. It is therefore possible that the neurons were protected from secondary degeneration and progressive cell loss. Previous studies in MPTP-treated mice have shown a pronounced microglia reaction (Czlonkowska et al., 1996) and inflammation may occur in PD because reactive microglia have been found in the SN of PD brains (McGeer et al., 1988). Microglial activation was reported to occur before massive death of the DA neurons and the trigger of apoptosis (Sugama et al., 2003b;

Vijitruth et al., 2006). Hence, SA may be more effective via its anti-inflammatory effects than its anti-oxidant properties as a neuroprotective agent in PD.

Recent studies on microglial pro-inflammatory and neurotoxic properties have suggested that good targets for therapeutic intervention include tumour necrosis factor (TNF)α, IL1β, TNF-related apoptosis-inducing ligant (TRAIL), iNOS, as well as glutamate and NADPH oxidase (Mizuno et al., 2005; Qian et al., 2006; Sriram et al., 2006; Takeuchi et al., 2006; Zipp and Aktas, 2006; Klegeris et al., 2007). This has led to the development of various strategies for neutralization of soluble TNFα as a potential anti-inflammatory treatment in PD (McCoy et al., 1983). A therapeutic antibody approach against a TNF receptor (TNFR1) in transplantation in rat straitum has also been examined (Clarke and Branton, 2002).

In conclusion, studies of SA treatment in a subchronic MPTP mouse model demonstrated that it was able to significantly rescue TH+ neurons and it may also provide neuroprotection via its anti-inflammatory action. A better understanding of its pharmacological action might be important to extend its protective ability to all neuronal subtypes and in improving therapeutic strategies for PD.

Figure 6.1

Dopamine synthesis and its metabolism by MAO-A and MAO-B

The pathway of dopamine synthesis proceeds from tyrosine via tyrosine hydroxylase (TH) catalysis to levodopa (L-DOPA), and subsequent decarboxylation by dopa decarboxylase (DDC) to dopamine. Dopamine is metabolized by intraneuronal monoamine oxidase A (MAO-A) and by glial and astrocyte MAO-A and MAO-B.

Purple boxes: Selective inhibitors of the enzymes involved in the metabolic pathway.

[Figure adapted from (Youdim et al., 2006)]

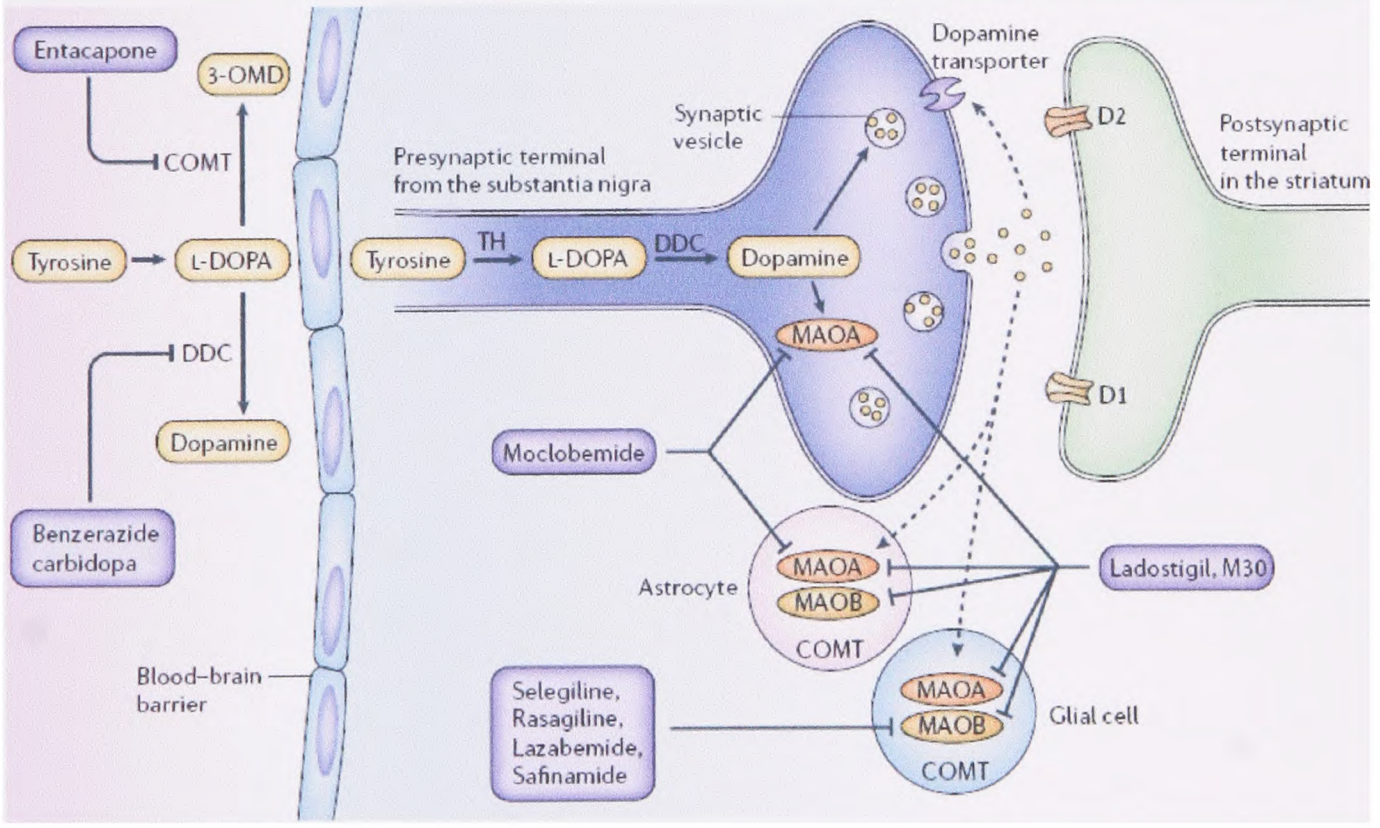


Figure 6.2

Sources of reactive oxygen species (ROS).

The primary source of ROS is leakage of electrons from the respiratory chain in the mitochondria during the reduction of molecular oxygen to water, to generate the superoxide anion, $O_2^{\cdot-}$. H_2O_2 is generated in cells from the breakdown of $O_2^{\cdot-}$, which is catalysed by superoxide dismutases (SODs), and from oxidases and β-oxidation of fatty acids in peroxisomes. Neither H_2O_2 nor $O_2^{\cdot-}$, are strongly reactive and their actions are local. More damaging is the generation from H_2O_2 of the highly reactive hydroxyl radical, $^{\cdot}OH$, which reacts indiscriminately with most cellular constituents. Production of $^{\cdot}OH$ is mediated in the Fenton reaction by reduced transition metal irons such as Fe^{2+}, which are oxidized in the process. The situation is exacerbated by the simultaneous presence of $O_2^{\cdot-}$ that reduces the Fe^{3+} to Fe^{2+} and hence, causes metal ion catalysis of the production of $^{\cdot}OH$. The mechanisms involved in metal ion homeostasis (for copper and iron ions) are therefore important in cellular defenses to minimize the formation of ROS.

Cells can also generate reactive nitrogen species from the reaction of the nitric oxide radical $NO^{\cdot}$ with $O_2^{\cdot-}$ to generate peroxynitrite ($ONOO^-$) and the nitrogen dioxide radical ($NO_2^{\cdot}$), which can nitrate aromatic amino acid residues, lesion DNA and oxidise thiols. Such oxidative stress plays a large part in the propagation of cellular injury that leads to PD neuropathology.

[Figure adapted from Temple, 2005]

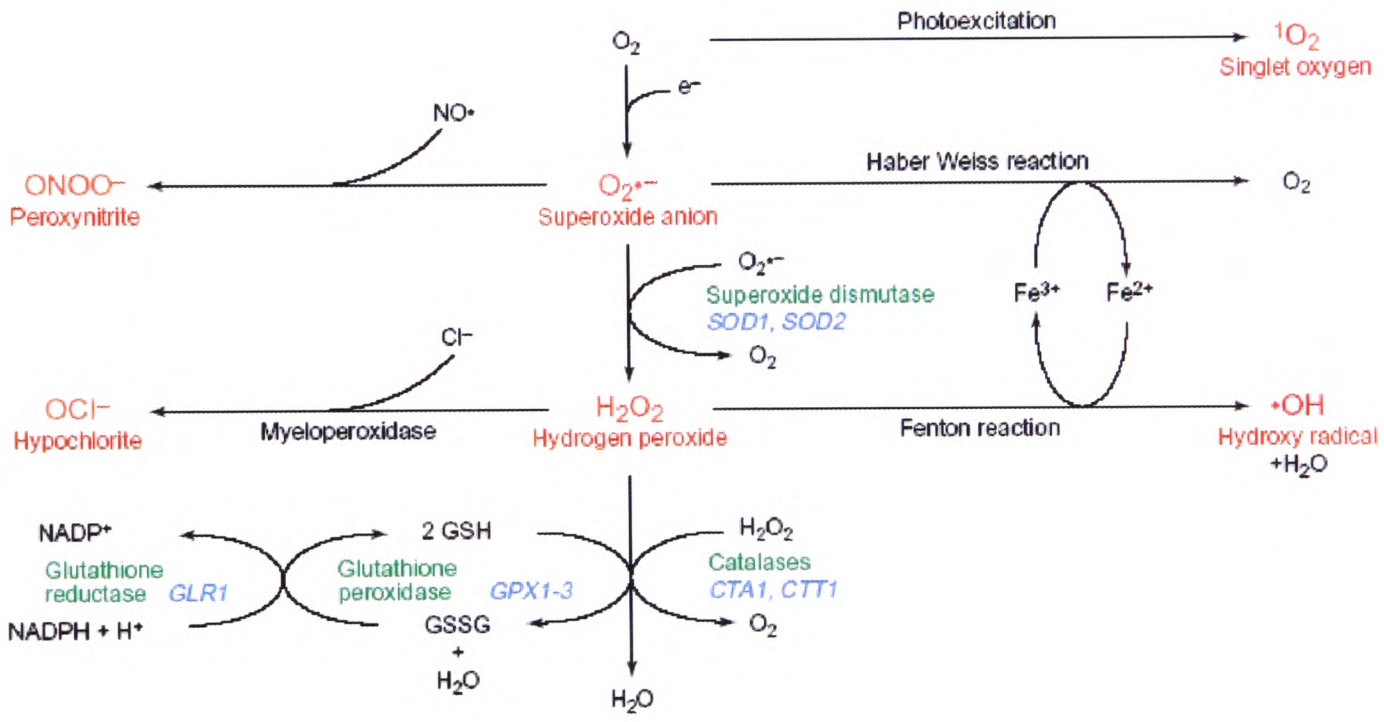

O_2
Photoexcitation
$^1O_2$
Singlet oxygen
e^-
$NO^•$
$ONOO^-$
Peroxynitrite
$O_2^{•-}$
Superoxide anion
Haber Weiss reaction
O_2
$O_2^{•-}$
Superoxide dismutase
SOD1, SOD2
O_2
Fe^{3+}
Fe^{2+}
Cl^-
OCl^-
Hypochlorite
Myeloperoxidase
H_2O_2
Hydrogen peroxide
Fenton reaction
$^•OH$
Hydroxy radical
$+H_2O$
NADP+
2 GSH
H_2O_2
Glutathione reductase
GLR1
Glutathione peroxidase
GPX1-3
Catalases
CTA1, CTT1
NADPH + H+
GSSG
+
H_2O
O_2
H_2O

Figure 6.3

Photomicrographs of nigral neurons in the probenecid-treated mice with no salicylic acid. **(A-C)** Photomicrographs of TH+, CB+ and TH+/CB+ neurons in the SN. The immunostaining patterns were similar to those observed in 1- and 3-month probenecid-treated mice, where TH+ neuronal cell bodies were present in the SNC, SNL and their projections in the SNR. CB+ cell bodies were mostly found in the SNC and SNL but not in the medial SNC. The merged image shows approximately 25% of the TH+ neuronal population was co-localised with CB, whereas almost all CB+ neurons were TH+/CB+. **(D-F)** Immunostaining of TH+ cell bodies and dendrites was found in the VTA, as well as CB+ cell bodies. The merged image shows about 75% of the TH+ neurons were co-localised with CB, whereas almost all CB+ neurons were TH+/CB+.

Scale bars = 100 μm

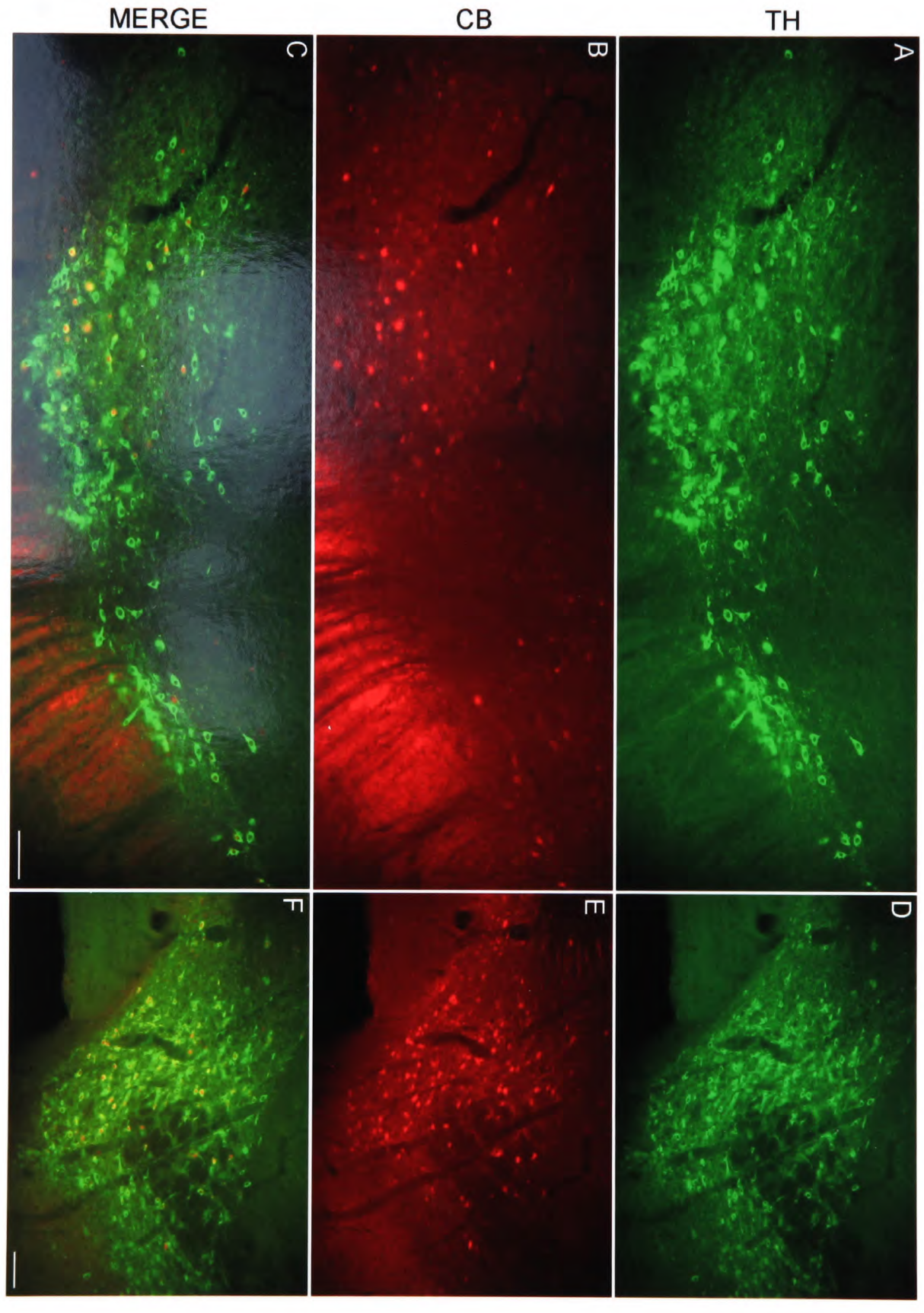

MERGE
CB
TH
C
B
A
F
E
D

Figure 6.4

Photomicrographs of nigral neurons in the probenecid-treated mice with salicylic acid.

(A-C) Photomicrographs of TH, CB and their co-localised immunoreactivities in the SN. TH+ neuronal cell bodies were abundant along the SNC, SNL and their processes reached into the SNR. CB+ cell bodies were mostly clustered in the SNC and SNL. The merged image shows approximately 50% of the TH+ neuronal population was co-localised with CB, whereas almost all CB+ neurons are TH+/CB+.

(D-F) In the VTA, immunostaining of TH+ cell bodies and dendrites were found, as well as CB+ cell bodies. The merged image shows over 75% of the TH+ neuronal population was co-localised with CB, whereas almost all CB+ neurons were TH+/CB+. The immunostaining patterns were similar to those observed in the probenecid-treated mice without salicylic acid.

Scale bars = 100 μm

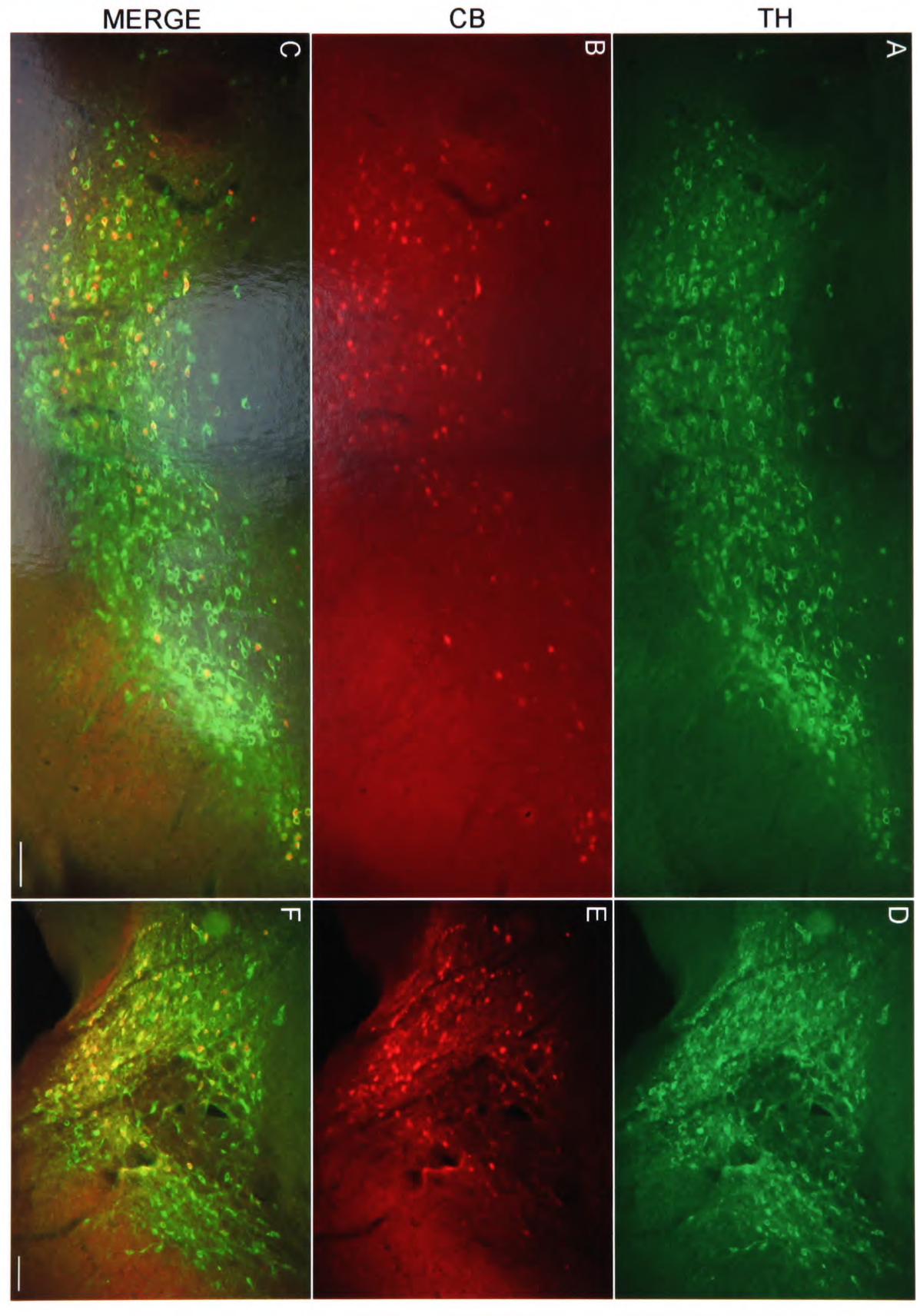

MERGE
CB
TH
C
B
A
F
E
D

Figure 6.5

Photomicrographs of nigral neurons in MPTP/probenecid-treated mice with no salicylic acid.

(A-C) Photomicrographs showing TH+, CB+ and TH+/CB+ neurons in the SN. TH+ neuronal cell bodies were observed in the SNC, SNL with their projections in the SNR. CB+ cell bodies were mostly found in the SNC and SNL. The merged image shows approximately 50% of the TH+ neuronal population was co-localised with CB, whereas almost all CB+ neurons were TH+/CB+.

(D-F) In the VTA, abundant number of TH+ neurons was observed, where CB+ cell bodies are also found. The merged image shows over 75% of the TH+ neuronal population was co-localised with CB, whereas almost all CB+ neurons are TH+/CB+.

Scale bars = 100 μm

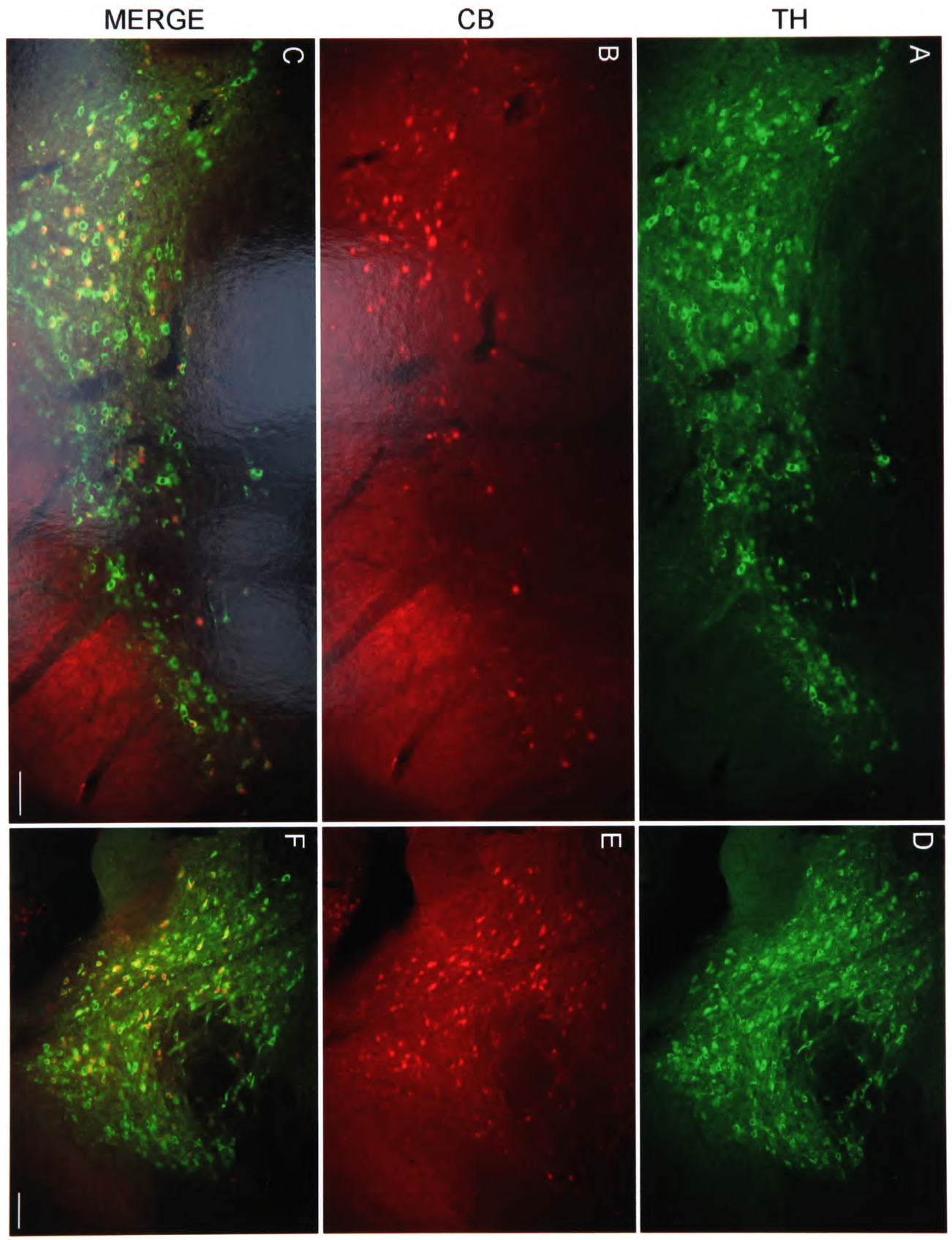

MERGE
CB
TH
C
B
A
F
E
D

Figure 6.6

Photomicrographs of nigral neurons in MPTP/probenecid-treated mice with salicylic acid.

(A-C) Photomicrographs showing TH+, CB+ and TH+/CB+ neurons in the SN. TH+ neuronal cell bodies were observed along the SNC. Fewer CB+ cell bodies were found in the SNC. The merged image shows approximately 50% of the TH+ neurons were co-localised with CB, whereas almost all CB+ neurons were TH+/CB+.

(D-F) TH+ and CB+ neurons were observed in the VTA. The merged image shows over 75% of the TH+ neurons were co-localised with CB, whereas almost all CB+ neurons were TH+/CB+. Immunostaining patterns between the salicylic acid-treated and untreated groups in the MPTP/probenecid mice were similar.

Scale bars = 100 μm

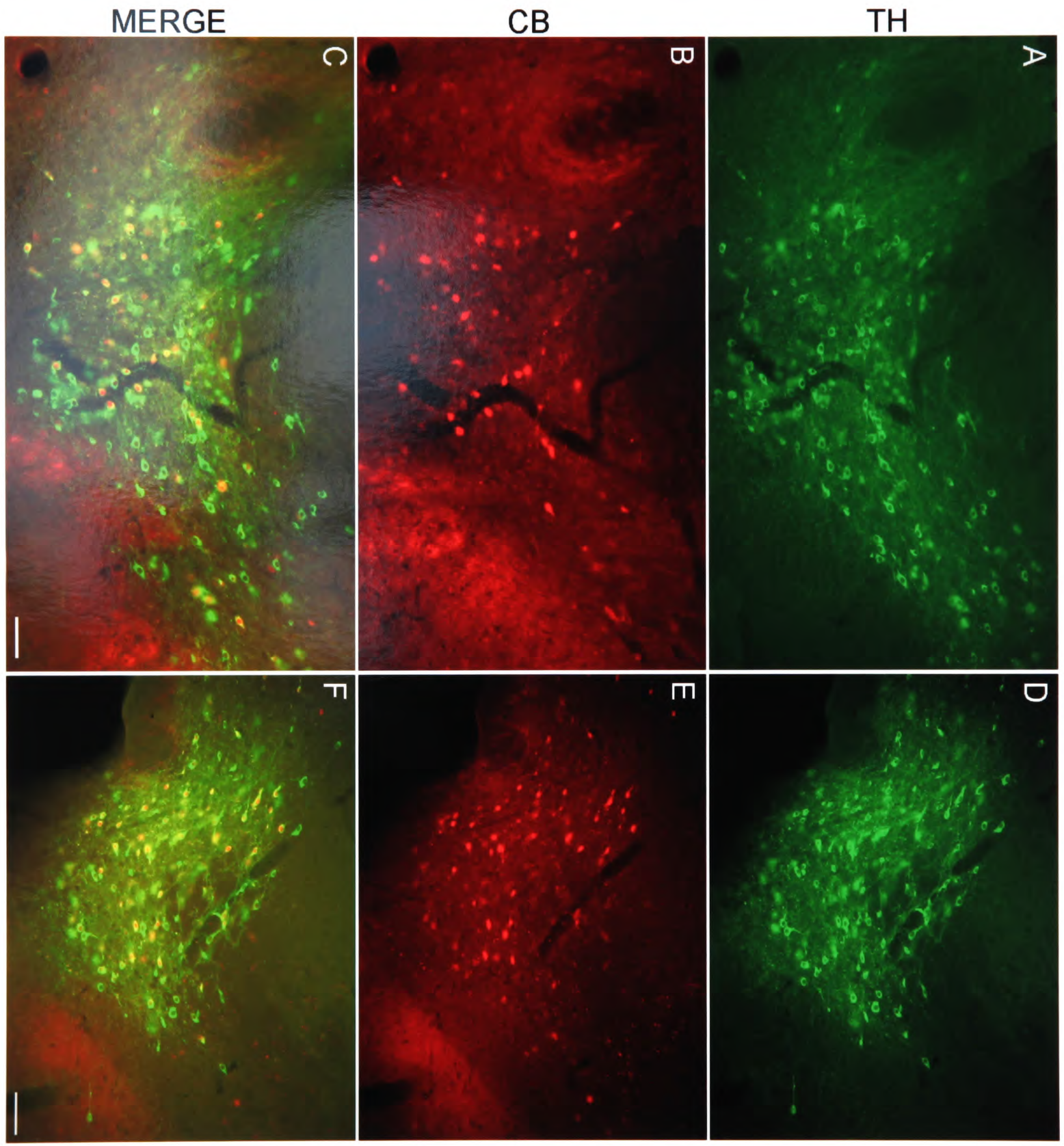

MERGE
CB
TH
C
B
A
F
E
D

Figure 6.7

Effects of the salicylic acid (SA) treatment on the MPTP/p and probenecid-treated mice.

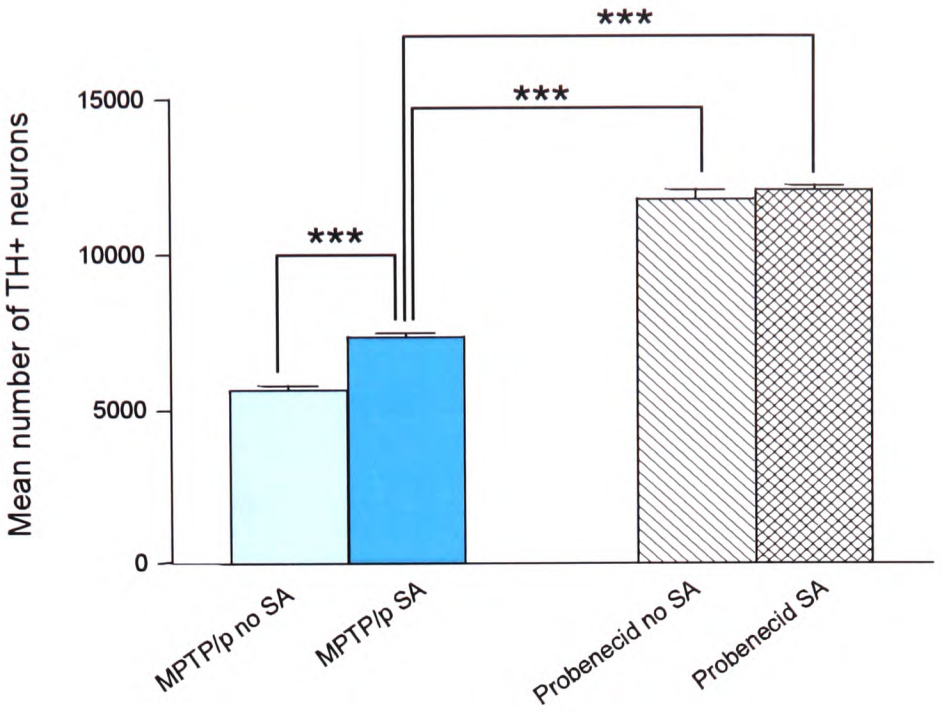
General linear modelling showed that there were significant differences among the cell count in the TH+, CB+ and TH+/CB+ populations ($F_{(2,18)} = 636.084$; $^{***}P < 0.0001$) as well as a count x treatment interaction ($F_{(6,18)} = 43.572$; $^{***}P < 0.0001$), implying that the three neuronal cell types responded differently to the treatment. There was also a significance in treatment ($F_{(3,9)} = 313.611$; $^{***}P < 0.0001$).

(A) In the TH+ population, there was no significant difference between the probenecid control with or without SA (Probenecid no SA vs Probenecid SA). In contrast, there was a significant increase of neuronal number in the SA-treated MPTP/p mice compared to the ones without (MPTP/p no SA vs MPTP SA, $^{***}P < 0.0001$). However, this improvement was still significantly poor compared to the probenecid control (MPTP/p SA vs Probenecid no SA, $^{***}P < 0.0001$; MPTP/p SA vs Probenecid SA, $^{***}P < 0.0001$).

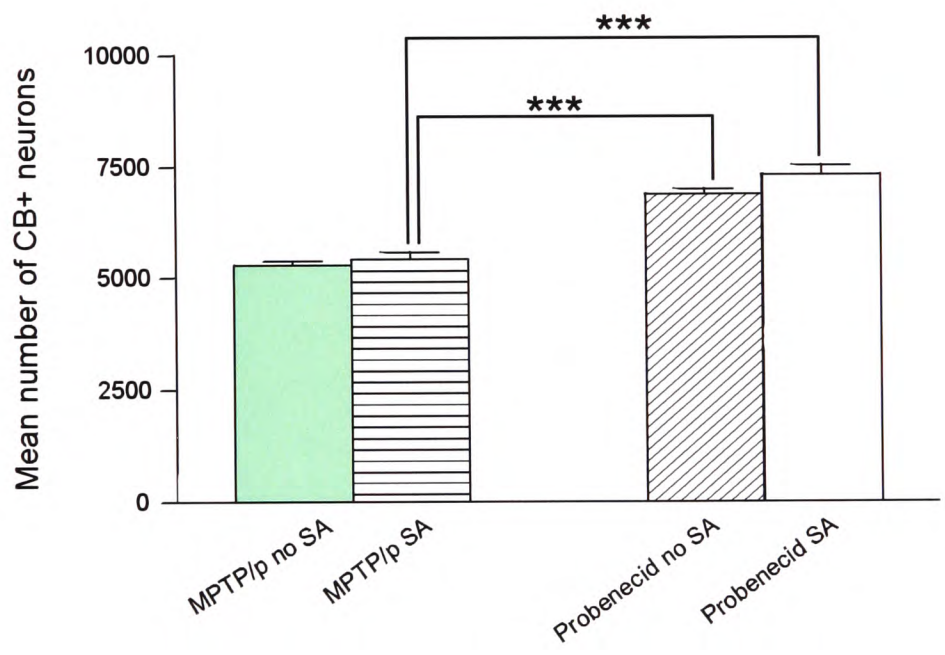
(B) In the CB+ population, there were no significant differences between the probenecid control with or without SA, or between the MPTP/p with or without SA treatment. As expected, the MPTP/p treatment caused significant reduction on the neuronal number compared to the control (all paired significance: $^{***}P < 0.0001$).

(C) In the TH+/CB+ population, there were also no significant differences between the probenecid control with or without SA, or between the MPTP/p with or without SA treatment. SA did not appear to have a positive effect on the MPTP/p-treated mice, since the neuronal number in the "MPTP/p SA" mice was still significantly lower than the probenecid controls (MPTP/p SA vs Probenecid no SA, $^{**}P = 0.014$, MPTP/p SA vs Probenecid SA, $^{***}P = 0.007$).

A


***
***
***
15000
10000
5000
0
Mean number of TH+ neurons
MPTP/p no SA
MPTP/p SA
Probenecid no SA
Probenecid SA

B


***
***
10000
7500
5000
2500
0
Mean number of CB+ neurons
MPTP/p no SA
MPTP/p SA
Probenecid no SA
Probenecid SA

C

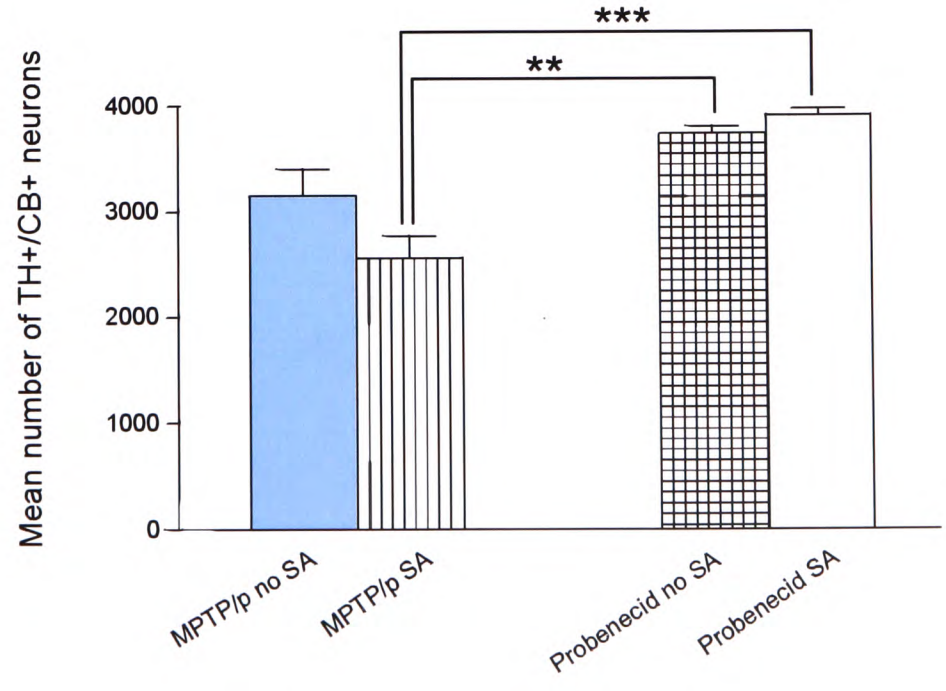

***
**
4000
3000
2000
1000
0
Mean number of TH+/CB+ neurons
MPTP/p no SA
MPTP/p SA
Probenecid no SA
Probenecid SA

Figure 6.8

Photomicrographs of MAC-1 immunostaining in the probenecid-treated mice with and without salicylic acid.

(A, B) In the SN, no MAC-1 immunoreactivity is observed in mice treated with or without salicylic acid.

(C, D) In the VTA and SNR, no MAC-1 immunoreactivity is observed in mice treated with or without salicylic acid. No activated microglia was found in other midbrain regions.

Scale bar = 100 μm

Probenecid without salicylic acid treatment

Probenecid with salicylic acid treatment

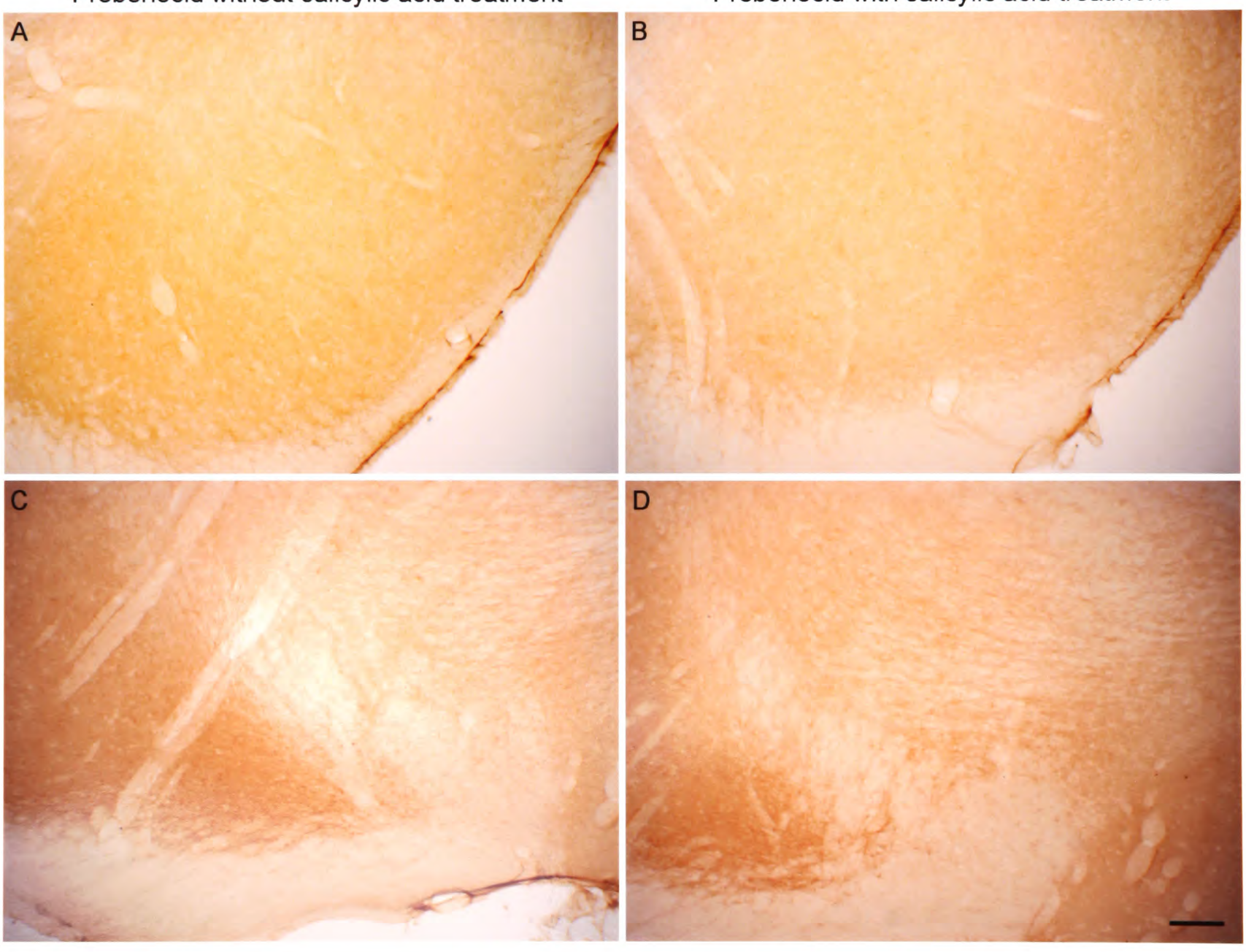


Figure 6.9

Microglial visualisation in the MPTP/probenecid-treated mice without (A and B) and with salicylic acid (C-F).

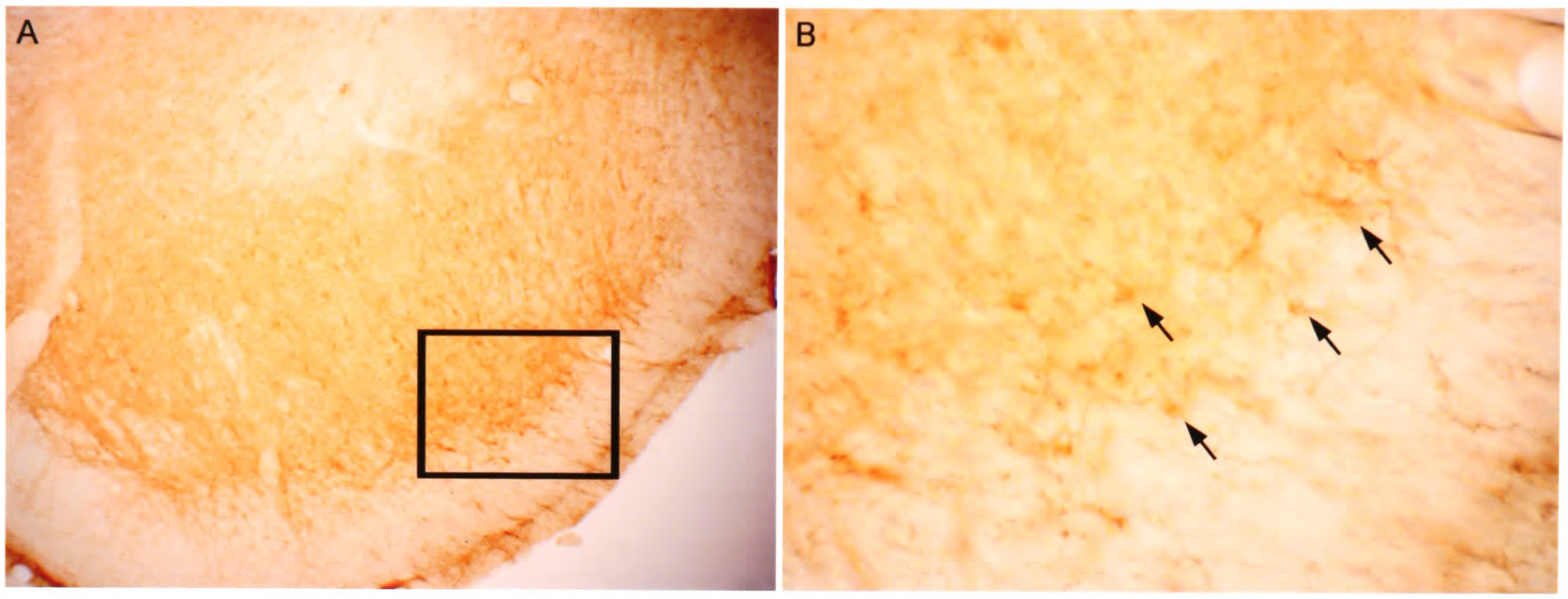
(A and B) Photomicrographs of the SNR with MAC-1 immunoreactivity. High-power micrograph of the boxed region shows individual microglial cells stained with MAC-1 immunohistochemistry (arrows).

(C and D) In MPTP/probenecid mice with salicylic acid, very few MAC-1 immunopositive cell bodies were observed in the SNR. High-power micrograph of the boxed region shows a few residual non-activated microglia (F, arrows).

(E and F) In the VTA, no MAC-1 immunoreactive cell bodies were observed at low or high magnification.

Scale bars: A-D = 50 μm; E-H = 100 μm

MPTP without salicylic acid treatment



MPTP with salicyclic acid treatment

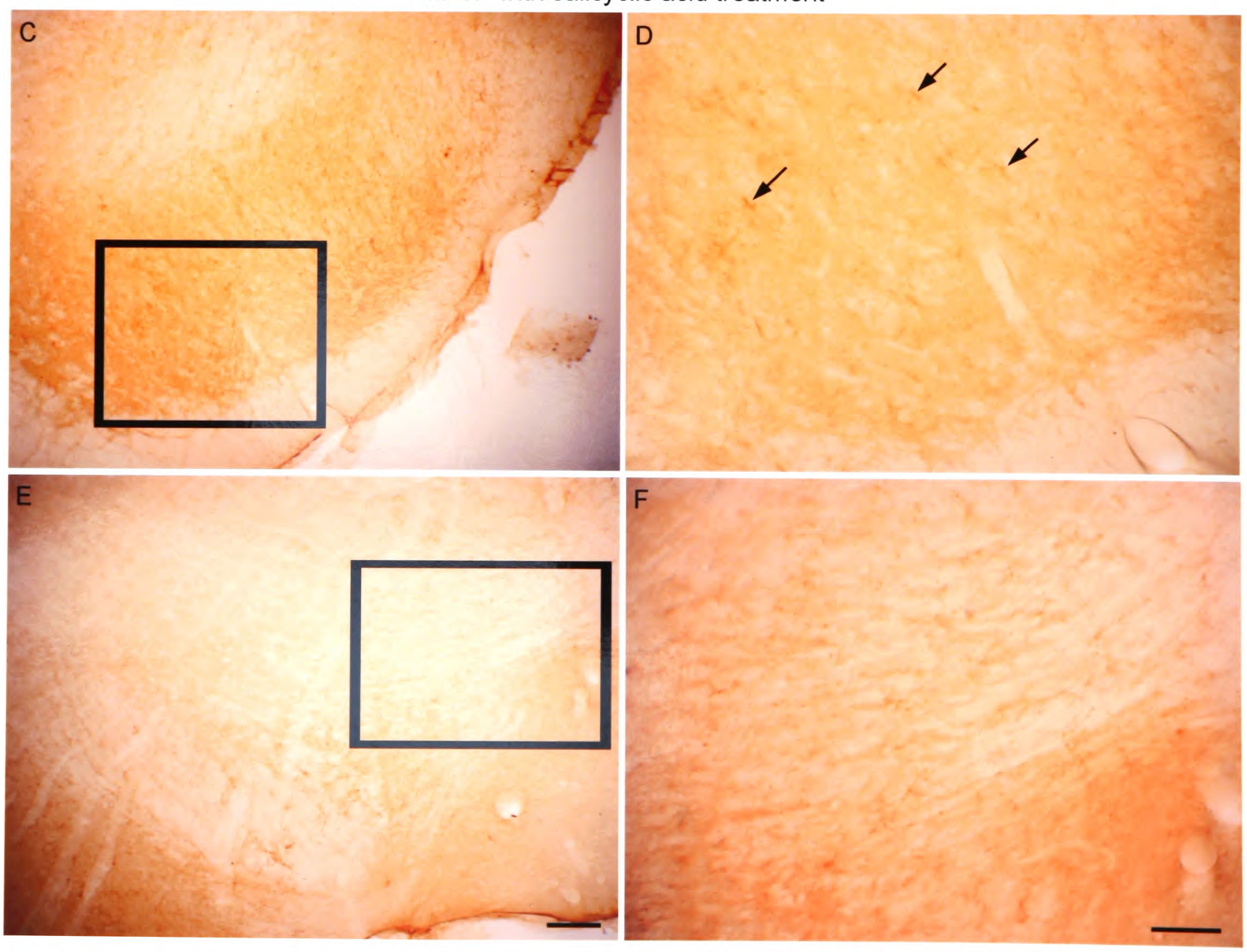


Figure 6.10

NSAIDs and the brain.

(1) Non-steroidal anti-inflammatory drugs (NSAIDs) such as aspirin and its main metabolite, salicylic acid (SA), exert their anti-inflammatory effects at least in part by inhibition of the enzyme cyclooxygenase (COX). (Vane, 1971; Vane, 1994). While aspirin inhibits COX activity by acetylating the active site of the enzyme, the mechanism of SA may be independent of COX inhibition and prostaglandin mediation.

(2) NSAIDs may ameliorate the effects of oxidative stress on α-synuclein, thereby reducing the rate of polymer aggregation and protein misfolding.

(3) Neuroinflammation and disease progression may also be influenced by NSAIDs acting on peripheral cells or immune cells, thereby altering the production of growth factors and cytokines, which can act across the blood-brain barrier (BBB).

[Figure adapted from Wyss-Coray, 2005]

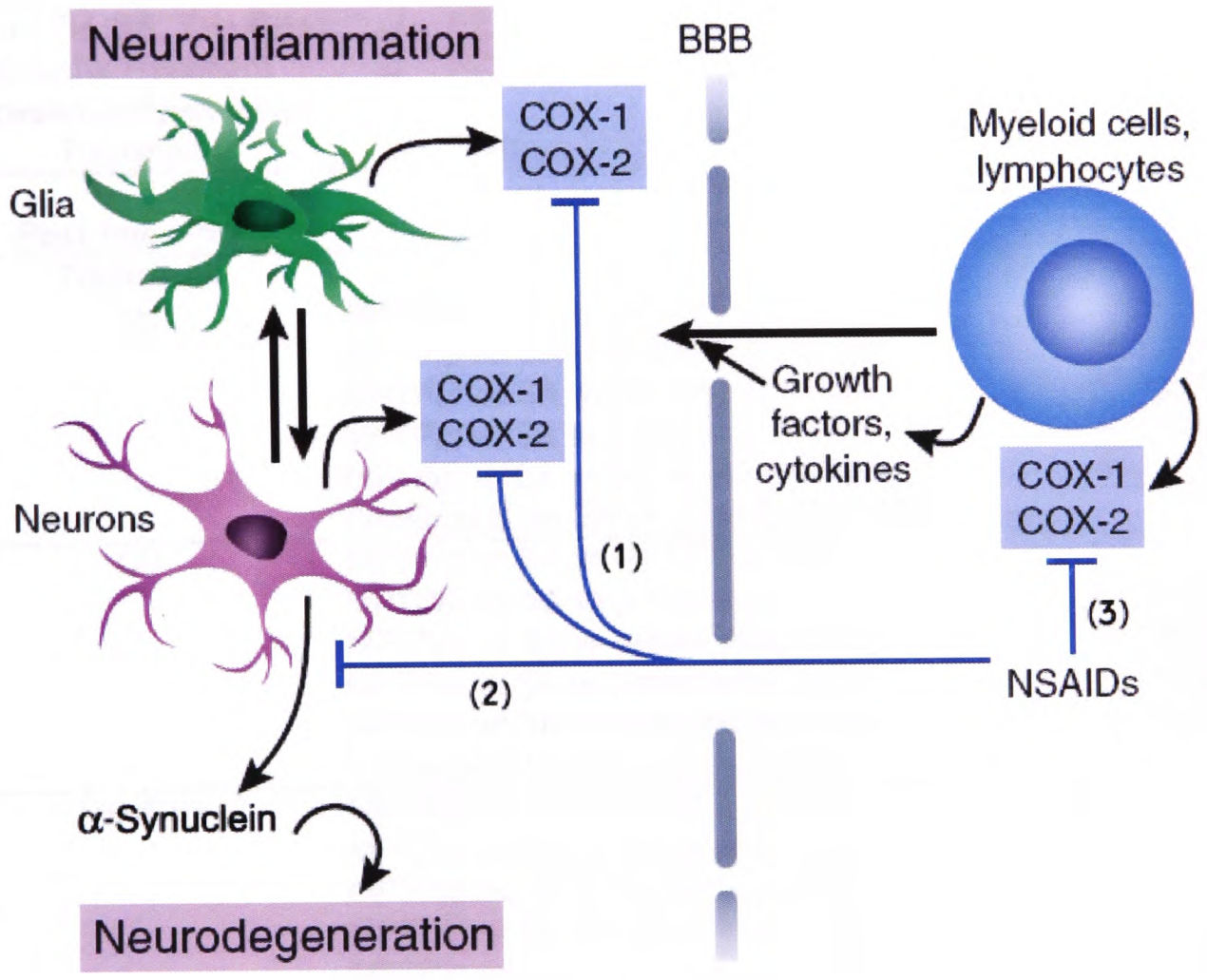

Neuroinflammation
BBB
COX-1
COX-2
Glia
Myeloid cells,
lymphocytes
COX-1
COX-2
Growth
factors,
cytokines
Neurons
(1)
COX-1
COX-2
(3)
(2)
NSAIDs
α-Synuclein
Neurodegeneration

Table 6.1

MPTP/p

	TH	SEM	CB	SEM	Coloc	SEM	% TH+ that are TH+/CB+
No SA	5646	153.6	5300	72.33	3146	255.1	56%
SA	7348	132.5	4520	159.8	2556	205.6	35%

Probenecid control

	TH	SEM	CB	SEM	Coloc	SEM	% TH+ that are TH+/CB+
No SA	11744	313	6870	125	3742	70	32%
SA	12052	160	7308	205	3910	63	32%

Statistical Analyses

GLM

Within-subject factors	Sig.	
Count (TH, CB, TH+/CB+)	√	$F(2,18) = 636.084$; $P < 0.0001$
Count x Treatment	√	$F(6,18) = 43.572$; $P < 0.0001$
Between-subject factor		
Treatment	√	$F(3,9) = 313.611$; $P < 0.0001$

***Post-hoc t*-test**

Treatment		Sig.	
TH	MPTP/p no SA vs MPTP/p w/ SA	√	$P < 0.0001$
	MPTP/p no SA vs probenecid no SA	√	$P < 0.0001$
	MPTP/p no SA vs probenecid w/ SA	√	$P < 0.0001$
	MPTP/p w/ SA vs probenecid no SA	√	$P < 0.0001$
	MPTP/p w/ SA vs probenecid w/ SA	√	$P < 0.0001$
	Probenecid No SA vs probenecid w/ SA	x	
CB	MPTP/p no SA vs MPTP/p w/ SA	x	
	MPTP/p no SA vs probenecid no SA	√	$P < 0.0001$
	MPTP/p no SA vs probenecid w/ SA	√	$P < 0.0001$
	MPTP/p w/ SA vs probenecid no SA	√	$P < 0.0001$
	MPTP/p w/ SA vs probenecid w/ SA	√	$P < 0.0001$
	Probenecid No SA vs probenecid w/ SA	x	
TH+/CB+	MPTP/p no SA vs MPTP/p w/ SA	x	
	MPTP/p no SA vs probenecid no SA	x	
	MPTP/p no SA vs probenecid w/ SA	x	
	MPTP/p w/ SA vs probenecid no SA	√	$P = 0.014$
	MPTP/p w/ SA vs probenecid w/ SA	√	$P = 0.007$
	Probenecid No SA vs probenecid w/ SA	x	

7 Arylamine N-acetyltransferase as a Vulnerability Factor in Sporadic Parkinson's Disease

7.1 Introduction

In previous chapters, I have examined the expression of CB in different stages of PD progression, the synaptic input to the CB+ neurons in the midbrain, as well as its expression in the salicylic acid-treated mouse model. Although further investigations remain to understand their contributions in PD pathogenesis, genetic vulnerability factors remain to be identified in most patients with PD who are either with the sporadic form of the disease, or only have a small number of affected relatives (Grundmann et al., 2004). Epidemiological studies have consistently identified both a positive family history and exposure to toxins as a risk factor for PD (Warner and Schapira, 2003). The emerging picture of sporadic PD is that it results from a combination of genetic and environmental factors, which likely interact with each other (Benmoyal-Segal and Soreq, 2006). One approach for identifying susceptibility genes for a specific disease is to determine the allelic frequency of known polymorphisms in the suspected candidate genes and to search for putative association of such polymorphisms with the disease status.

These types of study have immense power at detecting genes with small effects. To this date, at least 16 candidate genes were investigated with respect to the sporadic PD etiology. These include genes associated with dopaminergic transmission such as monoamine oxidase (Kurth et al., 1993; Costa et al., 1997), genes associated with protein aggregation and destruction such as alpha-synuclein (Kruger et al., 1999; Tan et al., 2000b; Mellick et al., 2005) and genes associated with xenobiotic metabolism.

The polymorphic arylamine *N*-acetyltransferase (NAT) enzymes are well characterised in the xenobiotic metabolism of arylamine, hydrazine and arylhydroxylamine substrates (Weber and Hein, 1985; Upton et al., 2001b). There are three *NAT* loci in humans: *NAT1* and *NAT2*

encode functional proteins, whereas the third locus is a pseudogene (Blum et al., 1990). The two human NAT isoforms, human NAT1 and human NAT2, have distinct but overlapping substrate specificities and expression profiles (Upton et al., 2001b; Hein, 2002). Whereas the expression of human NAT2 is predominantly in tissues engaged in xenobiotic metabolism, human NAT1 is more widespread. In addition to expression in liver and gut, human NAT1 activity has been detected in almost all tissues investigated including kidney, spleen, placenta, erythrocytes, bladder, skeletal muscle, breast and skin (Windmill et al., 2000; Upton et al., 2001a; Williams et al., 2001; Rodrigues-Lima et al., 2003). Comparison of the substrate specificities of human and mouse isozymes indicates that NAT2 in mice is equivalent to NAT1 in humans (Hein et al., 2000b; Kawamura et al., 2005).

An increasing number of reports have linked NAT polymorphism with neural dysfunction such as Parkinson's disease (Bandmann et al., 1997), Alzheimer's disease (Johnson et al., 2004), schizophrenia (Saiz et al., 2006) and brain astrocytoma and meningioma (Olivera et al., 2006). Three mutant alleles of *NAT2* were identified (M1, M2 and M3), which account for slow acetylators in humans. It was thought that carriers of two mutant alleles would be more susceptible to neurotoxin exposure and therefore more at risk to develop PD (Benmoyal-Segal and Soreq, 2006). Four of five studies that explored this working hypothesis reported a positive association (Agundez et al., 1998; Maraganore et al., 2000; Tan et al., 2000a; Chan et al., 2003), whereas one study that was conducted in Rotterdam reported a negative association (Harhangi et al., 1999). This possible association of NAT polymorphism and PD has been studied using different methodologies, diagnostic criteria and sample sizes which may result in conflicting observations (Harhangi et al., 1999). Alternatively, synergistic contributions of more than one polymorphism (e.g. in both CYP2D6 and *NAT2* genes) may underlie such differences, but this possibility was never explored (Benmoyal-Segal and Soreq, 2006). Recently, a study showed that intrastriatal 6-

OHDA treatment of NAT2 slow acetylator rats led to decrease of striatal dopamine levels as compared to identical treatment of NAT2 rapid acetylator (Grundmann et al., 2004). The aim of this study is therefore to investigate the role of NAT based on a single mouse model.

I have demonstrated the expression pattern of NAT *in vivo* using the fast acetylator C57Bl/6 mice, as used in the PD mouse model. A pure transgenic *Nat2-/-* mouse line has been generated on a C57Bl/6 background and can act as a comparison. Subsequently, *in vitro* substrate and inhibitor screening assays have been undertaken to investigate the endogenous role of NAT. Furthermore, I have used SHIRPA (**S**mithKline Beecham Pharmaceuticals, **H**arwell MRC Mouse Genome Centre, **I**mperial College School of Medicine at St Mary's, **R**oyal London Hospital, St Bartholomew's and the Royal London School of Medicine, **P**henotype, **A**ssessment), the primary behavioural tests, to compare the NAT wildtype and knockout mice as a whole system with particular focus on motor functions. This study will not only shed light onto the importance of genetic predisposition in PD, but will add an extra dimension showing the genetic-environment interactions in the disease pathology.

7.2 Aims

- To elucidate the expression pattern of mouse NAT2 in the adult mouse brain using immunohistochemical analysis and X-gal staining
- To investigate the potential function of NAT in its expressed cell types using substrate and inhibitor screening assays
- To compare the behavioural differences between the *Nat2+/+* and *Nat2-/-* mice using SHIRPA

7.3 Materials and Methods

7.3.1 Chemicals

Unless otherwise stated, all chemicals were purchased from Sigma-Aldrich Co. Ltd. (Poole, Dorset, UK.)

7.3.2 Generation of Nat2-/- mice

In human and in mice, there are two well-defined NAT isoforms, NAT1 and NAT2 (Hein et al., 1988). A transgenic mouse model with a null allele of *Nat2* has been generated using homologous recombination in embryonic stem cells (Cornish et al., 2003). When germline transmission has been obtained, the transgene was backcrossed onto the rapid acetylator, C57Bl/6 mouse strain (containing the deletion of α-synuclein from Harlan, Bicester). The genotypes of the offspring were determined by PCR.

All animals were genotyped with respect to the *Nat2* null allele (Cornish et al., 2003) using ear biopsies taken at the time of weaning (3-4 weeks). The genomic DNA was prepared from the tissue by phenol-chloroform extraction (Appendix 7.1). *Nat2* genotype was determined by polymerase chain reaction, using *Nat2* specific primers Nat2-1 and Nat2-910 to detect the wild-type allele and the NeoT with Nat-910 to detect the presence of the neomycin gene in the *Nat2* null allele as illustrated in Figure 7.1 (Cornish et al., 2003). The sequences are as follows:

mNat2-1: 5'-ATGGACATCGAAGCGTACTTTG-3',

mNAT2-910: 5'-TTCCAAGTACATGGAAGGACACC-3'

neo-T: 5'-CATCGCCTTCTATCGCCTTCT-3'.

Polymerase chain reaction (PCR) was performed using 50-500 ng of genomic DNA as template. A standard PCR reaction consisted of buffer (1x), 2 mM $MgCl_2$, 0.2 mM dNTP, 25 pmol antisense/sense primers as listed above, 1 U Taq polymerase in a total volume of 50 µl made up with endotoxin-free sterile water. PCR condition parameters were optimised by varying the concentration of $MgCl_2$ (1-8 mM). Amplifications were carried out using PTC-0200 Thermocycler (MJ Research). The first step, a hot start (94°C, 3 min), was followed by 34 cycles of denaturing (94°C, 30 sec), annealing (58°C, 30 sec) and extension steps (72°C, 45 sec). The samples underwent a final cycle at 94°C (30 sec), 58°C (30 sec) and an elongation step at 72°C for 7 min, and were finally stored at 4°C.

7.3.3 Antibody generation

Antibodies specific for human NAT1 and mouse NAT2 were generated in rabbits using the isoform-specific C-terminal peptide (Table 1) conjugated to bovine serum albumin as described previously (Stanley et al., 1996).

7.3.4 Tissue homogenisation

Frozen tissue samples were weighed and defrosted at 37°C. Homogenizing buffer (10 mM potassium phosphate buffer, pH 7.5, 1 mM EDTA, 1.15% (w/v) KCl, 1 mM DTT, 1x protease inhibitor cocktail) was added at 3 ml/(g tissue) and homogenised using a tissue grinder (Janke & Kunkel, IKA-Labortechnik, Ultra-Turrax T25) (20 – 30 sec at 8000 no load/min) (Smelt et al., 1997). The homogenate was centrifuged to pellet cell debris (14,000 g, 10 min, 4°C). The remaining homogenate supernatant was stored in liquid nitrogen until immunoblotting was performed.

7.3.5 Dot blotting and Western blotting

Dot blotting was used as a semi-quantitative technique for rapid screening of the experimental parameters (e.g. concentrations of protein samples, optimal dilution of the antibody, optimal time for antibody incubation). Protein samples were transferred directly onto a nitrocellulose membrane (Hybond™-C, Amersham) by "vacuum assisted solvent flow" using a 96-well Bio-Dot Microfiltration Apparatus (Bio-Rad). The membrane was pre-washed in TBS and placed into the apparatus. Protein samples (200 µl/well, diluted in TBS) were applied under vacuum for at least 1 hour. The membrane was washed three times in TBS (10 min) and probed using NAT antibodies.

Western blotting analysis was similar to that described previously (Stanley et al., 1996; Stanley et al., 1997), using human NAT1/mouse NAT2-specific antiserum 183 at a dilution of 1:4000 for 1 hour and peroxidase-conjugated goat anti-rabbit antibody (1:2000, Sigma) for 1 hour. Details on sodium dodecylsulfate-polyacrylamine gel electrophoresis (SDS-PAGE) and the Western blotting procedures are provided in Appendix 7.2 and 7.3 respectively.

7.3.6 X-gal staining

Free-floating mouse brain sections from Nat2 +/+ and Nat2 -/- mice (n=5/genotype) were assayed for β-galactosidase activity by X-gal staining as previously described (Hogan B, 1994; Rentschler et al., 2001; Cornish et al., 2003). Horizontal sections were used for analysis of lateral ventricles, SN and cerebellum and whole brains were used for analysis of choroid plexus. Essentially, samples were fixed in 4% paraformaldehyde:PBS, washed twice in PBS for 10 minutes each at room temperature and immersed in X-gal staining solution (0.1M phosphate buffer pH7.3 containing 2mM $MgCl_2$, 0.01% sodium deoxycholate, 0.02% Nonidet P-40, 5mM potassium ferricyanide, 5mM potassium ferrocyanide and 1mg/ml X-gal)

for 24 hours at 37°C in the dark. Samples were then washed in PBS, dehydrated through an ethanol series, cleared in xylene and mounted in VectaMount permanent mounting medium (Vector Laboratories). Brain slices and sections were mounted onto Superfrost slides (BDH) and visualized using a light microscope (Olympus BH2).

7.3.7 Immunohistochemistry

Mouse tissues from *Nat2* +/+ and *Nat2* -/- mice (n=5/genotype) were fixed by transcardial perfusion with a solution containing 4% paraformaldehyde in 0.1 M phosphate buffer. Serial 30 μm-thick horizontal sections of the whole brain were cut with a vibratome (Leica VT1000M) and stored in antifreeze solution at -20°C until further processing. The first two series of sections were processed for immunofluorescence and the third for X-gal staining.

Dual immunofluorescence was performed on free-floating mouse sections as previously described (Section 2.4.1). Briefly, sections were immersed in antiserum 183 (1:300) in PBS and 0.1% Triton X-100 at 4°C for 48 hours. This is followed by incubation with the secondary antibody, Alexa Fluor® 488 goat anti-rabbit IgG (H+L) (1:500, Molecular Probes) for 2 hours at room temperature. Sections were incubated with mouse monoclonal anti-TH antibody (1:1000, Clone TH-16, Sigma) or mouse monoclonal CB antibody (1: 2000, Swant) with 0.1% Triton X-100 at 4°C for 24 hours. The secondary antibody, Alexa Fluor® 568 goat anti-mouse IgG (H+L) (1:500, Molecular Probes), was incubated for 2 hours at room temperature. After final rinses in PBS, the sections were mounted on gelatin-coated slides in Vectashield HardSet™ mounting medium (Vector Laboratories). Fluorescent images were captured on a Leica DMRA2 fluorescent microscope by using Openlab 3.09 software, and figures prepared using Adobe PhotoShop (v.6.0).

7.3.8 Acetyl Coenzyme A (AcCoA) hydrolysis assay

7.3.8.1 Substrate Screening

The rate of hydrolysis of AcCoA by NAT, in the presence of a range of substrates, was determined by detecting the free CoA thiol group with Ellman's reagent, 5,5'-dithio-bis(2-nitrobenzoic acid) (DTNB) (Brooke et al., 2003b). The substrate (500 μM) and purified recombinant hamster NAT2 in 20 mM Tris-HCl buffer (pH8.0) were pre-incubated (37°C, 5 min) in 96-well flat bottom polystyrene plates (Costar®, Corning Inc.). AcCoA (400 μM) was added to start the reaction in a final volume of 100 μl. The reaction was quenched with the addition of 25 μl of guanidine HCl solution (6.4M guanidine.HCl, 0.1 M Tris-HCl, pH 7.3) containing 5 mM DTNB. The absorbance at 405 nm was measured on a plate-reader. Reactions in which substrate, AcCoA or NAT were replaced by assay buffer, were used as controls. The amount of CoA produced in the reaction was determined in comparison with a standard curve (A_{405} against varying concentrations of CoA). All measurements were performed in triplicates.

7.3.8.2 Inhibitor Screening

The method for inhibitor screening assay was based on the substrate screening assay except that inhibitors (30-100 μM) were pre-incubated with the protein and a substrate (*para*-aminobenzoyl glutamate, pABA) for 5 min at 37°C. The reaction was initiated by the addition of AcCoA. The reaction was quenched with the addition of DTNB solution.

7.3.9 Behavioural tests using SHIRPA

Primary behavioural screen of SHIRPA *(*Rogers *et al.,* 1997*)* was used. The detailed version of the original SHIRPA protocol can be found on the webpage of Harwell. 11 C57Bl/6

NAT2+/+ mice and 13 NAT-/- were taken to the test at random; their genotypes only being revealed after the assessments. The primary screen comprises a battery of 37 simple tests which provide a behavioural and functional profile by observational assessment. After recording their body weights, the undisturbed behaviour of the mice was evaluated in a viewing jar. The mouse was put under a clear Perspex box (15 x 25 cm), located above an arena. For 5 min, the body position, spontaneous activity, respiration rate and any sign of tremor were scored. Subsequently the mouse was transferred to the arena (30 x 50 cm) for observation of motor behaviour. Afterwards a sequence of manipulations using tail suspension was performed and visual acuity, grip strength, body tone and reflexes were recorded. The scores were analysed using chi-squared tests.

7.4 Results

7.4.1 Genotyping of Nat wildtype and knockout mice

The three PCR primers were designed such that Nat2-1 anneals to the 5' end of the wildtype *Nat2* coding sequence; Neo-T anneals to sequences within the selectable neomycin cassette present only in the null *Nat2* transgene, and Nat2-910 which serves as the reverse primer for both wildtype and null sequences, identical to sequences at the 3' end of the *Nat2* gene. The wildtype *Nat2+/+* mice therefore showed a single band of 910 bp after DNA amplification by PCR (Figure 7.2). The heterozygote *Nat2+/-* showed two bands of 910 bp and 500 bp and the knockout *Nat2-/-* mice showed a single band of 500 bp. No genomic DNA was added into the PCR reaction mix as a control to test for contamination and genomic DNA from a heterozygote *Nat2+/-* was used as the positive control.

7.4.2 Characterisation of hNAT1/mNAT2-specific antiserum 183

To confirm the specificity of antiserum 183 for human NAT1/mouse NAT2 prior to its use in immunohistochemistry, we have tested its reactivity against a series of prokaryotic and eukaryotic recombinant NAT proteins (Figure 7.3). Antiserum 183, like antiserum 184 (Stanley et al., 1996; Stanley et al., 1997; Stanley et al., 1998), was raised against the C-terminal 12 amino acid peptide of human NAT1/mouse NAT2. The isozymes mouse NAT2 and human NAT1 possess the same C-terminal dodecapeptide, as does hamster NAT2, which differs from that of human NAT2, mouse NAT1 and NAT3 (Table 1). There is no equivalent sequence in NAT from *Pseudomonas aeruginosa* NAT as determined by FASTA search of the entire sequence (Pearson and Lipman, 1988).

In order to confirm the predicted specificity, the detection of recombinant, pure NATs was used following SDS-PAGE. Coomassie blue staining was used to confirm that equal amounts of protein were loaded in each lane (Figure 7.3A). The molecular weight of Syrian hamster NAT2 is 34.2 kDa, human NAT1 is 34.3 kDa, human NAT2 with a hexa-histidine tag is 35.7 kDa (Kawamura et al., 2003) and NAT from *Pseudomonas aeruginosa* with a hexa-histidine tag is approximately 33.5 kDa (Westwood et al., 2005). Coomassie blue staining showed these proteins migrating according to the predicted molecular weight on SDS-PAGE (Figure 7.3A). Western blots of these gels, probed with antiserum 183, revealed hamster NAT2 and human NAT1 proteins, at the predicted molecular weight, but not human NAT2 or *Pseudomonas aeruginosa* NAT, indicating its specificity for mouse NAT2/human NAT1 (Figure 7.3B). Both recombinant human NAT2 and *Pseudomonas aeruginosa* NAT proteins contain a hexa-histidine tag. To confirm that the absence of bands corresponding to human NAT2 and *Pseudomonas aeruginosa* NAT was indeed due to the specificity of the antibody, equivalent blots were probed using an antibody against the hexa-histidine tag (Figure 7.3C).

Thus, Western blotting (Figure 7.3B) indicates that antiserum 183 is specific for hamster NAT2 and human NAT1.

These results validate the use of antiserum 183 to map mouse NAT2 expression. Indeed, as shown for antiserum 184 (Stanley et al., 1998). Western blot analysis of cerebellar homogenate from adult mice, using antiserum 183 to probe for mouse NAT2 protein, gives a single band of the predicted molecular weight. Further confirmation of the specificity of antiserum 183 comes from comparison of cerebellar homogenates from *Nat2* +/+ and *Nat2* -/- mice; immunoreactivity is not detected at 34 kDa in tissues from *Nat2* -/- mice (Figure 7.3D), supporting the suitability of this antibody for immunohistochemistry. Although the protein sequence of mouse NAT3 is similar to that of human NAT1/mouseNAT2/hamsterNAT2, there are 3 amino acid differences in the sequence. Furthermore, mouse NAT3 has a very low activity with pABA (*para*-aminobenzoyl glutamate) and the level of protein expression was hardly detectable (Upton et al., 2000; Boukouvala et al., 2002). Therefore it is unlikely that the antibodies cross-reacted with mouse NAT3.

7.4.3 Expression of mouse Nat2 in the adult brain

Using antiserum 183, neuronal NAT immunoreactivity is detected in the VTA and SN in adult mice (Figure 7.4). Not all NAT-immunoreactive neurons are immunopositive for TH, but approximately 75% of the midbrain TH+ neurons also express mouse NAT2. Mouse NAT2 was also found in the cerebellum (Figure 7.5) where fewer than 25% of the CB+ Purkinje cells were dual-labelled with NAT2.

The expression pattern of mouse *Nat2* was observed in *Nat2 -/-* mice, using β-galactosidase activity (Cornish et al., 2003). Mouse *Nat2* expression, represented by blue X-gal staining, is visible in the Purkinje cell layer of the cerebellum (Figure 7.6 A and B), and in the midbrain (Figure 7.6 C and D). Additional X-gal staining was observed in the glomerular layer in the olfactory bulb (Figure 7.6 E and F), as well as along the ependymal cells lining the lateral ventricle (Figure 7.6 G and H, arrowheads) and in the choroid plexus (Figure 7.6 G and H, asterisks). No X-gal staining was observed in the control brain sections of *Nat2* +/+ mice (data not shown).

A comparison of mouse NAT2 and human NAT1 expression in the central nervous tissue is detailed in Table 2. No detectable NAT immunolabelling was observed in other major brain regions such as the hippocampus.

7.4.4 Screening compounds as substrates/inhibitors of mouse NAT2

Although mNAT2 is expressed in the neurons of different functional subtypes, for example, in dopaminergic (in the midbrain) and GABAergic neurons (in the cerebellar Purkinje neurons), it is possible that NAT performs the same function within them. When the biosynthetic pathways of dopamine and GABA are compared, it is clear that both require the co-factor, pyridoxal phosphate (vitamin B-6) in their respective synthetic enzyme – L-aromatic amino acid decarboxylase in the catecholamine biosynthesis and glutamate decarboxylase (Figure 7.7). In addition, isoniazid, an arylamine substrate for NAT (Hein et al., 1982; Derewlany et al., 1994; Boukouvala and Fakis, 2005) has been used as a specific competitive inhibitor against pyridoxal phosphate (Johnston and White, 1965; Lheureux et al., 2005). It is therefore possible that pyridoxal phosphate is a substrate, or an inhibitor of NAT, and that NAT may consequently play a role in the neurotransmitter syntheses. To test this

hypothesis, pyridoxal phosphate and its derivatives, together with a series of chemically similar compounds (Figure 7.8) were screened *in vitro* as substrates and inhibitors of recombinant Syrian hamster NAT2 (shNAT2) (Kawamura et al., 2005).

The chemical interactions of shNAT2 and the compounds were studied using the DTNB assay (Brooke et al., 2003a). Its principle is described in Appendix 7.4. This assay is based on the observation that measurable hydrolysis of acetyl CoA (AcCoA) occurs only in the presence of an acceptor substrate and the enzyme (Kawamura, 2005). Control settings showed: a) no spontaneous hydrolysis of AcCoA was detected in the absence of an arylamine substrate over the period of the assay; b) no colour was detected in the absence of AcCoA or enzyme and c) pABA was used as the positive control such that acetylation was expected to occur with a subsequent increase in optical density (OD) at 405nm.

Under the optimal concentration of the enzyme, AcCoA and substrate/inhibitor, it was shown that none of the compounds were substrates of shNAT2. For example, pyridoxal 5'-phosphate and 4-pyridoxic acid were not acetylated, in contrast to the pABA control (Figure 7.9). On the other hand, when the compounds were tested as inhibitors against pABA, it was shown that pyridoxal 5'-phosphate and 4-pyridoxic acid were potential inhibitors, the former inhibited the acetylation of pABA by 96% and the latter inhibited the acetylation activity by 39% (Figure 7.10). A summary of the substrate/inhibitor screening is shown in Table 3.

7.4.5 SHIRPA behavioural study on NAT2 wildtype and knockout mice

The primary SHIRPA screen provides a comprehensive assessment of basic neurological and physical characteristics of the mice. The results were summarised in Table 4.

Both *Nat2+/+* and *Nat2-/-* mice appeared normal in a viewing box. However, when the mice were transferred from the viewing box to an arena, behavioural differences were observed. First, a significantly larger number of *Nat2-/-* mice showed brief freeze and fewer moved immediately to explore the arena, which was a sign of anxiety (Table 4, "1. Transfer Arousal"). Second, significantly fewer *Nat2-/-* mice showed fluid movement, in contrast to 100% movement fluidity in the *Nat2+/+* mice (Table 4, "2. Gait"), and significantly fewer *Nat2-/-* mice responded when the handler touched their foreheads (Table 4, "5. Touch response"). Third, a significantly fewer *Nat2-/-* mice were able to grasp onto a wire, implying some difficulties in balance and movement (Table 4, "6. Wire manoeuvre").

When the mice were directly handled above the arena, a significantly larger number of *Nat2-/-* mice struggled when they were held by the tail (Table 4, "7. Positional passivity"). While doing so, none of the knockout mice curled up their bodies (Table 4, "8. Trunk curl") but instead they tried to grasp their hindlimbs (Table 4, "9. Limb grasping"). Overall observations showed that fewer *Nat2-/-* mice urinated during the test (Table 4, "15. Urination") but no differences in defecation. Compared to the wildtype, more *Nat2-/-* mice responded by biting, but not by vocalising, when being handled (Table 4, "16. Biting in response to handling" and "17. Vocalisation in response to handling").

7.5 Discussion

Arylamine *N*-acetyltransferases play an important role in the detoxification and the potential metabolic activation of arylamines and hydrazines (Weber and Hein, 1985; Upton et al., 2001a). NAT polymorphism has been associated with cancer susceptibility and drug response phenotypes (Millikan et al., 1998; Alberg et al., 2004; Dairou et al., 2004). In this chapter, the possibility of an association between NAT and PD was investigated. NAT expression in

mouse brain was observed in epithelia lining the ventricles and in specific neuronal cell types in adults. In addition, mNAT2 expression has previously been demonstrated in adult spinal cord motor neurons, and in the developing nervous system (Stanley et al., 1998). NAT1 expression pattern in adult human brain was similarly found in the SN, brainstem in the vicinity of the pontine cerebllar tracts, choroid plexus in the fourth ventricles and in the cerebellum (Troen A.M., 2000). In the cerebellar folia, both the cytoplasm and dendrites of Purkinje cells were NAT1 immunoreactive, with weak NAT1 expression in occasional granule cells. The comparison illustrates the close correspondence between expression patterns of human *NAT1* and its mouse equivalent, *Nat2.* Furthermore, where tested, results obtained using immunohistochemical techniques on *Nat2*+/+ mice correlate well with those obtained by mapping *lacZ* reporter gene expression in *Nat* -/- mice.

The predominantly epithelial choroid plexus and ependymal cells serve to control the extracellular environment of neuronal and neuron-associated cells. Since the choroid plexus regulates the composition of the cerebrospinal fluid (Strazielle and Ghersi-Egea, 1999), the presence of mouse NAT2/human NAT1 in the choroid plexus and the ependymal cells of the lateral ventricles and cerebellum suggests a neuroprotective role. Several xenobiotic metabolising enzymes, including members of the cytochrome P450 and glutathione S-transferase families have also been shown to be expressed in the choroid plexus (Johnson et al., 1993; Lowndes et al., 1994; Stapleton et al., 1995; Martinasevic et al., 1998). Taken together, mNAT2 is located at specific brain regions and cell types where it could function as a detoxifying enzyme and has the capacity to protect the brain against environmental insults in sporadic PD etiology.

On the other hand, the specific expression pattern of NAT suggests a specific, or an additional, role to xenobiotic metabolism, which is more relevant to the function of particular neuronal types or circuits. The highly specific and persistent nature of *Nat2* expression within some postmitotic cells in the adult nervous system points to a specific role in neuronal function. After neurulation, expression of mouse *Nat2* persists in specific locations in the central nervous system. The cerebellum and choroid plexus have their ontogenetic origins in the roof of the fourth ventricle (reviewed in (Wang and Zoghbi, 2001). Expression of mouse *Nat2* in these structures at embryonic day 11.5 (Cornish VA, unpublished data) suggests that *Nat2* may be expressed continuously throughout the embryonic development of the cerebellar Purkinje cells and the choroid plexus. Further analysis is needed to determine whether this is indeed the case.

In order to examine the endogenous role of NAT, previous substrate/inhibitor screenings have been performed using the major neurotransmitters dopamine, serotonin, GABA, noradrenaline and acetylcholine with Syrian hamster NAT2 (shNAT2). None was found to be a potential substrate/inhibitor (Kawamura, 2005). Pyridoxal-5'-phosphate and 4-pyridoxic acid are, respectively, the essential coenzyme of vitamin B-6 and the major catabolite of vitamin B-6 metabolism, and play important roles in the synthesis or catabolism of neurotransmitters. Inadequate levels of pyridoxal phosphate in the brain cause neurological dysfunction, particularly epilepsy (Clayton, 2006). It was shown here that pyridoxal 5'-phosphate and 4-pyridoxic acid may be inhibitors of shNAT2; kinetic studies on the K_I values have to be determined to understand if this could hold true under physiological conditions. Their interactions with NAT could be a form of vitamin B-6 homeostasis, where NAT could indirectly modulate neurotransmitter syntheses in the brain. Preliminary metabolomic profiling from urine samples of the C57Bl/6 *Nat2*+/+ and *Nat2*-/- mice have

been performed with ^{1}H NMR analysis but without significant difference in their vitamin B-6 levels [Saggu R., Department of Biochemistry, Oxford University, data not shown].

Mouse *Nat2* is the genetic equivalent of human *NAT2*, but mouse *Nat2* encodes the functional equivalent of human NAT1 isozyme. These two proteins have the same pattern of expression and substrate specificity, acetylating pABA and p-aminobenzoylglutamate (p-ABglu) (Sim et al., 2000). However, both human *NAT1* and *NAT2* are polymorphic, whereas only one gene, mouse *Nat2*, shows polymorphism (Upton et al., 2001a). This implies that there may be an overlapping function or redundancy between mouse *Nat1* and *Nat2*. To support this hypothesis, recent findings showed that mouse *Nat1* is more widely expressed in adult mouse than previously thought and therefore could perform a compensatory role (Loehle et al., 2006). Moreover, the distinct substrate and role for mouse NAT3 are yet to be identified.

The *in vivo* and *in vitro* data, therefore, have to be interpreted with care when compared to human. Human NAT2 has been suggested as a genetic determinant in neurodegenerative diseases, such as Parkinson's disease (Bandmann et al., 1997; Bandmann et al., 2000; Tan et al., 2000a; van der Walt et al., 2003; Chaudhary et al., 2005). In four out of five studies, the slow acetylator genotype for human NAT was found to be more common in the Parkinson's disease group. Among Indians, the NAT2 genotype/phenotype was significantly associated with young onset PD and to a lesser extent with late onset PD (Chaudhary et al., 2005). Furthermore, there is a significant association between PD and NAT2 in Hong Kong Chinese (Chan et al., 2003). Grundmann *et al.* have shown that 6-OHDA lesion caused more deleterious effect at the level of striatal nerve endings in a slow NAT2 acetylator rat strain (Wistar-Kyoto) (Grundmann et al., 2004). The exception came from the Rotterdam study,

which concluded that slow NAT acetylator (NAT2) polymorphism is not a major genetic determinant of idiopathic PD (Harhangi et al., 1999). Such inconsistency is possibly due to the use of different methodologies, diagnostic criteria and most importantly, different population cohorts. The *Nat2-/-* mouse model, because of a likely *mNat1/hNAT2* functional overlap, could be used to demonstrate the association of PD and NAT polymorphism. Further experiments using double *Nat1/2*, or *Nat1/2/3* knockout mice in a 6-OHDA-lesioned paradigm will perhaps provide a more definitive answer to the population studies.

Experiments using single or double *Nat* mutants are possible because mice lacking either *Nat2* or both *Nat1* and *Nat2* are viable, fertile and described as aphenotypic (Cornish et al., 2003; Sugamori et al., 2003). However, when the wildtype and *Nat2-/-* mice were tested with SHIRPA screening, the *Nat2-/-* mice showed heightened anxiety compared to the wildtype animals – they were more reluctant to explore the unknown arena, more of them struggled when they were held and were more likely to bite. Surprisingly, they seemed to be less responsive to touch, which would contradict the hypothesis that they showed greater anxiety. One plausible explanation is that they were less spatially aware of any potential "danger" compared to the normal wildtype mice, but only became more anxious when provoked. Specific behavioural tests that distinguish different types of anxiety might be able to confirm this. The *Nat2-/-* mice also showed less fluid movement and experienced higher difficulty in the wire manoeuvre. It is possible that the role of *Nat2* in the brain is closely related to basal ganglia function, which governs anxiety and motor coordination, but is very subtle. Further behavioural studies specifically for movements, such as the rotarod test, would be able to distinguish between the *Nat2* wildtype and knockout animals. Furthermore, pharmacological stimuli may be required to test for a specific neuronal function in order to relate acetylator status to the etiology of sporadic PD.

Figure 7.1.

Schematic illustration showing the generation of the *Nat2*+/+ and *Nat2*-/- PCR products.

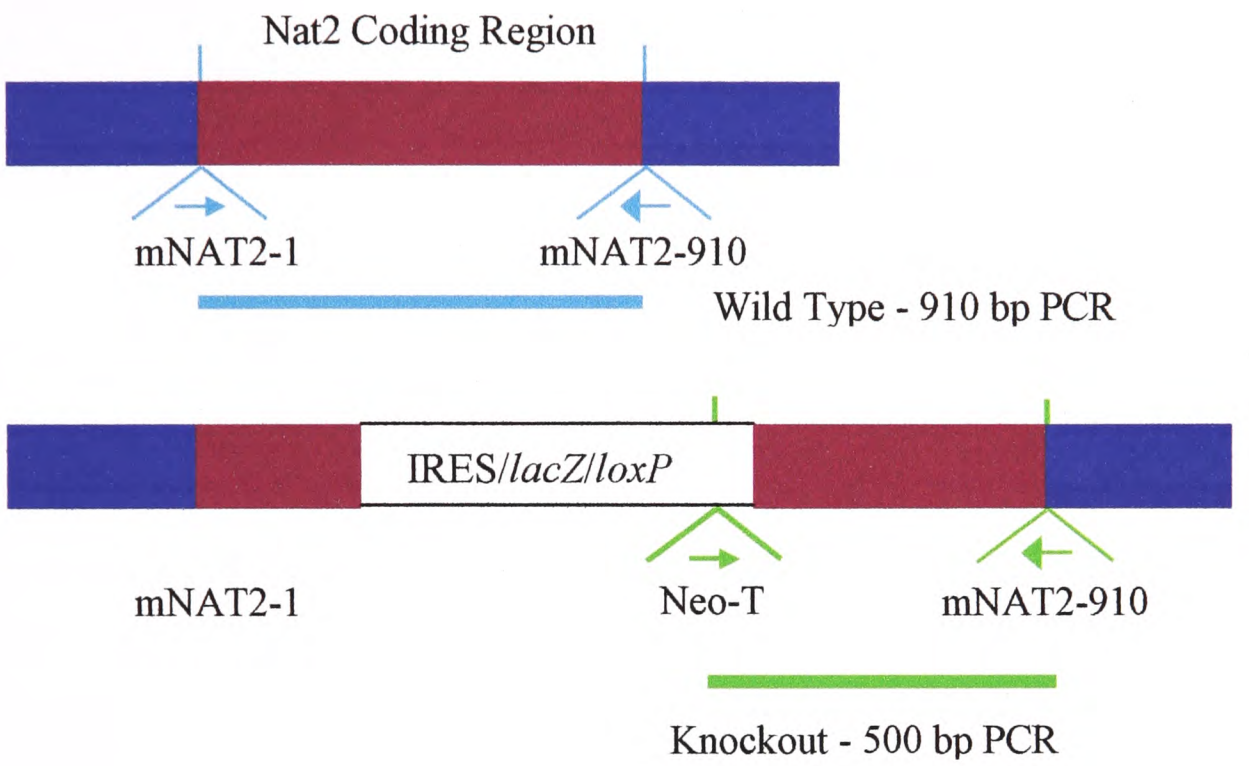


Figure 7.2

A schematic diagram of the *lacZ* construct and the PCR amplification for routine genotyping for *Nat2* knockout mice.

Genomic DNA extracted from tissue samples was PCR amplified with primers mNAT2-1, mNAT2-910 and Neo-T. The presence of the wildtype and knockout alleles results in PCR products of 910 and 500 bp respectively. M = Invitrogen 1 kb Plus DNA ladder; +/+ = *Nat2* wildtype; +/+ = *Nat2* heterozygote; -/- = *Nat2* null.

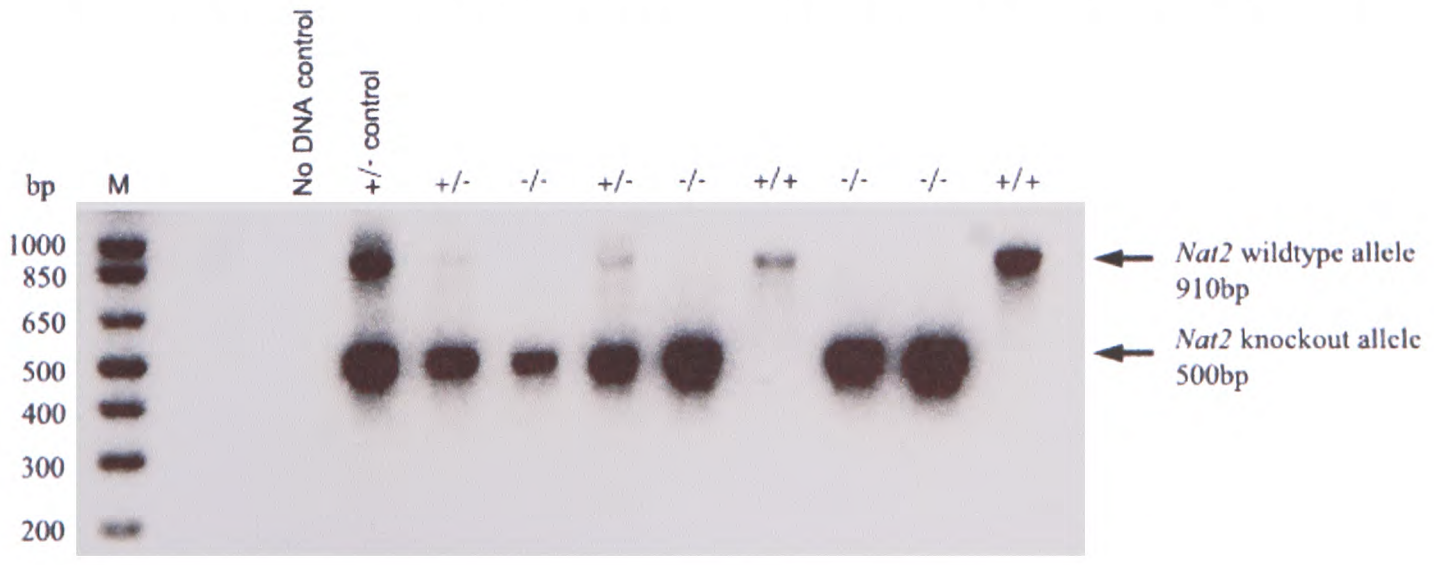


Figure 7.3

Characterisation of anti-mNAT2 antibody 183.

A series of recombinant prokaryotic and eukaryotic NAT proteins (35ng/lane) were loaded onto an SDS-PAGE gel as follows: purified Syrian hamster NAT2 (shNAT2), partially purified human NAT1 (hNAT1), partially purified human NAT2 with a hexa-histidine tag (hNAT2) and purified NAT from *Pseudomonas aeruginosa* with a hexa-histidine tag (PANAT). High-range Rainbow molecular weight marker (M) was loaded for molecular weight calculations. Proteins were separated by electrophoresis and gels were either stained with Coomassie blue (Figure 1A) or used for Western blotting with antiserum 183 (1:400) as primary antibody (Figure 1B). The blot from B was stripped and re-probed with an antibody against the His tag (QIA*express*® Penta-His™ HRP Conjugate antibody, Qiagen) to confirm that hNAT2 and PANAT protein were loaded (Figure 1C). Antiserum 183 was also used to detect NAT in cerebellar homogenates of the C57Bl/6 mouse strain of either *Nat2* +/+ or the corresponding *Nat2* -/- littermates from heterozygous intercrosses by Western blotting. A representative western blot is shown in Figure 1D. 0.5μg of purified Syrian hamster NAT2 was loaded for comparison. The amount of total protein loaded was indicated on top of each lane.

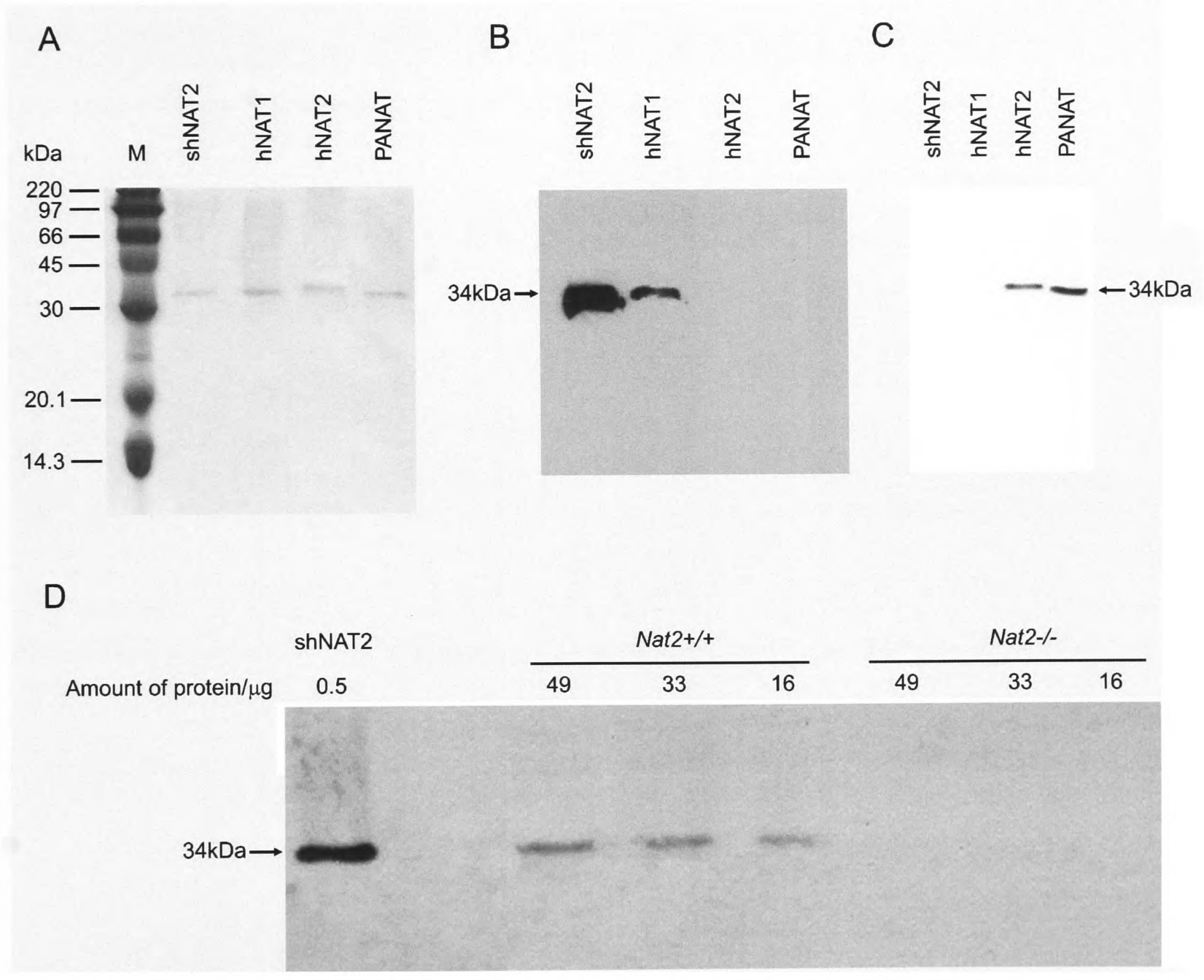

A
kDa
M
shNAT2
hNAT1
hNAT2
PANAT
220
97
66
45
30
20.1
14.3
B
shNAT2
hNAT1
hNAT2
PANAT
34kDa
C
shNAT2
hNAT1
hNAT2
PANAT
34kDa
D
shNAT2
Nat2+/+
Nat2-/-
Amount of protein/μg
0.5
49
33
16
49
33
16
34kDa

Figure 7.4

Dual labelling of the VTA and SN with anti-mouse NAT2 antibody and TH in adult mice.

(A) In the VTA, over 75% of NAT-labelled neurons (green, 1:300) are colocalised with TH+ dopaminergic neurons (red, 1:1000, Sigma) as indicated by the arrowheads. Neurons that are NAT-immunopositive but do not express TH are indicated by the arrows. (B) In the SN, colocalisation of NAT and TH is also observed (arrowheads), though some of the TH+ neurons do not express NAT (double arrowheads). Scale bars = 20 μm

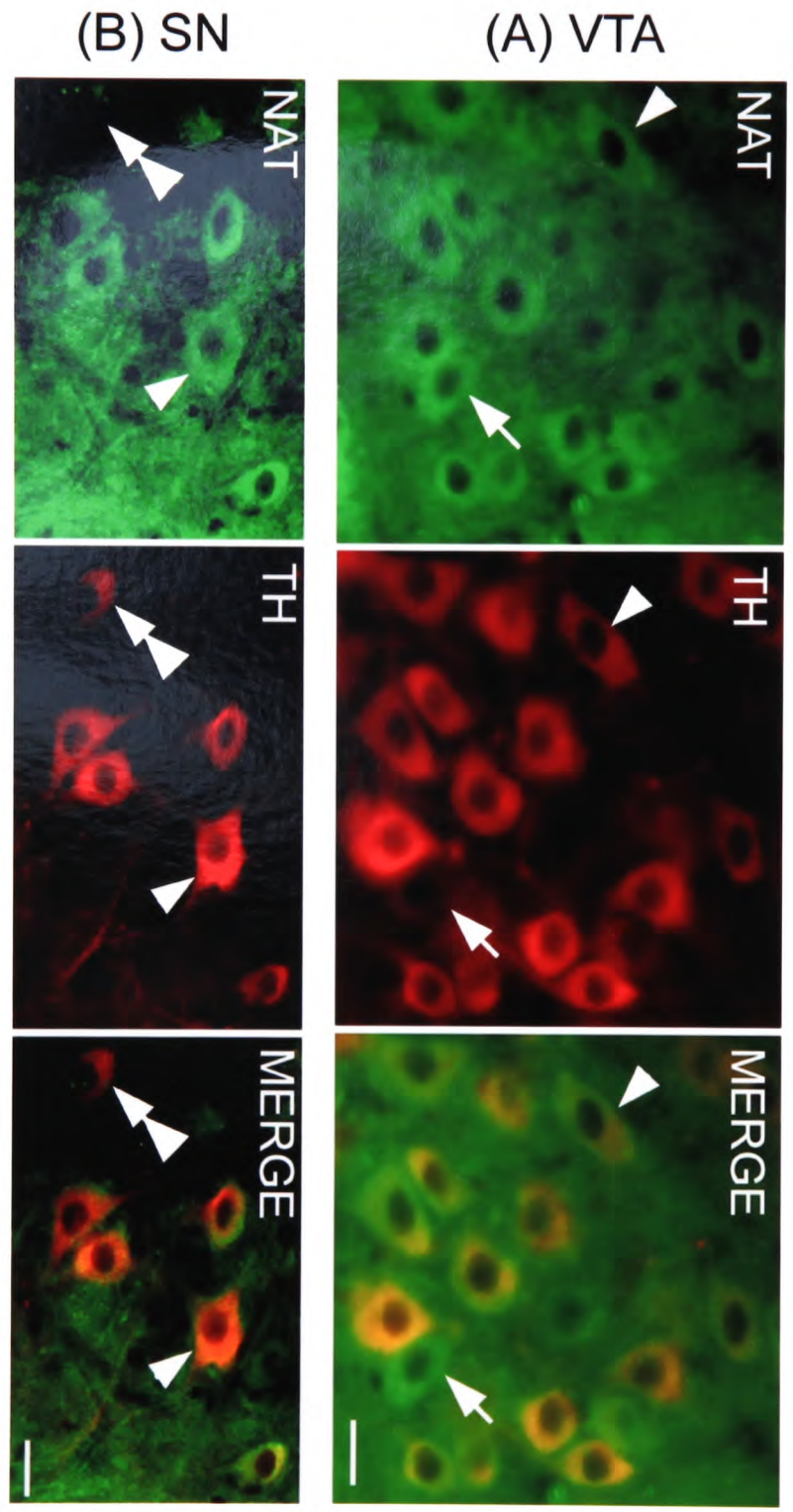

(B) SN
(A) VTA
NAT
NAT
TH
TH
MERGE
MERGE

Figure 7.5

Dual labelling of the cerebellum with anti-mouse NAT2 antibody and CB in adult mice.

In the cerebellar cortex, less than 25% of CB+ Purkinje neurons (red, 1:2000, Swant) are colocalised with NAT-labelled neurons (green, 1:300) as indicated by the arrows. The majority of the Purkinje cell layer is NAT-immunonegative. Scale bars = 30 μm

MERGE CALBINDIN NAT

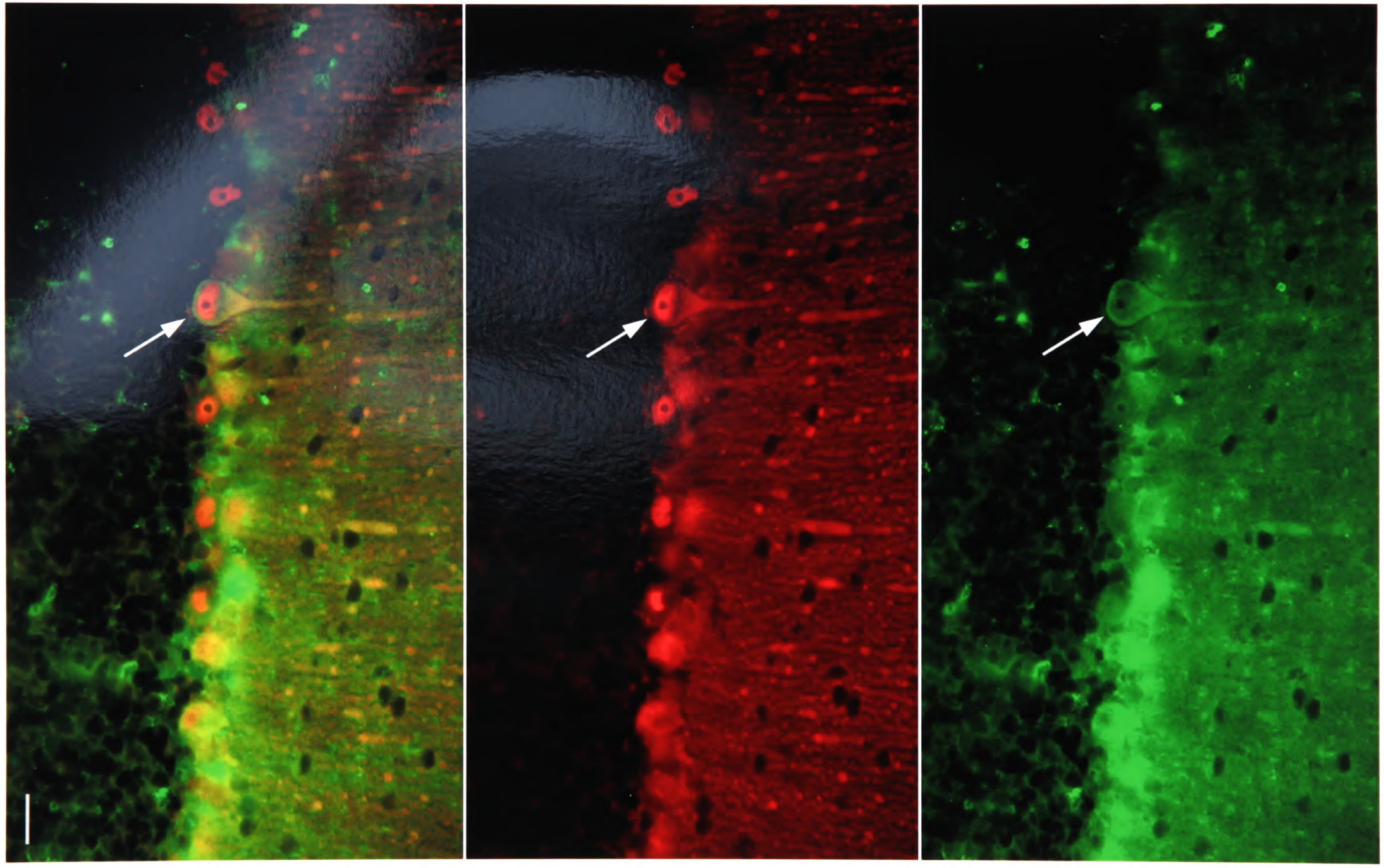


Figure 7.6

X-gal staining as a reporter for *Nat2* expression in adult mouse brain sections.

The blue X-gal product indicates expression of the *lacZ* transgene from the *Nat2* promoter. (A, B) X-gal staining is observed along the Purkinje cell layer in the cerebellar cortex. (C, D) X-gal staining is observed in the midbrain region which includes the SN and the VTA. (E, F) In the olfactory bulb, blue staining is observed predominantly in the glomerular layer. (G, H) Intense X-gal staining is also observed along the epithelial layer of the lateral ventricles (arrowheads) and in the choroid plexus (asterisks). Arrowheads mark reference point seen on higher magnification images. Scale bar = 100 μm in A, C, E and G; 50 μm in B, D, F and H.

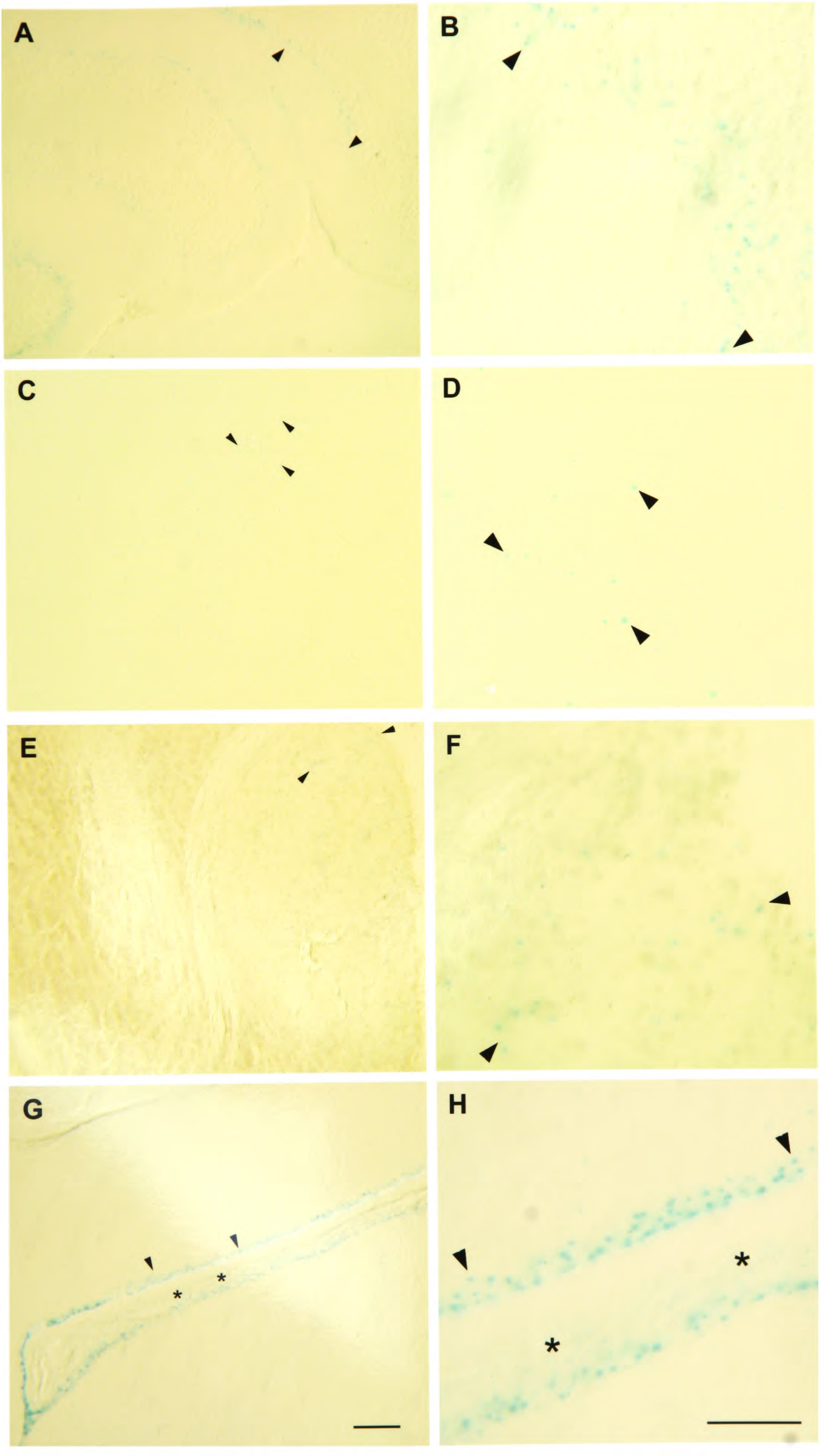

A
B
C
D
E
F
G
H

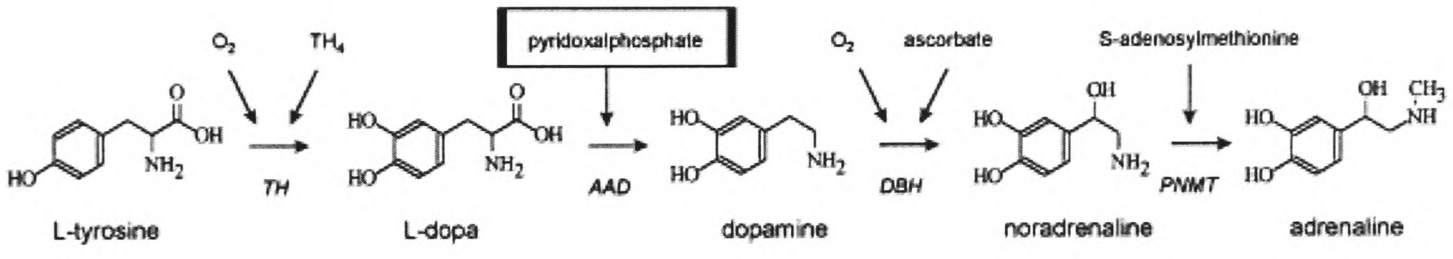
Figure 7.7

Biosynthetic pathways of catecholamines and GABA in the brain

In catecholamine synthesis, tyrosine is converted to DOPA by tyrosine hydroxylase (TH). DOPA is converted to dopamine by L-aromatic amino acid decarboxylase (AAD) using pyridoxal phosphate as a co-factor. Dopamine is transported into vesicles, where it is converted to noradrenaline by dopamine β-hydroxylase (DBH). Neurons that release dopamine as a neurotransmitter contain TH and AAD but lack DBH. Other neurons and the adrenal medullary cells release adrenaline, which is derived from noradrenaline by the action of phenylethanolamine-*N*-methyltransferase (PNMT).

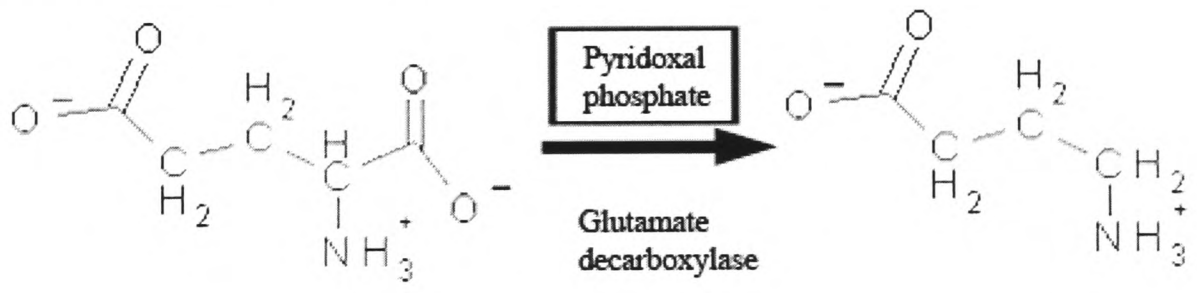
GABA is synthesized from glutamate by glutamate decarboxylase (GAD) using pyridoxal phosphate as a co-factor. Two forms of GAD are present in brain: GAD67 has a high affinity for pyridoxal phosphate and so may be constitutively active; GAD65 has a lower affinity and its activity may be rapidly regulated by co-factor availability.

Catecholamine pathway



[Adapted from Lehnert H., *European Journal of Endocrinology* (1998) **183** 363-367]

Biosynthesis of GABA



Glutamate

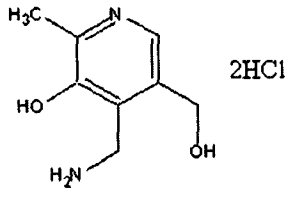
GABA

Figure 7.8

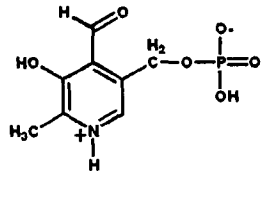
Chemical structures of the compounds tested as substrate/inhibitor of Syrian hamster NAT2 (shNAT2)

Pyridoxamine dihydrochloride, pyridoxal 5'-phosphate, 4-pyridoxic acid, retinoic acid, L-Kynurenine, anthranilic acid and gabaculine were tested as substrates or inhibitors of shNAT2, using *p*-aminobenzoic acid (pABA) as the positive control.

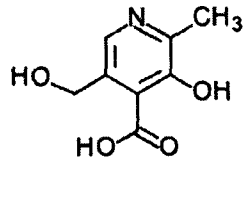
Pyridoxamine HCl



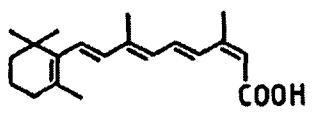
Pyridoxal phosphate



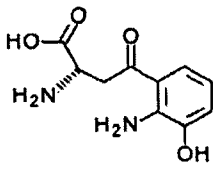
4-Pyridoxic acid



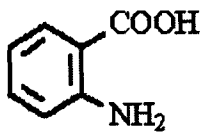
Retinoic acid



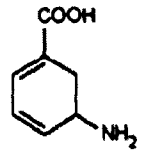
L-Kynurenine



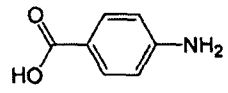
Anthranilic acid



Gabaculine



p-aminobenzoic acid



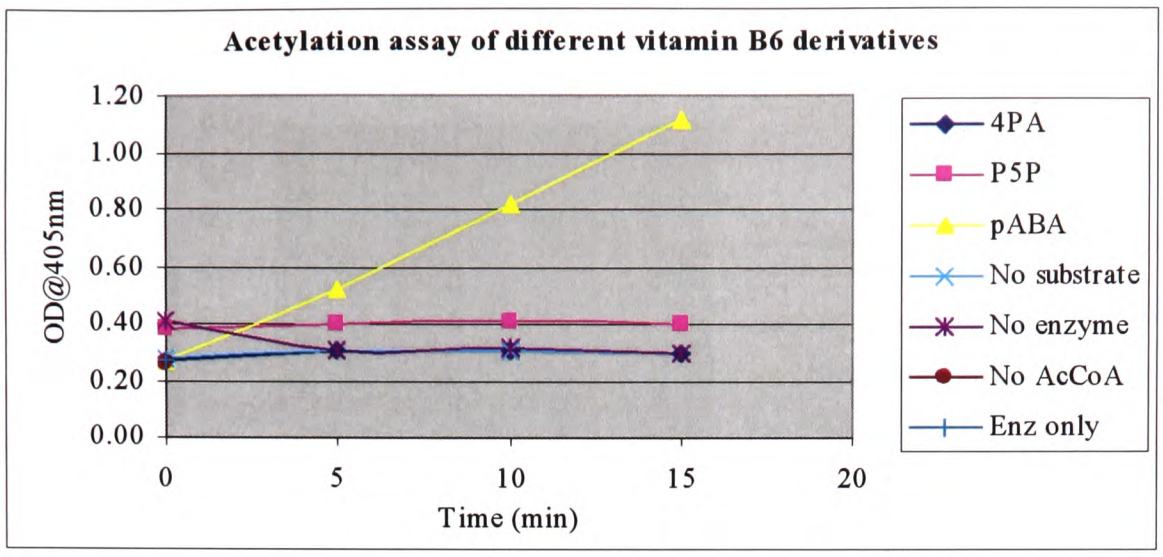
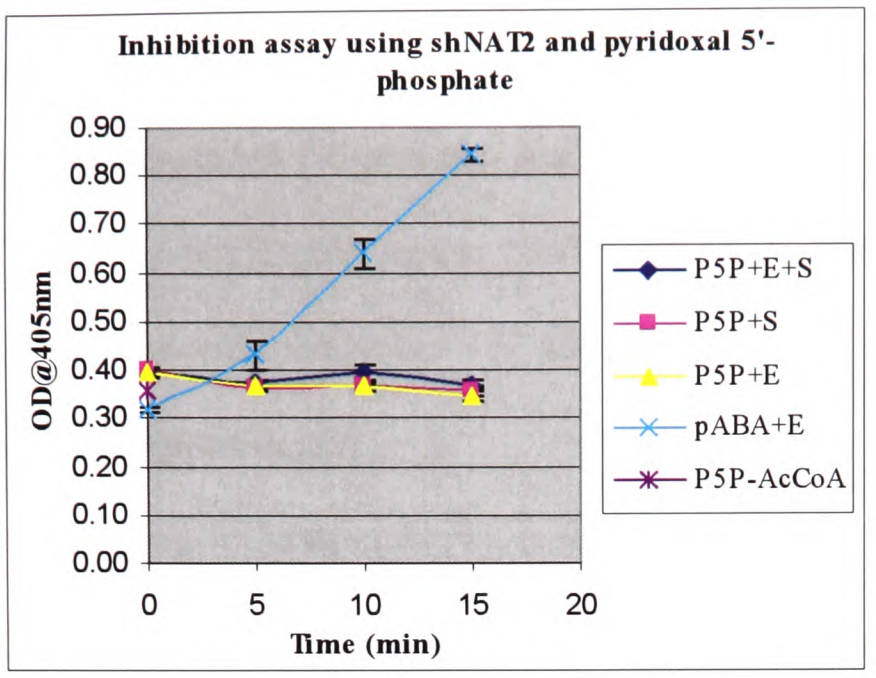


Figure 7.9

Measurement of shNAT2 activity with pyridoxal 5'-phosphate and 4-pyridoxic acid by hydrolysis of AcCoA

Purified recombinant shNAT2 (25 ng) was incubated with pABA, pyridoxal 5'-phosphate (P5P) or 4-pyridoxic acid (4PA) (each at 500 μM) in the presence of AcCoA (1 mM). The reaction was stopped after 5, 10, or 15 min and the DTNB was added to develop colour. Acetylation only occurred with pABA and the activity was in the linear range. Controls were performed with no enzyme, substrate or AcCoA. All measurements are described as mean ± standard deviation.



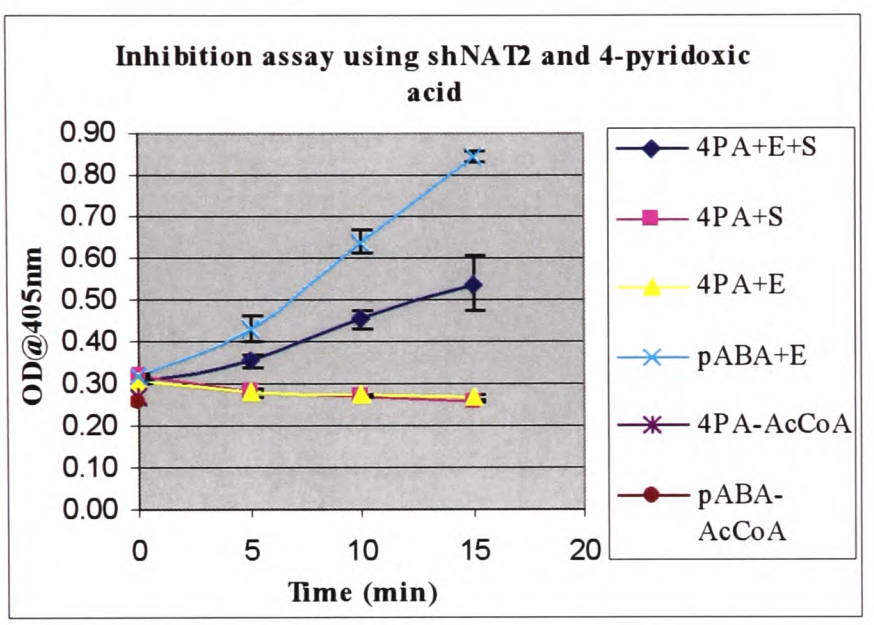


Figure 7.10

Screening of potential inhibitors for shNAT2 by measuring the hydrolysis of AcCoA

Purified recombinant shNAT2 (25 ng) was incubated with 100 μM of potential inhibitors such as pyridoxal 5'-phosphate (top panel) or 4-pyridoxic acid (bottom panel) in the presence of pABA (500 μM) and AcCoA (1mM). The reaction was stopped after 5, 10, or 15 min and the DTNB was added to develop colour. Pyridoxal 5'-phosphate almost reduced the acetylation of pABA to background levels, whereas 4-pyridoxic acid inhibited 38% of the pABA acetylation activity. Controls were performed with no enzyme, substrate, inhibitor or AcCoA. All measurements are described as mean ± standard deviation.

Table 1. Sequence alignment of NAT C-terminal dodeca-peptides. Alignment of human, hamster and mouse NAT C-terminal sequences shows 100% identity between the human NAT1, hamster NAT2 and mouse NAT2. This C-terminal dodecapeptide was used to raise isoform-specific antibodies 183 and 184. Identical residues across species and isoforms are highlighted in grey.

	C-terminal dodeca-peptide											
Immunisation hapten	L	V	P	K	H	G	D	R	F	F	T	I
human NAT1	L	V	P	K	H	G	D	R	F	F	T	I
hamster NAT2	L	V	P	K	H	G	D	R	F	F	T	I
mouse NAT2	L	V	P	K	H	G	D	R	F	F	T	I
mouse NAT3	L	V	P	K	**C**	G	**N**	**V**	F	F	T	I
human NAT2	L	V	P	K	**P**	G	D	**G**	**S**	**L**	T	I
hamster NAT1	**F**	V	P	K	**N**	G	**N**	**L**	**S**	F	**S**	I
mouse NAT1	**F**	V	P	K	H	G	**E**	**L**	**V**	F	T	I

Table 2: Mouse NAT2 and human NAT1 expression in adult Central Nervous System.

	Organism		
	Mouse		Human
Visualisation system / Brain region	**lacZ expression in Nat2-/- mice**	**Immunohistochemistry mouse NAT2**	**Immunohistochemistry human NAT1**
Cerebellum	++ Purkinje cells + granule cell layer - molecular layer	++ Purkinje cells[1] + granule cell layer - molecular layer	++ Purkinje cells + granule cell layer - molecular layer
Brainstem	not tested	not tested	+ cerebellar pontine tracts
Substantia nigra/Ventral tegmental area	++ neuronal cell bodies	++ TH +ve neurons ++ TH-ve neurons	++ pigmented neurons ++ non-pigmented neurons
Olfactory lobe	+	not tested	not tested
Hippocampus	-	-	-
Spinal cord	+	+ [2]	not tested
Choroid plexus	+++	not tested	+++
Lateral ventricles	+++ ependymal layer	not tested	+++ ependymal layer

\+ occasional cells are positive
++ some cells are positive
+++ most cells are positive
\- not detected

Additional evidence of NAT expression in these structures
[1] Acetylation of NAT2 specific substrates by cerebellar homogenate [Payton, 1999]
[2] Mouse NAT2 immunoreactivity in large motor neurons (Stanley et al 1998)

Compounds	As substrate Final conc	[AcCoA]	As inhibitor Final conc	pABA as substrate	[AcCoA]	Substrate?	Inhibitor?
Pyridoxol	500mM	1mM	100mM	500mM	1mM	x	x
Pyridoxal 5'-phosphate						x	√
Pyridoxamine dihydrochloride						x	x
Pyridoxamine 5'-phosphate							
4 Pyridoxic acid						x	√
Gabaculine						x	x
Anthranilic acid						x	x
L-Kynurenine						x	x
Retinoic acid						x	x

Table 3

Summary of the substrate/inhibitor screenings using different vitamin B-6 derivatives and other chemically-related compounds with shNAT2.

DTNB assays showed none of the tested compounds were potential substrate of shNAT2 (25 ng), though pyridoxal 5'-phosphate and 4-pyridoxic acid were shown to be potential inhibitors of shNAT2.

TABLE 4

Test	Scoring category	Wildtype (%)	*Nat2* Knockout (%)	Significance
VIEWING BOX				
Body position	Inactive	0	0	NS
	Active	100	100	
Tremor	Absent	100	100	NS
	Present	0	0	
Palpebral closure	Eyes open	100	100	NS
	Eyes closed	0	0	
Coat appearance	Well groomed	100	100	NS
	Irregular (e.g. piloerection)	0	0	
Whiskers	Absent	0	0	NS
	Present	100	100	
Lacrimation	Absent	100	100	NS
	Present	0	0	

Test	Scoring category	Wildtype (%)	*Nat2* Knockout (%)	P value	Significance
IN THE ARENA					
1. Transfer arousal	Extended freeze	0	0	0.0006	***
	Brief freeze	45	69		
	Immediate movement	55	31		
2. Gait	Fluid movement	100	85	<0.0001	***
	Lack of fluidity in movement	0	15		
3. Tail elevation	Horizontal extension	100	100	/	NS
	Elevated	0	0		
3. Startle response	Absent	45	38	0.32	NS
	Present	55	62		
4. Touch response	Absent	0	8	<0.0001	***
	Responds to touch	73	92		
	Flees prior to touch	27	0		
5. Wire maneouvre	Active grip with hind legs	55	23	<0.0001	***
	Difficult to grasp hind legs	27	47		
	Unable to grasp hind legs	0	0		
	Unable to lift hind legs; Falls within 10 seconds	9	15		
	Falls immediately	9	15		

Test	Scoring category	Wildtype (%)	*Nat2* Knockout (%)	P value	Significance
ABOVE ARENA					
6. Positional passivity	Struggles when held by the tail	27	85	<0.0001	***
7. Trunk curl	Absent	100	100	/	NS
	Present	0	0		
8. Limb grasping	Absent	100	85	<0.0001	***
	Present	0	15		
9. Skin colour	Blanched	0	0	/	NS
	Pink	100	100		
	Bright red	0	0		
10. Pinna reflex	Absent	0	0	/	NS
	Present	100	100		
11. Corneal reflex	Absent	0	0	/	NS
	Present	100	100		
12. Righting reflex	Absent	91	92	0.8	NS
	Present	9	8		
OVERALL BEHAVIOUR					
13. Defecation	Absent	0	0	/	NS
	Present	100	100		
14. Urination	Absent	82	92	0.04	*
	Present	18	8		
15. Biting in response to handling	Absent	18	8	0.04	*
	Present	82	92		
16. Vocalisation in response to handling	Absent	90	91	0.8	NS
	Present	10	9		

KEY

***: P<0.001

**: P = 0.001 to 0.01

*: P = 0.01 to 0.05

NS: Not significant, P >0.05

Appendix 7.1

Genomic DNA preparation for genotyping

The ear clip was treated with 30 µl lysis buffer (100 mM Tris HCl pH 8.5, 5 mM EDTA, 0.2% SDS, 200 mM NaCl, 10 mg/ml Proteinase K) at 55°C for 60 – 90 min. Proteinase K was denatured at 94°C for 10 min to terminate the lysis reaction. 30 µl phenol/chloroform solution was added to each sample and vortexed for 5 sec. After 5 min centrifugation at 12,000 rpm, the aqueous layer was removed. It was then stored at 4°C. 1-2 µl was used per PCR reaction.

Appendix 7.2

Sodium dodecylsulfate-Polyacrylamine Gel Electrophoresis (SDS-PAGE)

Proteins were separated using 12% acrylamide SDS-PAGE (Sambrook et al., 1989) and visualised by Coomassie blue staining or Western blotting. The separating gels contained 12% (v/v) acrylamide: bisacrylamide (29:1, Anachem), 375 mM Tris-HCl (pH 8.0), 0.125% (w/v) sodium dodecylsulfate (SDS), 0.05% (w/v) ammonium persulfate (APS) and 0.002% (v/v) *N,N,N',N'*-tetramethyl-ethylenediamine (TEMED). The stacking gel contained 6% (v/v) acrylamide: bisacrylamide 29:1, 125 mM Tris-HCl (pH 8.0), 0.125% (w/v) SDS, 0.05% APS and 0.002% TEMED. The gels were cast in a Hoefer vertical mini-gel apparatus. Protein samples were prepared by adding equivalent volumes of SDS-PAGE sample buffer (10 mM Tris-HCl, pH 6.8, 0.4% (w/v) SDS, 1% (v/v) 2-mercaptoethanol, 2% (v/v) glycerol, 10 μg/ml bromophenol blue, 83 mg/ml iodoacetamide) to the protein solution and heated at 95°C for 10 min. Electrophoresis was performed at 25 mA using running buffer (50 mM Tris-HCl, pH 8.3, 50 mM glycine, 1% (w/v) SDS). BioRad low range molecular markers were used as protein marker standards. Coomassie blue staining was carried out using staining buffer (0.375% (w/v) Coomassie Brilliant Blue in 18.75% (v/v) acetic acid, 45% (v/v) methanol) for 1 min and destained overnight in destaining buffer (0.5 M methanol, 0.75 M acetic acid).

Appendix 7.3

Western blotting

SDS-PAGE for Western blotting (Sambrook et al., 1989) was prepared and run using Rainbow markers (AP Biotech) as protein standards. Proteins were transferred from the gel to nitrocellulose membrane (Hybond™-C) (Amersham) at 25 V for 16 h at 4°C in transfer buffer (20 mM Na_2HPO_4, 20% (v/v methanol) in BioRad-Trans Blot™ cell. The nitrocellulose membrane was washed twice in TBST (50 mM Tris-HCl, pH 7.9, 150 mM NaCl, 0.05% (v/v) Tween® 20) for 5 min and was incubated with the following solutions at room temperature:

1. Blocking solution: TBST containing 10% (w/v) dried skimmed milk (2 h)
2. Primary antibody (NAT 183) incubation (1:4000) diluted in TBST containing 3% (w/v) dried skimmed milk (1 h)
3. Secondary antibody incubation: monoclonal HRP-anti rabbit IgG (Sigma) diluted 1:2000 in TBST containing 3% (w/v) dried skimmed milk (1 h)

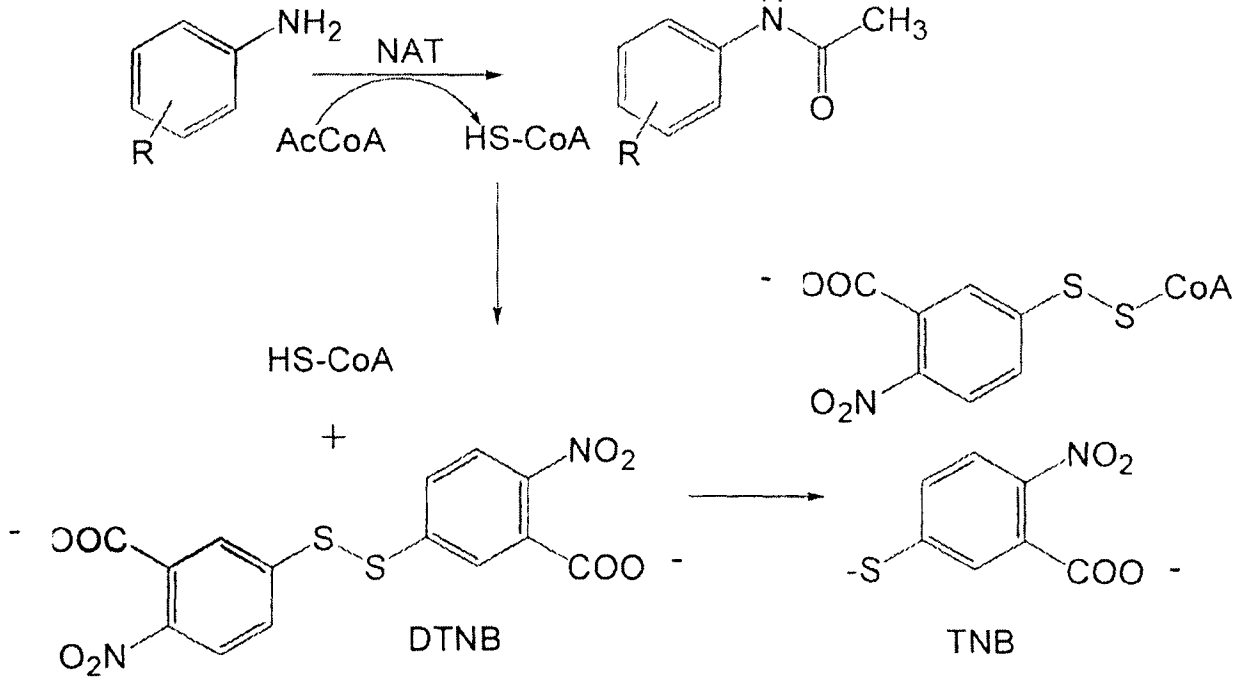
Between each step, the nitrocellulose membrane was washed (3 x 10 min) with TBST containing 3% (w/v) skimmed milk. Finally, the membrane was washed (3 x 10 min) in TBS. For Penta-his HRP conjugate antibody, the antibody incubation steps were performed according to the manufacturer's instructions.

Chemiluminescence using ECL™ western blot Detecting Reagents (Amersham) was used to detect the bound antibody. The chemiluminescent signal was captured using autoradiographic film (Kodak), developed using an X-OGraph Compact X2 automated film developer.

Appendix 7.4

Measurement of NAT activity by the DTNB assay

NAT activity can be determined by measuring the rate of hydrolysis of the acetyl-donor. Ellman's reagent (5,5'-dithio-bis(2nitrobenzoic acid) or DTNB) was used to measure the rate of acetyl CoA (AcCoA) hydrolysis in the presence of aromatic amines. The assay is based on the reaction of thiols with the chromogenic DTNB, which forms the yellow dianion 5-thio-2-nitrobenzoic acid (TNB). TNB is then measured at its absorption maximum 412 nm (Ellman, 1959). The NAT acetylation reaction utilises AcCoA: arylamine in a 1:1 ratio, therefore the reaction can be monitored by quantifying the free CoA liberated in the reaction, which corresponds to the amount of TNB produced (Kawamura, 2005).



8 Discussion

Summary of the experimental findings:

1. Partial nigrostriatal lesions were created in mice using 6-OHDA or MPTP/p, which could be used in examining PD-like pathological changes (Chapter 3, 4 and 6).
2. More CB+ DA neurons survived after neurotoxic treatments compared to CB- DA neurons (Chapter 3 and 4). In the midbrain, both CB+ and CB- DA neurons receive inputs from the striatum and the dorsal raphe. Electron microscopy showed TH+ and CB+ midbrain neurons both received synaptic inputs from the striatum and the dorsal raphe (Chapter 5). Hence, the difference between CB+ and CB- DA neurons is not likely to be due to input connectivity.
3. In the 6-OHDA PD model, there was no change in total midbrain volume but a significant decrease in the total number of midbrain neurons. Both DA neurons and GABAergic neurons were lost on the lesioned hemisphere compared to the unlesioned side (Chapter 3 and 4).
4. The extent of cell loss increased between one- and three-months post-lesion for DA cells but not for GABAergic cells (Chapter 4).
5. Salicylic acid (aspirin) showed neuroprotective effect on TH+/CB- neurons in the MPTP/p parkinsonian model, and showed observable amelioration in microgial activation (Chapter 6).
6. Murine arylamine *N*-acetyltransferase 2 (mNAT2) was preferentially expressed in midbrain DA neurons, Purkinje cells, choroid plexus and olfactory bulbs, with pyridoxal 5'-phosphate and 4-pyridoxic acid as potential inhibitors of mNAT2. Behavioural tests also showed that *Nat2-/-* mice have more difficulty in movement and increased anxiety in response to stimuli compared to controls. MNAT2 could therefore be a predisposing determinant of PD development (Chapter 7).

8.1 6-OHDA and MPTP/p Mouse Models of Parkinson's Disease

The present study created two Parkinsonian mouse models in which partial lesion of the nigrostriatal system was achieved. The dosage of neurotoxin, the volume administered and the minimum weight of the mice used were optimised in both the 6-OHDA and MPTP/p models to ensure minimum mobidity. Although the DA cell loss compromises movement and motivation for food, the mice were given high levels of post-operative support to accelerate their recovery. These are important parameters to consider when animal models are used because some publications to date have shown a high mortality rate, for example, MPTP treatment resulted in the death of eight of 22 wildtype and 13 of 26 CB null-mutant mice (Airaksinen et al., 1997).

This study validates, at least partially, both the 6-OHDA and MPTP/p-lesioned mice as PD models. The two models exhibit several phenotypic features of PD which have been listed in Chapter 1. Firstly, the neurotoxins both destroyed TH+ DA neurons, as shown by the extensive fiber loss in the striatum in the 6-OHDA-lesioned hemisphere and MPTP/p-treated animals. The addition of probenecid successfully increases the retention time of MPTP in neuron which produces a chronic lesion with a lower overall dose of the toxin. Secondly, a pronounced reduction of SN neurons was observed. Thirdly, the mice appeared to have a normal longevity and long lasting DA cell loss, as shown by the 1- and 3-month post-treatment studies, which allowed us to examine the progressive nature of PD. Fourthly, inclusion bodies in nigral neurons were observed under electron microscopy in the MPTP/p model which resembles the pathology of PD. Nevertheless, one study found no immunoreactive inclusion body formation in the MPTP/p model, and I did not examine the immunoreactivity of the inclusions I identified (Shimoji et al., 2005). Results from the present study are consistent with previous findings that inclusions containing dense and granular core, similar to that of the classical Lewy bodies, were found in the cytoplasm of

nigral and cortical neurons at 3 weeks after chronic MPTP/p treatment (Meredith et al., 2002; Novikova et al., 2006).

8.1.1 Differences between the 6-OHDA and MPTP/p models

Though both 6-OHDA and MPTP are substrates for the high-affinity dopamine reuptake system and both exert toxicity through generation of reactive oxygen species, evoking oxidative stress (Cohen, 1994), they generate different toxic mechanisms as described in Chapter 1. It has recently been found that 6-OHDA toxicity to DA neurons is associated with neuronal COX-2, whereas MPP^+ toxicity is COX independent (Carrasco et al., 2005), which will have a different implication to the use of salicylic acid as a therapeutic agent.

Different neurotoxic treatments may also lead to an increase in antigenicity of a protein. Fitzpatrick and colleagues showed in monkeys, there was an overall increase (22%) in the TH+/CB+ cell number in the dorsal tier of MPTP-treated cases, while there was a decrease in the TH+ cell number (65%) in the ventral tier. On the other hand, in 6-OHDA-lesioned rats, both TH+ neurons in the ventral tier (97%) and TH+/CB+ neurons in the dorsal tier (~40%) were lost. Hence, they have concluded that there was an increase in TH+/CB+ cell number in the dorsal tier in response to MPTP insult, which was not observed after 6-OHDA treatment. They further suggested that the increase in antigenicity was due to the dopaminergic reinnervation of the striatum in MPTP-treated cases (Fitzpatrick et al., 2005). However, the report compared monkeys to rats which might have introduced species variations. In this study, 6-OHDA and MPTP/p could have exerted the same effect on DA neurons, but the data were interpreted separately and no extrapolation was made between the two neurotoxin treatments with a change in antigenicity.

8.1.2 Limitations of the animal models

The 6-OHDA model does not mimic all pathological and clinical features of human parkinsonism (Schober, 2004). For example, the formation of inclusion bodies (Lewy bodies) has not been reported. Although a partial lesion has been achieved in this study, 6-OHDA treatment is still considered acute, which differs significantly from the slowly progressive pathology of human PD (Betarbet et al., 2002). It better represents the advanced phase of PD rather than the early phase. Also, in order to rule out a small but likely occurrence of a bilateral lesion, saline controls should be included in the future study using 6-OHDA.

Unlike the unilateral 6-OHDA model in which the intact hemisphere serves as an internal control structure (Perese et al., 1989), the major limitation of the MPTP/p model is the requirement for a relatively large number of control, vehicle (probenecid) and MPTP/p-treated animals. Consequently, a higher intra-animal variability might be introduced. If the model is used for testing new pharmacological therapies, the number of animals needed may be even higher to achieve a sufficient statistical power. Since the generation of the 6-OHDA and MPTP/p models at different survival time points requires a relatively long time, this study is limited by the number of animals used in each control and test groups. The continuation of this work with larger number of animals will be able to consolidate my findings.

There are several advantages in studying PD using mouse models. First, transgenic mice can be generated to manipulate genes that may be involved in the disease etiology. Second, the organisation of midbrain DA neurons in the mouse is similar to that in human (Liang et al., 1996a). Third, the economical, logistical and ethical constraints using primates in studying PD make mice a better alternative compared to primates (Cenci et al., 2002).

8.2 Midbrain CB+ and CB- Dopaminergic Neurons

The current study showed that, although CB+ neurons degenerated in the midbrain following toxin treatment, more CB+ DA neurons remained after 6-OHDA and MPTP/p treatments. One of the major challenges of quantifying the neuronal loss is the small sample size. After the neurotoxic treatments, particularly in the 6-OHDA-lesion model where only one side of the brain was counted as the test (lesioned) side and the other side as the control, the number of immunolabelled neurons present was relatively low. Hence, it was not possible to use unbiased stereology or to separate the midbrain into dorsal and ventral tier of the SNC, SNR, SNL, VTA and paranigral part of VTA, which may be essential to determining the exact pattern of dopamine cell loss.

However, the difficulty in obtaining a neuronal count is not completely due to our experimental limitations; the published numbers for TH+ neurons can span within a 2-fold estimation. For example, Chadi *et al.* used stereology on 27 C57Bl/6 male mice (12 weeks old) and estimated 6000 to 13700 TH+ neurons were present in the SN (Chadi et al., 1993). Moreover, the differences between the various published quantitative studies may be attributable to a number of variables, such as differences in staining protocols, different techniques for cell identification (neuromelanin versus immunohistochemistry), and differences in the delineation of the midbrain regions (Stark and Pakkenberg, 2004). By counting systematically in every serial section, the number of midbrain DA neurons estimated in this study is in agreement with the published data in C57Bl/6 mice: 7500 midbrain TH+ neurons (Joyce and Millan, 2005), ~3000 midbrain CB+ neurons (Sadikot, 2005).

Many reports suggested that CB+ DA neurons are less prone to neurodegeneration in PD. For example, CB+ cells in the dorsal tier of SNC are less affected in models of PD, whereas CB-

cells of the ventral tier of SNC, projecting to striosomes, are selectively sensitive to 6-OHDA (Rogers, 1992). Interestingly, the dorsal tier of SNC and VTA cells that project to the shell of nucleus accumbens are less affected in PD models (Zahm, 1991) and receive relatively few striatal inhibitory projections when compared with the ventral tier of SNC (Fallon and Loughlin, 1995). Furthermore, glial cell-line-derived neurotrophic factor (GDNF) significantly increased the number of surviving DA neurons and increased the density of CB+ neurons but without affecting the density of calretinin+ neurons in culture (Meyer et al., 1999). Cell type-specific gene expression of midbrain DA neurons (adult C57Bl mice), examined using laser capture microdissection and microarray analysis, revealed a higher expression of CB in A10 neurons (Chung et al., 2005). Together with the findings in this study, data support the notion that CB+ neurons are less vulnerable to PD neurodegeneration.

It was suggested that CB is not required for protection, but rather serves as a marker of less vulnerable neurons (Airaksinen et al., 1997; Korotkova et al., 2004). The two most published genes that have been associated with CB and a lower vulnerability are *Pitx3* and *HCN1*. *Pitx3* is a homeobox gene which affects a number of target genes functioning as either activators or repressors of eurkaryotic transcription (Korotkova et al., 2005). It is known that homeobox genes could act in a concentration-dependent way during the embryonal development (Manoukian and Krause, 1992; Lumsden and Krumlauf, 1996). Hence, different concentrations of a homeobox gene transcript may trigger activation of divergent downstream signally pathways. In the brain, *Pitx3* is confined to midbrain DA neurons and persists throughout adult life in both rodents and humans (Smidt et al., 1997), which implies a role in the maintenance of midbrain DA neurons. Moreover, *Pitx3* is differently expressed in VTA and SN, not only in the whole tissue but also at the single-cell level, with ~6x higher *Pitx3* expression in the VTA than in SN neurons (Korotkova et al., 2005). Furthermore, its expression is associated with CB: in CB+ neurons it is 3.6x higher than in CB- ones in the

VTA but not different in the SN. This is in keeping with the higher vulnerability of SN DA neurons in aphakia mice bearing the mutations in the *Pitx3* gene (Smidt et al., 1997; Hwang et al., 2003; Nunes et al., 2003; van den Munckhof et al., 2003; Sadikot, 2005): in SN 84% of neurons expressing *Pitx3* are CB- and only the ventral tier of SNC expressed *Pitx3* (van den Munckhof et al., 2003), hence more susceptible to neurodegeneration, whereas in the VTA nearly half of the Pitx3+ neurons express CB (Korotkova et al., 2005).

CB+ and CB- midbrain DA neurons also differ in their electrophysiological properties, expression of ion channels and projection patterns (Neuhoff et al., 2002), features that could be regulated by *Pitx3* expression (Korotkova et al., 2005). *In vitro* studies showed that DA midbrain neurons have low-frequency pacemaker activity, broad action potentials followed by a pronounced afterhyperpolarization, and a pronounced sag component that is mediated by hyperpolarization-activated, cyclic nucleotide-regulated cation channels (I_h, HCN) (Santoro and Tibbs, 1999). Single-cell RT-multiplex PCR experiments demonstrated that differential CB, but not calretinin, expression is associated with differential I_h channel densities: only the highly vulnerable class of DA neurons possesses the strong rebound activation, which might render these neurons more susceptible to glutamatergic input which was not investigated in this study (Beal, 2000). Moreover, the most vulnerable DA neurons possess the highest density of I_h channels, which could contribute to the different polarity and temporal structure of GABAergic integration in DA neurons, and might result in different pathophysiological responses to metabolic stress via K-ATP channel activation (Neuhoff et al., 2002).

If CB is now considered as a neurochemical marker for the less vulnerable DA neurons, then its function within the cell remains unknown. Perhaps it differs from the other calcium-binding proteins like calbindin D9k or parvalbumin, but its role in other neuronal types may

give us some clues. For example, in the spines and dendrites of cerebellar Purkinje cells, CB acts as an activity-dependent sensor that activates *myo*-inositol monophosphatase (IMPase), a key enzyme of the inositol-1,4,5-trisphosphate signalling cascade (Schmidt et al., 2005). Future experimentation will be necessary to study the functional consequences of CB, particularly in intracellular signalling.

8.3 Changes in Dopaminergic and GABAergic Neurons in Parkinson's Disease Models

The present study showed that GAD65/67-immunolabelled GABAergic neurons were expressed mostly in the SNR and a few was found in the VTA, in accordance with other reports (Diaz et al., 2003). The lack of GFP-GAD65 expression in the midbrain implies that GAD67 is the major isoform that contributed to the immunostaining. Both GAD65 and GAD67 mRNA transcripts are present in the SNR in rats (Rodriguez and Gonzalez-Hernandez, 1999), but it is possible that GAD65 mRNA is not translated: GAD67 protein is widely distributed throughout the neuron in its active form, saturated with the cofactor, and is pretranscriptionally regulated, whereas GAD65 is preferentially located in axon terminals as an inactive apoenzyme, and is activated by energy metabolites (Henry and Tappaz, 1991; Kaufman et al., 1991; Martin et al., 1991; Soghomonian and Chesselet, 1992; Esclapez et al., 1993; Martin and Rimvall, 1993; Esclapez et al., 1994; Rimvall and Martin, 1994; Rodriguez et al., 1994). It is not surprising that the two GAD isoforms are differentially regulated after modification in the nigrostriatal pathway by lesion.

This study also showed significant loss in the midbrain of both DA and GABAergic neurons after 6-OHDA treatment. Since 6-OHDA is a selective neurotoxin to DA neurons, the observed loss of GABAergic neurons would be secondary to the degeneration of DA neurons. However, not all GABAergic neurons appear to respond in the same way to DA cell

degeneration. The heterogeneity of midbrain GABAergic neurons is best described by Diaz *et al.* In their study using 6-OHDA-treated rats, GAD67 mRNA expression increases in the lateral region of SNR but decreases in the medial region of SNR (Diaz et al., 2003). The former region receives afferents from lateral striatal regions that receive afferents from somatosensory cortical areas, whereas the latter receives afferents from the medial striatal regions, which receive afferents from limbic and prelimbic cortical areas (Gerfen, 1985; Deniau and Chevalier, 1992; Deniau and Thierry, 1997). Thus the different response of GABAergic neurons in these two regions may correspond to a different adaptation in the motor and limbic components of basal ganglia to DA cell loss.

The different classification of cells is also reflected by their firing patterns. Although there was a decrease in GAD65/67-immunolabelled neurons, there might be a compensatory increase in GABA release. Indeed, DA cell degeneration increases the firing rate in regular-firing cells, but not in irregular and bursty cells, which causes subsets of GABAergic nigral neurons to react differentially to the striatal DA depletion (Diaz et al., 2003). Clinically, this increased firing of GABAergic SNR neurons is associated with catalepsy – an enhanced muscle tone in PD patients (Blandini et al., 2000). Thus, both firing rate and firing pattern of GABAergic neurons could be involved in the physiopathology of PD.

The responses of GABAergic neurons might be explained by the connectivity of CB- DA neurons. There is a distinct pattern of GABAergic dendritic innervation of the ventral tier DA neurons in the SNR (Fallon and Loughlin, 1995). The predominant post-inhibitory excitation in the CB- DA cells located in the ventral tier, due to higher expression of I_h channels, correlates to the more pronounced striatal feedback inhibition. On the other hand, higher post-inhibitory excitability might lead to higher metabolic demands on CB- cells. A combination of these factors, together with reduced responsiveness of K-ATP channels,

would render a neuron more vulnerable to metabolic stress (Korotkova et al., 2004). An initial loss of the most vulnerable cells leads to increased subthalamic nucleus excitatory input on the rest of the SNC population caused by an evolving imbalance in BG circuitry (Wichmann and DeLong, 1998). Hence, the two subsets of GABAergic neurons may also contribute to the differential neural vulnerability in PD. Further studies on the connectivity and electrophysiology of the nigral GABAergic subpopulation would lead to a better understanding of PD pathology.

8.4 The Relationship Between Early Neurotoxin Exposure and Progressive Neurotoxicity in Parkinson's Disease

DA neuronal loss differed significantly between the 1- and 3-month post-treatment mice. Although no epidemiological studies specifically address the issue of toxic exposure early in life, my study provided data that, in adult mice, 6-OHDA lesion exacerbated GABAergic neurodegeneration with time. This finding is similar to a "Two-hit model", where mice were exposed to paraquat (PQ) and the fungicide maneb (MB) during development, and subsequently exposed again as adults (Thiruchelvam et al., 2003) showed a more profound damage to DA neurons. Results in this study shows even initial and re-exposures that both occur during adulthood can cause greater neurodegeneration in the midbrain (Logroscino, 2005).

Other approaches subjecting young and older mice to neurotoxin have been developed to show an enhanced risk of PD with time (Thiruchelvam et al., 2003). The duration of microglial activation was longer in older mice compared to young ones (Sugama et al., 2003a). Because activated microglia precede DA neuronal loss following medial forebrain bundle axotomy (Sugama et al., 2003b), age-related microglia activation may be relevant to the higher susceptibility to MPTP neurotoxicity in older mice.

Molecular alterations that are qualitatively similar to those that occur in the nervous system during normal ageing are amplified in vulnerable neuronal populations by disease-related processes (Mattson and Magnus, 2006). For example, the amounts of oxidatively modified DNA bases, proteins and lipids in the brain increase progressively. Specific age-related modifications of proteins include carbonylation, nitration and covalent binding of the lipid peroxidation product 4-hydroxynonenal (Floyd and Hensley, 2002), which are found in vulnerable neurons in PD (Jenner, 2003). In addition to the synthesis of dopamine, which might increase oxidative stress, DA neurons are projection neurons with relatively long axons (Smith et al., 1987), which might be particularly vulnerable to ageing. This is because of their high energy requirement, reliance on axonal transport (anterograde and retrograde) for sustained function and trophic support, and a large cell surface area that increases exposure of the cells to toxic environmental conditions (Mattson and Magnus, 2006).

The progressive vulnerability of DA neurons also needs to be considered in terms of the penetration of 6-OHDA and MPTP/p through the blood-brain barrier (BBB). In rats, unilateral injections of 6-OHDA into the striatum or the medial forebrain bundle produced increased BBB leakage in the ipsilateral SN and striatum 10 and 34 days post-treatment (Carvey et al., 2005), though it is also possible that the leakage is caused by neuroinflammation produced by 6-OHDA. Long-term disruption of barrier function would expose the "hot spots" to higher quantities of neurotoxins, which could contribute to further disease progression. This supports the argument of the "Two-hit model". In addition, peripheral immunomediators may respond to a dysfunction BBB as previously suggested (McRae-Degueurce et al., 1988; Appel et al., 1992). On the other hand, the amount of MPTP reaching the brain was constant regardless of the age of mice (Ricaurte et al., 1987) and the concentration of MPP^+ in the brains of young and older mice were nearly identical (Ricaurte et al., 1987). Further studies examining the permeability of BBB in the 6-OHDA or MPTP/p

mouse models will be able to confirm whether peripheral molecules contribute to progressive DA vulnerability, or that the DA cell damage comes from within the brain.

8.5 Salicylic Acid As an Anti-oxidative and Anti-inflammatory Therapy for Parkinson's Disease

If the processes of ageing play a central role to neurodegenerative disorders, it would be expected that an intervention that slows this process would also guard against neurodegenerative disorders. Moreover, strong support in favour of a relationship between vulnerability to oxidative stress and neurodegeneration is provided by the observation that CB+ DA neurons, which were completely spared after paraquat exposure, showed no overt signs of lipid peroxidation (McCormack et al., 2006). This lack of oxidative stress in CB+ neurons was consistently found in both A9 and A10, implying that decreased susceptibility to injury is likely related to mechanisms that, within CB+ neurons, counteract oxidative damage. On the other hand, CB- DA neurons has a combination of high dopamine transporter (DAT) and low vesicular monoamine transporter 2 (VMAT2) levels which would result in higher oxidative stress in these neurons (Murase and McKay, 2006). Hence, anti-oxidants may be a potential preventative measure against PD.

This study showed that SA, through its anti-oxidant property, did not render CB+ or CB- DA neurons less vulnerable to MPTP/p treatment. It is, however, able to reduce TH+ neuronal death in the MPTP/p-treated mice and minimize microglial activation via its anti-inflammatory ability. To what extent is DA neuronal death attributable to microglial activation? Using the activated microglial inhibitor minocycline, Przedborski's group showed that activated microglia contribute to about 20% of the MPTP-induced TH+ cell death (Wu et al., 2002). The final effect of inflammation may vary depending on the balance between neurotrophic and neurotoxic factors released by activated microglia during the development

of PD. Thus, although SA may not rescue all types of midbrain neurons or restore degenerating DA neurons back to normal, chronic administration might give other beneficial effects such as reducing oxidative stress in ageing.

8.6 Gene-environment Interactions in Sporadic Parkinson's Disease

The incidence of sporadic PD cases is apparently affected by environmental factors (Semchuk et al., 1992; Priyadarshi et al., 2001). The emerging picture is that PD results from a combination of genetic and environmental factors, which likely interact with each other (Benmoyal-Segal and Soreq, 2006). However, both the nature and order of events leading to PD neurodegeneration are still being debated. One approach for identifying susceptibility genes for PD is to determine the allelic frequency of known polymorphisms in the suspected candidate genes and to search for putative association of such polymorphisms with the disease status. Hence, alleles involved with the emergence and/or progression of sporadic PD would be predictably found in patients at a frequency greater than those observed within the general population. To this date, at least 16 candidate genes were investigated with relation to the etiology of sporadic PD. One of them is arylamine *N*-acetyltransferase (NAT) (Borlak and Reamon-Buettner, 2006).

The study of NAT in the wildtype and knockout mice showed that, among other neuronal populations, murine NAT2 is expressed in some midbrain DA neurons. Its role in xenobiotic metabolism may relate to the efflux of environmental neurotoxins, and subsequently influence the vulnerability of DA neurons in PD. It is also plausible that NAT functions synergistically with more than one polymorphism, for example, with CYP2D6 but this possibility remains to be explored (Benmoyal-Segal and Soreq, 2006). Further experiments subjecting the wildtype and knockout mice to the 6-OHDA or MPTP/p paradigm should provide direct evidence of NAT's function in PD.

To elucidate factors related to selective DA neurodegeneration in PD, many studies using gene expression profiling have emerged. Between the SN and VTA DA neurons, several genes from different biological categories showed cell-specific expression patterns. At least five genes potentially related "neuroprotection" are higher in VTA DA neurons, one of which is calbindin (Liang et al., 1996b). For example, neuropeptide genes as a category are more highly expressed in VTA DA neurons than in those from the SN (Chung et al., 2005; Greene et al., 2005; Greene, 2006). On the other hand, multiple genes related to energy pathways, electron transport and mitochondria are more highly expressed in the SN than the VTA (Chung et al., 2005; Greene et al., 2005), which is especially relevant to the mitochondrial dysfunction aspect of PD pathology. These profiles suggest that SN DA neurons are more metabolically active than their counterparts in the VTA, that they rely more on oxidative energy metabolism, and/or that they have less energetic reserve capacity available to them (Greene, 2006).

This thesis set out to examine two toxin-based animal models of PD with particular reference to what they can tell us about the progression of cell loss and the vulnerability of different neuronal populations. I have shown that CB-containing neurons play an important role in the survival of DA neurons, and that they could be progressively lost over time. Their inputs from the striatum and dorsal raphe have also been illustrated. Moreover, GABAergic neurons are involved in the pathogenesis of PD. A salicylic acid treatment even after MPTP/p lesion could rescue some of the DA cell death and reduce inflammatory damage. The relationship between sporadic PD and environmental insults was also explored. Nevertheless, further work to examine the mechanism of CB in DA neurons and how a normal basal ganglia circuitry can be maintained is urgently needed if we are to improve the treatment of this devastating disease.

Bibliography

Abeliovich A, Schmitz Y, Farinas I, Choi-Lundberg D, Ho WH, Castillo PE, Shinsky N, Verdugo JM, Armanini M, Ryan A, Hynes M, Phillips H, Sulzer D, Rosenthal A (2000) Mice lacking alpha-synuclein display functional deficits in the nigrostriatal dopamine system. Neuron 25:239-252.

Aceves J, Floran B, Martinez-Fong D, Benitez J, Sierra A, Flores G (1992) Activation of D1 receptors stimulates accumulation of gamma-aminobutyric acid in slices of the pars reticulata of 6-hydroxydopamine-lesioned rats. Neurosci Lett 145:40-42.

Agundez JA, Jimenez-Jimenez FJ, Luengo A, Molina JA, Orti-Pareja M, Vazquez A, Ramos F, Duarte J, Coria F, Ladero JM, Alvarez-Cermeno JC, Benitez J (1998) Slow allotypic variants of the NAT2 gene and susceptibility to early-onset Parkinson's disease. Neurology 51:1587-1592.

Airaksinen MS, Thoenen H, Meyer M (1997) Vulnerability of midbrain dopaminergic neurons in calbindin-D28k-deficient mice: lack of evidence for a neuroprotective role of endogenous calbindin in MPTP-treated and weaver mice. Eur J Neurosci 9:120-127.

Alberg AJ, Daudt A, Huang HY, Hoffman SC, Comstock GW, Helzlsouer KJ, Strickland PT, Bell DA (2004) N-acetyltransferase 2 (NAT2) genotypes, cigarette smoking, and the risk of breast cancer. Cancer Detect Prev 28:187-193.

Albin RL, Young AB, Penney JB (1989) The functional anatomy of basal ganglia disorders. Trends Neurosci 12:366-375.

Albin RL, Young AB, Penney JB (1995) The functional anatomy of disorders of the basal ganglia. Trends Neurosci 18:63-64.

Albrecht M (2005) LRRK2 mutations and Parkinsonism. Lancet 365:1230.

Alexander GE, Crutcher MD (1990) Functional architecture of basal ganglia circuits: neural substrates of parallel processing. Trends Neurosci 13:266-271.

Anantharam V, Lehrmann E, Kanthasamy A, Yang Y, Banerjee P, Becker KG, Freed WJ, Kanthasamy AG (2007) Microarray analysis of oxidative stress regulated genes in mesencephalic dopaminergic neuronal cells: Relevance to oxidative damage in Parkinson's disease. Neurochem Int 50:834-847.

Andersen JK (2004) Oxidative stress in neurodegeneration: cause or consequence? Nat Med 10 Suppl:S18-25.

Apkarian AV, Hodge CJ (1989) Primate spinothalamic pathways: III. Thalamic terminations of the dorsolateral and ventral spinothalamic pathways. J Comp Neurol 288:493-511.

Appel SH, Le WD, Tajti J, Haverkamp LJ, Engelhardt JI (1992) Nigral damage and dopaminergic hypofunction in mesencephalon-immunized guinea pigs. Ann Neurol 32:494-501.

Aubin N, Curet O, Deffois A, Carter C (1998) Aspirin and salicylate protect against MPTP-induced dopamine depletion in mice. J Neurochem 71:1635-1642.

Bacon G (2002) The neuroanatomical basis for 5-HT-dopamine interactions in the rat substantia nigra and ventral tegmental area. In: Department of Pharmacology: Oxford University.

Baimbridge KG, Celio MR, Rogers JH (1992) Calcium-binding proteins in the nervous system. Trends Neurosci 15:303-308.

Bali B, Erdelyi F, Szabo G, Kovacs KJ (2005) Visualization of stress-responsive inhibitory circuits in the GAD65-eGFP transgenic mice. Neurosci Lett 380:60-65.

Ballard PA, Tetrud JW, Langston JW (1985) Permanent human parkinsonism due to 1-methyl-4-phenyl-1,2,3,6-tetrahydropyridine (MPTP): seven cases. Neurology 35:949-956.

Bandmann O, Vaughan J, Holmans P, Marsden CD, Wood NW (1997) Association of slow acetylator genotype for N-acetyltransferase 2 with familial Parkinson's disease. Lancet 350:1136-1139.

Bandmann O, Vaughan JR, Holmans P, Marsden CD, Wood NW (2000) Detailed genotyping demonstrates association between the slow acetylator genotype for N-acetyltransferase 2 (NAT2) and familial Parkinson's disease. Mov Disord 15:30-35.

Barbeau A (1984) Etiology of Parkinson's disease: A research strategy. Can J Neurol Sci 11:24-28.

Bassilana F, Mace N, Li Q, Stutzmann JM, Gross CE, Pradier L, Benavides J, Menager J, Bezard E (2005) Unraveling substantia nigra sequential gene expression in a progressive MPTP-lesioned macaque model of Parkinson's disease. Neurobiol Dis 20:93-103.

Beal MF (2000) Energetics in the pathogenesis of neurodegenerative diseases. Trends Neurosci 23:298-304.

Beal MF (2001) Experimental models of Parkinson's disease. Nat Rev Neurosci 2:325-334.

Benmoyal-Segal L, Soreq H (2006) Gene-environment interactions in sporadic Parkinson's disease. J Neurochem 97:1740-1755.

Betarbet R, Sherer TB, Greenamyre JT (2002) Animal models of Parkinson's disease. Bioessays 24:308-318.

Bevan MD, Bolam JP, Crossman AR (1994) Convergent synaptic input from the neostriatum and the subthalamus onto identified nigrothalamic neurons in the rat. Eur J Neurosci 6:320-334.

Blackburn TP, Cox B, Lee TF (1982a) Involvement of a central dopaminergic system in 5-methoxy-N,N-dimethyltryptamine-induced turning behaviour in rats with lesions of the dorsal raphe nuclei. Psychopharmacology (Berl) 78:261-265.

Blackburn TP, Foster GA, Heapy CG, Kemp JD (1980) Unilateral 5,7-dihydroxytryptamine lesions of the dorsal raphe nucleus (DRN) and rat rotational behaviour. Eur J Pharmacol 67:427-438.

Blackburn TP, Cox B, Heapy CG, Lee TF (1982b) Possible mechanism of 5-methoxy-N,N-dimethyltryptamine-induced turning behaviour in DRN lesioned rats. Pharmacol Biochem Behav 16:7-11.

Blandini F, Nappi G, Tassorelli C, Martignoni E (2000) Functional changes of the basal ganglia circuitry in Parkinson's disease. Prog Neurobiol 62:63-88.

Bloem BR, Irwin I, Buruma OJ, Haan J, Roos RA, Tetrud JW, Langston JW (1990) The MPTP model: versatile contributions to the treatment of idiopathic Parkinson's disease. J Neurol Sci 97:273-293.

Blum M, Grant DM, McBride W, Heim M, Meyer UA (1990) Human arylamine N-acetyltransferase genes: isolation, chromosomal localization, and functional expression. DNA Cell Biol 9:193-203.

Bobillier P, Seguin S, Petitjean F, Salvert D, Touret M, Jouvet M (1976) The raphe nuclei of the cat brain stem: a topographical atlas of their efferent projections as revealed by autoradiography. Brain Res 113:449-486.

Bolam JP (1992) Preparation of central nervous system tissue for light and electron microscopy. Oxford: Oxford University Press.

Bolam JP, Hodgson AJ, Smith AD, Somogyi P (1979) Demonstration of monosynaptic input to identified efferent neurones in the basal ganglia by a new morphological procedure [proceedings]. J Physiol 296:17P-18P.

Bonifati V, Rizzu P, van Baren MJ, Schaap O, Breedveld GJ, Krieger E, Dekker MC, Squitieri F, Ibanez P, Joosse M, van Dongen JW, Vanacore N, van Swieten JC, Brice A, Meco G, van Duijn CM, Oostra BA, Heutink P (2003) Mutations in the DJ-1 gene associated with autosomal recessive early-onset parkinsonism. Science 299:256-259.

Bonin M, Poths S, Osaka H, Wang YL, Wada K, Riess O (2004) Microarray expression analysis of gad mice implicates involvement of Parkinson's disease associated UCH-L1 in multiple metabolic pathways. Brain Res Mol Brain Res 126:88-97.
Borlak J, Reamon-Buettner SM (2006) N-acetyltransferase 2 (NAT2) gene polymorphisms in Parkinson's disease. BMC Med Genet 7:30.
Boukouvala S, Fakis G (2005) Arylamine N-acetyltransferases: what we learn from genes and genomes. Drug Metab Rev 37:511-564.
Boukouvala S, Price N, Sim E (2002) Identification and functional characterization of novel polymorphisms associated with the genes for arylamine N-acetyltransferases in mice. Pharmacogenetics 12:385-394.
Braak H, Del Tredici K, Rub U, de Vos RA, Jansen Steur EN, Braak E (2003) Staging of brain pathology related to sporadic Parkinson's disease. Neurobiol Aging 24:197-211.
Brooke E, Davies SG, Mulvaney AW, Okada M, Pompeo F, Sim E, Vickers RJ, Westwood IM (2003a) Synthesis and in vitro evaluation of novel small molecule inhibitors of bacterial arylamine N-acetyltransferases (NATs). Bioorganic and Medicinal Chemistry Letters 13:2527-2530.
Brooke EW, Davies SG, Mulvaney AW, Pompeo F, Sim E, Vickers RJ (2003b) An approach to identifying novel substrates of bacterial arylamine N-acetyltransferases. Bioorg Med Chem 11:1227-1234.
Brooks G, Yu XM, Wang Y, Crabbe MJ, Shattock MJ, Harper JV (2003) Non-steroidal anti-inflammatory drugs (NSAIDs) inhibit vascular smooth muscle cell proliferation via differential effects on the cell cycle. J Pharm Pharmacol 55:519-526.
Bunney BS, Aghajanian GK (1976) The precise localization of nigral afferents in the rat as determined by a retrograde tracing technique. Brain Res 117:423-435.
Burns RS, Chiueh CC, Markey SP, Ebert MH, Jacobowitz DM, Kopin IJ (1983) A primate model of parkinsonism: selective destruction of dopaminergic neurons in the pars compacta of the substantia nigra by N-methyl-4-phenyl-1,2,3,6-tetrahydropyridine. Proc Natl Acad Sci U S A 80:4546-4550.
Butterfield DA, Castegna A, Lauderback CM, Drake J (2002) Evidence that amyloid beta-peptide-induced lipid peroxidation and its sequelae in Alzheimer's disease brain contribute to neuronal death. Neurobiol Aging 23:655-664.
Cabello CR, Thune JJ, Pakkenberg H, Pakkenberg B (2002) Ageing of substantia nigra in humans: cell loss may be compensated by hypertrophy. Neuropathol Appl Neurobiol 28:283-291.
Calne DB, Langston JW (1983) Aetiology of Parkinson's disease. Lancet 2:1457-1459.
Carr DB, Sesack SR (2000) Projections from the rat prefrontal cortex to the ventral tegmental area: target specificity in the synaptic associations with mesoaccumbens and mesocortical neurons. J Neurosci 20:3864-3873.
Carrasco E, Casper D, Werner P (2005) Dopaminergic neurotoxicity by 6-OHDA and MPP+: differential requirement for neuronal cyclooxygenase activity. J Neurosci Res 81:121-131.
Carvey PM, Zhao CH, Hendey B, Lum H, Trachtenberg J, Desai BS, Snyder J, Zhu YG, Ling ZD (2005) 6-Hydroxydopamine-induced alterations in blood-brain barrier permeability. Eur J Neurosci 22:1158-1168.
Castellano MA, Diaz-Palarea MD, Barroso J, Rodriguez M (1989) Behavioral lateralization in rats and dopaminergic system: individual and population laterality. Behav Neurosci 103:46-53.
Cavalieri B (1966) Geometria Degli Indivisibili. Torino: Unione Tipografico, Editrice.
Celio MR (1990) Calbindin D-28k and parvalbumin in the rat nervous system. Neuroscience 35:375-475.
Cenci MA, Whishaw IQ, Schallert T (2002) Animal models of neurological deficits: how relevant is the rat? Nat Rev Neurosci 3:574-579.

Chadi G, Moller A, Rosen L, Janson AM, Agnati LA, Goldstein M, Ogren SO, Pettersson RF, Fuxe K (1993) Protective actions of human recombinant basic fibroblast growth factor on MPTP-lesioned nigrostriatal dopamine neurons after intraventricular infusion. Exp Brain Res 97:145-158.

Chan DK, Lam MK, Wong R, Hung WT, Wilcken DE (2003) Strong association between N-acetyltransferase 2 genotype and PD in Hong Kong Chinese. Neurology 60:1002-1005.

Chan P, DeLanney LE, Irwin I, Langston JW, Di Monte D (1991) Rapid ATP loss caused by 1-methyl-4-phenyl-1,2,3,6-tetrahydropyridine in mouse brain. J Neurochem 57:348-351.

Chao J, Nestler EJ (2004) Molecular neurobiology of drug addiction. Annu Rev Med 55:113-132.

Charara A, Smith Y, Parent A (1996) Glutamatergic inputs from the pedunculopontine nucleus to midbrain dopaminergic neurons in primates: Phaseolus vulgaris-leucoagglutinin anterograde labeling combined with postembedding glutamate and GABA immunohistochemistry. J Comp Neurol 364:254-266.

Chaudhary S, Behari M, Dihana M, Swaminath PV, Govindappa ST, Jayaram S, Singh S, Muthane UB, Juyal RC, B KT (2005) Association of N-acetyl transferase 2 gene polymorphism and slow acetylator phenotype with young onset and late onset Parkinson's disease among Indians. Pharmacogenet Genomics 15:731-735.

Chen EY, Kallwitz E, Leff SE, Cochran EJ, Mufson EJ, Kordower JH, Mandel RJ (2000) Age-related decreases in GTP-cyclohydrolase-I immunoreactive neurons in the monkey and human substantia nigra. J Comp Neurol 426:534-548.

Chen H, Jacobs E, Schwarzschild MA, McCullough ML, Calle EE, Thun MJ, Ascherio A (2005) Nonsteroidal antiinflammatory drug use and the risk for Parkinson's disease. Ann Neurol 58:963-967.

Chiueh CC, Rauhala P (1998) Free radicals and MPTP-induced selective destruction of substantia nigra compacta neurons. Adv Pharmacol 42:796-800.

Chiueh CC, Huang SJ, Murphy DL (1992a) Enhanced hydroxyl radical generation by 2'-methyl analog of MPTP: suppression by clorgyline and deprenyl. Synapse 11:346-348.

Chiueh CC, Murphy DL, Miyake H, Lang K, Tulsi PK, Huang SJ (1993) Hydroxyl free radical (.OH) formation reflected by salicylate hydroxylation and neuromelanin. In vivo markers for oxidant injury of nigral neurons. Ann N Y Acad Sci 679:370-375.

Chiueh CC, Krishna G, Tulsi P, Obata T, Lang K, Huang SJ, Murphy DL (1992b) Intracranial microdialysis of salicylic acid to detect hydroxyl radical generation through dopamine autooxidation in the caudate nucleus: effects of MPP+. Free Radic Biol Med 13:581-583.

Choi J, Sullards MC, Olzmann JA, Rees HD, Weintraub ST, Bostwick DE, Gearing M, Levey AI, Chin LS, Li L (2006) Oxidative damage of DJ-1 is linked to sporadic Parkinson and Alzheimer diseases. J Biol Chem 281:10816-10824.

Chu Y, Kompoliti K, Cochran EJ, Mufson EJ, Kordower JH (2002) Age-related decreases in Nurr1 immunoreactivity in the human substantia nigra. J Comp Neurol 450:203-214.

Chung CY, Seo H, Sonntag KC, Brooks A, Lin L, Isacson O (2005) Cell type-specific gene expression of midbrain dopaminergic neurons reveals molecules involved in their vulnerability and protection. Hum Mol Genet 14:1709-1725.

Cicchetti F, Brownell AL, Williams K, Chen YI, Livni E, Isacson O (2002) Neuroinflammation of the nigrostriatal pathway during progressive 6-OHDA dopamine degeneration in rats monitored by immunohistochemistry and PET imaging. Eur J Neurosci 15:991-998.

Clarke DJ, Branton RL (2002) A role for tumor necrosis factor alpha in death of dopaminergic neurons following neural transplantation. Exp Neurol 176:154-162.

Clayton DF, George JM (1999) Synucleins in synaptic plasticity and neurodegenerative disorders. J Neurosci Res 58:120-129.
Clayton PT (2006) B(6)-responsive disorders: A model of vitamin dependency. J Inherit Metab Dis 29:317-326.
Cohen G, Werner, P. (1994) Free radicals, oxidative stress, and neurodegeneration. Philadelphia: W.B. Saunders.
Colonnier M (1968) Synaptic patterns on different cell types in the different laminae of the cat visual cortex. An electron microscope study. Brain Res 9:268-287.
Conway KA, Harper JD, Lansbury PT, Jr. (2000) Fibrils formed in vitro from alpha-synuclein and two mutant forms linked to Parkinson's disease are typical amyloid. Biochemistry 39:2552-2563.
Conway KA, Rochet JC, Bieganski RM, Lansbury PT, Jr. (2001) Kinetic stabilization of the alpha-synuclein protofibril by a dopamine-alpha-synuclein adduct. Science 294:1346-1349.
Cornish VA, Pinter K, Boukouvala S, Johnson N, Labrousse C, Payton M, Priddle H, Smith AJ, Sim E (2003) Generation and analysis of mice with a targeted disruption of the arylamine N-acetyltransferase type 2 gene. Pharmacogenomics J 3:169-177.
Corsini G.U. MRaVF (2002) Molecular and cellular events regulating dopamine neuron survival: Springer, Berlin.
Corsini GU, Pintus S, Chiueh CC, Weiss JF, Kopin IJ (1985) 1-Methyl-4-phenyl-1,2,3,6-tetrahydropyridine (MPTP) neurotoxicity in mice is enhanced by pretreatment with diethyldithiocarbamate. Eur J Pharmacol 119:127-128.
Corvaja N, Doucet G, Bolam JP (1993) Ultrastructure and synaptic targets of the raphe-nigral projection in the rat. Neuroscience 55:417-427.
Costa P, Checkoway H, Levy D, Smith-Weller T, Franklin GM, Swanson PD, Costa LG (1997) Association of a polymorphism in intron 13 of the monoamine oxidase B gene with Parkinson disease. Am J Med Genet 74:154-156.
Cote PY, Sadikot AF, Parent A (1991) Complementary Distribution of Calbindin D-28k and Parvalbumin in the Basal Forebrain and Midbrain of the Squirrel Monkey. Eur J Neurosci 3:1316-1329.
Curzon G, Gumpert EJ, Sharpe DM (1971) Amine metabolites in the lumbar cerebrospinal fluid of humans with restricted flow of cerebrospinal fluid. Nat New Biol 231:189-191.
Czlonkowska A, Kohutnicka M, Kurkowska-Jastrzebska I, Czlonkowski A (1996) Microglial reaction in MPTP (1-methyl-4-phenyl-1,2,3,6-tetrahydropyridine) induced Parkinson's disease mice model. Neurodegeneration 5:137-143.
Czlonkowska A, Kurkowska-Jastrzebska I, Czlonkowski A, Peter D, Stefano GB (2002) Immune processes in the pathogenesis of Parkinson's disease - a potential role for microglia and nitric oxide. Med Sci Monit 8:RA165-177.
Dairou J, Atmane N, Rodrigues-Lima F, Dupret JM (2004) Peroxynitrite irreversibly inactivates the human xenobiotic-metabolizing enzyme arylamine N-acetyltransferase 1 (NAT1) in human breast cancer cells: a cellular and mechanistic study. J Biol Chem 279:7708-7714.
Damier P, Hirsch EC, Agid Y, Graybiel AM (1999a) The substantia nigra of the human brain. I. Nigrosomes and the nigral matrix, a compartmental organization based on calbindin D(28K) immunohistochemistry. Brain 122 (Pt 8):1421-1436.
Damier P, Hirsch EC, Agid Y, Graybiel AM (1999b) The substantia nigra of the human brain. II. Patterns of loss of dopamine-containing neurons in Parkinson's disease. Brain 122 (Pt 8):1437-1448.
Date I, Felten DL, Felten SY (1990a) Long-term effect of MPTP in the mouse brain in relation to aging: neurochemical and immunocytochemical analysis. Brain Res 519:266-276.

Date I, Notter MF, Felten SY, Felten DL (1990b) MPTP-treated young mice but not aging mice show partial recovery of the nigrostriatal dopaminergic system by stereotaxic injection of acidic fibroblast growth factor (aFGF). Brain Res 526:156-160.
Dauer W, Przedborski S (2003) Parkinson's disease: mechanisms and models. Neuron 39:889-909.
Dawson T, Mandir A, Lee M (2002) Animal models of PD: pieces of the same puzzle? Neuron 35:219-222.
Dawson TM, Dawson VL (2002) Neuroprotective and neurorestorative strategies for Parkinson's disease. Nat Neurosci 5 Suppl:1058-1061.
Dawson TM, Dawson VL (2003) Molecular pathways of neurodegeneration in Parkinson's disease. Science 302:819-822.
Day BJ, Patel M, Calavetta L, Chang LY, Stamler JS (1999) A mechanism of paraquat toxicity involving nitric oxide synthase. Proc Natl Acad Sci U S A 96:12760-12765.
DeLong MR (1990) Primate models of movement disorders of basal ganglia origin. Trends Neurosci 13:281-285.
Deniau JM, Chevalier G (1992) The lamellar organization of the rat substantia nigra pars reticulata: distribution of projection neurons. Neuroscience 46:361-377.
Deniau JM, Thierry AM (1997) Anatomical segregation of information processing in the rat substantia nigra pars reticulata. Adv Neurol 74:83-96.
Denner LA, Wu JY (1985) Two forms of rat brain glutamic acid decarboxylase differ in their dependence on free pyridoxal phosphate. J Neurochem 44:957-965.
Derewlany LO, Knie B, Koren G (1994) Arylamine N-acetyltransferase activity of the human placenta. J Pharmacol Exp Ther 269:756-760.
Dervan AG, Meshul CK, Beales M, McBean GJ, Moore C, Totterdell S, Snyder AK, Meredith GE (2004) Astroglial plasticity and glutamate function in a chronic mouse model of Parkinson's disease. Exp Neurol 190:145-156.
Deumens R, Blokland A, Prickaerts J (2002) Modeling Parkinson's disease in rats: an evaluation of 6-OHDA lesions of the nigrostriatal pathway. Exp Neurol 175:303-317.
Dexter DT, Carter CJ, Wells FR, Javoy-Agid F, Agid Y, Lees A, Jenner P, Marsden CD (1989) Basal lipid peroxidation in substantia nigra is increased in Parkinson's disease. J Neurochem 52:381-389.
Diaz MR, Barroso-Chinea P, Acevedo A, Gonzalez-Hernandez T (2003) Effects of dopaminergic cell degeneration on electrophysiological characteristics and GAD65/GAD67 expression in the substantia nigra: different action on GABA cell subpopulations. Mov Disord 18:254-266.
Diaz Palarea MD, Gonzalez MC, Rodriguez M (1987) Behavioral lateralization in the T-maze and monoaminergic brain asymmetries. Physiol Behav 40:785-789.
Ding SL, Elberger AJ (1995) A modification of biotinylated dextran amine histochemistry for labeling the developing mammalian brain. J Neurosci Methods 57:67-75.
Dowd DR, MacDonald PN, Komm BS, Haussler MR, Miesfeld RL (1992) Stable expression of the calbindin-D28K complementary DNA interferes with the apoptotic pathway in lymphocytes. Mol Endocrinol 6:1843-1848.
Dray A, Gonye TJ, Oakley NR, Tanner T (1976) Evidence for the existence of a raphe projection to the substantia nigra in rat. Brain Res 113:45-57.
Duke DC, Moran LB, Kalaitzakis ME, Deprez M, Dexter DT, Pearce RK, Graeber MB (2006) Transcriptome analysis reveals link between proteasomal and mitochondrial pathways in Parkinson's disease. Neurogenetics 7:139-148.
Duque A. ZL (2006) Juxtacellular labeling of individual neurons in vivo: from electrophysiology to synaptology. In: Neuroanatomical Tract-Tracing 3: Molecules, Neurons and Systems (L. Zaborszky FWaJL, ed): Springer.

Ellis CE, Schwartzberg PL, Grider TL, Fink DW, Nussbaum RL (2001) alpha-synuclein is phosphorylated by members of the Src family of protein-tyrosine kinases. J Biol Chem 276:3879-3884.
Emborg ME, Ma SY, Mufson EJ, Levey AI, Taylor MD, Brown WD, Holden JE, Kordower JH (1998) Age-related declines in nigral neuronal function correlate with motor impairments in rhesus monkeys. J Comp Neurol 401:253-265.
Erdélyi F SG, Katarova Z, Hájos N, Pálhalmi J, Freund TF, Mugnaini E, Szabó G (2002) GAD65-GFP transgenic mice expressing GFP in the GABAergic nervous system. FENS Abstr 1:A0113.
Erlander MG, Tobin AJ (1991) The structural and functional heterogeneity of glutamic acid decarboxylase: a review. Neurochem Res 16:215-226.
Erlander MG, Tillakaratne NJ, Feldblum S, Patel N, Tobin AJ (1991) Two genes encode distinct glutamate decarboxylases. Neuron 7:91-100.
Esclapez M, Tillakaratne NJ, Tobin AJ, Houser CR (1993) Comparative localization of mRNAs encoding two forms of glutamic acid decarboxylase with nonradioactive in situ hybridization methods. J Comp Neurol 331:339-362.
Esclapez M, Tillakaratne NJ, Kaufman DL, Tobin AJ, Houser CR (1994) Comparative localization of two forms of glutamic acid decarboxylase and their mRNAs in rat brain supports the concept of functional differences between the forms. J Neurosci 14:1834-1855.
Estrada L, Kanelakis KC, Levy GN, Weber WW (2000) Tissue- and gender-specific expression of N-acetyltransferase 2 (Nat2*) during development of the outbred mouse strain CD-1. Drug Metab Dispos 28:139-146.
Evans WE, Relling MV (1999) Pharmacogenomics: translating functional genomics into rational therapeutics. Science 286:487-491.
Fabre E, Monserrat J, Herrero A, Barja G, Leret ML (1999) Effect of MPTP on brain mitochondrial H2O2 and ATP production and on dopamine and DOPAC in the striatum. J Physiol Biochem 55:325-331.
Fallon JH, Loughlin SE (1995) The Rat Nervous System
Chapter 12 Substantia Nigra, Second Edition Edition: Academic Press, Inc.
Farivar RS, Chobanian AV, Brecher P (1996) Salicylate or aspirin inhibits the induction of the inducible nitric oxide synthase in rat cardiac fibroblasts. Circ Res 78:759-768.
Farrer M, Kachergus J, Forno L, Lincoln S, Wang DS, Hulihan M, Maraganore D, Gwinn-Hardy K, Wszolek Z, Dickson D, Langston JW (2004) Comparison of kindreds with parkinsonism and alpha-synuclein genomic multiplications. Ann Neurol 55:174-179.
FDA Advisory Committee Briefing Document. NDA 20-998/S-009: Celebrex Capsules (Celecoxib): Medical Officer Review. In.
Fearnley JM, Lees AJ (1991) Ageing and Parkinson's disease: substantia nigra regional selectivity. Brain 114 (Pt 5):2283-2301.
Feher JJ (1983) Facilitated calcium diffusion by intestinal calcium-binding protein. Am J Physiol 244:C303-307.
Ferger B, Teismann P, Earl CD, Kuschinsky K, Oertel WH (1999) Salicylate protects against MPTP-induced impairments in dopaminergic neurotransmission at the striatal and nigral level in mice. Naunyn Schmiedebergs Arch Pharmacol 360:256-261.
FitzGerald GA (2003) COX-2 and beyond: Approaches to prostaglandin inhibition in human disease. Nat Rev Drug Discov 2:879-890.
Fitzpatrick E, Ashkan K, Wallace BA, Benabid AL, Mitrofanis J (2005) Differential survival patterns among midbrain dopaminergic cells of MPTP-treated monkeys and 6OHDA-lesioned rats. Anat Embryol (Berl) 210:101-123.
Floran B, Aceves J, Sierra A, Martinez-Fong D (1990) Activation of D1 dopamine receptors stimulates the release of GABA in the basal ganglia of the rat. Neurosci Lett 116:136-140.

Floyd RA, Hensley K (2002) Oxidative stress in brain aging. Implications for therapeutics of neurodegenerative diseases. Neurobiol Aging 23:795-807.
Gaspar P, Heizmann CW, Kaas JH (1993) Calbindin D-28K in the dopaminergic mesocortical projection of a monkey (Aotus trivirgatus). Brain Res 603:166-172.
Gaspar P, Ben Jelloun N, Febvret A (1994) Sparing of the dopaminergic neurons containing calbindin-D28k and of the dopaminergic mesocortical projections in weaver mutant mice. Neuroscience 61:293-305.
Gerfen CR (1985) The neostriatal mosaic. I. Compartmental organization of projections from the striatum to the substantia nigra in the rat. J Comp Neurol 236:454-476.
Gerfen CR (1992) The neostriatal mosaic: multiple levels of compartmental organization. Trends Neurosci 15:133-139.
Gerfen CR, Sawchenko PE (1984) An anterograde neuroanatomical tracing method that shows the detailed morphology of neurons, their axons and terminals: immunohistochemical localization of an axonally transported plant lectin, Phaseolus vulgaris leucoagglutinin (PHA-L). Brain Res 290:219-238.
Gerfen CR, Wilson CJ (1996) The Basal Ganglia. Handbook of Chemical Neuroanatomy: Integrated Systems of the CNS: Elsevier Science.
Gerfen CR, Herkenham M, Thibault J (1987) The neostriatal mosaic: II. Patch- and matrix-directed mesostriatal dopaminergic and non-dopaminergic systems. J Neurosci 7:3915-3934.
German DC, Liang CL (1993) Neuroactive peptides exist in the midbrain dopaminergic neurons that contain calbindin-D28k. Neuroreport 4:491-494.
German DC, Manaye KF, Sonsalla PK, Brooks BA (1992) Midbrain dopaminergic cell loss in Parkinson's disease and MPTP-induced parkinsonism: sparing of calbindin-D28k-containing cells. Ann N Y Acad Sci 648:42-62.
German DC, Dubach M, Askari S, Speciale SG, Bowden DM (1988) 1-Methyl-4-phenyl-1,2,3,6-tetrahydropyridine-induced parkinsonian syndrome in Macaca fascicularis: which midbrain dopaminergic neurons are lost? Neuroscience 24:161-174.
German DC, Manaye K, Smith WK, Woodward DJ, Saper CB (1989) Midbrain dopaminergic cell loss in Parkinson's disease: computer visualization. Ann Neurol 26:507-514.
Gervais J, Rouillard C (2000) Dorsal raphe stimulation differentially modulates dopaminergic neurons in the ventral tegmental area and substantia nigra. Synapse 35:281-291.
Gibb WR, Lees AJ (1991) Anatomy, pigmentation, ventral and dorsal subpopulations of the substantia nigra, and differential cell death in Parkinson's disease. J Neurol Neurosurg Psychiatry 54:388-396.
Gilks WP, Abou-Sleiman PM, Gandhi S, Jain S, Singleton A, Lees AJ, Shaw K, Bhatia KP, Bonifati V, Quinn NP, Lynch J, Healy DG, Holton JL, Revesz T, Wood NW (2005) A common LRRK2 mutation in idiopathic Parkinson's disease. Lancet 365:415-416.
Gimenez-Amaya JM, de las Heras S, Erro E, Mengual E, Lanciego JL (2000) Considerations on the thalamostriatal system with some functional implications. Histol Histopathol 15:1285-1292.
Giovannelli L, Decorosi F, Dolara P, Pulvirenti L (2003) Vulnerability to DNA damage in the aging rat substantia nigra: a study with the comet assay. Brain Res 969:244-247.
Goldberg MS, Fleming SM, Palacino JJ, Cepeda C, Lam HA, Bhatnagar A, Meloni EG, Wu N, Ackerson LC, Klapstein GJ, Gajendiran M, Roth BL, Chesselet MF, Maidment NT, Levine MS, Shen J (2003) Parkin-deficient mice exhibit nigrostriatal deficits but not loss of dopaminergic neurons. J Biol Chem 278:43628-43635.
Gonzalez-Hernandez T, Barroso-Chinea P, Rodriguez M (2004) Response of the GABAergic and dopaminergic mesostriatal projections to the lesion of the contralateral dopaminergic mesostriatal pathway in the rat. Mov Disord 19:1029-1042.

Gonzalez-Hernandez T, Barroso-Chinea P, Acevedo A, Salido E, Rodriguez M (2001) Colocalization of tyrosine hydroxylase and GAD65 mRNA in mesostriatal neurons. Eur J Neurosci 13:57-67.
Goodwin FK, Post RM, Dunner DL, Gordon EK (1973) Cerebrospinal fluid amine metabolites in affective illness: the probenecid technique. Am J Psychiatry 130:73-79.
Gordon EK, Oliver J, Kopin IJ (1975) The effect of probenecid on catecholamine metabolites in human cerebrospinal fluid analyzed by mass fragmentography. Life Sci 16:1527-1531.
Gordon EK, Markey SP, Sherman RL, Kopin IJ (1976) Conjugated 3,4 dihydroxy phenyl acetic acid (DOPAC) in human and monkey cerebrospinal fluid and rat brain and the effects of probenecid treatment. Life Sci 18:1285-1292.
Graybiel AM (2000) The basal ganglia. Curr Biol 10:R509-511.
Graybiel AM, Rauch SL (2000) Toward a neurobiology of obsessive-compulsive disorder. Neuron 28:343-347.
Greenamyre JT, Hastings TG (2004) Biomedicine. Parkinson's--divergent causes, convergent mechanisms. Science 304:1120-1122.
Greene JG (2006) Gene expression profiles of brain dopamine neurons and relevance to neuropsychiatric disease. J Physiol 575:411-416.
Greene JG, Dingledine R, Greenamyre JT (2005) Gene expression profiling of rat midbrain dopamine neurons: implications for selective vulnerability in parkinsonism. Neurobiol Dis 18:19-31.
Grunblatt E, Mandel S, Youdim MB (2000) Neuroprotective strategies in Parkinson's disease using the models of 6-hydroxydopamine and MPTP. Ann N Y Acad Sci 899:262-273.
Grunblatt E, Mandel S, Maor G, Youdim MB (2001) Gene expression analysis in N-methyl-4-phenyl-1,2,3,6-tetrahydropyridine mice model of Parkinson's disease using cDNA microarray: effect of R-apomorphine. J Neurochem 78:1-12.
Grundmann M, Earl CD, Sautter J, Henze C, Oertel WH, Bandmann O (2004) Slow N-acetyltransferase 2 status leads to enhanced intrastriatal dopamine depletion in 6-hydroxydopamine-lesioned rats. Exp Neurol 187:199-202.
Grunewald T, Beal MF (1999) NOS knockouts and neuroprotection. Nat Med 5:1354-1355.
Guengerich FP (1992) Metabolic activation of carcinogens. Pharmacol Ther 54:17-61.
Guridi J, Herrero MT, Luquin MR, Guillen J, Ruberg M, Laguna J, Vila M, Javoy-Agid F, Agid Y, Hirsch E, Obeso JA (1996) Subthalamotomy in parkinsonian monkeys. Behavioural and biochemical analysis. Brain 119 (Pt 5):1717-1727.
Haber SN, Ryoo H, Cox C, Lu W (1995) Subsets of midbrain dopaminergic neurons in monkeys are distinguished by different levels of mRNA for the dopamine transporter: comparison with the mRNA for the D2 receptor, tyrosine hydroxylase and calbindin immunoreactivity. J Comp Neurol 362:400-410.
Halliwell B (1989) Free radicals in biology and medicine, 2nd Edition: Oxford: Clarendon.
Hammond C, Bergman H, Brown P (2007) Pathological synchronization in Parkinson's disease: networks, models and treatments. Trends Neurosci.
Hamre K, Tharp R, Poon K, Xiong X, Smeyne RJ (1999) Differential strain susceptibility following 1-methyl-4-phenyl-1,2,3,6-tetrahydropyridine (MPTP) administration acts in an autosomal dominant fashion: quantitative analysis in seven strains of Mus musculus. Brain Res 828:91-103.
Hanrott K, Gudmunsen L, O'Neill MJ, Wonnacott S (2006) 6-hydroxydopamine-induced apoptosis is mediated via extracellular auto-oxidation and caspase 3-dependent activation of protein kinase Cdelta. J Biol Chem 281:5373-5382.
Harhangi BS, Oostra BA, Heutink P, van Duijn CM, Hofman A, Breteler MM (1999) N-acetyltransferase-2 polymorphism in Parkinson's disease: the Rotterdam study. J Neurol Neurosurg Psychiatry 67:518-520.

Hatano Y, Li Y, Sato K, Asakawa S, Yamamura Y, Tomiyama H, Yoshino H, Asahina M, Kobayashi S, Hassin-Baer S, Lu CS, Ng AR, Rosales RL, Shimizu N, Toda T, Mizuno Y, Hattori N (2004) Novel PINK1 mutations in early-onset parkinsonism. Ann Neurol 56:424-427.

Hefti F, Melamed E, Sahakian BJ, Wurtman RJ (1980) Circling behavior in rats with partial, unilateral nigro-striatal lesions: effect of amphetamine, apomorphine, and DOPA. Pharmacol Biochem Behav 12:185-188.

Heikkila RE, Hess A, Duvoisin RC (1984) Dopaminergic neurotoxicity of 1-methyl-4-phenyl-1,2,5,6-tetrahydropyridine in mice. Science 224:1451-1453.

Hein DW (2002) Molecular genetics and function of NAT1 and NAT2: role in aromatic amine metabolism and carcinogenesis. Mutat Res 506-507:65-77.

Hein DW, Grant DM, Sim E (2000a) Update on consensus arylamine N-acetyltransferase gene nomenclature [letter]. Pharmacogenetics 10:291-292.

Hein DW, Omichinski JG, Brewer JA, Weber WW (1982) A unique pharmacogenetic expression of the N-acetylation polymorphism in the inbred hamster. J Pharmacol Exp Ther 220:8-15.

Hein DW, Trinidad A, Yerokun T, Ferguson RJ, Kirlin WG, Weber WW (1988) Genetic control of acetyl coenzyme A-dependent arylamine N-acetyltransferase, hydrazine N-acetyltransferase, and N-hydroxy-arylamine O-acetyltransferase enzymes in C57BL/6J, A/J, AC57F1, and the rapid and slow acetylator A.B6 and B6.A congenic inbred mouse. Drug Metabolism and Disposition 16:341-347.

Hein DW, Doll MA, Fretland AJ, Leff MA, Webb SJ, Xiao GH, Devanaboyina US, Nangju NA, Feng Y (2000b) Molecular genetics and epidemiology of the NAT1 and NAT2 acetylation polymorphisms. Cancer Epidemiology, Biomarkers and Prevention 9:29-42.

Heizmann CW, Braun K (1992) Changes in Ca(2+)-binding proteins in human neurodegenerative disorders. Trends Neurosci 15:259-264.

Henry S, Tappaz M (1991) Relative enrichment of the lighter 59 kDa form of glutamic acid decarboxylase in nerve endings: an immunoblotting study in pituitary neurointermediate lobe. Neurosci Lett 131:253-256.

Hensley K, Maidt ML, Yu Z, Sang H, Markesbery WR, Floyd RA (1998) Electrochemical analysis of protein nitrotyrosine and dityrosine in the Alzheimer brain indicates region-specific accumulation. J Neurosci 18:8126-8132.

Herrero MT, Hirsch EC, Kastner A, Ruberg M, Luquin MR, Laguna J, Javoy-Agid F, Obeso JA, Agid Y (1993) Does neuromelanin contribute to the vulnerability of catecholaminergic neurons in monkeys intoxicated with MPTP? Neuroscience 56:499-511.

Hickman D, Risch A, Buckle V, Spurr NK, Jeremiah SJ, McCarthy A, Sim E (1994) Chromosomal localization of human genes for arylamine N-acetyltransferase. Biochemical Journal 297 (Pt 3):441-445.

Hickman D, Pope J, Patil SD, Fakis G, Smelt V, Stanley LA, Payton M, Unadkat JD, Sim E (1998) Expression of arylamine N-acetyltransferase in human intestine. Gut 42:402-409.

Hogan B BR, Costantini F, Lacy E (1994) Manipulating the Mouse Embryo: A Laboratory Manual. New York: Cold Spring Harbor Laboratory.

Hornykiewicz O, Kish SJ (1987) Biochemical pathophysiology of Parkinson's disease. Adv Neurol 45:19-34.

Hsu LJ, Sagara Y, Arroyo A, Rockenstein E, Sisk A, Mallory M, Wong J, Takenouchi T, Hashimoto M, Masliah E (2000) alpha-synuclein promotes mitochondrial deficit and oxidative stress. Am J Pathol 157:401-410.

Hunot S, Vila M, Teismann P, Davis RJ, Hirsch EC, Przedborski S, Rakic P, Flavell RA (2004) JNK-mediated induction of cyclooxygenase 2 is required for

neurodegeneration in a mouse model of Parkinson's disease. Proc Natl Acad Sci U S A 101:665-670.
Hwang DY, Ardayfio P, Kang UJ, Semina EV, Kim KS (2003) Selective loss of dopaminergic neurons in the substantia nigra of Pitx3-deficient aphakia mice. Brain Res Mol Brain Res 114:123-131.
Hyun DH, Lee M, Hattori N, Kubo S, Mizuno Y, Halliwell B, Jenner P (2002) Effect of wild-type or mutant Parkin on oxidative damage, nitric oxide, antioxidant defenses, and the proteasome. J Biol Chem 277:28572-28577.
Iacopino A, Christakos S, German D, Sonsalla PK, Altar CA (1992) Calbindin-D28K-containing neurons in animal models of neurodegeneration: possible protection from excitotoxicity. Brain Res Mol Brain Res 13:251-261.
Iancu R, Mohapel P, Brundin P, Paul G (2005) Behavioral characterization of a unilateral 6-OHDA-lesion model of Parkinson's disease in mice. Behav Brain Res 162:1-10.
Imai H, Steindler DA, Kitai ST (1986) The organization of divergent axonal projections from the midbrain raphe nuclei in the rat. J Comp Neurol 243:363-380.
Insel (1996) Analgesic-antipyretic and anti-inflammatory agents and drugs employed in the treatment of gout., 9th edition Edition. New York: McGraw-Hill.
Irwin I, DeLanney LE, Langston JW (1993) MPTP and aging. Studies in the C57BL/6 mouse. Adv Neurol 60:197-206.
Irwin I, Finnegan KT, Delanney LE, Di Monte D, Langston JW (1992) The relationships between aging, monoamine oxidase, striatal dopamine and the effects of MPTP in C57BL/6 mice: a critical reassessment. Brain Res 572:224-231.
Itier JM, Ibanez P, Mena MA, Abbas N, Cohen-Salmon C, Bohme GA, Laville M, Pratt J, Corti O, Pradier L, Ret G, Joubert C, Periquet M, Araujo F, Negroni J, Casarejos MJ, Canals S, Solano R, Serrano A, Gallego E, Sanchez M, Denefle P, Benavides J, Tremp G, Rooney TA, Brice A, Garcia de Yebenes J (2003) Parkin gene inactivation alters behaviour and dopamine neurotransmission in the mouse. Hum Mol Genet 12:2277-2291.
Itoh K, Weis S, Mehraein P, Muller-Hocker J (1996) Cytochrome c oxidase defects of the human substantia nigra in normal aging. Neurobiol Aging 17:843-848.
Iwata S, Nomoto M, Morioka H, Miyata A (2004) Gene expression profiling in the midbrain of striatal 6-hydroxydopamine-injected mice. Synapse 51:279-286.
Izzo PN (1991) A note on the use of biocytin in anterograde tracing studies in the central nervous system: application at both light and electron microscopic level. J Neurosci Methods 36:155-166.
Jain S, Wood NW, Healy DG (2005) Molecular genetic pathways in Parkinson's disease: a review. Clin Sci (Lond) 109:355-364.
Jande SS, Maler L, Lawson DE (1981) Immunohistochemical mapping of vitamin D-dependent calcium-binding protein in brain. Nature 294:765-767.
Javitch JA, D'Amato RJ, Strittmatter SM, Snyder SH (1985) Parkinsonism-inducing neurotoxin, N-methyl-4-phenyl-1,2,3,6 -tetrahydropyridine: uptake of the metabolite N-methyl-4-phenylpyridine by dopamine neurons explains selective toxicity. Proc Natl Acad Sci U S A 82:2173-2177.
Jellinger KA (2001) The pathology of Parkinson's disease. Adv Neurol 86:55-72.
Jenne JW (1965) Partial purification and properties of the isoniazid transacetylase in human liver: its relationship to the acetylation of p-aminosalicylic acid. J Clin Invest 44:1992-2002.
Jenner P (2003) Oxidative stress in Parkinson's disease. Ann Neurol 53 Suppl 3:S26-36; discussion S36-28.
Jeon BS, Jackson-Lewis V, Burke RE (1995) 6-Hydroxydopamine lesion of the rat substantia nigra: time course and morphology of cell death. Neurodegeneration 4:131-137.

Jha N, Kumar MJ, Boonplueang R, Andersen JK (2002) Glutathione decreases in dopaminergic PC12 cells interfere with the ubiquitin protein degradation pathway: relevance for Parkinson's disease? J Neurochem 80:555-561.

Jin J, Meredith GE, Chen L, Zhou Y, Xu J, Shie FS, Lockhart P, Zhang J (2005) Quantitative proteomic analysis of mitochondrial proteins: relevance to Lewy body formation and Parkinson's disease. Brain Res Mol Brain Res 134:119-138.

Joel D, Weiner I (2000) The connections of the dopaminergic system with the striatum in rats and primates: an analysis with respect to the functional and compartmental organization of the striatum. Neuroscience 96:451-474.

Johnson JA, el Barbary A, Kornguth SE, Brugge JF, Siegel FL (1993) Glutathione S-transferase isoenzymes in rat brain neurons and glia. J Neurosci 13:2013-2023.

Johnson N, Bell P, Jonovska V, Budge M, Sim E (2004) NAT gene polymorphisms and susceptibility to Alzheimer's disease: identification of a novel NAT1 allelic variant. BMC Med Genet 5:6.

Johnston FA, White SL (1965) The effect of vitamin B6 deficiency and of isoniazid on the pyridoxal phosphate content of rat brain. Biochem Pharmacol 14:1481-1483.

Jonsson G (1980) Chemical neurotoxins as denervation tools in neurobiology. Annu Rev Neurosci 3:169-187.

Jossan SS, Sakurai E, Oreland L (1989) MPTP toxicity in relation to age, dopamine uptake and MAO-B activity in two rodent species. Pharmacol Toxicol 64:314-318.

Joyce JN, Millan MJ (2005) Dopamine D3 receptor antagonists as therapeutic agents. Drug Discov Today 10:917-925.

Kaufman DL, Houser CR, Tobin AJ (1991) Two forms of the gamma-aminobutyric acid synthetic enzyme glutamate decarboxylase have distinct intraneuronal distributions and cofactor interactions. J Neurochem 56:720-723.

Kaur H, Whiteman M, Halliwell B (1997) Peroxynitrite-dependent aromatic hydroxylation and nitration of salicylate and phenylalanine. Is hydroxyl radical involved? Free Radic Res 26:71-82.

Kawamura A (2005) Structural investigations of arylamine *N*-acetyltransferases from eukaryotes. In: Department of Pharmacology, p 162: University of Oxford.

Kawamura A, Sandy J, A. U, Noble M, Sim E (2003) Structural investigation of mutant *Mycobacterium smegmatis* arylamine N-acetyltransferase: a model for a naturally occuring functional polymorphism in *Mycobacterium tuberculosis* arylamine N-acetyltransferase. Protein Expression and Purification 27:75-84.

Kawamura A, Graham J, Mushtaq A, Tsiftsoglou SA, Vath GM, Hanna PE, Wagner CR, Sim E (2005) Eukaryotic arylamine N-acetyltransferase. Investigation of substrate specificity by high-throughput screening. Biochem Pharmacol 69:347-359.

Khan NL, Jain S, Lynch JM, Pavese N, Abou-Sleiman P, Holton JL, Healy DG, Gilks WP, Sweeney MG, Ganguly M, Gibbons V, Gandhi S, Vaughan J, Eunson LH, Katzenschlager R, Gayton J, Lennox G, Revesz T, Nicholl D, Bhatia KP, Quinn N, Brooks D, Lees AJ, Davis MB, Piccini P, Singleton AB, Wood NW (2005) Mutations in the gene LRRK2 encoding dardarin (PARK8) cause familial Parkinson's disease: clinical, pathological, olfactory and functional imaging and genetic data. Brain 128:2786-2796.

King MA, Louis PM, Hunter BE, Walker DW (1989) Biocytin: a versatile anterograde neuroanatomical tract-tracing alternative. Brain Res 497:361-367.

Kirik D, Rosenblad C, Bjorklund A (1998) Characterization of behavioral and neurodegenerative changes following partial lesions of the nigrostriatal dopamine system induced by intrastriatal 6-hydroxydopamine in the rat. Exp Neurol 152:259-277.

Kish SJ, Shannak K, Rajput A, Deck JH, Hornykiewicz O (1992) Aging produces a specific pattern of striatal dopamine loss: implications for the etiology of idiopathic Parkinson's disease. J Neurochem 58:642-648.
Kita H, Armstrong W (1991) A biotin-containing compound N-(2-aminoethyl)biotinamide for intracellular labeling and neuronal tracing studies: comparison with biocytin. J Neurosci Methods 37:141-150.
Kitada T, Asakawa S, Hattori N, Matsumine H, Yamamura Y, Minoshima S, Yokochi M, Mizuno Y, Shimizu N (1998) Mutations in the parkin gene cause autosomal recessive juvenile parkinsonism. Nature 392:605-608.
Klegeris A, McGeer EG, McGeer PL (2007) Therapeutic approaches to inflammation in neurodegenerative disease. Curr Opin Neurol 20:351-357.
Klein C, Schlossmacher MG (2006) The genetics of Parkinson disease: Implications for neurological care. Nat Clin Pract Neurol 2:136-146.
Klivenyi P, Andreassen OA, Ferrante RJ, Lancelot E, Reif D, Beal MF (2000a) Inhibition of neuronal nitric oxide synthase protects against MPTP toxicity. Neuroreport 11:1265-1268.
Klivenyi P, Andreassen OA, Ferrante RJ, Dedeoglu A, Mueller G, Lancelot E, Bogdanov M, Andersen JK, Jiang D, Beal MF (2000b) Mice deficient in cellular glutathione peroxidase show increased vulnerability to malonate, 3-nitropropionic acid, and 1-methyl-4-phenyl-1,2,5,6-tetrahydropyridine. J Neurosci 20:1-7.
Knapowski J, Wieczorowska-Tobis K, Witowski J (2002) Pathophysiology of ageing. J Physiol Pharmacol 53:135-146.
Knott C, Stern G, Wilkin GP (2000) Inflammatory regulators in Parkinson's disease: iNOS, lipocortin-1, and cyclooxygenases-1 and -2. Mol Cell Neurosci 16:724-739.
Kohler G, Milstein C (1975) Continuous cultures of fused cells secreting antibody of predefined specificity. Nature 256:495-497.
Kohr G, Lambert CE, Mody I (1991) Calbindin-D28K (CaBP) levels and calcium currents in acutely dissociated epileptic neurons. Exp Brain Res 85:543-551.
Korotkova TM, Ponomarenko AA, Brown RE, Haas HL (2004) Functional diversity of ventral midbrain dopamine and GABAergic neurons. Mol Neurobiol 29:243-259.
Korotkova TM, Ponomarenko AA, Haas HL, Sergeeva OA (2005) Differential expression of the homeobox gene Pitx3 in midbrain dopaminergic neurons. Eur J Neurosci 22:1287-1293.
Kruger R, Kuhn W, Muller T, Woitalla D, Graeber M, Kosel S, Przuntek H, Epplen JT, Schols L, Riess O (1998) Ala30Pro mutation in the gene encoding alpha-synuclein in Parkinson's disease. Nat Genet 18:106-108.
Kruger R, Vieira-Saecker AM, Kuhn W, Berg D, Muller T, Kuhnl N, Fuchs GA, Storch A, Hungs M, Woitalla D, Przuntek H, Epplen JT, Schols L, Riess O (1999) Increased susceptibility to sporadic Parkinson's disease by a certain combined alpha-synuclein/apolipoprotein E genotype. Ann Neurol 45:611-617.
Kubis N, Faucheux BA, Ransmayr G, Damier P, Duyckaerts C, Henin D, Forette B, Le Charpentier Y, Hauw JJ, Agid Y, Hirsch EC (2000) Preservation of midbrain catecholaminergic neurons in very old human subjects. Brain 123 (Pt 2):366-373.
Kukar T, Murphy MP, Eriksen JL, Sagi SA, Weggen S, Smith TE, Ladd T, Khan MA, Kache R, Beard J, Dodson M, Merit S, Ozols VV, Anastasiadis PZ, Das P, Fauq A, Koo EH, Golde TE (2005) Diverse compounds mimic Alzheimer disease-causing mutations by augmenting Abeta42 production. Nat Med 11:545-550.
Kulisevsky J, Roldan E (2004) Hallucinations and sleep disturbances in Parkinson's disease. Neurology 63:S28-30.
Kunikowska G, Jenner P (2003) Alterations in m-RNA expression for Cu,Zn-superoxide dismutase and glutathione peroxidase in the basal ganglia of MPTP-treated marmosets and patients with Parkinson's disease. Brain Res 968:206-218.

Kurth JH, Kurth MC, Poduslo SE, Schwankhaus JD (1993) Association of a monoamine oxidase B allele with Parkinson's disease. Ann Neurol 33:368-372.
Lang AE, Lozano AM (1998a) Parkinson's disease. Second of two parts. N Engl J Med 339:1130-1143.
Lang AE, Lozano AM (1998b) Parkinson's disease. First of two parts. N Engl J Med 339:1044-1053.
Langston JW, Langston EB, Irwin I (1984) MPTP-induced parkinsonism in human and non-human primates--clinical and experimental aspects. Acta Neurol Scand Suppl 100:49-54.
Laprade N, Soghomonian JJ (1999) Gene expression of the GAD67 and GAD65 isoforms of glutamate decarboxylase is differentially altered in subpopulations of striatal neurons in adult rats lesioned with 6-OHDA as neonates. Synapse 33:36-48.
Lau YS, Fung YK (1986) Pharmacological effects of 1-methyl-4-phenyl-1,2,3,6-tetrahydropyridine (MPTP) on striatal dopamine receptor system. Brain Res 369:311-315.
Lau YS, Crampton JM, Wilson JA (1988) Urinary excretion of MPTP and its primary metabolites in mice. Life Sci 43:1459-1464.
Lau YS, Trobough KL, Crampton JM, Wilson JA (1990) Effects of probenecid on striatal dopamine depletion in acute and long-term 1-methyl-4-phenyl-1,2,3,6-tetrahydropyridine (MPTP)-treated mice. Gen Pharmacol 21:181-187.
Lavoie B, Parent A (1991) Dopaminergic neurons expressing calbindin in normal and parkinsonian monkeys. Neuroreport 2:601-604.
Lee CR, Tepper JM (2007) Morphological and physiological properties of parvalbumin- and calretinin-containing gamma-aminobutyric acidergic neurons in the substantia nigra. J Comp Neurol 500:958-972.
Levine MS, Cepeda C, Hickey MA, Fleming SM, Chesselet MF (2004) Genetic mouse models of Huntington's and Parkinson's diseases: illuminating but imperfect. Trends Neurosci 27:691-697.
Lheureux P, Penaloza A, Gris M (2005) Pyridoxine in clinical toxicology: a review. Eur J Emerg Med 12:78-85.
Liang CL, Sinton CM, German DC (1996a) Midbrain dopaminergic neurons in the mouse: co-localization with Calbindin-D28K and calretinin. Neuroscience 75:523-533.
Liang CL, Sinton CM, Sonsalla PK, German DC (1996b) Midbrain dopaminergic neurons in the mouse that contain calbindin-D28k exhibit reduced vulnerability to MPTP-induced neurodegeneration. Neurodegeneration 5:313-318.
Lindefors N, Brene S, Herrera-Marschitz M, Persson H (1989) Region specific regulation of glutamic acid decarboxylase mRNA expression by dopamine neurons in rat brain. Exp Brain Res 77:611-620.
Liu Y, Fallon L, Lashuel HA, Liu Z, Lansbury PT, Jr. (2002) The UCH-L1 gene encodes two opposing enzymatic activities that affect alpha-synuclein degradation and Parkinson's disease susceptibility. Cell 111:209-218.
Lobo MK, Karsten SL, Gray M, Geschwind DH, Yang XW (2006) FACS-array profiling of striatal projection neuron subtypes in juvenile and adult mouse brains. Nat Neurosci 9:443-452.
Loehle JA, Cornish V, Wakefield L, Doll MA, Neale JR, Zang Y, Sim E, Hein DW (2006) N-acetyltransferase (Nat) 1 and 2 expression in Nat2 knockout mice. J Pharmacol Exp Ther 319:724-728.
Logroscino G (2005) The role of early life environmental risk factors in Parkinson disease: what is the evidence? Environ Health Perspect 113:1234-1238.
Lotharius J, Brundin P (2002) Impaired dopamine storage resulting from alpha-synuclein mutations may contribute to the pathogenesis of Parkinson's disease. Hum Mol Genet 11:2395-2407.

Lowndes HE, Beiswanger CM, Philbert MA, Reuhl KR (1994) Substrates for neural metabolism of xenobiotics in adult and developing brain. Neurotoxicology 15:61-73.
Lumsden A, Krumlauf R (1996) Patterning the vertebrate neuraxis. Science 274:1109-1115.
Luthman J, Fredriksson A, Sundstrom E, Jonsson G, Archer T (1989) Selective lesion of central dopamine or noradrenaline neuron systems in the neonatal rat: motor behavior and monoamine alterations at adult stage. Behav Brain Res 33:267-277.
Ma SY, Ciliax BJ, Stebbins G, Jaffar S, Joyce JN, Cochran EJ, Kordower JH, Mash DC, Levey AI, Mufson EJ (1999) Dopamine transporter-immunoreactive neurons decrease with age in the human substantia nigra. J Comp Neurol 409:25-37.
Mandel S, Grunblatt E, Maor G, Youdim MB (2002) Early and late gene changes in MPTP mice model of Parkinson's disease employing cDNA microarray. Neurochem Res 27:1231-1243.
Mann DM, Yates PO, Marcyniuk B (1984) Monoaminergic neurotransmitter systems in presenile Alzheimer's disease and in senile dementia of Alzheimer type. Clin Neuropathol 3:199-205.
Manoukian AS, Krause HM (1992) Concentration-dependent activities of the even-skipped protein in Drosophila embryos. Genes Dev 6:1740-1751.
Maraganore DM, Farrer MJ, Hardy JA, McDonnell SK, Schaid DJ, Rocca WA (2000) Case-control study of debrisoquine 4-hydroxylase, N-acetyltransferase 2, and apolipoprotein E gene polymorphisms in Parkinson's disease. Mov Disord 15:714-719.
Markey SP, Johannessen JN, Chiueh CC, Burns RS, Herkenham MA (1984) Intraneuronal generation of a pyridinium metabolite may cause drug-induced parkinsonism. Nature 311:464-467.
Martin DL, Rimvall K (1993) Regulation of gamma-aminobutyric acid synthesis in the brain. J Neurochem 60:395-407.
Martin DL, Martin SB, Wu SJ, Espina N (1991) Regulatory properties of brain glutamate decarboxylase (GAD): the apoenzyme of GAD is present principally as the smaller of two molecular forms of GAD in brain. J Neurosci 11:2725-2731.
Martin JH (2003) Neuroanatomy text and atlas, Third edition Edition. United States: McGraw-Hill.
Martinasevic MK, King CD, Rios GR, Tephly TR (1998) Immunohistochemical localization of UDP-glucuronosyltransferases in rat brain during early development. Drug Metab Dispos 26:1039-1041.
Masliah E, Rockenstein E, Veinbergs I, Mallory M, Hashimoto M, Takeda A, Sagara Y, Sisk A, Mucke L (2000) Dopaminergic loss and inclusion body formation in alpha-synuclein mice: implications for neurodegenerative disorders. Science 287:1265-1269.
Mattson MP, Magnus T (2006) Ageing and neuronal vulnerability. Nat Rev Neurosci 7:278-294.
Mattson MP, Rychlik B, Chu C, Christakos S (1991) Evidence for calcium-reducing and excito-protective roles for the calcium-binding protein calbindin-D28k in cultured hippocampal neurons. Neuron 6:41-51.
Mayer RA, Kindt MV, Heikkila RE (1986) Prevention of the nigrostriatal toxicity of 1-methyl-4-phenyl-1,2,3,6-tetrahydropyridine by inhibitors of 3,4-dihydroxyphenylethylamine transport. J Neurochem 47:1073-1079.
McCormack AL, Atienza JG, Langston JW, Di Monte DA (2006) Decreased susceptibility to oxidative stress underlies the resistance of specific dopaminergic cell populations to paraquat-induced degeneration. Neuroscience 141:929-937.
McCormack AL, Atienza JG, Johnston LC, Andersen JK, Vu S, Di Monte DA (2005) Role of oxidative stress in paraquat-induced dopaminergic cell degeneration. J Neurochem 93:1030-1037.

McCormack AL, Thiruchelvam M, Manning-Bog AB, Thiffault C, Langston JW, Cory-Slechta DA, Di Monte DA (2002) Environmental risk factors and Parkinson's disease: selective degeneration of nigral dopaminergic neurons caused by the herbicide paraquat. Neurobiol Dis 10:119-127.

McCormack AL, Di Monte DA, Delfani K, Irwin I, DeLanney LE, Langston WJ, Janson AM (2004) Aging of the nigrostriatal system in the squirrel monkey. J Comp Neurol 471:387-395.

McCoy E, Anders M, Rosenkranz H (1983) The basis of the insensitivity of Salmonella typhimurium strain TA98/1,8-DNP6 to the mutagenic action of nitroarenes. Mutat Res 121:17-23.

McGeer PL, McGeer EG, Suzuki JS (1977) Aging and extrapyramidal function. Arch Neurol 34:33-35.

McGeer PL, Itagaki S, Boyes BE, McGeer EG (1988) Reactive microglia are positive for HLA-DR in the substantia nigra of Parkinson's and Alzheimer's disease brains. Neurology 38:1285-1291.

McNeill TH, Koek LL (1990) Differential effects of advancing age on neurotransmitter cell loss in the substantia nigra and striatum of C57BL/6N mice. Brain Res 521:107-117.

McNeill TH, Koek LL, Brown SA, Rafols JA (1988) Age-related changes in the nigrostriatal system. Ann N Y Acad Sci 515:239-248.

McRae-Degueurce A, Klawans HL, Penn RD, Dahlstrom A, Tanner CM, Goetz CG, Carvey PM (1988) An antibody in the CSF of Parkinson's disease patients disappears following adrenal medulla transplantation. Neurosci Lett 94:192-197.

McRitchie DA, Halliday GM (1995) Calbindin D28k-containing neurons are restricted to the medial substantia nigra in humans. Neuroscience 65:87-91.

Mehta JL, Chen J, Yu F, Li DY (2004) Aspirin inhibits ox-LDL-mediated LOX-1 expression and metalloproteinase-1 in human coronary endothelial cells. Cardiovasc Res 64:243-249.

Mellick GD (2006) CYP450, genetics and Parkinson's disease: gene x environment interactions hold the key. J Neural Transm Suppl:159-165.

Mellick GD, Maraganore DM, Silburn PA (2005) Australian data and meta-analysis lend support for alpha-synuclein (NACP-Rep1) as a risk factor for Parkinson's disease. Neurosci Lett 375:112-116.

Meltzer HY (1995) Role of serotonin in the action of atypical antipsychotic drugs. Clin Neurosci 3:64-75.

Meredith GE, Halliday GM, Totterdell S (2004) A critical review of the development and importance of proteinaceous aggregates in animal models of Parkinson's disease: new insights into Lewy body formation. Parkinsonism Relat Disord 10:191-202.

Meredith GE, Totterdell S, Petroske E, Santa Cruz K, Callison RC, Jr., Lau YS (2002) Lysosomal malfunction accompanies alpha-synuclein aggregation in a progressive mouse model of Parkinson's disease. Brain Res 956:156-165.

Meyer M, Zimmer J, Seiler RW, Widmer HR (1999) GDNF increases the density of cells containing calbindin but not of cells containing calretinin in cultured rat and human fetal nigral tissue. Cell Transplant 8:25-36.

Meyer-Lindenberg A, Miletich RS, Kohn PD, Esposito G, Carson RE, Quarantelli M, Weinberger DR, Berman KF (2002) Reduced prefrontal activity predicts exaggerated striatal dopaminergic function in schizophrenia. Nat Neurosci 5:267-271.

Miettinen RA, Kalesnykas G, Koivisto EH (2002) Estimation of the total number of cholinergic neurons containing estrogen receptor-alpha in the rat basal forebrain. J Histochem Cytochem 50:891-902.

Miller JJ, Richardson TL, Fibiger HC, McLennan H (1975) Anatomical and electrophysiological identification of a projection from the mesencephalic raphe to the caudate-putamen in the rat. Brain Res 97:133-136.

Miller LP, Martin DL, Mazumder A, Walters JR (1978) Studies on the regulation of GABA synthesis: substrate-promoted dissociation of pyridoxal-5'-phosphate from GAD. J Neurochem 30:361-369.
Millikan RC, Pittman GS, Newman B, Tse CK, Selmin O, Rockhill B, Savitz D, Moorman PG, Bell DA (1998) Cigarette smoking, N-acetyltransferases 1 and 2, and breast cancer risk. Cancer Epidemiol Biomarkers Prev 7:371-378.
Mitchell JA, Akarasereenont P, Thiemermann C, Flower RJ, Vane JR (1993) Selectivity of nonsteroidal antiinflammatory drugs as inhibitors of constitutive and inducible cyclooxygenase. Proc Natl Acad Sci U S A 90:11693-11697.
Mizuno T, Kuno R, Nitta A, Nabeshima T, Zhang G, Kawanokuchi J, Wang J, Jin S, Takeuchi H, Suzumura A (2005) Protective effects of nicergoline against neuronal cell death induced by activated microglia and astrocytes. Brain Res 1066:78-85.
Mohanakumar KP, Muralikrishnan D, Thomas B (2000) Neuroprotection by sodium salicylate against 1-methyl-4-phenyl-1,2,3, 6-tetrahydropyridine-induced neurotoxicity. Brain Res 864:281-290.
Molho ES, Factor SA (2001) Parkinson's disease: the treatment of drug-induced hallucinations and psychosis. Curr Neurol Neurosci Rep 1:320-328.
Morgan DW, Welton AF, Heick AE, Christakos S (1986) Specific in vitro activation of Ca,Mg-ATPase by vitamin D-dependent rat renal calcium binding protein (calbindin D28K). Biochem Biophys Res Commun 138:547-553.
Morrish PK, Sawle GV, Brooks DJ (1995) Clinical and [18F] dopa PET findings in early Parkinson's disease. J Neurol Neurosurg Psychiatry 59:597-600.
Mrak RE, Griffin WS (1997) The role of chronic self-propagating glial responses in neurodegeneration: implications for long-lived survivors of human immunodeficiency virus. J Neurovirol 3:241-246.
Mrak RE, Griffin ST, Graham DI (1997) Aging-associated changes in human brain. J Neuropathol Exp Neurol 56:1269-1275.
Murase S, McKay RD (2006) A specific survival response in dopamine neurons at most risk in Parkinson's disease. J Neurosci 26:9750-9760.
Murphy GF, Robinson D, Sharman DF (1969) The effect of tropolone on the formation of 3,4-dihydroxyphenylacetic acid and 4-hydroxy-3-methoxyphenylacetic acid in the brain of the mouse. Br J Pharmacol 36:107-115.
Muthane U, Yasha TC, Shankar SK (1998) Low numbers and no loss of melanized nigral neurons with increasing age in normal human brains from India. Ann Neurol 43:283-287.
Nanopoulos D, Belin MF, Maitre M, Vincendon G, Pujol JF (1982) Immunocytochemical evidence for the existence of GABAergic neurons in the nucleus raphe dorsalis. Possible existence of neurons containing serotonin and GABA. Brain Res 232:375-389.
Naoi M, Maruyama W (1999) Cell death of dopamine neurons in aging and Parkinson's disease. Mech Ageing Dev 111:175-188.
Nemoto C, Hida T, Arai R (1999) Calretinin and calbindin-D28k in dopaminergic neurons of the rat midbrain: a triple-labeling immunohistochemical study. Brain Res 846:129-136.
Neuhoff H, Neu A, Liss B, Roeper J (2002) I(h) channels contribute to the different functional properties of identified dopaminergic subpopulations in the midbrain. J Neurosci 22:1290-1302.
Ng MC, Iacopino AM, Quintero EM, Marches F, Sonsalla PK, Liang CL, Speciale SG, German DC (1996) The neurotoxin MPTP increases calbindin-D28k levels in mouse midbrain dopaminergic neurons. Brain Res Mol Brain Res 36:329-336.
Nishikawa K, Li H, Kawamura R, Osaka H, Wang YL, Hara Y, Hirokawa T, Manago Y, Amano T, Noda M, Aoki S, Wada K (2003) Alterations of structure and hydrolase

activity of parkinsonism-associated human ubiquitin carboxyl-terminal hydrolase L1 variants. Biochem Biophys Res Commun 304:176-183.
Nishioka K, Hayashi S, Farrer MJ, Singleton AB, Yoshino H, Imai H, Kitami T, Sato K, Kuroda R, Tomiyama H, Mizoguchi K, Murata M, Toda T, Imoto I, Inazawa J, Mizuno Y, Hattori N (2006) Clinical heterogeneity of alpha-synuclein gene duplication in Parkinson's disease. Ann Neurol 59:298-309.
Novikova L, Garris BL, Garris DR, Lau YS (2006) Early signs of neuronal apoptosis in the substantia nigra pars compacta of the progressive neurodegenerative mouse 1-methyl-4-phenyl-1,2,3,6-tetrahydropyridine/probenecid model of Parkinson's disease. Neuroscience 140:67-76.
Nunes I, Tovmasian LT, Silva RM, Burke RE, Goff SP (2003) Pitx3 is required for development of substantia nigra dopaminergic neurons. Proc Natl Acad Sci U S A 100:4245-4250.
Obata T, Chiueh CC (1992) In vivo trapping of hydroxyl free radicals in the striatum utilizing intracranial microdialysis perfusion of salicylate: effects of MPTP, MPDP+, and MPP+. J Neural Transm Gen Sect 89:139-145.
Obeso JA, Rodriguez-Oroz MC, Rodriguez M, Arbizu J, Gimenez-Amaya JM (2002) The basal ganglia and disorders of movement: pathophysiological mechanisms. News Physiol Sci 17:51-55.
Obeso JA, Rodriguez-Oroz MC, Rodriguez M, Lanciego JL, Artieda J, Gonzalo N, Olanow CW (2000) Pathophysiology of the basal ganglia in Parkinson's disease. Trends Neurosci 23:S8-19.
Ohashi S, Mori A, Kurihara N, Mitsumoto Y, Nakai M (2006) Age-related severity of dopaminergic neurodegeneration to MPTP neurotoxicity causes motor dysfunction in C57BL/6 mice. Neurosci Lett 401:183-187.
Ohsako S, Deguchi T (1990) Cloning and expression of cDNAs for polymorphic and monomorphic arylamine N-acetyltransferases from human liver. Journal of Biological Chemistry 265:4630-4634.
Olivera M, Martinez C, Molina JA, Alonso-Navarro H, Jimenez-Jimenez FJ, Garcia-Martin E, Benitez J, Agundez JA (2006) Increased frequency of rapid acetylator genotypes in patients with brain astrocytoma and meningioma. Acta Neurol Scand 113:322-326.
Olszewski J. BD (1954) Cytoarchitecture of the Human Brain Stem. Basel: Karger.
Osaka H, Wang YL, Takada K, Takizawa S, Setsuie R, Li H, Sato Y, Nishikawa K, Sun YJ, Sakurai M, Harada T, Hara Y, Kimura I, Chiba S, Namikawa K, Kiyama H, Noda M, Aoki S, Wada K (2003) Ubiquitin carboxy-terminal hydrolase L1 binds to and stabilizes monoubiquitin in neuron. Hum Mol Genet 12:1945-1958.
Ostrerova-Golts N, Petrucelli L, Hardy J, Lee JM, Farer M, Wolozin B (2000) The A53T alpha-synuclein mutation increases iron-dependent aggregation and toxicity. J Neurosci 20:6048-6054.
Ouimet CC, Miller PE, Hemmings HC, Jr., Walaas SI, Greengard P (1984) DARPP-32, a dopamine- and adenosine 3':5'-monophosphate-regulated phosphoprotein enriched in dopamine-innervated brain regions. III. Immunocytochemical localization. J Neurosci 4:111-124.
Owen AD, Schapira AH, Jenner P, Marsden CD (1996) Oxidative stress and Parkinson's disease. Ann N Y Acad Sci 786:217-223.
Pacifici GM, Bencini C, Rane A (1986) Acetyltransferase in humans: development and tissue distribution. Pharmacology 32:283-291.
Packard MG, Knowlton BJ (2002) Learning and memory functions of the Basal Ganglia. Annu Rev Neurosci 25:563-593.
Paisan-Ruiz C, Jain S, Evans EW, Gilks WP, Simon J, van der Brug M, Lopez de Munain A, Aparicio S, Gil AM, Khan N, Johnson J, Martinez JR, Nicholl D, Carrera IM, Pena AS, de Silva R, Lees A, Marti-Masso JF, Perez-Tur J, Wood NW, Singleton AB

(2004) Cloning of the gene containing mutations that cause PARK8-linked Parkinson's disease. Neuron 44:595-600.
Pakkenberg H, Andersen BB, Burns RS, Pakkenberg B (1995) A stereological study of substantia nigra in young and old rhesus monkeys. Brain Res 693:201-206.
Palacino JJ, Sagi D, Goldberg MS, Krauss S, Motz C, Wacker M, Klose J, Shen J (2004) Mitochondrial dysfunction and oxidative damage in parkin-deficient mice. J Biol Chem 279:18614-18622.
Parent A, Bouchard C, Smith Y (1984) The striatopallidal and striatonigral projections: two distinct fiber systems in primate. Brain Res 303:385-390.
Parent A, Fortin M, Cote PY, Cicchetti F (1996) Calcium-binding proteins in primate basal ganglia. Neurosci Res 25:309-334.
Paxinos G, Franklin KBJ (2004) The Mouse Brain in stereotaxic coordinates, Second Edition Edition: Elsevier Academic Press.
Pearce RK, Owen A, Daniel S, Jenner P, Marsden CD (1997) Alterations in the distribution of glutathione in the substantia nigra in Parkinson's disease. J Neural Transm 104:661-677.
Pearson WR, Lipman DJ (1988) Improved tools for biological sequence comparison. Proc Natl Acad Sci U S A 85:2444-2448.
Pedersen WA, Fu W, Keller JN, Markesbery WR, Appel S, Smith RG, Kasarskis E, Mattson MP (1998) Protein modification by the lipid peroxidation product 4-hydroxynonenal in the spinal cords of amyotrophic lateral sclerosis patients. Ann Neurol 44:819-824.
Pedneault S, Soghomonian JJ (1994) Glutamate decarboxylase (GAD65) mRNA levels in the striatum and pallidum of MPTP-treated monkeys. Brain Res Mol Brain Res 25:351-354.
Perese DA, Ulman J, Viola J, Ewing SE, Bankiewicz KS (1989) A 6-hydroxydopamine-induced selective parkinsonian rat model. Brain Res 494:285-293.
Perry TL, Yong VW (1986) Idiopathic Parkinson's disease, progressive supranuclear palsy and glutathione metabolism in the substantia nigra of patients. Neurosci Lett 67:269-274.
Perry TL, Godin DV, Hansen S (1982) Parkinson's disease: a disorder due to nigral glutathione deficiency? Neurosci Lett 33:305-310.
Peters A, Sethares C, Harriman KM (1990) Different kinds of axon terminals forming symmetric synapses with the cell bodies and initial axon segments of layer II/III pyramidal cells. II. Synaptic junctions. J Neurocytol 19:584-600.
Petroske E, Meredith GE, Callen S, Totterdell S, Lau YS (2001) Mouse model of Parkinsonism: a comparison between subacute MPTP and chronic MPTP/probenecid treatment. Neuroscience 106:589-601.
Poewe WH, Wenning GK (1998) The natural history of Parkinson's disease. Ann Neurol 44:S1-9.
Polymeropoulos MH, Lavedan C, Leroy E, Ide SE, Dehejia A, Dutra A, Pike B, Root H, Rubenstein J, Boyer R, Stenroos ES, Chandrasekharappa S, Athanassiadou A, Papapetropoulos T, Johnson WG, Lazzarini AM, Duvoisin RC, Di Iorio G, Golbe LI, Nussbaum RL (1997) Mutation in the alpha-synuclein gene identified in families with Parkinson's disease. Science 276:2045-2047.
Potashkin JA, Meredith GE (2006) The role of oxidative stress in the dysregulation of gene expression and protein metabolism in neurodegenerative disease. Antioxid Redox Signal 8:144-151.
Prensa L, Cossette M, Parent A (2000) Dopaminergic innervation of human basal ganglia. J Chem Neuroanat 20:207-213.
Priyadarshi A, Khuder SA, Schaub EA, Priyadarshi SS (2001) Environmental risk factors and Parkinson's disease: a metaanalysis. Environ Res 86:122-127.

Przedborski S, Levivier M, Jiang H, Ferreira M, Jackson-Lewis V, Donaldson D, Togasaki DM (1995) Dose-dependent lesions of the dopaminergic nigrostriatal pathway induced by intrastriatal injection of 6-hydroxydopamine. Neuroscience 67:631-647.
Przedborski S, Kostic V, Jackson-Lewis V, Naini AB, Simonetti S, Fahn S, Carlson E, Epstein CJ, Cadet JL (1992) Transgenic mice with increased Cu/Zn-superoxide dismutase activity are resistant to N-methyl-4-phenyl-1,2,3,6-tetrahydropyridine-induced neurotoxicity. J Neurosci 12:1658-1667.
Przedborski S, Chen Q, Vila M, Giasson BI, Djaldatti R, Vukosavic S, Souza JM, Jackson-Lewis V, Lee VM, Ischiropoulos H (2001) Oxidative post-translational modifications of alpha-synuclein in the 1-methyl-4-phenyl-1,2,3,6-tetrahydropyridine (MPTP) mouse model of Parkinson's disease. J Neurochem 76:637-640.
Purisai MG, McCormack AL, Cumine S, Li J, Isla MZ, Di Monte DA (2007) Microglial activation as a priming event leading to paraquat-induced dopaminergic cell degeneration. Neurobiol Dis 25:392-400.
Qian L, Block ML, Wei SJ, Lin CF, Reece J, Pang H, Wilson B, Hong JS, Flood PM (2006) Interleukin-10 protects lipopolysaccharide-induced neurotoxicity in primary midbrain cultures by inhibiting the function of NADPH oxidase. J Pharmacol Exp Ther 319:44-52.
Quik M (2004) Smoking, nicotine and Parkinson's disease. Trends Neurosci 27:561-568.
Ramos-Vara JA (2005) Technical aspects of immunohistochemistry. Vet Pathol 42:405-426.
Ravina B, Janis S, Keleti J, Marler JM (2004) Funding evidence: the National Institute of Neurological Disorders and Stroke Clinical Trials Program. NeuroRx 1:317-322.
Reader TA, Dewar KM (1999) Effects of denervation and hyperinnervation on dopamine and serotonin systems in the rat neostriatum: implications for human Parkinson's disease. Neurochem Int 34:1-21.
Reisner PD, Christakos S, Vanaman TC (1992) In vitro enzyme activation with calbindin-D28k, the vitamin D-dependent 28 kDa calcium binding protein. FEBS Lett 297:127-131.
Rentschler S, Vaidya DM, Tamaddon H, Degenhardt K, Sassoon D, Morley GE, Jalife J, Fishman GI (2001) Visualization and functional characterization of the developing murine cardiac conduction system. Development 128:1785-1792.
Reynolds ES (1963) The use of lead citrate at high pH as an electron-opaque stain in electron microscopy. J Cell Biol 17:208-212.
Ricaurte GA, Irwin I, Forno LS, DeLanney LE, Langston E, Langston JW (1987) Aging and 1-methyl-4-phenyl-1,2,3,6-tetrahydropyridine-induced degeneration of dopaminergic neurons in the substantia nigra. Brain Res 403:43-51.
Richard A. Goldsby TJK, Barbara A Osborne (2000) Kuby Immunology, Fourth Edition Edition. New York: W.H. Freeman and Company.
Rimvall K, Martin DL (1994) The level of GAD67 protein is highly sensitive to small increases in intraneuronal gamma-aminobutyric acid levels. J Neurochem 62:1375-1381.
Robertson GS, Vincent SR, Fibiger HC (1992) D1 and D2 dopamine receptors differentially regulate c-fos expression in striatonigral and striatopallidal neurons. Neuroscience 49:285-296.
Rodrigues-Lima F, Cooper RN, Goudeau B, Atmane N, Chamagne AM, Butler-Browne G, Sim E, Vicart P, Dupret JM (2003) Skeletal muscles express the xenobiotic-metabolizing enzyme arylamine N-acetyltransferase. J Histochem Cytochem 51:789-796.
Rodriguez M, Gonzalez-Hernandez T (1999) Electrophysiological and morphological evidence for a GABAergic nigrostriatal pathway. J Neurosci 19:4682-4694.
Rodriguez M, Martin L, Santana C (1994) Ontogenic development of brain asymmetry in dopaminergic neurons. Brain Res Bull 33:163-171.

Rodriguez M, Gomez C, Alonso J, Afonso D (1992) Laterality, alternation, and perseveration relationships on the T-maze test. Behav Neurosci 106:974-980.
Rodriguez M, Barroso-Chinea P, Abdala P, Obeso J, Gonzalez-Hernandez T (2001) Dopamine cell degeneration induced by intraventricular administration of 6-hydroxydopamine in the rat: similarities with cell loss in parkinson's disease. Exp Neurol 169:163-181.
Roffler-Tarlov S, Sharman DF, Tegerdine P (1971) 3,4-dihydroxyphenylacetic acid and 4-hydroxy-3-methoxyphenylacetic acid in the mouse striatum: a reflection of intra- and extra-neuronal metabolism of dopamine? Br J Pharmacol 42:343-351.
Rogers DC, Fisher EM, Brown SD, Peters J, Hunter AJ, Martin JE (1997) Behavioral and functional analysis of mouse phenotype: SHIRPA, a proposed protocol for comprehensive phenotype assessment. Mamm Genome 8:711-713.
Rogers JH (1992) Immunohistochemical markers in rat brain: colocalization of calretinin and calbindin-D28k with tyrosine hydroxylase. Brain Res 587:203-210.
Rogers MA, Bradshaw JL, Pantelis C, Phillips JG (1998) Frontostriatal deficits in unipolar major depression. Brain Res Bull 47:297-310.
Rozovsky I, Finch CE, Morgan TE (1998) Age-related activation of microglia and astrocytes: in vitro studies show persistent phenotypes of aging, increased proliferation, and resistance to down-regulation. Neurobiol Aging 19:97-103.
Sachs C, Jonsson G (1975) Mechanisms of action of 6-hydroxydopamine. Biochem Pharmacol 24:1-8.
Sadikot AF, Luk, K.C., van den Munckhof, P., Pymar, V.V., Leung, K., Gandhi, R., Drouin, J. (2005) Pitx3 is necessary for survival of midbrain dopaminergic neuron subsets relevant to Parkinson's disease: Springer USA.
Sairam K, Saravanan KS, Banerjee R, Mohanakumar KP (2003) Non-steroidal anti-inflammatory drug sodium salicylate, but not diclofenac or celecoxib, protects against 1-methyl-4-phenyl pyridinium-induced dopaminergic neurotoxicity in rats. Brain Res 966:245-252.
Saito Y, Kawashima A, Ruberu NN, Fujiwara H, Koyama S, Sawabe M, Arai T, Nagura H, Yamanouchi H, Hasegawa M, Iwatsubo T, Murayama S (2003) Accumulation of phosphorylated alpha-synuclein in aging human brain. J Neuropathol Exp Neurol 62:644-654.
Saiz PA, Garcia-Portilla MP, Arango C, Morales B, Alvarez V, Coto E, Fernandez JM, Bousono M, Bobes J (2006) N-acetyltransferase-2 polymorphisms and schizophrenia. Eur Psychiatry 21:333-337.
Sajadi A, Schneider BL, Aebischer P (2004) Wlds-mediated protection of dopaminergic fibers in an animal model of Parkinson disease. Curr Biol 14:326-330.
Saka E, Graybiel AM (2003) Pathophysiology of Tourette's syndrome: striatal pathways revisited. Brain Dev 25 Suppl 1:S15-19.
Sanghera MK, Manaye KF, Liang CL, Lacopino AM, Bannon MJ, German DC (1994) Low dopamine transporter mRNA levels in midbrain regions containing calbindin. Neuroreport 5:1641-1644.
Santoro B, Tibbs GR (1999) The HCN gene family: molecular basis of the hyperpolarization-activated pacemaker channels. Ann N Y Acad Sci 868:741-764.
Schmidt H, Schwaller B, Eilers J (2005) Calbindin D28k targets myo-inositol monophosphatase in spines and dendrites of cerebellar Purkinje neurons. Proc Natl Acad Sci U S A 102:5850-5855.
Schober A (2004) Classic toxin-induced animal models of Parkinson's disease: 6-OHDA and MPTP. Cell Tissue Res 318:215-224.
Seaton TA, Cooper JM, Schapira AH (1997) Free radical scavengers protect dopaminergic cell lines from apoptosis induced by complex I inhibitors. Brain Res 777:110-118.
Selkoe DJ (2001) Alzheimer's disease: genes, proteins, and therapy. Physiol Rev 81:741-766.

Semchuk KM, Love EJ, Lee RG (1992) Parkinson's disease and exposure to agricultural work and pesticide chemicals. Neurology 42:1328-1335.

Semina EV, Reiter RS, Murray JC (1997) Isolation of a new homeobox gene belonging to the Pitx/Rieg family: expression during lens development and mapping to the aphakia region on mouse chromosome 19. Hum Mol Genet 6:2109-2116.

Shimoji M, Zhang L, Mandir AS, Dawson VL, Dawson TM (2005) Absence of inclusion body formation in the MPTP mouse model of Parkinson's disease. Brain Res Mol Brain Res 134:103-108.

Shimura H, Hattori N, Kubo S, Mizuno Y, Asakawa S, Minoshima S, Shimizu N, Iwai K, Chiba T, Tanaka K, Suzuki T (2000) Familial Parkinson disease gene product, parkin, is a ubiquitin-protein ligase. Nat Genet 25:302-305.

Sian J, Dexter DT, Lees AJ, Daniel S, Agid Y, Javoy-Agid F, Jenner P, Marsden CD (1994) Alterations in glutathione levels in Parkinson's disease and other neurodegenerative disorders affecting basal ganglia. Ann Neurol 36:348-355.

Siddiqi Z, Kemper TL, Killiany R (1999) Age-related neuronal loss from the substantia nigra-pars compacta and ventral tegmental area of the rhesus monkey. J Neuropathol Exp Neurol 58:959-971.

Sim E, Payton M, Noble M, Minchin R (2000) An update on genetic, structural and functional studies of arylamine *N*-acetyltransferases in eucaryotes and procaryotes. Hum Mol Genet 9:2435-2441.

Simon H, Le Moal M, Calas A (1979) Efferents and afferents of the ventral tegmental-A10 region studied after local injection of [3H]leucine and horseradish peroxidase. Brain Res 178:17-40.

Singer TP, Castagnoli N, Jr., Ramsay RR, Trevor AJ (1987) Biochemical events in the development of parkinsonism induced by 1-methyl-4-phenyl-1,2,3,6-tetrahydropyridine. J Neurochem 49:1-8.

Singleton AB, Farrer M, Johnson J, Singleton A, Hague S, Kachergus J, Hulihan M, Peuralinna T, Dutra A, Nussbaum R, Lincoln S, Crawley A, Hanson M, Maraganore D, Adler C, Cookson MR, Muenter M, Baptista M, Miller D, Blancato J, Hardy J, Gwinn-Hardy K (2003) alpha-Synuclein locus triplication causes Parkinson's disease. Science 302:841.

Sirinathsinghji DJ, Kupsch A, Mayer E, Zivin M, Pufal D, Oertel WH (1992) Cellular localization of tyrosine hydroxylase mRNA and cholecystokinin mRNA-containing cells in the ventral mesencephalon of the common marmoset: effects of 1-methyl-4-phenyl-1,2,3,6-tetrahydropyridine. Brain Res Mol Brain Res 12:267-274.

Smelt VA, Mardon HJ, Redman CW, Sim E (1997) Acetylation of arylamines by the placenta. European Journal of Drug Metabolism and Pharmacokinetics 22:403-408.

Smidt MP, van Schaick HS, Lanctot C, Tremblay JJ, Cox JJ, van der Kleij AA, Wolterink G, Drouin J, Burbach JP (1997) A homeodomain gene Ptx3 has highly restricted brain expression in mesencephalic dopaminergic neurons. Proc Natl Acad Sci U S A 94:13305-13310.

Smith DE, Saji M, Joh TH, Reis DJ, Pickel VM (1987) Ibotenic acid-induced lesions of striatal target and projection neurons: ultrastructural manifestations in dopaminergic and non-dopaminergic neurons and in glia. Histol Histopathol 2:251-263.

Smith Y, Bevan MD, Shink E, Bolam JP (1998) Microcircuitry of the direct and indirect pathways of the basal ganglia. Neuroscience 86:353-387.

Sobal G, Menzel JE, Sinzinger H (2000) Influence of acetylsalicylic acid on oxidation of native and glycated low-density lipoprotein. Life Sci 66:1987-1998.

Soghomonian JJ, Chesselet MF (1992) Effects of nigrostriatal lesions on the levels of messenger RNAs encoding two isoforms of glutamate decarboxylase in the globus pallidus and entopeduncular nucleus of the rat. Synapse 11:124-133.

Soghomonian JJ, Laprade N (1997) Glutamate decarboxylase (GAD67 and GAD65) gene expression is increased in a subpopulation of neurons in the putamen of Parkinsonian monkeys. Synapse 27:122-132.
Soghomonian JJ, Gonzales C, Chesselet MF (1992) Messenger RNAs encoding glutamate-decarboxylases are differentially affected by nigrostriatal lesions in subpopulations of striatal neurons. Brain Res 576:68-79.
Soghomonian JJ, Pedneault S, Audet G, Parent A (1994) Increased glutamate decarboxylase mRNA levels in the striatum and pallidum of MPTP-treated primates. J Neurosci 14:6256-6265.
Somogyi P, Bolam JP, Smith AD (1981a) Monosynaptic cortical input and local axon collaterals of identified striatonigral neurons. A light and electron microscopic study using the Golgi-peroxidase transport-degeneration procedure. J Comp Neurol 195:567-584.
Somogyi P, Bolam JP, Totterdell S, Smith AD (1981b) Monosynaptic input from the nucleus accumbens--ventral striatum region to retrogradely labelled nigrostriatal neurones. Brain Res 217:245-263.
Song DK, Im YB, Jung JS, Suh HW, Huh SO, Song JH, Kim YH (1999) Central injection of nicotine increases hepatic and splenic interleukin 6 (IL-6) mRNA expression and plasma IL-6 levels in mice: involvement of the peripheral sympathetic nervous system. Faseb J 13:1259-1267.
Specht CG, Schoepfer R (2001) Deletion of the alpha-synuclein locus in a subpopulation of C57BL/6J inbred mice. BMC Neurosci 2:11.
Spillantini MG, Schmidt ML, Lee VM, Trojanowski JQ, Jakes R, Goedert M (1997) Alpha-synuclein in Lewy bodies. Nature 388:839-840.
SPSS (1999) SPSS advanced models 10.0. Chicago: Statistical Package for Social Sciences.
Sriram K, Miller DB, O'Callaghan JP (2006) Minocycline attenuates microglial activation but fails to mitigate striatal dopaminergic neurotoxicity: role of tumor necrosis factor-alpha. J Neurochem 96:706-718.
Sriram SR, Li X, Ko HS, Chung KK, Wong E, Lim KL, Dawson VL, Dawson TM (2005) Familial-associated mutations differentially disrupt the solubility, localization, binding and ubiquitination properties of parkin. Hum Mol Genet 14:2571-2586.
Stanley LA, Mills IG, Sim E (1997) Localization of polymorphic N-acetyltransferase (NAT2) in tissues of inbred mice. Pharmacogenetics 7:121-130.
Stanley LA, Coroneos E, Cuff R, Hickman D, Ward A, Sim E (1996) Immunochemical detection of arylamine N-acetyltransferase in normal and neoplastic bladder. J Histochem Cytochem 44:1059-1067.
Stanley LA, Copp AJ, Pope J, Rolls S, Smelt V, Perry VH, Sim E (1998) Immunochemical detection of arylamine N-acetyltransferase during mouse embryonic development and in adult mouse brain. Teratology 58:174-182.
Stapleton G, Steel M, Richardson M, Mason JO, Rose KA, Morris RG, Lathe R (1995) A novel cytochrome P450 expressed primarily in brain. J Biol Chem 270:29739-29745.
Stark AK, Pakkenberg B (2004) Histological changes of the dopaminergic nigrostriatal system in aging. Cell Tissue Res 318:81-92.
Stephenson DT, Li Q, Simmons C, Connell MA, Meglasson MD, Merchant K, Emborg ME (2005) Expression of GAD65 and GAD67 immunoreactivity in MPTP-treated monkeys with or without L-DOPA administration. Neurobiol Dis 20:347-359.
Sterio DC (1984) The unbiased estimation of number and sizes of arbitrary particles using the disector. J Microsc 134:127-136.
Strazielle N, Ghersi-Egea JF (1999) Demonstration of a coupled metabolism-efflux process at the choroid plexus as a mechanism of brain protection toward xenobiotics. J Neurosci 19:6275-6289.

Sugama S, Yang L, Cho BP, DeGiorgio LA, Lorenzl S, Albers DS, Beal MF, Volpe BT, Joh TH (2003a) Age-related microglial activation in 1-methyl-4-phenyl-1,2,3,6-tetrahydropyridine (MPTP)-induced dopaminergic neurodegeneration in C57BL/6 mice. Brain Res 964:288-294.

Sugama S, Cho BP, Degiorgio LA, Shimizu Y, Kim SS, Kim YS, Shin DH, Volpe BT, Reis DJ, Cho S, Joh TH (2003b) Temporal and sequential analysis of microglia in the substantia nigra following medial forebrain bundle axotomy in rat. Neuroscience 116:925-933.

Sugamori KS, Wong S, Gaedigk A, Yu V, Abramovici H, Rozmahel R, Grant DM (2003) Generation and functional characterization of arylamine N-acetyltransferase Nat1/Nat2 double-knockout mice. Mol Pharmacol 64:170-179.

Svenningsson P, Nishi A, Fisone G, Girault JA, Nairn AC, Greengard P (2004) DARPP-32: an integrator of neurotransmission. Annu Rev Pharmacol Toxicol 44:269-296.

Takeuchi H, Jin S, Wang J, Zhang G, Kawanokuchi J, Kuno R, Sonobe Y, Mizuno T, Suzumura A (2006) Tumor necrosis factor-alpha induces neurotoxicity via glutamate release from hemichannels of activated microglia in an autocrine manner. J Biol Chem 281:21362-21368.

Tan EK, Khajavi M, Thornby JI, Nagamitsu S, Jankovic J, Ashizawa T (2000a) Variability and validity of polymorphism association studies in Parkinson's disease. Neurology 55:533-538.

Tan EK, Matsuura T, Nagamitsu S, Khajavi M, Jankovic J, Ashizawa T (2000b) Polymorphism of NACP-Rep1 in Parkinson's disease: an etiologic link with essential tremor? Neurology 54:1195-1198.

Tanaka M, Kim YM, Lee G, Junn E, Iwatsubo T, Mouradian MM (2004) Aggresomes formed by alpha-synuclein and synphilin-1 are cytoprotective. J Biol Chem 279:4625-4631.

Tanner CM, Goldman SM (1996) Epidemiology of Parkinson's disease. Neurol Clin 14:317-335.

Tatton WG, Greenwood CE, Seniuk NA, Salo PT (1992) Interactions between MPTP-induced and age-related neuronal death in a murine model of Parkinson's disease. Can J Neurol Sci 19:124-133.

Teismann P, Ferger B (2001) Inhibition of the cyclooxygenase isoenzymes COX-1 and COX-2 provide neuroprotection in the MPTP-mouse model of Parkinson's disease. Synapse 39:167-174.

Teismann P, Vila M, Choi DK, Tieu K, Wu DC, Jackson-Lewis V, Przedborski S (2003) COX-2 and neurodegeneration in Parkinson's disease. Ann N Y Acad Sci 991:272-277.

Thiruchelvam M, McCormack A, Richfield EK, Baggs RB, Tank AW, Di Monte DA, Cory-Slechta DA (2003) Age-related irreversible progressive nigrostriatal dopaminergic neurotoxicity in the paraquat and maneb model of the Parkinson's disease phenotype. Eur J Neurosci 18:589-600.

Tipton KF, Singer TP (1993) Advances in our understanding of the mechanisms of the neurotoxicity of MPTP and related compounds. J Neurochem 61:1191-1206.

Tomas-Camardiel M, Herrera AJ, Venero JL, Cruz Sanchez-Hidalgo M, Cano J, Machado A (2002) Differential regulation of glutamic acid decarboxylase mRNA and tyrosine hydroxylase mRNA expression in the aged manganese-treated rats. Brain Res Mol Brain Res 103:116-129.

Ton TG, Heckbert SR, Longstreth WT, Jr., Rossing MA, Kukull WA, Franklin GM, Swanson PD, Smith-Weller T, Checkoway H (2006) Nonsteroidal anti-inflammatory drugs and risk of Parkinson's disease. Mov Disord.

Torres EM, Meldrum A, Kirik D, Dunnett SB (2006) An investigation of the problem of two-layered immunohistochemical staining in paraformaldehyde fixed sections. J Neurosci Methods 158:64-74.
Troen A.M. (2000) A role for one-carbon metabolism in Alzheimer's disease. In: Department of Pharmacology: University of Oxford.
Uchida K, Kihara N, Hashimoto K, Nakayama H, Yamaguchi R, Tateyama S (2003) Age-related histological changes in the canine substantia nigra. J Vet Med Sci 65:179-185.
Ungerstedt U (1968) 6-Hydroxy-dopamine induced degeneration of central monoamine neurons. Eur J Pharmacol 5:107-110.
Ungerstedt U (1971) Stereotaxic mapping of the monoamine pathways in the rat brain. Acta Physiol Scand Suppl 367:1-48.
Ungerstedt U, Arbuthnott GW (1970) Quantitative recording of rotational behavior in rats after 6-hydroxy-dopamine lesions of the nigrostriatal dopamine system. Brain Res 24:485-493.
Upton A, Johnson N, Sandy J, Sim E (2001a) Arylamine N-acetyltransferases – of mice, men and microorganisms. Trends in Pharmacological Sciences 22:140-146.
Upton A, Smelt V, Mushtaq A, Aplin R, Johnson N, Mardon H, Sim E (2000) Placental arylamine N-acetyltransferase type 1: potential contributory source of urinary folate catabolite p-acetamidobenzoylglutamate during pregnancy. BIOCHIMICA ET BIOPHYSICA ACTA-GENERAL SUBJECTS 1524:143-148.
Upton A, Mushtaq A, Victor TC, Sampson SL, Sandy J, Smith D-M, van Helden PV, Sim E (2001b) Arylamine N-acetyltransferase of Mycobacterium tuberculosis is a polymorphic enzyme and a site of isoniazid metabolism. Molecular Microbiology 42:309-319.
Valente EM, Abou-Sleiman PM, Caputo V, Muqit MM, Harvey K, Gispert S, Ali Z, Del Turco D, Bentivoglio AR, Healy DG, Albanese A, Nussbaum R, Gonzalez-Maldonado R, Deller T, Salvi S, Cortelli P, Gilks WP, Latchman DS, Harvey RJ, Dallapiccola B, Auburger G, Wood NW (2004) Hereditary early-onset Parkinson's disease caused by mutations in PINK1. Science 304:1158-1160.
Van Bockstaele EJ, Biswas A, Pickel VM (1993) Topography of serotonin neurons in the dorsal raphe nucleus that send axon collaterals to the rat prefrontal cortex and nucleus accumbens. Brain Res 624:188-198.
Van Bockstaele EJ, Cestari DM, Pickel VM (1994) Synaptic structure and connectivity of serotonin terminals in the ventral tegmental area: potential sites for modulation of mesolimbic dopamine neurons. Brain Res 647:307-322.
van den Munckhof P, Luk KC, Ste-Marie L, Montgomery J, Blanchet PJ, Sadikot AF, Drouin J (2003) Pitx3 is required for motor activity and for survival of a subset of midbrain dopaminergic neurons. Development 130:2535-2542.
van der Walt JM, Martin ER, Scott WK, Zhang F, Nance MA, Watts RL, Hubble JP, Haines JL, Koller WC, Lyons K, Pahwa R, Stern MB, Colcher A, Hiner BC, Jankovic J, Ondo WG, Allen FH, Jr., Goetz CG, Small GW, Mastaglia F, Roses AD, Stajich JM, Booze MW, Fujiwara K, Gibson RA, Middleton LT, Scott BL, Pericak-Vance MA, Vance JM (2003) Genetic polymorphisms of the N-acetyltransferase genes and risk of Parkinson's disease. Neurology 60:1189-1191.
Varastet M, Riche D, Maziere M, Hantraye P (1994) Chronic MPTP treatment reproduces in baboons the differential vulnerability of mesencephalic dopaminergic neurons observed in Parkinson's disease. Neuroscience 63:47-56.
Veenman CL, Reiner A, Honig MG (1992) Biotinylated dextran amine as an anterograde tracer for single- and double-labeling studies. J Neurosci Methods 41:239-254.
Vercelli A, Repici M, Garbossa D, Grimaldi A (2000) Recent techniques for tracing pathways in the central nervous system of developing and adult mammals. Brain Res Bull 51:11-28.

Vertes RP (1991) A PHA-L analysis of ascending projections of the dorsal raphe nucleus in the rat. J Comp Neurol 313:643-668.
Vijitruth R, Liu M, Choi DY, Nguyen XV, Hunter RL, Bing G (2006) Cyclooxygenase-2 mediates microglial activation and secondary dopaminergic cell death in the mouse MPTP model of Parkinson's disease. J Neuroinflammation 3:6.
Vila M, Przedborski S (2004) Genetic clues to the pathogenesis of Parkinson's disease. Nat Med 10 Suppl:S58-62.
Vila M, Vukosavic S, Jackson-Lewis V, Neystat M, Jakowec M, Przedborski S (2000) Alpha-synuclein up-regulation in substantia nigra dopaminergic neurons following administration of the parkinsonian toxin MPTP. J Neurochem 74:721-729.
Volles MJ, Lee SJ, Rochet JC, Shtilerman MD, Ding TT, Kessler JC, Lansbury PT, Jr. (2001) Vesicle permeabilization by protofibrillar alpha-synuclein: implications for the pathogenesis and treatment of Parkinson's disease. Biochemistry 40:7812-7819.
von Coelln R, Dawson VL, Dawson TM (2004) Parkin-associated Parkinson's disease. Cell Tissue Res 318:175-184.
Walsh SL, Wagner GC (1989) Age-dependent effects of 1-methyl-4-phenyl-1,2,3,6-tetrahydropyridine (MPTP): correlation with monoamine oxidase-B. Synapse 3:308-314.
Wang VY, Zoghbi HY (2001) Genetic regulation of cerebellar development. Nat Rev Neurosci 2:484-491.
Warner M, Gustafsson JA (1994) Effect of ethanol on cytochrome P450 in the rat brain. Proc Natl Acad Sci U S A 91:1019-1023.
Warner TT, Schapira AH (2003) Genetic and environmental factors in the cause of Parkinson's disease. Ann Neurol 53 Suppl 3:S16-23; discussion S23-15.
Weber WW, Hein DW (1985) N-acetylation pharmacogenetics. Pharmacol Rev 37:25-79.
West MJ (1993) New stereological methods for counting neurons. Neurobiol Aging 14:275-285.
West MJ, Gundersen HJ (1990) Unbiased stereological estimation of the number of neurons in the human hippocampus. J Comp Neurol 296:1-22.
Westwood IM, Holton SJ, Rodrigues-Lima F, Dupret JM, Bhakta S, Noble ME, Sim E (2005) Expression, purification, characterization and structure of Pseudomonas aeruginosa arylamine N-acetyltransferase. Biochem J 385:605-612.
Wichmann T, DeLong MR (1998) Models of basal ganglia function and pathophysiology of movement disorders. Neurosurg Clin N Am 9:223-236.
Wichmann T, DeLong MR (2003) Pathophysiology of Parkinson's disease: the MPTP primate model of the human disorder. Ann N Y Acad Sci 991:199-213.
Williams JA, Stone EM, Fakis G, Johnson N, Cordell JA, Meinl W, Glatt H, Sim E, Phillips DH (2001) N-Acetyltransferases, sulfotransferases and heterocyclic amine activation in the breast. Pharmacogenetics 11:373-388.
Windmill KF, Gaedigk A, Hall PM, Samaratunga H, Grant DM, McManus ME (2000) Localization of N-acetyltransferases NAT1 and NAT2 in human tissues. Toxicol Sci 54:19-29.
Wirtshafter D, Stratford TR, Asin KE (1987) Evidence that serotonergic projections to the substantia nigra in the rat arise in the dorsal, but not the median, raphe nucleus. Neurosci Lett 77:261-266.
Wolfart J, Neuhoff H, Franz O, Roeper J (2001) Differential expression of the small-conductance, calcium-activated potassium channel SK3 is critical for pacemaker control in dopaminergic midbrain neurons. J Neurosci 21:3443-3456.
Wood-Kaczmar A, Gandhi S, Wood NW (2006) Understanding the molecular causes of Parkinson's disease. Trends Mol Med 12:521-528.
Wouterlood FG, Jorritsma-Byham B (1993) The anterograde neuroanatomical tracer biotinylated dextran-amine: comparison with the tracer Phaseolus vulgaris-

leucoagglutinin in preparations for electron microscopy. J Neurosci Methods 48:75-87.

Wu DC, Jackson-Lewis V, Vila M, Tieu K, Teismann P, Vadseth C, Choi DK, Ischiropoulos H, Przedborski S (2002) Blockade of microglial activation is neuroprotective in the 1-methyl-4-phenyl-1,2,3,6-tetrahydropyridine mouse model of Parkinson disease. J Neurosci 22:1763-1771.

Yamada T, McGeer PL, Baimbridge KG, McGeer EG (1990) Relative sparing in Parkinson's disease of substantia nigra dopamine neurons containing calbindin-D28K. Brain Res 526:303-307.

Yoshida D, Hasegawa T, Sugibayashi K (2002) Targeting of salicylate to skin and muscle following topical injections in rats. Int J Pharm 231:177-184.

Youdim MB, Edmondson D, Tipton KF (2006) The therapeutic potential of monoamine oxidase inhibitors. Nat Rev Neurosci 7:295-309.

Young SN, Lal S, Martin JB, Ford RM, Sourkes TL (1973) 5-Hydroxyindoleacetic acid, homovanillic acid and tryptophan levels in CSF above and below a complete block of CSF flow. Psychiatr Neurol Neurochir 76:439-444.

Zahm DS (1991) Compartments in rat dorsal and ventral striatum revealed following injection of 6-hydroxydopamine into the ventral mesencephalon. Brain Res 552:164-169.

Zarranz JJ, Alegre J, Gomez-Esteban JC, Lezcano E, Ros R, Ampuero I, Vidal L, Hoenicka J, Rodriguez O, Atares B, Llorens V, Gomez Tortosa E, del Ser T, Munoz DG, de Yebenes JG (2004) The new mutation, E46K, of alpha-synuclein causes Parkinson and Lewy body dementia. Ann Neurol 55:164-173.

Zecca L, Gallorini M, Schunemann V, Trautwein AX, Gerlach M, Riederer P, Vezzoni P, Tampellini D (2001) Iron, neuromelanin and ferritin content in the substantia nigra of normal subjects at different ages: consequences for iron storage and neurodegenerative processes. J Neurochem 76:1766-1773.

Zhang J, Graham DG, Montine TJ, Ho YS (2000) Enhanced N-methyl-4-phenyl-1,2,3,6-tetrahydropyridine toxicity in mice deficient in CuZn-superoxide dismutase or glutathione peroxidase. J Neuropathol Exp Neurol 59:53-61.

Zimprich A, Biskup S, Leitner P, Lichtner P, Farrer M, Lincoln S, Kachergus J, Hulihan M, Uitti RJ, Calne DB, Stoessl AJ, Pfeiffer RF, Patenge N, Carbajal IC, Vieregge P, Asmus F, Muller-Myhsok B, Dickson DW, Meitinger T, Strom TM, Wszolek ZK, Gasser T (2004) Mutations in LRRK2 cause autosomal-dominant parkinsonism with pleomorphic pathology. Neuron 44:601-607.

Zipp F, Aktas O (2006) The brain as a target of inflammation: common pathways link inflammatory and neurodegenerative diseases. Trends Neurosci 29:518-527.

Zocchi A, Girlanda E, Varnier G, Sartori I, Zanetti L, Wildish GA, Lennon M, Mugnaini M, Heidbreder CA (2003) Dopamine responsiveness to drugs of abuse: A shell-core investigation in the nucleus accumbens of the mouse. Synapse 50:293-302.

Zuddas A, Fascetti F, Corsini GU, Piccardi MP (1994) In brown Norway rats, MPP+ is accumulated in the nigrostriatal dopaminergic terminals but it is not neurotoxic: a model of natural resistance to MPTP toxicity. Exp Neurol 127:54-61.

Zuddas A, Corsini GU, Schinelli S, Johannessen JN, di Porzio U, Kopin IJ (1989) MPTP treatment combined with ethanol or acetaldehyde selectively destroys dopaminergic neurons in mouse substantia nigra. Brain Res 501:1-10.